Facultat de Física
Departamento de Física Teórica

INTERACTION OF HADRONS AND TESTS FOR THE NATURE OF RESONANCES

Ph.D. THESIS

Submitted by:
Francesca Aceti

Supervised by:
Eulogio Oset Baguena

"He felt even freer than usual, attuned to the registers of his lower brain and gaining distance from the need to take inspired action, make original judgements, maintain independent principles and convictions, all the reasons why people are fucked up and birds and rats are not."

COSMOPOLIS, Don DeLillo

D. Eulogio Oset Báguena, Catedrático de Física Teórica de la Universidad de Valencia,

> CERTIFICA: Que la presente Memoria *Interaction of Hadrons and Tests for the Nature of Resonances* ha sido realizada bajo mi dirección en el Departamento de Física Teórica de la Universidad de Valencia por Francesca Aceti como Tesis para obtener el grado de Doctor en Física

Y para que así conste presenta la referida Memoria, firmando el presente certificado.

Fdo: Eulogio Oset Báguena

CONTENTS

LIST OF FIGURES

LIST OF TABLES

AGRADECIMIENTOS

Alla mia famiglia per l'amore e il supporto incondizionati.
Ai migliori amici che potessi incontrare, e non importa quanti chilometri ci separino.
A Carlo per la pazienza e la rassicurante presenza.
Ad Annalisa per le cure, le lacrime, le gag in salotto, le confessioni e le lezioni imparate.
A Flavio, e a questo legame che non smette di sorprendermi.
A Isabella e Dario per essere un esempio, pure se non l'ho mai detto loro apertamente.
A Viviana per le chiacchierate illuminanti.
A Valentina, perché lo so che è lì sempre e comunque e mi pare incredibile.
Ad Eleonora, per le sue analisi, le risate e i concerti.
Ad Adriano per quel caffé.
A mis compañeros de trabajo, Astrid, Miguel, Carlos, Raquel, Javier, Eduardo, Pedro, Uchino, Vinicius, por el ánimo, la paciencia y los momentos divertidos compartidos, pero sobre todo por su amistad.
A Manolo Vicente, Juan Nieves y Luis Álvarez por su apoyo y por los valiosos consejos, tanto profesionales como personales, que me han dado.
Y, obviamente, a mi director de Tesis, Eulogio Oset, por todo lo que fue capaz de enseñarme, por creer en mí y por su increíble y contagioso entusiasmo.

CHAPTER 1

INTRODUCTION

The idea of this Thesis work is to give a contribution to the extensive efforts made to understand the structure of hadronic particles done in the last decades, one of the most important issues in hadron physics.

During the 50s, the development of particle accelerators and the measurement of scattering cross sections revealed the existence of new particles in the form of resonances, corresponding to states with an extremely small lifetime and a considerable width (10 to 200 MeV).

The first resonance was discovered by Anderson, Fermi, Long and Nagle at the Chicago Cyclotron in 1952 [1] in the πp system with $J = \frac{3}{2}$, and it is now known as the $\Delta(1232)$. Many others followed, like the $\Sigma(1385)$, discovered at the Lawrence Radiation Laboratory in 1960 [2] and the observation of the first mesonic resonances, the $K^*(980)$ [3], the ρ [4] and the ω [5], particles with spin $J = 1$. With this proliferation of particles and resonances, a pattern appeared and an organizing scheme became necessary in order to describe it.

The solution was initially found in the generalization of the concept of isospin, a quantum number originally introduced to explain the properties of the nucleons. In the Fermi-Yang model of 1959 [6], the neutron and the proton appear as fundamental objects and the other particles as their combinations, considering for example the pion as a bound state of a nucleon and an anti-nucleon, $\bar{n}p \rightarrow \pi^+$ [7]. Later, Sakata proposed to extend the model from $SU(2)$ to $SU(3)$ including the Λ as one of the building blocks, in order to accommodate mesons and baryons with strangeness [8].

However, the real turning point arrived in 1961 when Gell-Mann [9] and, independently, Ne'maan [10] proposed that each isospin, or $SU(3)$, multiplet had to be composed of particles sharing the same values of spin and parity. While in the Sakata model the baryons p, n and Λ formed a triplet of $SU(3)$ and the pseudoscalars were in an octet, in the Gell-Mann-Ne'eman model the

baryons constitute an octect, including the Σ isotriplet and the Ξ isodoublet in addition to the nucleons and the Λ. Thus, all the particles are grouped in octets, which are the basic entity of the model, or in multiplets deriving from the combination of octects following rules analogous to the ones for the addition of angular momenta. By means of the "*eightfold way*", the name Gell-Mann gave to the theory, it was possible to arrange already observed states, but also to predict new ones, later discovered with appropriate properties, in order to fill the multiplets. For example, the known pseudoscalars at that time were only the π^+, π^0, π^-, K^+, K^0, $\bar{K}^0$ and the K^-, implying the existence of another one yet to be found, now known as the η, observed not long afterwards [11]. The $SU(3)$ symmetry is not exact, and its slight violation not only contributes to the mass difference between the proton and the neutron, but also to break the mass degeneracy in the multiplets. The model had great success and all the hadrons known could be arranged. The three octets of $J = \frac{1}{2}$ baryons, pseudoscalars mesons and vector mesons are shown in **Figure 1.1** and **Figure 1.2**. The baryonic resonances could also be organized in the decuplet with $J = 3/2$, shown in **Figure 1.3**. The three figures are taken from Ref. [12]. Some sort of periodic table of the hadrons had been invented, and physicist had complete faith in considering $SU(3)$ as the correct symmetry to represent physical reality.

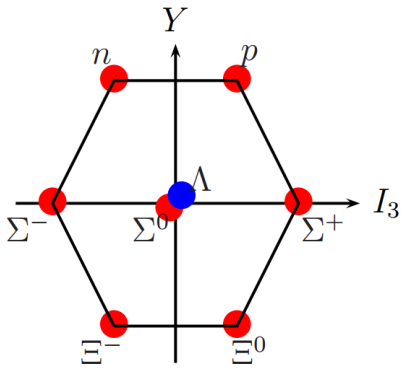

Figure 1.1: Octet of the baryons with $J = \frac{1}{2}$ [12].

The idea of the existence of three basic constituents, called *quarks*, building all the hadrons and able to explain the classification in multiplets of $SU(3)$, was proposed independently by Gell-Mann [13] and Zweig [14] in 1964. They are now known as "up", "down" and "strange" quark. In this scheme, baryons result as made up of three quarks (qqq) while mesons as quark-antiquark systems ($q\bar{q}$). However, at the time, hadrons where still considered as "soft" objects, with a diffuse internal structure. Although the simplicity and effectiveness of the scheme, the scientific community was sceptical about the possibility of

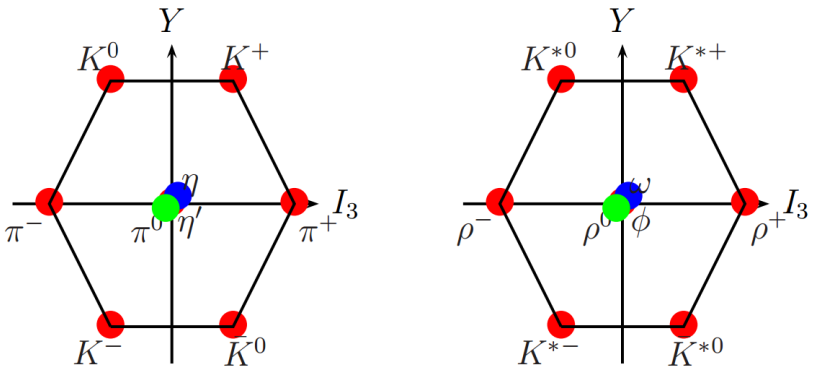

Figure 1.2: Octet and singlet of pseudoscalars (left panel) and vectors (right panel) mesons [12].

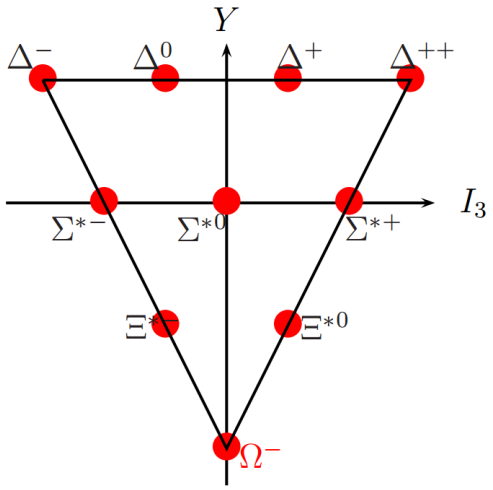

Figure 1.3: Decuplet of the baryons with $J = \frac{3}{2}$ [12].

an internal structure for the nucleons and kept considering quarks only as a convenient mathematical construction.

Their existence was intensely debated, also due to the impossibility to isolate them as free particles regardless the energy supplied to the nucleon. Thanks to a series of experiments of deep inelastic scattering (DIS) on an hydrogen target, carried out at the Stanford linear accelerator (SLAC) at the end of the 60s, it was possible to reveal the internal structure of the nucleon. The structure functions in the cross section for the scattering on nucleons present a phenomenon called scaling, first anticipated theoretically by Bjorken in 1967, proving the pointlike nature of these constituents. By 1973, different kinds of high energy scattering experiments (electron-nucleon, neutrino-nucleon, electron-positron, proton-proton), had already provided enough evidence for the nucleon constituents and for the expected quantum numbers, though they had never been observed yet as isolated entities.

Motivated by the big success obtained by gauge theories in unifying electromagnetic and weak interactions, theorists decided to apply the same framework to the strong force and demonstrated that in certain gauge theories the quark-quark interaction can become really weak at short distances, explaining the behaviour of the DIS cross sections. This phenomenon, called *asymptotic freedom* [15, 16], is one of the very peculiar features of the new theory that emerged, called Quantum Chromodynamics (QCD). In this scheme, the interactions among quarks are described by means of the exchange of massless vector particles, called gluons, the gauge bosons of the theory. The underlying symmetry group is $SU(3)$, such that each quark appears in three different versions, "red", "blue" and "green". This new quantum number, "color", is the equivalent of the electric charge in the case of strong interactions. The concept of color is supported by direct tests, like the prediction of the ratio of the total hadronic cross section to the muon pair production cross section in e^+e^- annihilation and the decay width of the pion to $\gamma\gamma$.

Now we know that quarks exist in three flavours more than initially expected, "charm", "bottom" and "top", and their existence has been confirmed experimentally by detailed analysis of jets of hadrons emerged from high energy e-p collisions. While the $SU(3)$ flavor symmetry is only approximately realized, $SU(3)$ color is an exact symmetry. More specifically, QCD is an unbroken non-Abelian gauge theory, and this characteristic has two significant consequences. We already mentioned the first one, which is asymptotic freedom, making the strength of the interaction weaker and weaker as we go to shorter distances, that is inside the hadron itself. The other one is complementary and makes the interaction stronger at larger distances, implying that it is impossible to separate the quarks composing the hadrons and to observe them as free particles. Only objects not carrying color charge can be seen as

free, which are the hadrons. This phenomenon is called *confinement*.

These two features have strong practical implications when trying to exploit the theory to solve strong interaction problems. Indeed, in the high energy regime, where perturbation theory can be applied due to asymptotic freedom, the theory proved successful in describing a variety of phenomena with large momentum transfer. On the other hand, at low energies, due to confinement, perturbative methods fail making the analysis of QCD phenomena in terms of quark as fundamental degrees of freedom very difficult.

Furthermore, while in principle QCD was supposed to provide all the answers about the nature of hadrons, it soon became clear that the classification of mesons and baryons in terms of $q\bar{q}$ and qqq systems was insufficient to describe the hadronic spectrum, that was becoming richer and richer as new resonances were discovered at different facilities and added to the Particle Data Group [17]. In fact, some new particles seemed to have properties that cannot fit into the constituent quark description. One of the most popular example is the case of the $\Lambda(1405)$, whose mass is anomalously light compared with the ones of other negative parity baryons, while the lightest scalar mesons ($f_0(500) = \sigma$, $K_0^* = \kappa$, $f_0(980)$, and $a_0(980)$) exhibit inverted spectrum from what is expected with a $q\bar{q}$ description. In the last forty years, the amount of experimental proofs of the inadequacy of the constituent quark model kept growing. Among others, for example, the discovery of XYZ hadrons, charmoniumlike or bottomoniumlike states that are seen decaying to final states containing a heavy quark and a heavy anti-quark, either a c or a b, but that cannot be accommodated in an unassigned $Q\bar{Q}$ level. **Figure 1.4** and **Figure 1.5**, taken from Ref. [18], show the state of charmonium and charmoniumlike below 4500 MeV, and bottomonium and bottomoniumlike respectively.

Due to the lack of understanding of the long-distance regime of QCD and the rapidly increasing number of resonances in the hadronic spectrum, many alternative models based on color symmetry have been formulated. For example, just like it is possible to combine the triplet of $q = u, d, s$ light quarks with the anti-triplet to form multiplets of mesons, one can combine two triplets of quarks and build multiplets of "diquarks". Even though diquarks are not color singlets and cannot exist as free particles, they can combine with other colored objects to form structures much more complex than $q\bar{q}$ and qqq and which are color neutral. These multiquark states are called "exotic" and include pentaquark baryons, six-quark H-dibaryons, tetraquark mesons, glueballs (mesons made only of gluons) and hybrids (a q, $\bar{q}$ and gluon combination) [19, 20]. Another possibility consists in hadronic molecules, deuteron-like bound states of two (or more) constituent common hadrons kept together by strong interaction. The $\bar{K}N$ quasi-bound picture of the $\Lambda(1405)$ is one of the examples

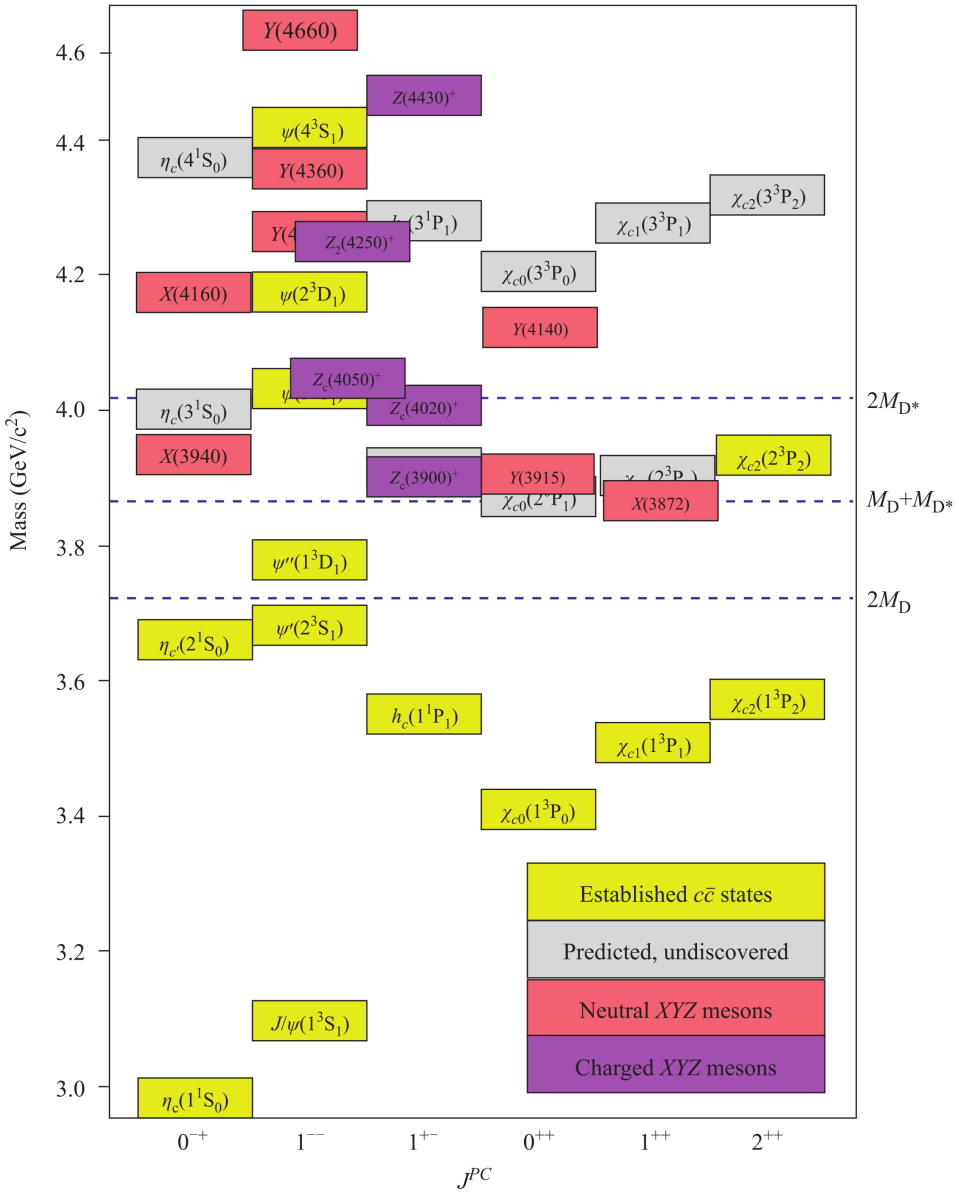

Figure 1.4: Spectrum of charmonium and charmoniumlike states [18].

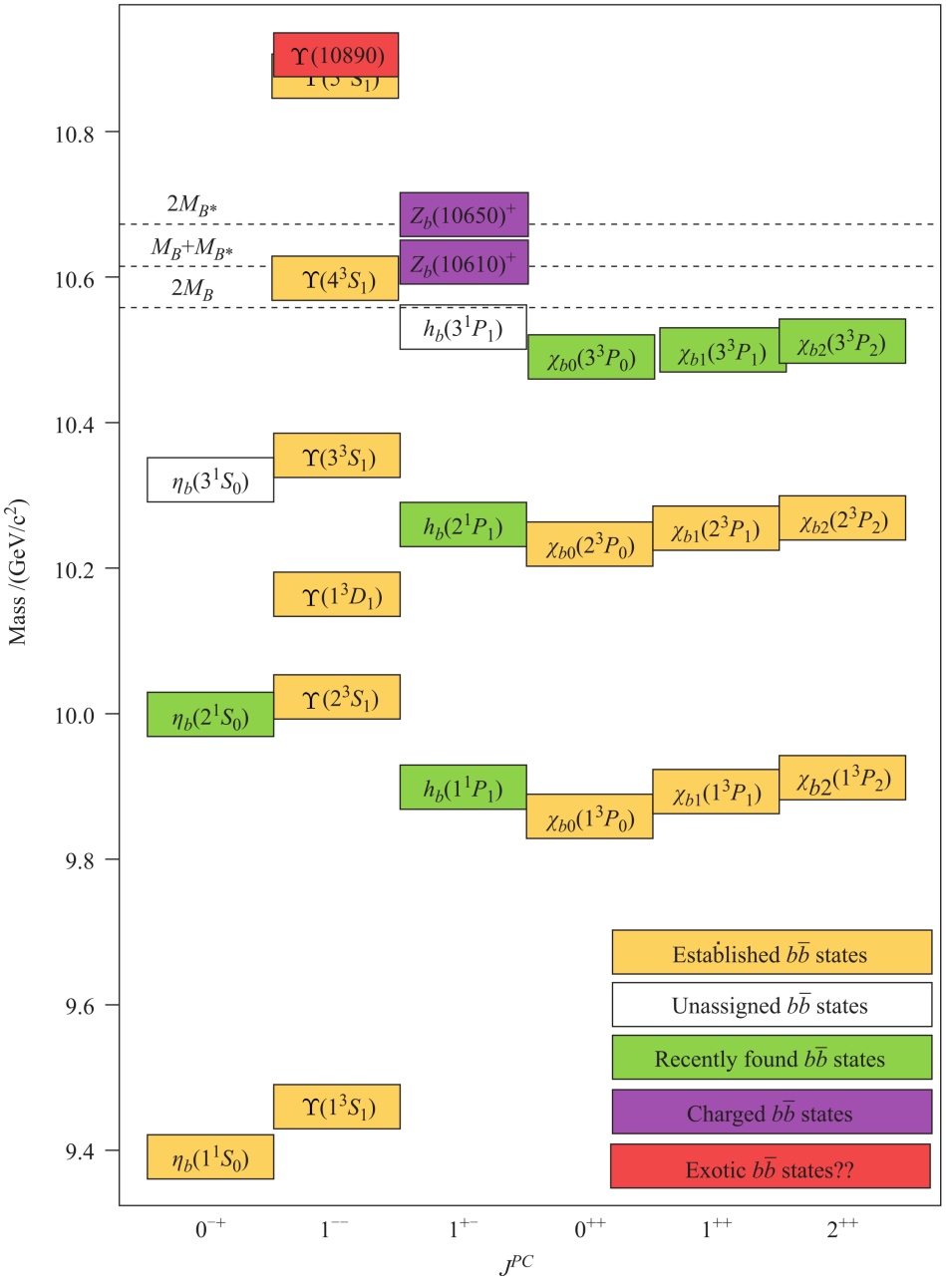

Figure 1.5: Spectrum of bottomonium and bottomoniumlike states [18].

[21–23]. All of them are illustrated in **Figure 1.6** (see Ref. [18] for a more thorough review).

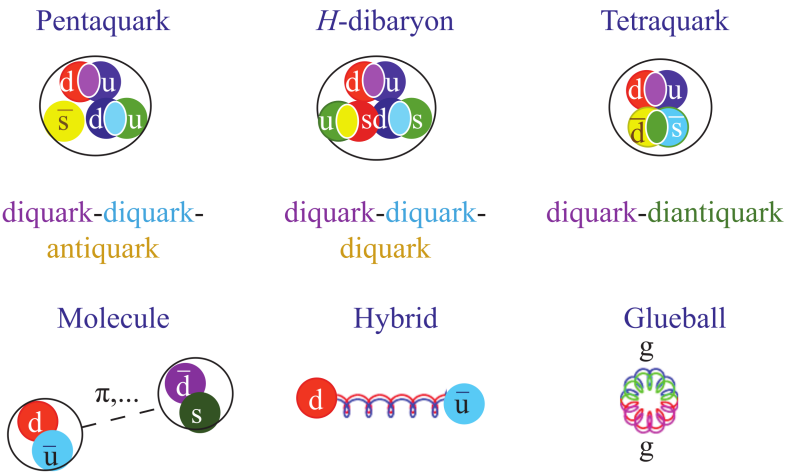

Figure 1.6: Representation of exotic multiquark states [18].

In recent years, chiral perturbation theory (χPT) [24, 25] has been remarkably successful in describing hadron structures. This effective approach to QCD at low energy makes use of Chiral Lagrangians, in which the ground states of mesons and baryons appear as fundamental degrees of freedom [25–28]. With these Lagrangians one can make predictions for meson-meson interaction and meson-baryon interaction at lowest order and obtain very good results in a systematic and technically simple way. Unfortunately, due to its limited range of convergence, this methods proved to be insufficient to describe the hadron spectrum in the region of resonances.

The method was improved combining unitarity constraints in coupled channels of mesons and baryons with the use of chiral Lagrangians in order to widen the range of applicability. The first attempt to combine unitarity and χPT was done in Ref. [21], where πN and $\bar{K}N$ scattering were studied in the region of the $N^*(1525)$ and $\Lambda(1405)$. The theory resulting from this extension is usually referred to as *chiral unitary approach* [21, 22, 29–39] and it allows to explain many mesons and baryons in terms of the meson-meson and meson-baryon interactions provided by chiral Lagrangians, interpreting them as composite states of hadrons. This kind of resonances are commonly known as "dynamically generated". In Ref. [30], the author could reproduce meson-meson scattering in s-wave up to 1.2 GeV, while in Ref. [22] the study of the meson-baryon interaction with $S = -1$ led to a good reproduction of the $\bar{K}N$ scattering properties and to generate dynamically the $\Lambda(1405)$. In Refs. [40, 41], the authors could dynamically generate all the resonances up to 1.2

GeV, $\sigma(500)$, $f_0(980)$, $a_0(980)$, $\kappa(900)$, ρ and K^* (although the last two are consequence of the use of higher order Lagrangians and do not correspond to molecular states). Many more states followed extrapolating the method at higher energies, like the $\Lambda(1670)$ [42], the $\Xi(1620)$ [43], the $N^*(1535)$ [29, 44], the two $\Lambda(1405)$ [33–35, 38, 45, 46] and the $\Lambda(1520)$ [47, 48]. Moreover, also the interaction of pseudoscalar mesons with vector mesons can be approached by means of chiral largrangians [49] in a unitary scheme. This led to the dynamical generation of the low lying axial vectors mesons $h_1(1170)$, $h_1(1380)$, $f_1(1285)$, $b_1(1235)$, $a_1(1260)$, $K_1(1270)$ [50–54].

The extrapolation of these ideas to the charm sector led to the prediction of many new states [55–58]. In Ref. [59], for example, the scalar resonances $D_{s0}^*(2317)$ and $D_0^*(2400)$ are interpreted as a DK bound state and a $D\pi$ resonance respectively, while in Ref. [56] a richer scenario is found for axial resonances, some of them identified with observed states like the controversial $X(3872)$, the $D_{s1}(2460)$ and the $D_1(2430)$.

A deeper understanding of the properties of the resonances that, in the last years, seemed to fit into the the dynamically generated scheme and have been classified as good candidates to be composite hadron-hadron states, is the motivation of my research work and the purpose of this Thesis. Exploiting the techniques of chiral unitary approach, better analyzed in **Chapter 2**, together with other useful theoretical tools, we could address a large variety of problems.

In **Chapter 3** we try to develop a general method to quantify the weight of the composite character of a given resonance or bound state with respect to other components (genuine or "exotic") that can coexist in the wave function. The procedure, that takes advantage of a very convenient sum rule, will be applied to concrete cases of meson resonances commonly considered as genuine and, for the first time, to baryons. We will see how, unlike the case of bound states, the nature of resonances itself makes really hard to give an interpretation of the different terms of the sum rule. We try to give our own in **Chapter 4**.

The multiplet of light scalar mesons, among them the $f_0(980)$ and the $a_0(980)$, is still a very poorly understood sector of the hadronic spectrum. The intense debate of the last years did not lead to any inference about their structure and many different models have been suggested, like tetraquarks and glueballs. In **Chapter 5**, we investigate different decays which involve the $a_0(980)$ and $f_0(980)$ as intermediate states. The assumption of a molecular pseudoscalar-pseudoscalar nature for these resonances allows us to use a specific decay mechanism leading to results that seem to corroborate it.

Two chapters of this Thesis are devoted to the study of some of the XYZ states we mentioned above. In 2013, BESIII observed a peak in the reaction

$e^+e^- \to \pi^+\pi^- J/\psi$ in the $\pi J/\psi$ invariant mass with energy around 3900 MeV. Right after, Belle and CLEO also measured enhancements with slightly different energies and widths, bringing up the question: are they the same state? In **Chapter 6** we try to find an answer and to describe the $Z_c(3900)$ in terms of a molecular $D\bar{D}^*$ state of $I = 1$. In the invariant $(D^*\bar{D}^*)^\mp$ distribution for the reaction $e^+e^- \to \pi^\pm(D^*\bar{D}^*)^\mp$, BESIII reports of a peak around 4025 MeV that we try to interpret as a $D^*\bar{D}^*$ molecule. We also consider the possibility of a molecular nature for the $Z_b(10610)$ and $Z_b(10650)$ keeping into account many different possible sources of interaction between the two hadrons in $I = 1$. On the other hand, **Chapter 7** is devoted to the $X(3872)$. We study three possible decays of this resonance in the dynamically generated picture of Ref. [56] in order to give support to this assumption. In the last chapter we will make a summary of the results obtained and draw some conclusions.

CHAPTER 2

THEORETICAL TOOLS

2.1 Introduction

The aim of this Chapter is to introduce the tools we will need throughout this Thesis work as they chronologically appeared since the first attempts at describing strong interactions and the hadronic spectrum.

We will start, in **Section** 2.2, briefly discussing Quantum Chromodynamics (QCD), the gauge field theory of strong interaction, which describes the color interaction of quarks and gluons. This theory is one of the fundamental blocks of the Standard Model (SM) of Particle Physics being the $SU(3)$ component of the $SU(3) \times SU(2) \times U(1)$ gauge theory of the SM, where the $SU(2) \times U(1)$ gauge group describes the electroweak interactions.

This theory is very well understood and it has been shown to be reliable by experimental tests at high energies, where, thanks to its asymptotically-free character, perturbation theory can be safely applied. Unfortunately, this perturbation theory is not suitable to describe low energy interactions. In fact, in this domain, the growing of the running coupling constant and the consequent confinement of quarks and gluons into hadrons make the application of perturbative methods fail.

This is when effective field theories come into play, taking into account only the degrees of freedom which are relevant at low energy. The effective field theory of QCD, called Chiral Perturbation Theory (χPT) [24, 25], is built on one of its fundamental symmetries, chiral symmetry, and provides the interactions between the ground states of mesons and baryons. Following essentially Ref. [60], and with some further help from Refs. [61] and [62], we address the most important characteristic of χPT in **Section** 2.3.

Due to its limitations in terms of predictive power and range of convergence, χPT had to be improved by implementing unitarity constraints in the

formalism. A new technique, called Chiral Unitary Approach [21, 22, 29–39], followed, and **Section** 2.4 is dedicated to this.

The last section is devoted to the Hidden Gauge Symmetry formalism, one of the possible methods to implement spin 1 particles in the theory. The interaction of pseudoscalar mesons with vector mesons can be, in principle, dealt with using chiral Lagrangians [49]. These chiral Lagrangians are also obtained through the local hidden gauge approach [63–66], exchanging vector mesons between the vectors and the pseudoscalars in the limit of small momentum transfers. Interesting developments using these Lagrangians within a unitary scheme in coupled channels led, for example, to the generation of the low lying axial vectors from the interaction of these mesons [50–54].

2.2 The QCD Lagrangian

The gauge theory describing the strong interactions among quarks and gluons is called Quantum Chromodynamics. Its underlying gauge group is color $SU(3)$ ($SU(3)_C$), introduced for the first time into the quark model in order to account for the Pauli exclusion principle in the wave functions of baryons. The matter fields of this theory are called quarks, spin $1/2$ fermions existing in three different flavours in addition to the three possible colors. We will denote these fields as q_f, consisting, for every flavour f, in a color triplet

$$q_f = \begin{pmatrix} q_{f,r} \\ q_{f,g} \\ q_{f,b} \end{pmatrix} , \tag{2.1}$$

with r="red", g="green" and b="blue".

The free Lagrangian for these fields, can be written as

$$\mathcal{L}_0 = \sum_f \bar{q}_f (i\gamma^\mu \partial_\mu - m_f) q_f \, , \tag{2.2}$$

where γ^μ are the Dirac matrices, and it is invariant under arbitrary global $SU(3)_C$ transformation in color space,

$$q_f^\alpha \to (q_f^\alpha)' = U_\beta^\alpha q_f^\beta \, , \tag{2.3}$$

with $UU^\dagger = U^\dagger U = 1$ and $\det U = 1$. The matrix U can be written as

$$U = \exp\left(-ig\frac{\lambda^a}{2}\theta_a\right) , \tag{2.4}$$

where θ_a are arbitrary parameters. The λ^a $(a = 1, ..., 8)$ matrices are the generators of the fundamental representation of the $SU(3)_C$ algebra, which are traceless and satisfy the commutation relations

$$[\lambda^a, \lambda^b] = 2if_{abc}\lambda^c\,, \tag{2.5}$$

with f_{abc} the $SU(3)_C$ structure constants.

According to the gauge principle, the gauge invariance must hold locally, so we require the Lagrangian to be invariant under local transformation of $SU(3)_C$, $\theta_a = \theta_a(x)$, leading to the introduction of a covariant derivative,

$$D_\mu q_f = \left(\partial_\mu - ig_s\frac{\lambda^a}{2}\mathcal{A}^a_\mu\right) q_f\,, \tag{2.6}$$

which contains the eight different gauge fields needed, A^a_μ, the so called gluons. The quantity g_s is the strong coupling constant.

The covariant derivative must transform exactly as the quark fields, that is

$$D^\mu \to (D^\mu)' = UD^\mu U^\dagger\,, \tag{2.7}$$

and it fixes the transformation of the gauge fields

$$\mathcal{A}^\mu \to (\mathcal{A}^\mu)' = U\mathcal{A}^\mu U^\dagger - \frac{i}{g_s}(\partial^\mu U)U^\dagger\,. \tag{2.8}$$

In the last equation we defined $(\mathcal{A}_\mu)_{\alpha\beta} \equiv \left(\frac{\lambda^a}{2}\right)_{\alpha\beta}\mathcal{A}^a_\mu$. The covariant derivative acts on color and Dirac indices but it is independent of flavour. The behaviour of the fields under infinitesimal transformations of $SU(3)_C$ reads

$$q^\alpha_f \;\to\; (q^\alpha_f)' = q^\alpha_f - ig_s\left(\frac{\lambda^a}{2}\right)_{\alpha\beta}\delta\theta_a q^\beta_f\,, \tag{2.9}$$

$$\mathcal{A}^a_\mu \;\to\; (\mathcal{A}^a_\mu)' = \mathcal{A}^a_\mu - \partial_\mu(\delta\theta^a) + g_s f_{abc}\delta\theta^b\mathcal{A}^c_\mu\,. \tag{2.10}$$

In order to build a gauge-invariant kinetic term for the gluon fields, we must introduce the field strength tensor,

$$\begin{aligned}\mathcal{G}_{\mu\nu} &\equiv \frac{\lambda^a}{2}\mathcal{G}^a_{\mu\nu}\\ \mathcal{G}^a_{\mu\nu} &= \partial_\mu\mathcal{A}^a_\nu - \partial_\mu\mathcal{A}^a_\mu + g_s f_{abc}\mathcal{A}^b_\mu\mathcal{A}^c_\nu\,,\end{aligned} \tag{2.11}$$

whose transformation under $SU(3)_C$ is given by

$$\mathcal{G}_{\mu\nu} \to (\mathcal{G}_{\mu\nu})' = U\mathcal{G}_{\mu\nu}U^\dagger\,. \tag{2.12}$$

At this point we have all the ingredients to write the $SU(3)_C$ invariant QCD Lagrangian, that reads

$$\mathcal{L}_{QCD} = \sum_f \bar{q}_f (i \not{D} - m_f) q_f - \frac{1}{4} G^a_{\mu\nu} G^{a\mu\nu} \,, \tag{2.13}$$

The second term in Eq. (2.13) gives rise to gauge fields self-interactions involving vertices with three and four gauge fields, characteristic of non-Abelian theories.

2.2.1 Running Coupling and Confinement

We define a Quantum Field Theory renormalizable when it is possible to reabsorb all the ultraviolet divergences through a redefinition of the original fields and couplings. This redefinition is meaningful only if self-consistent, in the sense that all the ultraviolet divergent contributions to all the possible scattering processes must be eliminated through the same redefinition of the coupling. Gauge theories such as QED or QCD have an underlying gauge symmetry that guarantees the renormalizability of the theory.

The redefinition introduces a dependence on an arbitrary energy scale μ, depending on the chosen renormalization scheme, such that for the renormalized coupling we have $\alpha_R = g_s^2/4\pi = \alpha_s(\mu^2)$, that we call running coupling constant. For a given process, the scale μ can be identified with the momentum transfer $Q^2 = -q^2$, such that $\alpha_s(\mu^2) = \alpha_s(Q^2)$.

The scale dependence is regulated by the so called β-function by means of the following equations:

$$\mu \frac{d\alpha_s}{d\mu} \equiv \alpha_s \beta(\alpha_s) \,, \qquad\qquad \beta(\alpha_s) = \beta_1 \alpha_s + \beta_2 \alpha_s^2 + \dots \,. \tag{2.14}$$

At the one loop level the β-function reduces to the first coefficient β_1 and, from the calculation of the relevant diagrams one gets [15, 16]

$$\beta_1 = \frac{N_f - 11\, N_c}{6} \,. \tag{2.15}$$

The positive contribution proportional to N_f is generated by the $q\bar{q}$-loops and, up to a constant, it is the same that one finds in the case of QED. The negative contribution proportional to N_c is the novelty of QCD and it is introduced by the self-interactions among gluons, due to the non-Abelian character of the theory. This contribution is responsible for the completely different behaviour of QCD with respect to QED. In fact, for $N_f \leq 16$, $\beta_1 < 0$ such that, for the corresponding QCD running coupling

$$\alpha_s(Q^2) = \frac{\alpha_s(Q_0^2)}{1 - \beta_1 \frac{\alpha_s(Q_0^2)}{2\pi} \ln(Q^2/Q_0^2)} \,, \tag{2.16}$$

one finds

$$\lim_{Q^2\to\infty} \alpha_s(Q^2) = 0\,. \tag{2.17}$$

This last equation is the formalization of *asymptotic freedom*, one of the features of QCD, discovered independently by Gross and Wilczek [15] and by Politzer [16]. This phenomenon implies that at very small distances the quarks behave as free particles. The important consequence is that, at least at high energies, the use of perturbative methods to evaluate diagrams is allowed and successful.

Apart from the introduction of a dependence on the energy, we need a reference scale to decide whether a given Q^2 can be considered large or not. Solving the differential equation (2.14) at one loop, one gets

$$\ln\mu + \frac{\pi}{\beta_1\alpha_s(\mu^2)} = \ln\Lambda\,, \tag{2.18}$$

where $\ln\Lambda$ is an integration constant. It follows

$$\alpha_s(\mu^2) = \frac{2\pi}{-\beta_1\ln(\mu^2/\Lambda^2)}\,. \tag{2.19}$$

When $\mu >> \Lambda$, $\alpha_s(\mu^2) \to 0$, and asymptotic freedom is recovered. On the other hand, at lower energies the running coupling gets bigger and we have that for $\mu \to \Lambda$, $\alpha_s(\mu^2) \to \infty$, such that perturbation theory is no longer applicable and Λ provides the scale when the coupling of QCD blows up. Although this is not a proof, since perturbation theory is no longer valid at $\mu \to \Lambda$, this last argument tells us that the phenomenon of *confinement* is plausible in QCD.

Gluons are massless particles, like photons. Yet, the range of strong interactions is extremely small. Almost certainly, this apparent contradiction is tied to the behaviour of the coupling constants α_s. Let us consider the colour force between a quark and an antiquark bound in a meson. If α_s really increases with increasing distance, whatever finite amount of energy we supply to the system, the quark and the antiquark will not become free particles. Increasing the separation, the colour force will become even stronger, and this is caused by the gluon self-coupling. Through the coupling of gluons to one another the colour fields line of force between the quark and the antiquark are obliged to form a tube as if there where attractive forces between the field lines. As the $q\bar{q}$ distance r increases, the potential energy of the system increases in proportion to r and the quarks and the gluons cannot be freed. This gives rise to the total confinement of quarks and gluons inside hadrons, which are color neutral, or singlets and that are the only observable states [67].

This is why, in order to do quantitative calculation in this energy regime we need other methods like, for example, Effective Field Theories [24], where

	Flavor	Mass
Light Sector	u	$(1.8 - 3.0)$ MeV
	d	$(4.5 - 5.3)$ MeV
	s	(95 ± 5) MeV
Heavy Sector	c	(1.275 ± 0.025) GeV
	b	$(4.1 - 4.7)$ GeV
	t	$\simeq 174$ GeV

Table 2.1: Masses of the six different quarks [17].

one uses the the most general Lagrangian involving the relevant degrees of freedom at the energy scale of interest that is consistent with the underlying symmetries. This will be the subject of the next section.

2.3 Hints of Chiral Perturbation Theory

Chiral Perturbation Theory (χPT) is the effective theory of QCD in the low energy regime and it is based on the chiral symmetry properties of QCD. Effective field theories are the appropriate theoretical tool to study low-energy physics since the basic idea is to take explicitly into account only the relevant degrees of freedom, i.e. the lighter particles with mass $m \ll \Lambda$, where Λ is the energy scale of the problem. Thus, the dynamics are described by effective Lagrangians containing only the interactions among the light states, organized as an expansion in powers of E/Λ. The information about the heavier degrees of freedom is contained in the couplings of the low-energy Lagrangian, which also incorporate all the symmetries of the underlying fundamental theory.

We know that quarks exist in six different flavors that can be divided into the three light ones (u, d, s) and the three heavy flavors (c, b, t), whose masses are listed in Table 2.1. Due to the pronounced separation between the light and the scalar sector, it seems reasonable to start the discussion from a Lagrangian, that we will call $\mathcal{L}^0_{QCD}$, containing only the fields of the light quarks in the limit $m_u, m_d, m_s \to 0$, which is known as chiral limit.

2.3.1 Chiral Symmetry

The QCD Lagrangian, in the limit of massless u, d and s quarks, can be written as

$$\mathcal{L}^0_{QCD} = -\frac{1}{4} G^a_{\mu\nu} G^{a\,\mu\nu} + i\bar{q}_L \gamma_\mu D^\mu q_L + i\bar{q}_R \gamma_\mu D^\mu q_R \,, \tag{2.20}$$

where $q_{R,L} = \frac{1}{2}(1 \pm \gamma_5)q$. This lagrangian exhibits a global symmetry

$$SU(3)_L \times SU(3)_R \times U(1)_V \times U(1)_A \,. \tag{2.21}$$

The question arises whether or not the hadron spectrum is, at least approximately, in accordance with these symmetries.

At the hadronic level, $U(1)_V$ is realized as the baryon number conservation and trivially realized in the meson sector, while the axial $U(1)_A$ is not a symmetry at the quantum level (Abelian anomaly [68–70]). Under the chiral group $G \equiv SU(3)_L \times SU(3)_R$, the left- and right-handed fields transform as

$$q_L \xrightarrow{G} g_L q_L \,, \qquad q_R \xrightarrow{G} g_R q_R \qquad g_{L,R} \in SU(3)_{L,R} \,. \tag{2.22}$$

The Noether currents of the chiral group G are

$$J^{a\,\mu}_{R,L} = \bar{q}_{R,L}\gamma^\mu \frac{\lambda^a}{2} q_{R,L} \,, \qquad (a = 1, ..., 8) \,, \tag{2.23}$$

with the corresponding charges given by

$$Q_{R,L} = \int d^3x J^{a\,0}_{R,L}(x) \tag{2.24}$$

and satisfying the commutation relations $[Q^a_A, Q^b_B] = i\delta_{AB} f_{abc} Q^c_A$, where $A = R, L$ and $B = R, L$.

However, chiral symmetry is not even approximately realized in the hadronic spectrum. Yet, from the 16 generators of the chiral group G in Eq. (2.24), it is possible to construct the linear combinations

$$Q^a_V = Q^a_R + Q^a_L \,, \qquad Q^a_A = Q^a_R - Q^a_L \,, \qquad (a = 1, ..., 8) \,, \tag{2.25}$$

which represent the vectorial and axial charges respectively. The generators Q^a_V form a Lie algebra corresponding to the subgroup $H = SU(3)_V$ of the chiral group G.

In Ref. [71] it was shown that, in the chiral limit, the ground state is necessarily invariant under the group H, which means that the generators annihilate the ground state, i.e.

$$Q^a_V |0\rangle = 0 \,. \tag{2.26}$$

In a very famous paper of 1966, Coleman showed that the symmetry of the energy spectrum is determined by the symmetry of the ground state [72], and we then expect the symmetry pattern of the hadron spectrum to follow $SU(3)_V$ symmetry. This is actually the situation at the experimental level, since hadrons are organized in multiplets of $SU(3)_V$. On the other hand, no

degeneration between the $J^P = 0^+$ and $J^P = 0^-$ is observed, indicating that the axial generators Q_A^a do not annihilate the ground state. This means that the ground state is not invariant under the full symmetry group, which is spontaneously broken to $SU(3)_V$.

According to the Goldstone theorem [73, 74], to each generator that commutes with the Hamiltonian and does not annihilate the ground state corresponds a massless Goldstone boson, whose properties are strictly related to the ones of the generator. The generators Q_A^a have negative parity, baryon number zero and transform as an octet under the subgroup $SU(3)_V$. Hence, one expects the Goldstone bosons to have the same properties. Although not exactly massless, the octet of the light pseudoscalar mesons (π, K, η) is identified with the Goldstone bosons, and the finite masses of the physical states are interpreted as a consequence of the explicit symmetry breaking due to the finite masses of the u, d and s quarks [75].

Due to the mass gap separating the pseudoscalars from the rest of the hadronic spectrum, the most natural thing to do is to construct an Effective Field Theory containing only these degrees of freedom, whose interactions are strongly constrained by their Goldstone nature. In the following subsection we will derive the most general theory describing the dynamics of the Goldstone bosons associated with the spontaneous breaking of chiral symmetry.

2.3.2 The lowest-order effective Lagrangian

We want our Lagrangian to contain exactly eight pseudoscalar degrees of freedom transforming as an octet under the subgroup $H = SU(3)_V$. These eight variables can be collected in the 3×3 unitary matrix transforming, under the chiral group G, as

$$U(\phi) \xrightarrow{G} g_R\, U(\phi)\, g_L^{-1}\,, \qquad\qquad (g_L, g_R) \in G\,. \tag{2.27}$$

There exist different parametrizations for $U(\phi)$ but the most convenient is the exponential one which, for $N_f = 3$, reads

$$U(\phi) = u(\phi)^2 = \exp\left(i\frac{\sqrt{2}\phi}{f}\right)\,, \tag{2.28}$$

with

$$\phi(x) = \frac{\lambda^a}{\sqrt{2}}\phi^a = \begin{pmatrix} \frac{\eta_8}{\sqrt{6}} + \frac{\pi^0}{\sqrt{2}} & \pi^+ & K^+ \\ \pi^- & \frac{\eta_8}{\sqrt{6}} - \frac{\pi^0}{\sqrt{2}} & K^0 \\ K^- & \bar{K}^0 & -\frac{2\eta_8}{\sqrt{6}} \end{pmatrix}\,. \tag{2.29}$$

The constant f in Eq. (2.28) turns out to be the pion decay constant in the chiral limit, $f = 93$ MeV.

In order to get the low-energy effective Lagrangian, we must write the most general Lagrangian we can write containing the matrix $U(\phi)$ and respecting chiral symmetry. This Lagrangian can be organized in terms of increasing powers of momentum, which is equivalent to say increasing number of derivatives. Due to parity conservation, the number of derivatives must be even, such that

$$\mathcal{L}_{eff} = \sum_n \mathcal{L}_{2n}\,, \tag{2.30}$$

with n the order of the expansion. Since the U matrix is unitary, we need at least two derivatives to have a non-trivial interaction. Thus, at lowest-order, the effective chiral Lagrangian is given by one single term:

$$\mathcal{L}_2 = \frac{f^2}{4}\langle \partial_\mu U^\dagger \partial^\mu U\rangle\,, \tag{2.31}$$

where $\langle\ \rangle$ stands for the trace and the constant $f^2/4$ in Eq. (2.31) is fixed to properly normalize the kinetic terms.

Expanding the exponential in $U(\phi)$ in powers of ϕ we can explicitly write the kinetic term plus the interactions involving an always increasing number of pseudoscalar mesons:

$$\mathcal{L}_2 = \frac{1}{2}\langle \partial_\mu \phi\, \partial^\mu \phi\rangle + \frac{1}{12f^2}\langle (\phi \overleftrightarrow{\partial_\mu} \phi)(\phi \overleftrightarrow{\partial^\mu} \phi)\rangle + \mathcal{O}(\phi^6/f^4)\,. \tag{2.32}$$

It is important to stress that all the interactions among the Goldstone bosons are fixed by the single coupling f.

2.3.3 Coupling to external sources

It is necessary to distinguish between dynamical and external fields, needed to incorporate electromagnetic and leptonic interactions. The idea is to extend the chiral invariant QCD Lagrangian of Eq. (2.13) by coupling the quarks to external hermitian matrix fields, v_μ, a_μ, s and p such that ([25, 76])

$$\mathcal{L} = \mathcal{L}^0_{QCD} + \bar{q}\gamma^\mu(v_\mu + \gamma_5 a_\mu)q - \bar{q}(s - i\gamma_5 p)q\,. \tag{2.33}$$

The external photons and W boson fields are among the gauge fields v_μ and a_μ:

$$\begin{aligned} r_\mu &\equiv v_\mu + a_\mu = eQA^{ext}_\mu + \dots\,, \\ l_\mu &\equiv v_\mu - a_\mu = eQA^{ext}_\mu + \frac{e}{\sqrt{2}\sin\theta_W}(W^\dagger_\mu T_+ + \text{h.c.}) + \dots\,, \end{aligned} \tag{2.34}$$

with

$$Q = \frac{1}{3}\,\text{diag}(2,-1,-1) \tag{2.35}$$

the quark charge matrix and

$$T_+ = \begin{pmatrix} 0 & V_{ud} & V_{us} \\ 0 & 0 & 0 \\ 0 & 0 & 0 \end{pmatrix} , \tag{2.36}$$

where V_{ij} are the Kobayashi-Maskawa mixing matrix elements.

The Lagrangian in Eq. (2.33) is invariant under the following local $SU(3)_L \times SU(3)_R$ transformations

$$\begin{aligned} & q_L \to g_L \, q_L \, , \\ & q_R \to g_R \, q_R \, , \\ & s + ip \to g_R \, (s + ip) \, g_L^\dagger \, , \\ & l_\mu \to g_L \, l_\mu \, g_L^\dagger + i g_L \, \partial_\mu \, g_L^\dagger \, , \\ & r_\mu \to g_R \, r_\mu \, g_R^\dagger + i g_R \, \partial_\mu \, g_R^\dagger \, . \end{aligned} \tag{2.37}$$

It is then possible to build the generalized effective Lagrangian for the Goldstone bosons in presence of external sources as

$$\mathcal{L}_2 = \frac{f^2}{4} \langle D_\mu U^\dagger D^\mu U + U^\dagger \chi + \chi^\dagger U \rangle \, , \tag{2.38}$$

where now the covariant derivative D_μ will contain the gauge fields v_μ and a_μ in order to respect local invariance,

$$\begin{aligned} & D_\mu U = \partial_\mu U - i r_\mu \, U + i U \, l_\mu \, , \\ & D_\mu U^\dagger = \partial_\mu U^\dagger + i U^\dagger \, r_\mu - i l_\mu \, U^\dagger \, . \end{aligned} \tag{2.39}$$

The matrix χ in Eq. (2.38) is defined as

$$\chi = 2 B_0 (s + ip) \, , \tag{2.40}$$

with B_0 a constant which, like f, is not fixed by the symmetry.

One can incorporate the explicit breaking of chiral symmetry by means of the quark masses fixing the scalar term

$$s = \mathcal{M} = \mathrm{diag}(m_u, m_d, m_s) \tag{2.41}$$

and $p = 0$. Hence, the χ term in Eq. (2.38) will give rise, apart from other interactions proportional to the quark masses, to a quadratic pseudoscalar mass term from where it is possible to derive, in the isospin limit ($m_u =$

$m_d = \hat{m}$), the following relations between the quark masses and the ones of the Goldstone bosons:

$$\begin{aligned} m_\pi^2 &= 2\hat{m}B_0\,, \\ m_K^2 &= (\hat{m}+m_s)B_0\,, \\ m_{\eta_8}^2 &= \frac{2}{3}(\hat{m}+2m_s)B_0\,, \end{aligned} \tag{2.42}$$

with $\hat{m} = (m_u + m_d)/2$. Using Eqs. (2.42) we can write the mass matrix χ as

$$\chi = \begin{pmatrix} m_\pi^2 & 0 & 0 \\ 0 & m_\pi^2 & 0 \\ 0 & 0 & 2m_K^2 - m_\pi^2 \end{pmatrix}\,. \tag{2.43}$$

If we limit the expansion to the Lagrangian of Eq. (2.38), we are taking into account only tree-level diagrams. This can be easily seen remembering that, for a general connected diagram with N_d vertices of $\mathcal{O}(p^d)$, $d = 2, 4, ...$ and L loops, the chiral dimension is given by the formula [24]

$$D = 2L + 2 + \sum_d N_d(d-2)\,. \tag{2.44}$$

From this last equation it is clear that when $D = 2$, that is at lowest order, one must have $L = 0$ and $d = 2$, which means that only tree-level contributions can come from $\mathcal{L}_2$. In order to include corrections we need to go to higher orders. For instance, at $\mathcal{O}(p^4)$ there are contributions at tree-level from $\mathcal{L}_4$ (for $L = 0$, $d = 4$ and $N_4 = 1$) and also one-loop diagrams coming from $\mathcal{L}_2$ (with $L = 1$, $d = 2$). In the next section we shortly introduce the structure of the $\mathcal{L}_4$ Lagrangian.

2.3.4 Chiral Lagrangian at $\mathcal{O}(p^4)$

The most general Lagrangian invariant under the local chiral transformations of Eqs. (2.37), parity, charge conjugation and Lorentz transformations is given by [76]

$$\begin{aligned} \mathcal{L}_4 = {} & L_1\langle D_\mu U^\dagger D^\mu U\rangle^2 + L_2\langle D_\mu U^\dagger D_\nu U\rangle\langle D^\mu U^\dagger D^\nu U\rangle \\ & + L_3\langle D_\mu U^\dagger D^\mu U D_\nu U^\dagger D^\nu U\rangle + L_4\langle D_\mu U^\dagger D^\mu U\rangle\langle U^\dagger\chi + \chi^\dagger U\rangle \\ & + L_5\langle D_\mu U^\dagger D^\mu U(U^\dagger\chi + \chi^\dagger U)\rangle + L_6\langle U^\dagger\chi + \chi^\dagger U\rangle^2 \\ & + L_7\langle U^\dagger\chi - \chi^\dagger U\rangle^2 + L_8\langle\chi^\dagger U\chi^\dagger U + U^\dagger\chi U^\dagger\chi\rangle \\ & - iL_9\langle F_R^{\mu\nu} D_\mu U D_\nu U^\dagger + F_L^{\mu\nu} D_\mu U^\dagger D_\nu U\rangle + L_{10}\langle U^\dagger F_R^{\mu\nu} U F_{L\mu\nu}\rangle \\ & + H_1\langle F_R^{\mu\nu} F_{R\mu\nu} + F_L^{\mu\nu} F_{L\mu\nu}\rangle + H_2\langle\chi^\dagger\chi\rangle\,, \end{aligned} \tag{2.45}$$

where

$$\begin{aligned} F_L^{\mu\nu} &= \partial^\mu l^\nu - \partial^\nu l^\mu - i[l^\mu, l^\nu]\,, \\ F_R^{\mu\nu} &= \partial^\mu r^\nu - \partial^\nu r^\mu - i[r^\mu, r^\nu] \end{aligned} \tag{2.46}$$

are the strength tensors for the l_μ and r_μ fields. The terms proportional to H_1 and H_2 do not contain the pseudoscalar fields. This means that they are not directly measurable.

Thus, at $\mathcal{O}(p^4)$ we have ten additional couplings, L_i, called low energy constants (LEC). These constants are not fixed by chiral symmetry. Analogously to the couplings f and B_0, they contain information on the underlying QCD dynamics. In principle, it should be possible to calculate all the LEC as functions of the QCD scale Λ_{QCD} and of the quark masses, but, at present time, the information about these couplings comes mainly from low-energy phenomenology.

From a practical point of view, these coefficients are also required for renormalization purposes. Indeed, the Goldstone loops are divergent and need to be renormalized. If one uses a regularization method preserving the symmetries of the theory, such as dimensional regularization, the counter-terms needed to renormalize the theory are symmetric. Since we built an effective Lagrangian containing all the possible terms allowed by symmetry, the divergences can be reabsorbed in the renormalization of the coupling constants contained in the Lagrangian. The one-loop diagrams calculated using vertices of $\mathcal{L}_2$ generate infinities that are of $\mathcal{O}(p^4)$ and cannot be reabsorbed by a renormalization of the couplings f and B_0 and must be necessarily reabsorbed in the LEC contained in Eq. (2.45). The renormalized coupling L_i^r will depend on an arbitrary scale of dimensional regularization μ.

Though the number of constants is quite big at $\mathcal{O}(p^4)$, a given observable only takes contributions from a few of them. For example, in absence of external sources, Eq. (2.45) only contains the first three terms, implying that elastic $\pi\pi$ and πK scattering is only sensitive to the values of L_1, L_2 and L_3, while L_4 and L_5 generate mass corrections to the meson decay constants and so on. The present status of the phenomenological determination of the LEC is reported in Table 2.2. The values listed refer to a renormalization scale $\mu = M_\rho$.

χPT is an expansion in terms of momenta over some typical hadronic scale Λ_χ, which is called scale of Spontaneous Chiral Symmetry Breaking (SCSB) and considered $\Lambda_{\chi PT} \simeq 1$ GeV, that is the energy region where resonances start to appear. One can make an estimate of the expected size of the LEC L_i in terms of the SCSB scale comparing the Lagrangians $\mathcal{L}_2$ and $\mathcal{L}_4$,

$$L_i \sim \frac{f^2/4}{\Lambda_{\chi PT}^2} \sim 10^{-3}\,, \tag{2.47}$$

i	$L_i^r(M_\rho) \times 10^3$
1	0.4 ± 0.3
2	1.4 ± 0.3
3	-3.5 ± 1.1
4	-0.3 ± 0.5
5	1.4 ± 0.5
6	-0.2 ± 0.3
7	-0.4 ± 0.2
8	0.9 ± 0.3
9	6.9 ± 0.7
10	-5.5 ± 0.7

Table 2.2: Phenomenological values of the renormalized couplings $L_i^r(M_\rho)$.

in agreement with what reported in Table 2.2. This means that below the resonance region, $p < M_\rho$, we have a good convergence of the expansion.

Hence, we saw that ten additional coupling appear in the Lagrangian at $\mathcal{O}(p^4)$. The first attempt to construct the most general Lagragian in $SU(3)$ at $\mathcal{O}(p^6)$ was made in Ref. [77]. Although it was found in there that the original list of terms contained redundant structures, even the final number of 94 parameters is very large and it seems unlikely that all of them can be fixed through comparison with experimental data as in the case of $\mathcal{L}_4$. Such a rapid increase in the number of couplings needed to describe the theory at higher orders, implies a fast loss of predictive power.

2.4 Non-perturbative methods

We saw that, although χPT is a very powerful tool in the low energy region, its Lagrangian consists of an expansion in the powers of the external momenta of the Goldstone bosons over some typical scale Λ_χ, which is smaller than the masses of the heavier particles. In QCD, resonances typically appear for $\sqrt{s} \geq 0.8$ GeV, so that $\Lambda_{\chi PT} \leq 1$ GeV, and when this happens, there is no way to reproduce them from a perturbative expansion, since they are associated to poles in the scattering amplitude. If one includes higher orders corrections, χPT results valid up to energies around 500 MeV with $\Lambda_{\chi PT} \simeq 1$ GeV.

As mentioned at the end of the previous section, another drawback of this effective theory is the fact that its predictive power is rapidly lost when trying to increase the energy region of applicability going to higher orders. While at $\mathcal{O}(p^2)$ the χPT Lagrangian without baryons contains only the masses of pions, kaons and etas and f_π, at $\mathcal{O}(p^4)$ there are 12 free parameters, that

become more than 100 at $\mathcal{O}(p^6)$. For these two reasons, the development of non-perturbative methods capable of extending the validity of the theory without losing predictive power, became necessary.

Different independent non-perturbative approaches have been used rather successfully to reproduce important features of meson-meson interactions including resonances, and they are the inverse amplitude method (IAM), the Bethe-Salpeter (BS) equation method and the N/D method. Although formally different, these three methods share an important feature consisting in the imposition of unitarity.

The IAM was first suggested in Refs. [78, 79] and makes use of the lowest order chiral Lagrangian as well as the next to leading order ($\mathcal{O}(p^4)$). The method, although rather successfull in generating the ρ, K^* and σ resonances, had strong limitations due to the imposition of only elastic unitarity, that does not allow a coupled channel treatment necessary to obtain the poles of the $a_0(980)$ and the $f_0(980)$. The formalism based on the N/D method [80], on the other hand, was developed in Ref. [41] in order to provide the most general structure for an arbitrary partial wave amplitude when the unphysical cuts are neglected or, changing the perspective, treated perturbatively, so that the method can be considered as the zero order of a most general approach. The main conclusion of Ref. [41] is that it is possible to obtain an accurate description of the scalar sector compared to experiment. Moreover, contrary to what happens for the vector sector, for the scalar sector the unitarization of the $\mathcal{O}(p^2)$ χPT amplitude is sufficient to produce meson-meson states like the $\sigma(500)$, $a_0(980)$, $\kappa(900)$ and a strong contribution to the $f_0(980)$.

However, the method we will use throughout this thesis work is the LS Equation method, first developed in Ref. [30] to investigate the $J = 0$ sector alone. In the next section we will make a brief summary of the idea behind this approach.

2.4.1 The Bethe-Salpeter equation method

The starting point of the method is the standard chiral Lagrangian of χPT at lowest order, $\mathcal{L}_2$, since it contains the most general interactions among the mesons of the pseudoscalar octet. The amplitudes derived from this Lagrangian are the potentials that will be used in the coupled channels scattering equation. The basic assumption in the method is that the lowest order Hamiltonian provides the potential V_{ij} (where i is the initial and j the final channel) that must be iterated in the Lippmann-Schwinger (or Bether-Salpeter if we use relativistic propagators) in coupled channels. For example, in the case of

only two coupled channels, the coupled channels equations read

$$\begin{aligned} T_{11} &= V_{11} + V_{11}G_{11}T_{11} + V_{12}G_{22}T_{21}\,, \\ T_{21} &= V_{21} + V_{21}G_{11}T_{11} + V_{22}G_{22}T_{21}\,, \\ T_{22} &= V_{22} + V_{21}G_{11}T_{12} + V_{22}G_{22}T_{22}\,, \end{aligned} \tag{2.48}$$

with

$$G_{ii} = i\frac{1}{q^2 - m_{1i}^2 + i\epsilon}\frac{1}{(P-q)^2 - m_{2i}^2 + i\epsilon}\,, \tag{2.49}$$

where P is the total four-momentum of the meson-meson system. The term VGT in Eqs. (2.48) stands for

$$VGT = \int \frac{dq^4}{(2\pi)^4} V(k,p,q)G(P,q)T(q,k',p')\,. \tag{2.50}$$

At the diagrammatic level, Eq. (2.50) implies the series in Figure 2.1. In this approach, the loop in Eq. (2.50) is regularized using a cutoff q_{max}. This parameter, is the only degree of freedom in the model and it is fixed by experimental data.

In principle, V and T in Eq. (2.50) should be taken off-shell but it is shown in Ref. [30] that only the on-shell informations are needed. Following Ref. [30], we will summarize the argument in the case of one loop and one channel, for simplicity.

The on-shell amplitudes can be obtained simply taking $p_i^2 = m_i^2$, where p_i is the four-momentum of the particle. This means that we can separate the off-shell and the on-shell part of the tree-level potentials V as

$$V = V_{on} + \beta \sum_i (p_i^2 - m_i^2)\,, \tag{2.51}$$

leading to

$$V^2 = V_{on}^2 + 2\,\beta\, V_{on} \sum_i (p_i^2 - m_i^2) + \beta^2 \sum_{ij} (p_i^2 - m_i^2)(p_j^2 - m_j^2)\,. \tag{2.52}$$

Let us assume that in the second term of Eq. (2.52) we have $(P-q)^2 - m_2^2$. the term will cancel the second propagator of Eq. (2.49) and the remaining integration gives

$$2\,\beta\, V_{on}\, i \int \frac{d^4q}{(2\pi)^4}\frac{1}{q^2 - m_1^2} = \frac{2\,\beta\, V_{on}}{(2\pi)^3}\int \frac{d^3q}{2\omega_1} = \beta\frac{V_{on}}{2\pi^2}\int d\omega_1\; q\,. \tag{2.53}$$

For the second pole the procedure is identical. The last expression, for a large energy scale Λ compared to the masses, goes as $V_{on}\Lambda^2$ and has, in the

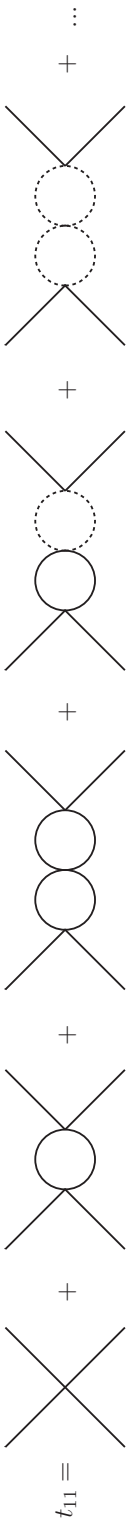

Figure 2.1: Diagrammatic representation of T_{11} in Eqs. (2.48).

dynamical variables, the same structure as the tree-level diagrams. The term proportional to β^2 in Eq. (2.53) gives rise, for the pole $q^0 = \omega_1(q)$, to a term

$$\frac{\beta^2}{(2\pi)^3}\int \frac{d^3q}{2\omega_1}[(P^0-\omega_1)^2-\omega_2^2] = \frac{\beta^2}{(2\pi)^3}\int \frac{d^3q}{2\omega_1}[P^{02}-2\omega_1 P^0+(m_1^2-m_2^2)]\,, \quad (2.54)$$

while in the case of the second pole, $q^0 = P^0 + \omega_2(q)$, we get

$$\frac{\beta^2}{(2\pi)^3}\int \frac{d^3q}{2\omega_2}[P^{02}+2\omega_2 P^0+(m_2^2-m_1^2)]\,. \quad (2.55)$$

The terms linear in P^0 in the last two equations cancel exactly, while the term proportional to $[P^{02}-2\omega_1 P^0+(m_1^2-m_2^2)]$ leads to a contribution of the type $[P^{02}+(m_1^2-m_2^2)]\Lambda^2$, and an analogous structure, $[P^{02}+(m_2^2-m_1^2)]\Lambda^2$, is generated by the quadratic term in Eq. (2.55). These terms, together with the $V_{on}\Lambda^2$ one, combine with the tree level contributions, generating an amplitude with the same structure of the tree-level one but with renormalized parameters, f and masses. Once physical values are taken for these parameters, these terms can be simply omitted. Thus, V and T can be taken on-shell and factorized outside the integral. The integration in dq^0 can be done analytically by choosing the contour in the lower half of the complex plane, such that the factorized on-shell coupled-channels equations read

$$T_{ij} = V_{ij} + V_{il}\, G_{ll}\, T_{lj}\,, \quad (2.56)$$

with

$$G_{ll} = \int_0^{q_{max}} \frac{dq}{(2\pi)^2}\,\frac{q^2\,(\omega_1+\omega_2)}{\omega_1\,\omega_2\,(s-(\omega_1+\omega_2)^2+i\epsilon)}\,. \quad (2.57)$$

In Eqs. (2.56) and (2.57), $s = P^{02}$ is the center of mass energy of the meson-meson system, $\omega_i = \sqrt{q^2+m_i^2}$ and the subindex $i = 1, 2$ stands for the two intermediate particles in the l channel. In matrix form, Eqs. (2.56) can be written as

$$T = V + VGT\,, \quad (2.58)$$

or equivalently as

$$T = [1 - VG]^{-1}\, V\,. \quad (2.59)$$

This is the matrix form of the *Bethe-Salpeter equation*, that we will use to evaluate scattering amplitudes in coupled channels throughout this Thesis work.

At this point, the coupled channels equations of Eqs. (2.48) reduce to a set of algebraic equations:

$$AT = V\,, \quad (2.60)$$

with

$$T = \begin{pmatrix} T_{11} \\ T_{21} \\ T_{22} \end{pmatrix} , \qquad V = \begin{pmatrix} V_{11} \\ V_{21} \\ V_{22} \end{pmatrix} , \tag{2.61}$$

$$A = \begin{pmatrix} 1 - V_{11}G_{11} & -V_{12}G_{22} & 0 \\ -V_{21}G_{11} & 1 - V_{22}G_{22} & 0 \\ 0 & -V_{21}G_{11} & 1 - V_{22}G_{22} \end{pmatrix} . \tag{2.62}$$

The loop function G of Eq. (2.57) can also be expressed, in dimensional regularization [41], as

$$\begin{aligned} G_{ll} &= \frac{1}{16\pi^2}(\alpha_j(\mu) + \log\frac{m_1^2}{\mu^2} + \frac{m_2^2 - m_1^2 + s}{2s}\log\frac{m_2^2}{m_1^2} \\ &+ \frac{p}{\sqrt{s}}(\log\frac{s - m_2^2 + m_1^2 + 2p\sqrt{s}}{-s + m_2^2 - m_1^2 + 2p\sqrt{s}} \\ &+ \log\frac{s + m_2^2 - m_1^2 + 2p\sqrt{s}}{-s - m_2^2 + m_1^2 + 2p\sqrt{s}})) . \end{aligned} \tag{2.63}$$

The equivalence between the two prescriptions has been shown in Ref. [33]. In Eq. (2.63), p is the three-momentum of the mesons in the centre of mass

$$p = \frac{\sqrt{(s - (m_1 + m_2)^2)(s - (m_1 - m_2)^2)}}{2\sqrt{s}} = \frac{\lambda^{1/2}(s, m_1^2, m_2^2)}{2\sqrt{s}} , \tag{2.64}$$

and μ is the arbitrary scale of the regularization and λ is the Källén function. Changes in the scale are reabsorbed by the subtraction constant $\alpha(\mu)$, such that the result is independent of the scale. From a comparison between Eqs. (2.57) and (2.63) it is possible to determine the subtraction constant for every intermediate state of the scattering problem.

2.4.2 Equivalence between IAM and the Bethe-Salpeter equation method

In Ref. [32] the equivalence between the IAM method and the use of the Bethe-Salpeter equation is shown. The IAM consists in a resummation of χPT based on the expansion of T^{-1}. Unitarity is implemented in coupled channels by means of the formula

$$\mathrm{Im}T_{if} = T_{in}\,\sigma_{nn}\,T^*_{nf} , \tag{2.65}$$

where σ is the diagonal matrix whose elements account for the phase-space of the two mesonic intermediate states n which are physically accessible, defined

in our normalization as

$$\sigma_{nn}(s) = -\frac{p}{8\pi\sqrt{s}}\,\theta(s-(m_1-m_2)^2)\,. \tag{2.66}$$

Using the informations contained in χPT up to $\mathcal{O}(p^4)$ to approximate the amplitude T, one arrives to write it as

$$T = T_2\,[T_2 - T_4]^{-1}\,T_2\,. \tag{2.67}$$

Eq. (2.67) is the generalization to multiple coupled channels of the IAM of Refs. [78, 81], which makes the method more general allowing for transition cross sections and inelasticities.

However, Eq. (2.67) requires the complete evaluation of T_4, which can be complicated when dealing with many channels, and a technically simpler but still accurate approximation could be useful. The loop function G of Eq. (2.57) has the property

$$\mathrm{Im}G_{nn}(s) = \sigma_{nn}\,. \tag{2.68}$$

As we already said, the real part of G is divergent and needs to be regularized. We assume that by means of a suitable choice of the cutoff q_{max} we can write the approximation

$$\mathrm{Re}T_4 \;\simeq T_2\,\mathrm{Re}G\,T_2\,. \tag{2.69}$$

Using Eq. (2.69), its straightforward to show that the IAM amplitude leads to the one of the Bethe-Salpeter Equation method. In fact, from Eq. (2.67),

$$\begin{aligned} T &= T_2\,[T_2 - \mathrm{Re}T_4 - \mathrm{Im}T_4]^{-1}\,T_2 \\ &= T_2\,[T_2 - T_2\mathrm{Re}G\,T_2 - \mathrm{Im}T_4]^{-1}\,T_2\,, \end{aligned} \tag{2.70}$$

and recalling that, above threshold,

$$\mathrm{Im}T_4 = T_2\,\sigma\,T_2 = T_2\,\mathrm{Im}G\,T_2\,, \tag{2.71}$$

it follows

$$T = [1 - T_2\,G]^{-1}\,T_2\,, \tag{2.72}$$

that is exactly Eq. (2.59).

2.5 Poles and couplings

The identification of resonances proceeds by means of their association to the poles of the scattering matrix. According to the scattering theory, when we have a pole for $\mathrm{Im}(p) > 0$ and $\mathrm{Re}(p) = 0$, corresponding to the real s axis below the lowest threshold, we found a *bound state*. On the other hand, *resonances*

appear for $\mathrm{Im}(p) < 0$ and $\mathrm{Re}(s)$ above the lowest threshold, which is called the second Riemann sheet of the function $T(s)$. If these poles are not too far from the real axis, their imaginary part can be identified with half the width of the state, such that $\sqrt{s_P} = (m_R \pm i\frac{\Gamma}{2})$. However, what is really physically meaningful is the amplitude evaluated for real values of $\sqrt{s}$, corresponding to the reflection of the pole on the real axis.

We will denote the amplitude in the second Riemann sheet by

$$T^{II} = [1 - VG^{II}]^{-1} V \,, \tag{2.73}$$

and in order to evaluate it, we need the loop function G_{jj} extrapolated to the second Riemann sheet, G^{II}_{jj}. As explained in Refs. [30, 51], G^{II}_{jj} can be evaluated by means of the Schwartz reflection theorem: if a function $f(z)$ is analytic in a region of the complex plane including a portion of the real axis in which f is real, then

$$[f(z^*)]^* = f(z) \,. \tag{2.74}$$

The conditions above are satisfied by the G function and consequently, for $\mathrm{Re}\sqrt{s} > m_1 + m_2$,

$$G_{jj}(\sqrt{s} - i\epsilon) = [G_{jj}(\sqrt{s} + i\epsilon)]^* = G_{jj}(\sqrt{s} + i\epsilon) - i\, 2\, \mathrm{Im} G_{jj}(\sqrt{s} + i\epsilon) \,. \tag{2.75}$$

The equation above, since the beginning of the second Riemann sheet coincides with the end of the first one, can be rewritten as

$$G^{II}_{jj}(\sqrt{s} + i\epsilon) = G^{I}_{jj}(\sqrt{s} - i\epsilon) = G^{II}_{jj}(\sqrt{s} + i\epsilon) - i\, 2\, \mathrm{Im} G^{I}_{jj}(\sqrt{s} + i\epsilon) \,, \tag{2.76}$$

with

$$\mathrm{Im} G^{I}_{jj} = -\frac{p}{8\pi\sqrt{s}} \,, \tag{2.77}$$

and $G^{I}_{jj}(\sqrt{s})$ is given by Eq. (2.63). Eqs. (2.76) and (2.77) should hold only very close to the real axis, but since the analytic continuation to the rest of the complex plane is unique, in general one can write

$$G^{II}_{jj}(\sqrt{s}) = G^{I}_{jj}(\sqrt{s}) + i\frac{p}{4\pi\sqrt{s}} \,, \qquad \mathrm{Im}(p) > 0 \,. \tag{2.78}$$

This last equation allows the evaluation of the scattering amplitude and, therefore, to systematically look for resonances searching for its poles. Throughout this work, we will consider as *dynamically generated* all those resonance appearing as poles in the second Riemann sheet of the scattering amplitude evaluated by means of Eq. (2.59), that is from the coupled-channels Bethe-Salpeter equation where the hadron-hadron tree-level potentials coming from the chiral Lagrangians at $\mathcal{O}(p^2)$ are used as the kernel. In Eq. (2.59), we will

use G^{II}_{jj} when the j channel is open, that is when $\mathrm{Re}\sqrt{s} > m_1+m_2$, and G^{I}_{jj} for $\mathrm{Re}\sqrt{s} < m_1 + m_2$. This also allows, when we are below the lowest threshold, to obtain poles corresponding to pure bound states.

At this point, it is also possible to evaluate the couplings g_i of the state to the different hadron-hadron channels remembering that, close to the pole of the resonance, the amplitude in the complex plane for a diagonal transition can be written as

$$T_{ii}(s) \simeq \frac{g_i^2}{s - s_R}\,, \tag{2.79}$$

where s_R is the position of the resonance. Hence, the coupling can be evaluated as the residue at the pole of $T_{ii}(s)$, using the formula

$$\int_0^{2\pi} T_{ii}(z(\theta))\, i\, r\, e^{i\theta} d\theta = 2\pi i\, \mathrm{Res}(T_{ii}) = 2\pi i\, g_i^2\,, \tag{2.80}$$

with $z = z_0 + r\, e^{i\theta}$ and $z_0 = m_R + i\Gamma/2$.

2.6 Hidden Gauge Formalism

Among all the method that could be used to implement spin 1 particles in the effective theory (see Ref. [49] for a review), one is the formalism of hidden gauge for vector mesons [63, 64], an internally consistent scheme naturally implementing chiral symmetry. As reported in Ref. [82], in this formalism the vector mesons are gauge bosons of a hidden local symmetry transforming inhomogeneously. After taking the unitary gauge, the vector meson fields transform exactly as in the nonlinear realization of chiral symmetry [26]. This method is ideal since it provides a way to deal simultaneously with vector mesons and pseudoscalars and it leads to the same lowest order chiral Lagrangian of Ref. [76].

Another important feature of the approach is that, although much simpler, it has been proven in Refs. [83] to be equivalent to using the tensor formalism for vector mesons [84], where the vectors transform inhomogeneously under a non linear realization of chiral symmetry, with the use of couplings implied in the vector meson dominance formalism. Moreover, besides the interaction of vector mesons with pseudoscalars, the formalisms of hidden gauge also contain the interaction of vector mesons with themselves, for which there were no Lagrangians available in the formalism of Ref. [84].

In Refs. [64, 65, 85] the axial vector mesons are introduced as elementary particles in the hidden gauge symmetry Lagrangian, but in Ref. [82] they are treated as generated by the interaction of mesons and this allows the inclusion of photons in the theory. When axial resonances are considered as

composite particles of vector and pseudoscalars, the coupling to the photon is made through its component, and proceeds through loop diagrams involving the corresponding vector and pseudoscalar mesons of each channel.

Following Ref. [82] we can write the Lagrangian involving pseudoscalars, vector mesons and photons as

$$\mathcal{L} = \mathcal{L}_2 + \mathcal{L}_{III}\,, \tag{2.81}$$

where $\mathcal{L}_2$ is the chiral Lagrangian at $\mathcal{O}(p^2)$ of Eq. (2.38) while

$$\mathcal{L}_{III} = -\frac{1}{4}\langle V_{\mu\nu}V^{\mu\nu}\rangle + \frac{1}{2}M_V^2\langle\left(V_\mu - \frac{i}{g}\Gamma_\mu\right)^2\rangle\,, \tag{2.82}$$

with $\langle\ \rangle$ is the $SU(3)$ trace. The V_μ matrix is the $SU(3)$ matrix containing the vector mesons,

$$V_\mu = \begin{pmatrix} \frac{\omega}{\sqrt{2}} + \frac{\rho^0}{\sqrt{2}} & \rho^+ & K^{*+} \\ \rho^- & \frac{\omega}{\sqrt{2}} - \frac{\rho^0}{\sqrt{2}} & K^{*0} \\ K^{*-} & \bar{K}^{*0} & \phi \end{pmatrix}_\mu\,, \tag{2.83}$$

while the matrix of the pseudoscalars ϕ is the one of Eq. (2.29).

Expanding the matrix U (Eq. (2.28)) up to terms containing four fields ϕ, one gets

$$\tilde{\mathcal{L}}_2 = \frac{1}{12f^2}\langle[\phi,\partial_\mu\phi]^2 + M\phi^4\rangle\,, \tag{2.84}$$

with $M = \mathrm{diag}(m_\pi^2, m_\pi^2, 2m_K^2 - m_\pi^2)$. Recalling Eqs. (2.34) and (2.39), we can write the part of the covariant derivative in $\tilde{\mathcal{L}}_2$ containing the photon as

$$D_\mu U = \partial_\mu U - ieQ\,A_\mu U + ieUQ\,A_\mu\,, \tag{2.85}$$

where $Q = \mathrm{diag}(2,-1,-1)/3$, $e = -|e|$ is the electron charge and A_μ is the photon field. Hence, the Lagrangian of Eq. (2.84) provides the coupling between the pseudoscalars (P) and one photon (γ), given by

$$\mathcal{L}_{\gamma PP} = -ieA^\mu\langle Q[\phi,\partial_\mu\phi]\rangle\,. \tag{2.86}$$

The tensor $V_{\mu\nu}$ in $\mathcal{L}_{III}$ is defined as

$$V_{\mu\nu} = \partial_\mu V_\nu - \partial_\nu V_\mu - ig[V_\mu, V_\nu]\,, \tag{2.87}$$

while

$$\Gamma_\mu = \frac{1}{2}[u^\dagger(\partial_\mu - ieQA_\mu)u + u(\partial_\mu - ieQA_\mu)u^\dagger]\,. \tag{2.88}$$

The hidden gauge coupling g is related to the constant f and to the vector meson mass M_V by the formula

$$g = \frac{M_V}{2f} \,. \tag{2.89}$$

Expanding the term with $(V_\mu - i\frac{i}{g}\Gamma_\mu)^2$ up to two meson fields, it is possible to obtain the interactions among pseudoscalars, photons and vector mesons:

$$\mathcal{L}_{V\gamma} = -M_V^2 \frac{e}{g} A_\mu \langle V^\mu Q \rangle \,, \tag{2.90}$$

$$\mathcal{L}_{V\gamma PP} = e\frac{M_V^2}{4gf^2} A_\mu \langle V^\mu (Q\phi^2 + \phi^2 Q - 2\phi Q \phi) \rangle \,, \tag{2.91}$$

$$\mathcal{L}_{VPP} = -ig \, \langle V^\mu [\phi, \partial_\mu \phi] \rangle \,, \tag{2.92}$$

$$\mathcal{L}_{\gamma PP} = ie \, A_\mu \langle Q [\phi, \partial_\mu \phi] \rangle \,, \tag{2.93}$$

$$\mathcal{L}_{PPPP} = -\frac{1}{8f^2} \langle [\phi, \partial_\mu \phi]^2 \rangle \,. \tag{2.94}$$

The term in Eq. (2.93) is exactly cancelled by the term coming from $\tilde{\mathcal{L}}_2$ of Eq. (2.86), such that in the end the photon couples to the pseudoscalar mesons via vector meson exchange, which is the basic feature of vector meson dominance [86]. The term in Eq. (2.94) has the same derivative structure we can find in Eq. (2.84) and, added to $\tilde{\mathcal{L}}_2^{(2)}$, it would break chiral symmetry. However, this term is cancelled by the exchange of vector mesons between pseudoscalars resulting from the vertices described by $\mathcal{L}_{VPP}$ of Eq. (2.92) in the limit $q^2/M_V^2 \to 0$, where q is the momentum carried by the vector meson in the exchange. This result was already reported in Ref. [26].

From the term $-\frac{1}{4}\langle V_{\mu\nu} V^{\mu\nu} \rangle$ in $\mathcal{L}_{III}$, two different types of interaction can be derived: a contact interaction, coming from the $[V_\mu, V_\nu]$ term,

$$\mathcal{L}^{(c)} = \frac{g^2}{2} \langle V_\mu V_\nu V^\mu V^\nu - V_\nu V_\mu V^\mu V^\nu \rangle \,, \tag{2.95}$$

and the three-vector vertex

$$\mathcal{L}^{(3V)} = ig \langle (\partial_\mu V_\nu - \partial_\nu V_\mu) V^\mu V^\nu \rangle \,. \tag{2.96}$$

The Lagrangian $\mathcal{L}^{(3V)}$ produces the $VV \to VV$ interaction by means of the exchange of one vector meson.

As reported in Ref. [82], beside the vertices listed above, processes could get relevant contributions also from diagrams involving the VVP vertex. This interaction is anomalous, accounts for processes not conserving intrinsic parity

and can be obtained from the gauged Wess-Zumino term [66, 87]. Although expected to give small contributions due to their higher order nature, these diagrams have shown to be relevant in some cases like in radiative decays of scalar mesons [84, 88, 89] and in kaon photoproduction [90]. The Lagrangian describing the VVP vertex is given by

$$\mathcal{L}_{VVP} = \frac{G}{\sqrt{2}}\epsilon^{\mu\nu\alpha\beta}\langle\partial_\mu V_\nu \partial_\alpha V_\beta P\rangle \ , \tag{2.97}$$

where $G = 3M_V^2/16\pi^2 f^3$ and $\epsilon^{\mu\nu\alpha\beta}$ is the completely antisymmetric tensor.

Eqs. (2.90), (2.92), (2.95), (2.96) and (2.97) will be used in the next chapter for the evaluation of diagrams involving vector mesons.

CHAPTER **3**

COMPOSITENESS OF HADRON STATES: MESON RESONANCES

3.1 Introduction

One of the challenges in hadron spectroscopy is to find a way to determine, simply from experimental data, the nature of the states and whether they are composed of other stable particles or something different. An early attempt to answer this question was made by Weinberg in his work of 1965 [91], in which he determined that the deuteron was a bound state of a proton and a neutron. However, his approach was only suitable for s-waves and small binding energies. Later, more work on this issue has been done in Refs. [92, 93]. A generalization of Weinberg's work to more heavily bound systems and using many coupled channels was made in Ref. [94] and, with a different derivation, also in Ref. [95]. Finally, in Ref. [96] also resonances are considered, but still all the work was limited to the case of s-waves.

In this chapter we generalize the theorem to higher partial waves. We start with the case of bound states in **Section 3.2**, considering first a single channel and then including many coupled scattering channels. We follow the approach of Ref. [94], which was, however, limited to bound states in the case of interactions in s-wave. We first make a thorough study of the relationship between scattering amplitudes and wave functions, deriving the expression of the wave function in momentum space. The normalization condition for the wave function is then used to obtain a different formulation of the compositeness condition of Weinberg. We then move to the coordinate space and, after analysing the asymptotic behaviour of the wave function, we establish the relation between the coupling of the bound state to the two interacting hadrons and the wave function at the origin.

In **Section 3.3** we extend the formalism to the case of open channels. We will see that, even though the compositeness condition cannot be derived from the normalization of the wave function, which is not finite in the case of resonances, it still holds at the pole.

The sum rule derived in **Section 3.3** can be applied to concrete cases to find out whether a resonance is created by the interaction of two particles or not. In **Section 3.4** we quantify the composite nature of two meson resonances, the ρ and the K^*. The content of this Chapter can be found in Refs. [97] and [98].

3.2 The case of bound states

We want to study the non-relativistic dynamics of a bound state generated by the interaction of two particles of masses m_1 and m_2 in a generic l-wave.

The system is described by the Hamiltonian $H = H_0 + V$, with H_0 the free Hamiltonian and V the interaction potential. In order to illustrate the results, we need to choose a potential V. As done in Refs. [94, 96], we use a separable function in momentum space with the modulating factor being a step function Θ. However, the basic results hold unaltered using other types of potentials, as in the case of Ref. [94]. Our potential, projected in a generic l-wave (instead of s-wave), is given by

$$\langle \vec{p}\,'|V|\vec{p}\rangle = V(\vec{p},\vec{p}\,') = v(2l+1)\Theta(\Lambda-p)\Theta(\Lambda-p')P_l(\cos\theta)|\vec{p}\,|^l\,|\vec{p}\,'|^l\ , \quad (3.1)$$

where Λ is a cutoff in the momentum space.

The non-relativistic Lippmann-Schwinger equation describing the scattering process can be written as

$$T = V + V\frac{1}{E-H_0}T \quad (3.2)$$

and also as

$$T = V + V\frac{1}{E-H}V\ . \quad (3.3)$$

Considering Eq. (3.2) and substituting the expression of the potential inside the second term, we can write

$$\begin{aligned}\langle \vec{p}\,|T^{(2)}|\vec{p}\,'\rangle = \langle\vec{p}\,|(2l+1)v\,\Theta(\Lambda-p)\int_{p''<\Lambda} d^3p''P_l(\hat{p},\hat{p}'')\frac{|\vec{p}\,|^l|\vec{p}\,''|^l}{E-m_1-m_2-\frac{\vec{p}\,''^2}{2\mu}}\\ \times(2l+1)v\,\Theta(\Lambda-p')P_l(\hat{p}'',\hat{p}')|\vec{p}\,''|^l|\vec{p}\,'|^l|\vec{p}\,'\rangle\,,\end{aligned} \quad (3.4)$$

where μ is the reduced mass of the two interacting particles of masses m_1 and m_2. The states are normalized such that

$$\begin{aligned} |\vec{p}\rangle\langle\vec{p}| &\equiv \int d^3p \ , \\ \langle\vec{p}|\vec{p}\,'\rangle &= \delta^{(3)}(\vec{p}-\vec{p}\,') \, . \end{aligned} \tag{3.5}$$

Using the expression of the Legendre functions in terms of the spherical harmonics,

$$P_l(\hat{p},\hat{p}'') = \frac{4\pi}{2l+1}\sum_m Y_{lm}(\hat{p})Y^*_{lm}(\hat{p}'') \, , \tag{3.6}$$

and their normalization condition,

$$\int d\Omega Y^*_{lm}(\hat{p})Y_{l'm'}(\hat{p}) = \delta_{ll'}\delta_{mm'} \, , \tag{3.7}$$

Eq. (3.4) becomes

$$\begin{aligned} T^{(2)} = (2l+1)v\Theta(\Lambda-p)v\Theta(\Lambda-p')P_l(\hat{p},\hat{p}')|\vec{p}\,|^l|\vec{p}\,'|^l \\ \times \int_{p''<\Lambda} d^3p'' \frac{|\vec{p}\,''|^{2l}}{E-m_1-m_2-\frac{\vec{p}\,''^2}{2\mu}} \, . \end{aligned} \tag{3.8}$$

The procedure can be repeated for all the other terms in the Lippmann-Schwinger equation, leading to the expression of the scattering amplitude

$$T = (2l+1)P_l(\hat{p},\hat{p}')\Theta(\Lambda-p)\Theta(\Lambda-p')|\vec{p}\,|^l|\vec{p}\,'|^l t \, , \tag{3.9}$$

with

$$t = v + v\ G\ t \ , \qquad t = \frac{v}{(1-vG)} = \frac{1}{v^{-1}-G} \, , \tag{3.10}$$

where

$$G = \int_{p''<\Lambda} d^3p'' \frac{|\vec{p}\,''|^{2l}}{E-m_1-m_2-\frac{\vec{p}\,''^2}{2\mu}} \, . \tag{3.11}$$

We can see that the factor $2l+1$ does not appear in the equation for t.

It is important to highlight that v in Eq. (3.10) does not contain $|\vec{p}\,|^l$, which is now absorbed into the definition of the loop function G of Eq. (3.11). This is unusual, since other approaches for p-waves, like the one of Refs. [99] and [100], factorize on shell $|\vec{p}\,|^l$ and associate it to the potential. In those cases, G does not have the factor $|\vec{p}\,''|^{2l}$ that we find in Eq. (3.11). The procedure leads to the same imaginary part of the amplitude T but can induce differences in the real part. Later on we will show that the option chosen here, which stems from the form of the potential in Eq. (3.1), allows one to generalize the sum rule for the couplings found in Ref. [94], which is lost if one uses the on shell factorized form.

3.2.1 Wave function in momentum space

We now want to derive the expression of the wave function in momentum space. From the Schrödinger equation it follows

$$|\Psi\rangle = \frac{V}{E - H_0}|\Psi\rangle\,, \tag{3.12}$$

which has the solution

$$\langle\vec{p}\,|\Psi\rangle = \int d^3k \int d^3k' \langle\vec{p}\,|\frac{1}{E - H_0}|\vec{k}\rangle\langle\vec{k}|V|\vec{k}'\rangle\langle\vec{k}'|\Psi\rangle\,. \tag{3.13}$$

Substituting the potential of Eq. (3.1) in this last equation and using the fact that

$$\langle\vec{p}\,|\frac{1}{E - H_0}|\vec{k}\rangle = \delta^{(3)}(\vec{p} - \vec{k})\frac{1}{E - m_1 - m_2 - \frac{\vec{p}^{\,2}}{2\mu}}\,, \tag{3.14}$$

we obtain

$$\begin{aligned}\langle\vec{p}\,|\Psi\rangle &= \int_{k'<\Lambda} d^3k'(2l+1)v\,\Theta(\Lambda - p)\frac{1}{E - m_1 - m_2 - \frac{\vec{p}^{\,2}}{2\mu}}|\vec{p}\,|^l|\vec{k}'|^l P_l(\hat{p},\hat{k}')\langle\vec{k}'|\Psi\rangle \\ &= 4\pi\sum_m \frac{\Theta(\Lambda - p)|\vec{p}\,|^l v}{E - m_1 - m_2 - \frac{\vec{p}^{\,2}}{2\mu}}Y_{lm}(\hat{p})\int_{k<\Lambda} d^3k Y^*_{lm}(\hat{k})|\vec{k}|^l\langle\vec{k}|\Psi\rangle\,,\end{aligned} \tag{3.15}$$

which gives us the expression of the wave function in momentum space.

Defining $\langle\vec{k}|\tilde{\Psi}\rangle$ as

$$\langle\vec{k}|\Psi\rangle \cong (4\pi)^{1/2}\sum_{m'} a_{m'}Y_{lm'}(\hat{k})\langle\vec{k}|\tilde{\Psi}\rangle\,, \tag{3.16}$$

and normalizing the coefficients $a_{m'}$ as

$$\sum_{m'}|a_{m'}|^2 = 1\,, \tag{3.17}$$

we can write Eq. (3.15) as

$$\begin{aligned}\langle\vec{p}\,|\Psi\rangle &= (4\pi)^{1/2}\sum_m a_m Y_{lm}(\hat{p})\langle\vec{p}\,|\tilde{\Psi}\rangle \\ &= (4\pi)^{1/2}\sum_m \frac{\Theta(\Lambda - p)|\vec{p}\,|^l v}{E - m_1 - m_2 - \frac{\vec{p}^{\,2}}{2\mu}}a_m Y_{lm}(\hat{p})\int_{k<\Lambda} d^3k|\vec{k}|^l\langle\vec{k}|\tilde{\Psi}\rangle\,,\end{aligned} \tag{3.18}$$

that leads to

$$\langle\vec{p}\,|\tilde{\Psi}\rangle = \frac{\Theta(\Lambda - p)|\vec{p}\,|^l v}{E - m_1 - m_2 - \frac{\vec{p}^{\,2}}{2\mu}}\int_{k<\Lambda} d^3k|\vec{k}|^l\langle\vec{k}|\tilde{\Psi}\rangle\,. \tag{3.19}$$

Integrating in d^3p and multiplying both sides by $|\vec{p}|^l$, Eq. (3.19) becomes

$$\begin{aligned}\int d^3p|\vec{p}|^l\langle\vec{p}|\tilde{\Psi}\rangle &= \int_{p<\Lambda} d^3p\frac{|\vec{p}|^{2l}v}{E-m_1-m_2-\frac{\vec{p}^2}{2\mu}}\int_{k<\Lambda} d^3k\langle\vec{k}|\tilde{\Psi}\rangle|\vec{k}|^l \\ &= G\ v\ \int_{k<\Lambda} d^3k\langle\vec{k}|\tilde{\Psi}\rangle|\vec{k}|^l\,.\end{aligned} \tag{3.20}$$

This last expression gives us the condition for a pole in the t-matrix corresponding to a bound state,

$$1-G(E)\ v=0\ , \tag{3.21}$$

which will occur for some value of the energy below the scattering threshold.

Let now $E_\alpha < m_1+m_2$ be the solution of Eq. (3.21). Since we are dealing with a bound state, its wave function will satisfy the normalization condition

$$\int d^3p|\langle\vec{p}|\Psi\rangle|^2=1\,. \tag{3.22}$$

We can now substitute the expression of the wave function of Eq. (3.18) in the above equation,

$$\begin{aligned}\int d^3p|\langle\vec{p}|\Psi\rangle|^2 &= \int d^3p(4\pi)^{1/2}\sum_m\frac{\Theta(\Lambda-p)|\vec{p}|^l v}{E-m_1-m_2-\frac{\vec{p}^2}{2\mu}}\ a_m^*Y_{lm}^*(\hat{p})\int_{k<\Lambda} d^3k\langle\tilde{\Psi}|\vec{k}\rangle|\vec{k}|^l \\ &\times(4\pi)^{1/2}\sum_{m'}\frac{\Theta(\Lambda-p)|\vec{p}|^l v}{E-m_1-m_2-\frac{\vec{p}^2}{2\mu}}\ a_{m'}Y_{lm'}(\hat{p})\int_{k'<\Lambda} d^3k'\langle\vec{k}'|\tilde{\Psi}\rangle|\vec{k}'|^l \\ &= \int_{p<\Lambda} d^3p\left(\frac{|\vec{p}|^l v}{E-m_1-m_2-\frac{\vec{p}^2}{2\mu}}\right)^2\sum_m|a_m|^2\left|\int_{k<\Lambda} d^3k|\vec{k}|^l\langle\vec{k}|\tilde{\Psi}\rangle\right|^2\,.\end{aligned} \tag{3.23}$$

Taking into account the normalization in Eq. (3.17) and Eq. (3.11), we obtain

$$-\frac{dG}{dE}\ v^2\left|\int_{k<\Lambda} d^3k|\vec{k}|^l\langle\vec{k}|\tilde{\Psi}\rangle\right|^2=1\,. \tag{3.24}$$

3.2.2 The compositeness condition

Eq. (3.24) is relevant for our purposes. By construction, the left-hand side is the probability that the bound state found couples to the hadron-hadron component under consideration. We shall see in the following sections that, when we have several interacting hadron-hadron pairs, it is replaced by a sum

over the different coupled channels and each one of the terms indicates the probability to find the hadron-hadron pair in the wave function. Yet, it could be that a physical state couples not only to hadron-hadron pairs, but also to a different component of non-molecular type, say $q\bar{q}$ for mesons or qqq for baryons. One example of this can be found in studies with the chiral bag model [101] where the Δ has a big qqq component and a smaller πN one. In this case the normalization would be given by

$$-\frac{dG}{dE}\, v^2 \left| \int_{k<\Lambda} d^3k |\vec{k}|^l \langle \vec{k}|\tilde{\Psi}\rangle \right|^2 + |\langle \beta|\Psi\rangle|^2 = 1\,, \tag{3.25}$$

that we can rewrite as

$$-\frac{dG}{dE}\, v^2 \left| \int_{k<\Lambda} d^3k |\vec{k}|^l \langle \vec{k}|\tilde{\Psi}\rangle \right|^2 = 1 - Z\ ; \qquad Z = |\langle \beta|\Psi\rangle|^2\,, \tag{3.26}$$

where $|\beta\rangle$ is the genuine component of the state (the qqq in the bag model of Ref. [101], for instance).

This is the statement of the *compositeness condition of Weinberg*, although derived and formulated in a different way. The idea is that the first term in Eq. (3.24) represents the probability to find the hadron-hadron component in the wave function, and its diversion from unity is the probability to find some other components which could have not been taken into account if one has neglected important channels of the more general coupled channels problem.

Yet, the theorem can be stated in a more practical way resorting to the coupling of the state to the channel considered. To do that, we need to use the other form of the Lippmann-Schwinger equation, Eq. (3.3). We have

$$\langle \vec{p}|T|\vec{p}\,'\rangle = \langle \vec{p}|V|\vec{p}\,'\rangle + \sum_{nn'} \langle \vec{p}|V|n\rangle\langle n|\frac{1}{E-H}|n'\rangle\langle n'|V|\vec{p}\,'\rangle\,, \tag{3.27}$$

where $|n\rangle$ and $|n'\rangle$ are complete sets of eigenstates of the full Hamiltonian H.

In the vicinity of the pole, where $E = E_\alpha$, we can take into account only the dominant contribution coming from the eigenstate $|\alpha\rangle$. Then,

$$\langle \vec{p}|T|\vec{p}\,'\rangle \sim \langle \vec{p}|V|\vec{p}\,'\rangle + \int d^3k \int d^3k' \langle \vec{p}|V|\vec{k}\rangle\langle \vec{k}|\alpha\rangle \frac{1}{E-E_\alpha}\langle \alpha|\vec{k}'\rangle\langle \vec{k}'|V|\vec{p}\,'\rangle\,, \tag{3.28}$$

and we can write Eq. (3.28) explicitly

$$\begin{aligned}\langle\vec{p}|T|\vec{p}\,'\rangle &= 4\pi\Theta(\Lambda-p)\Theta(\Lambda-p')t|\vec{p}|^l|\vec{p}\,'|^l\sum_m Y_{lm}(\hat{p})Y^*_{lm}(\hat{p}')\\ &= 4\pi\Theta(\Lambda-p)\Theta(\Lambda-p')v|\vec{p}|^l|\vec{p}\,'|^l\sum_m Y_{lm}(\hat{p})Y^*_{lm}(\hat{p}')\\ &+\int_{k<\Lambda}d^3k\int_{k'<\Lambda}d^3k'4\pi\Theta(\Lambda-p)v|\vec{p}|^l|\vec{k}|^l\sum_{m'}Y_{lm'}(\hat{p})Y^*_{lm'}(\hat{k})\\ &\times\langle\vec{k}|\alpha\rangle\frac{1}{E-E_\alpha}\langle\alpha|\vec{k}'\rangle 4\pi\Theta(\Lambda-p')v|\vec{k}'|^l|\vec{p}\,'|^l\sum_{m''}Y_{lm''}(\hat{k}')Y^*_{lm''}(\hat{p}')\,.\end{aligned} \tag{3.29}$$

We can write

$$\begin{aligned}\langle\vec{k}|\alpha\rangle &= (4\pi)^{1/2}\sum_{m'}a_{m'}Y_{lm'}(\vec{k})\langle\vec{k}|\tilde{\alpha}\rangle\,,\\ \langle\alpha|\vec{k}\,'\rangle &= (4\pi)^{1/2}\sum_{m''}a^*_{m''}Y^*_{lm''}(\vec{k}\,')\langle\tilde{\alpha}|\vec{k}\,'\rangle\,.\end{aligned} \tag{3.30}$$

Taking into account that

$$|\tilde{\alpha}\rangle\frac{1}{E-E_\alpha}\langle\tilde{\alpha}|\to|\tilde{\alpha}\rangle\frac{1}{E-E_\alpha}\langle\tilde{\alpha}|\delta_{m'm''}\,, \tag{3.31}$$

since $|\tilde{\alpha}\rangle$ states with same third component of angular momentum have the same energy (a sum over α is intended in Eq. (3.29)), we can write

$$\langle\vec{k}|\alpha\rangle\frac{1}{E-E_\alpha}\langle\alpha|\vec{k}'\rangle\to 4\pi\frac{1}{E-E_\alpha}\langle\vec{k}|\tilde{\alpha}\rangle\langle\tilde{\alpha}|\vec{k}'\rangle\sum_{m'}Y_{lm'}(\hat{k})Y^*_{lm'}(\hat{k}')\,, \tag{3.32}$$

and using this relation in Eq. (3.29) we can easily find

$$t=v+v^2\frac{1}{E-E_\alpha}\left|\int_{k<\Lambda}d^3k\langle\vec{k}|\tilde{\alpha}\rangle|\vec{k}|^l\right|^2\,. \tag{3.33}$$

Now, remembering that close to the pole the coupling g is defined such that the amplitude can be written as

$$t=\frac{g^2}{E-E_\alpha}\,, \tag{3.34}$$

we get

$$g^2=\lim_{E\to E_\alpha}(E-E_\alpha)\;t=v^2\left|\int_{k<\Lambda}d^3k\langle\vec{k}|\tilde{\alpha}\rangle|\vec{k}|^l\right|^2\,. \tag{3.35}$$

Eq. (3.35) allows us to write $v^2 \left| \int_{k<\Lambda} d^3k \langle \vec{k}|\tilde{\alpha}\rangle |\vec{k}|^l \right|^2$ in terms of the couplings, which can be determined experimentally. This means that Eq. (3.24) can be stated, for a composite state, as

$$-g^2 \frac{dG}{dE} = 1 \tag{3.36}$$

and, in the general case we have coupling to a genuine component, as

$$-g^2 \frac{dG}{dE} = 1 - Z\,, \tag{3.37}$$

with Z the probability to find this component in the wave function. Since g can be determined experimentally, one can simply evaluate Eq. (3.37) to determine the nature of the states, as has been made manifest in Refs. [91] and [92].

In this Section we have been assuming implicitly that v is energy independent. Indeed, Eq. (3.36) can be obtained from Eq. (3.10) using l'Hôpital rule

$$g^2 = \lim_{E\to E_\alpha} (E - E_\alpha)t = \lim_{E\to E_\alpha} \frac{E - E_\alpha}{v^{-1} - G} = \frac{1}{-\frac{dG}{dE}}\,, \tag{3.38}$$

where, in the last step, the assumption is used. Now it is clear the convenience of avoiding the incorporation of the vertex $|\vec{p}|^{2l}$ in v, that is the on shell factorization. In that case the new v would be necessarily energy dependent and Eq. (3.38) could not be obtained so straightforwardly.

Actually, as seen in Refs. [91] and [92], Z means the probability of having the genuine component of the state. When dealing with a physical system in which $Z \neq 0$, one can accommodate it in the present formalism by taking an energy independent potential v, which accounts for the couplings to the hadron-hadron component, and a CDD pole term [102] of the type $a/(E-E_R)$, which accounts for the coupling to the genuine component. As shown in Ref. [41], this is a good tool for the analysis of data that returns $Z \leq 1$ as it should be, with Z related to the strength of the CDD pole, a.

3.2.3 Wave function in coordinate space

We can also evaluate the wave function in coordinate space as

$$\begin{aligned}\langle \vec{x}|\Psi\rangle &= \int d^3p \langle \vec{x}|\vec{p}\rangle\langle \vec{p}|\Psi\rangle = \int \frac{d^3p}{(2\pi)^{3/2}} e^{i\vec{p}\vec{x}} \langle \vec{p}|\Psi\rangle \\ &= \int_{p<\Lambda} \frac{d^3p}{(2\pi)^{3/2}} e^{i\vec{p}\vec{x}} \frac{|\vec{p}|^l}{E - m_1 - m_2 - \frac{\vec{p}^2}{2\mu}} g(4\pi)^{1/2} \sum_m a_m Y_{lm}(\hat{p})\,,\end{aligned} \tag{3.39}$$

where we have used Eqs. (3.18) and (3.36) in the expression of the wave function in momentum space.

Recalling the expansion of a plane wave in terms of spherical harmonics and Bessel functions

$$e^{i\vec{p}\,\vec{x}} = 4\pi \sum_{lm} i^l j_l(pr) Y^*_{lm}(\hat{p}) Y_{lm}(\hat{r})\,, \tag{3.40}$$

Eq. (3.39) becomes

$$\langle \vec{x}|\Psi\rangle = g \int_{p<\Lambda} \frac{d^3p}{(2\pi)^{3/2}}\; i^l j_l(pr) \frac{|\vec{p}|^l}{E - m_1 - m_2 - \frac{\vec{p}^{\,2}}{2\mu}} (4\pi)^{1/2} \sum_m a_m Y_{lm}(\hat{r})\,, \tag{3.41}$$

that gives us the expression of the wave function in coordinate space.

The Bessel functions satisfy the condition

$$j_l(z) \stackrel{z\to\infty}{\longrightarrow} \frac{1}{z} \cos\left[z - \frac{l+1}{2}\pi\right]\,. \tag{3.42}$$

Substituting this expression in the wave function in coordinate space of Eq. (3.41), taking into account that

$$\cos\left[z - \frac{l+1}{2}\pi\right] = \frac{1}{2}\left[(-i)^{l+1} e^{iz} + i^{l+1} e^{-iz}\right] \tag{3.43}$$

and the symmetries of the integrand, we can write

$$\begin{aligned}\langle \vec{x}|\Psi\rangle &\stackrel{pr\to\infty}{\longrightarrow} g \int_{-\Lambda}^{\Lambda} \frac{4\pi\, dp}{(2\pi)^{3/2}} \frac{i^l}{r} \frac{|\vec{p}|^l}{E - m_1 - m_2 - \frac{\vec{p}^{\,2}}{2\mu}} \frac{1}{2} \frac{e^{ipr}}{i^{l+1}} (4\pi)^{1/2} \sum_m a_m Y_{lm}(\hat{r}) \\ &= -g\, 2\mu \int_{-\Lambda}^{\Lambda} \frac{4\pi\, dp}{(2\pi)^{3/2}} \frac{i^l}{r} \frac{|\vec{p}|^l}{(p - i\gamma)(p + i\gamma)} \frac{1}{2} \frac{e^{ipr}}{i^{l+1}} (4\pi)^{1/2} \sum_m a_m Y_{lm}(\hat{r})\,,\end{aligned} \tag{3.44}$$

where in the last step we defined $\gamma = \sqrt{2\mu|E_B|}$, with E_B the binding energy, $E_B = E - m_1 - m_2 < 0$. Integrating Eq. (3.44) by means of the Cauchy theorem, the asymptotic behaviour of the wave function is easily found

$$\langle \vec{x}|\Psi\rangle \stackrel{r\to\infty}{\longrightarrow} -g\; 2\mu\; \sqrt{2}\pi \left(1 + O\left(\frac{1}{\Lambda}\right)\right) \sum_m a_m Y_{lm}(\hat{r}) (i\gamma)^l\; \frac{e^{-\gamma r}}{r}\,. \tag{3.45}$$

Now we want to establish the relation between the coupling and the wave function at the origin of coordinate space. From the behaviour of the Bessel functions for small values of the argument,

$$j_l(pr) \longrightarrow \frac{|\vec{p}|^l |\vec{r}\,|^l}{(2l+1)!!} \qquad\qquad |\vec{p}||\vec{r}\,| \to 0\,, \tag{3.46}$$

follows the expression of the wave function at the origin

$$\Psi(\vec{x} \to 0) = \langle \vec{x} \to 0 | \Psi \rangle = g\ G\ \frac{i^l |\vec{r}\,|^l}{(2\pi)^{3/2}(2l+1)!!}(4\pi)^{1/2} \sum_m a_m Y_{lm}(\hat{r})\,. \quad (3.47)$$

Eq. (3.47) leads to the relation between the coupling and the wave function

$$g = G^{-1}\ \hat{\Psi}\ , \quad (3.48)$$

where we have defined

$$\hat{\Psi} = \frac{(2\pi)^{3/2}(2l+1)!!}{i^l |\vec{r}\,|^l (4\pi)^{1/2} \sum_m a_m Y_{lm}(\hat{r})}\ \Psi(\vec{x} \to 0)\,. \quad (3.49)$$

For $l = 0$ this equation leads to

$$(2\pi)^{3/2}\Psi(0) = gG\,, \quad (3.50)$$

which is the same result obtained in Ref. [94].

3.2.4 Generalization to coupled channels

In the case of multiple two body scattering channels, we can use the same expression for the interaction potential,

$$\langle \vec{p}\,|V|\vec{p}\,'\rangle \equiv (2l+1)\ v\ \Theta(\Lambda - p)\Theta(\Lambda - p)|\vec{p}\,|^l |\vec{p}\,'|^l P_l(\cos\theta)\,, \quad (3.51)$$

but now v is a $N \times N$ matrix, with N the number of the different hadron-hadron channels.

All the expressions obtained in the previous section can be generalized to many channels. We can write the t matrix as

$$t = [1 - vG]^{-1} v\ , \quad (3.52)$$

where G is the diagonal matrix

$$\begin{pmatrix} G_1 & & & \\ & G_2 & & \\ & & \ddots & \\ & & & G_N \end{pmatrix} \quad (3.53)$$

with G_i given by Eq. (3.11) for each channel. This can also be rewritten as

$$t = \frac{Av}{\det(1 - vG)}\,, \quad (3.54)$$

where A is defined as

$$A = [\det(1 - vG)](1 - vG)^{-1} \tag{3.55}$$

and introduced to single out the source of the pole in coupled channels, given by the condition

$$\det(1 - vG) = 0\,. \tag{3.56}$$

Now we have for the couplings

$$g_i g_j = \lim_{E \to E_\alpha} (E - E_\alpha)\; t_{ij} = \left[\frac{(Av)_{ij}}{\frac{d}{dE}\det(1 - vG)} \right]_{E=E_\alpha}\,, \tag{3.57}$$

which, hence, implies

$$\frac{g_j}{g_i} = \left[\frac{(Av)_{ij}}{(Av)_{ii}} \right]_{E=E_\alpha}\,. \tag{3.58}$$

Eq. (3.18) is generalized as follows

$$\langle \vec{p}|\Psi_i\rangle = \frac{|\vec{p}|^l \Theta(\Lambda - p)(2l+1)}{E - M_i - \frac{\vec{p}^2}{2\mu_i}} \sum_j v_{ij} \int_{k<\Lambda} d^3k |\vec{k}|^l P_l(\hat{k}, \hat{p}) \langle \vec{k}|\Psi_j\rangle\,, \tag{3.59}$$

and using Eq. (3.16) we find

$$\langle \vec{p}|\tilde{\Psi}_i\rangle = \frac{|\vec{p}|^l \Theta(\Lambda - p)}{E - M_i - \frac{\vec{p}^2}{2\mu_i}} \sum_j v_{ij} \int_{k<\Lambda} d^3k |\vec{k}|^l \langle \vec{k}|\tilde{\Psi}_j\rangle\,, \tag{3.60}$$

where $M_i = m_{1i} + m_{2i}$.

Integrating in d^3p and multiplying by $|\vec{p}|^l$ both sides, we obtain the following equation, written in matrix form

$$\int d^3p |\vec{p}|^l \langle \vec{p}|\tilde{\Psi}\rangle = G\; v \int_{k<\Lambda} d^3k |\vec{k}|^l \langle \vec{k}|\tilde{\Psi}\rangle\,. \tag{3.61}$$

From Eq. (3.61) follows again the condition to find the pole

$$\det(1 - Gv) = 0\;. \tag{3.62}$$

This last equation can be rewritten as

$$\sum_j v_{ij} \int d^3p |\vec{p}|^l \langle \vec{p}|\tilde{\Psi}_j\rangle = [G_i^\alpha]^{-1} \int d^3p |\vec{p}|^l \langle \vec{p}|\tilde{\Psi}_i\rangle\,, \tag{3.63}$$

which, substituted in Eq. (3.60), gives

$$\langle \vec{p}|\tilde{\Psi}_i\rangle = \frac{|\vec{p}|^l \Theta(\Lambda - p)}{E - M_i - \frac{\vec{p}^2}{2\mu_i}} [G_i^\alpha]^{-1} \int_{k<\Lambda} d^3k |\vec{k}|^l \langle \vec{k}|\tilde{\Psi}_i\rangle\,. \tag{3.64}$$

We can now define the partial probability

$$P_i = \int d^3p |\langle \vec{p}|\Psi_i\rangle|^2 \tag{3.65}$$

and write the normalization condition for the wave functions as

$$\sum_i P_i = 1 \ . \tag{3.66}$$

Substituting Eq. (3.59) in the last equation we find the generalization to many channels of Eq. (3.24)

$$P_i = \left[-\frac{dG_i}{dE}\right]_{E=E_\alpha} \frac{1}{[G_i^\alpha]^2} \left| \int_{k<\Lambda} d^3k |\vec{k}|^l \langle \vec{k}|\tilde{\Psi}_i\rangle \right|^2 . \tag{3.67}$$

We now move to the coordinate space, where we have

$$\begin{aligned} \langle \vec{x}|\Psi_i\rangle = \int \frac{d^3p}{(2\pi)^{3/2}} e^{i\vec{p}\vec{x}} \langle \vec{p}|\Psi_i\rangle = \int_{p<\Lambda} \frac{d^3p}{(2\pi)^{3/2}} e^{i\vec{p}\vec{x}} (4\pi)^{1/2} \\ \times \sum_m a_m Y_{lm}(\hat{p}) \frac{|\vec{p}|^l}{E - M_i - \frac{\vec{p}^2}{2\mu_i}} \frac{1}{G_i^\alpha} \int_{k<\Lambda} d^3k |\vec{k}|^l \langle \vec{k}|\tilde{\Psi}_i\rangle \, , \end{aligned} \tag{3.68}$$

which, expanding the plane wave by means of Eq. (3.40), becomes

$$\begin{aligned} \Psi_i(\vec{x}) = \langle \vec{x}|\Psi_i\rangle = \int_{p<\Lambda} \frac{d^3p}{(2\pi)^{3/2}} (4\pi)^{1/2} \sum_m a_m Y_{lm}(\hat{r}) \ i^l \ j_l(pr) \\ \times \frac{|\vec{p}|^l}{E - M_i - \frac{\vec{p}^2}{2\mu_i}} \frac{1}{G_i^\alpha} \int_{k<\Lambda} d^3k |\vec{k}|^l \langle \vec{k}|\tilde{\Psi}_i\rangle \, . \end{aligned} \tag{3.69}$$

As in the case of only one channel, we obtain the expression of the wave function at the origin in coordinate space using Eq. (3.46):

$$\Psi_i(\vec{x} \equiv 0) = \frac{(4\pi)^{1/2} \sum_m a_m Y_{lm}(\hat{r}) i^l |\vec{r}|^l}{(2\pi)^{3/2}(2l+1)!!} \int_{k<\Lambda} d^3k |\vec{k}|^l \langle \vec{k}|\tilde{\Psi}_i\rangle \, . \tag{3.70}$$

Now we go back to Eq. (3.61). Defining as in the previous section

$$\hat{\Psi}_i \equiv \Psi_i(\vec{x} \to 0) \left[\frac{(4\pi)^{1/2} \sum_m a_m Y_{lm}(\hat{r}) i^l |\vec{r}|^l}{(2\pi)^{3/2}(2l+1)!!}\right]^{-1} = \int_{k<\Lambda} d^3k |\vec{k}|^l \langle \vec{k}|\tilde{\Psi}\rangle \, , \tag{3.71}$$

we are allowed to rewrite Eq. (3.61) as

$$\hat{\Psi} = G \ v \ \hat{\Psi} \ . \tag{3.72}$$

Eq. (3.72) requires for its solution

$$\det(1 - vG) = 0 \,, \tag{3.73}$$

which is guaranteed for a bound eigenstate of energy E_α. So, this equation can be rewritten as

$$[G^\alpha]^{-1}\,\hat{\Psi} = v\hat{\Psi}\,, \tag{3.74}$$

which allows us to write the expression of the wave function in momentum space in terms of the wave function at the origin of coordinate space, as

$$\langle \vec{p}|\Psi_i\rangle = (4\pi)^{1/2}\sum_m a_m Y_{lm}(\hat{p})\frac{\Theta(\Lambda - p)|\vec{p}|^l}{E - M_i - \frac{\vec{p}^{\,2}}{2\mu_i}}\,[G_i^\alpha]^{-1}\,\hat{\Psi}_i\,. \tag{3.75}$$

From the normalization condition in Eq. (3.66) it follows again

$$\begin{aligned}\sum_i \langle\Psi_i|\Psi_i\rangle &= \int d^3p \sum_i |\langle\vec{p}|\Psi_i\rangle|^2 \\ &= -\sum_i \left[\frac{dG_i}{dE}\right]_{E=E_\alpha} \frac{1}{[G_i^\alpha]^2}\hat{\Psi}_i^{\,2} = 1\,.\end{aligned} \tag{3.76}$$

To define the couplings in terms of $\hat{\Psi}_i$ we use once again the version of Eq. (3.3) for the Lippmann-Schwinger equation. Recalling that close to the pole of the eigenfunction of the Hamiltonian associated to the E_α, only this state $|\alpha\rangle$ contributes in the sum over the eigenstates, we find

$$t_{ij} = v_{ij} + \sum_{mn} v_{im}\hat{\Psi}_m \frac{1}{E - E_\alpha}\hat{\Psi}_n v_{nj}\,. \tag{3.77}$$

When we look for the couplings as the residues in the pole of the t-matrix, we obtain

$$\begin{aligned} g_i g_j &= \lim_{E\to E_\alpha}(E - E_\alpha)t_{ij} = \sum_{mn} v_{im}\hat{\Psi}_m v_{nj}\hat{\Psi}_n \\ &= \left[G_i^{-1}\hat{\Psi}_i G_j^{-1}\hat{\Psi}_j\right]_{E=E_\alpha}\,, \end{aligned} \tag{3.78}$$

which leads to the expression of the couplings in terms of the wave function at the origin of coordinate space,

$$g_i = [G_i^\alpha]^{-1}\,\hat{\Psi}_i\,. \tag{3.79}$$

Eq. (3.76) can then be rewritten as

$$\sum_i g_i^2 \left[\frac{dG_i}{dE}\right]_{E=E_\alpha} = -1\,, \tag{3.80}$$

in complete analogy with the case of only one channel. Each one of the terms in Eq. (3.80) (with opposite sign) gives the probability to find a certain channel in the wave function of the bound states.

3.3 Generalization to open channels

Now we want to adapt the formalism to the case of open channels. We work directly in coupled channels where at least one is open. We take again

$$\langle \vec{p}|V|\vec{p}\,'\rangle \equiv (2l+1)v\,\Theta(\Lambda-p)\Theta(\Lambda-p')|\vec{p}|^l|\vec{p}\,'|^l P_l(\cos\theta)\,. \tag{3.81}$$

In order to create a resonance from the interaction of many channels at a certain energy, we must take a channel which is open at this energy and make the two particles collide, starting from an infinite separation at $t=-\infty$. We call this channel, which is asymptotically the scattering state, channel 1.

The equations we have to solve are

$$|\Psi\rangle = |\Phi\rangle + \frac{1}{E-H_0}V|\Psi\rangle\,, \tag{3.82}$$

where

$$|\Psi\rangle = \begin{Bmatrix} |\Psi_1\rangle \\ |\Psi_2\rangle \\ \vdots \\ |\Psi_N\rangle \end{Bmatrix}\,, \qquad |\Phi\rangle = \begin{Bmatrix} |\Phi_1\rangle \\ 0 \\ \vdots \\ 0 \end{Bmatrix}\,, \tag{3.83}$$

and $|\Phi\rangle = |\vec{p}\,'\rangle$. Once again μ_i is the reduced mass of the system of total mass $M_i = m_{1i} + m_{2i}$.

3.3.1 Wave functions and couplings

We can proceed analogously to the bound states case and write the wave functions in momentum space as

$$\begin{aligned}
\langle \vec{p}|\Psi_1\rangle - \langle \vec{p}|\Phi_1\rangle &= (4\pi)^{1/2}\sum_m a_m Y_{lm}(\hat{p})\frac{|\vec{p}|^l\Theta(\Lambda-p)}{E-M_1-\frac{\vec{p}^{\,2}}{2\mu_1}+i\epsilon}\sum_j v_{1j}\int_{k<\Lambda} d^3k|\vec{k}|^l\langle\vec{k}|\tilde{\Psi}_j\rangle\,,\\
\langle \vec{p}|\Psi_i\rangle &= (4\pi)^{1/2}\sum_m a_m Y_{lm}(\hat{p})\frac{|\vec{p}|^l\Theta(\Lambda-p)}{E-M_i-\frac{\vec{p}^{\,2}}{2\mu_i}+i\epsilon}\sum_j v_{ij}\int_{k<\Lambda} d^3k|\vec{k}|^l\langle\vec{k}|\tilde{\Psi}_j\rangle\,, \qquad i\neq 1\,.
\end{aligned} \tag{3.84}$$

In the bound state case we had $E < M_i$ and, consequently, $E - M_i - \vec{p}^{\,2}/2\mu$ could not be zero for any value of E. We only had discrete eigenstates for some energies. Now, we are dealing with open channels and, since any value of E is allowed and we can have singularities when $E = M_i + \vec{p}^{\,2}/2\mu_i$, we need to put $+i\epsilon$ in order to guarantee a solution to the Lippmann-Schwinger equations.

In order to make the problem technically easy we shall prepare the state $|\Phi_1\rangle$ such that it contains only the l-wave:

$$|\Phi_1\rangle = \int d^3p' a(\vec{p}\,')|\vec{p}\,'\rangle \,. \tag{3.85}$$

We can choose $a(\vec{p}\,')$ such that

$$a(\vec{p}\,') = (4\pi)^{1/2} Y_{lm}(\hat{p'}) a(p') \,, \tag{3.86}$$

where $a(p')$ is, for instance, a Gaussian around p_1 and m is fixed. Thus, we find that

$$\begin{aligned} \langle \vec{p}|\Phi_1\rangle &= \int d^3p' (4\pi)^{1/2} Y_{lm}(\hat{p}\,') a(p') \langle \vec{p}|\vec{p}\,'\rangle \\ &= \int d^3p' (4\pi)^{1/2} Y_{lm}(\hat{p}\,') \delta^{(3)}(\vec{p} - \vec{p}\,') a(p') \\ &= (4\pi)^{1/2} Y_{lm}(\hat{p}) a(p) \,, \end{aligned} \tag{3.87}$$

with $a(p)$ normalized such that $\int d^3p\ a(p)|\vec{p}|^l = 1$.

Now all the terms in $|\Psi_i\rangle$ have the same angular dependence and we can write

$$\begin{aligned} \langle \vec{p}|\tilde{\Psi}_1\rangle &= a(p) + \frac{\Theta(\Lambda - p)|\vec{p}|^l}{E - M_1 - \frac{\vec{p}^{\,2}}{2\mu_1} + i\epsilon} \sum_j v_{1j} \int_{k<\Lambda} d^3k |\vec{k}|^l \langle \vec{k}|\tilde{\Psi}_j\rangle \,, \\ \langle \vec{p}|\tilde{\Psi}_i\rangle &= \frac{\Theta(\Lambda - p)|\vec{p}|^l}{E - M_i - \frac{\vec{p}^{\,2}}{2\mu_i} + i\epsilon} \sum_j v_{ij} \int_{k<\Lambda} d^3k |\vec{k}|^l \langle \vec{k}|\tilde{\Psi}_j\rangle \,, \qquad i \neq 1 \,. \end{aligned} \tag{3.88}$$

Now we integrate again in d^3p and multiply by $|\vec{p}|^l$, and since

$$\int d^3p |\vec{p}|^l \langle \vec{p}|\tilde{\Phi}_1\rangle = 1 \,, \tag{3.89}$$

we find

$$\begin{aligned} \int d^3p |\vec{p}|^l \langle \vec{p}|\tilde{\Psi}_1\rangle &= 1 + G_1 \sum_j v_{1j} \int_{k<\Lambda} d^3k |\vec{k}|^l \langle \vec{k}|\tilde{\Psi}_j\rangle \,, \\ \int d^3p |\vec{p}|^l \langle \vec{p}|\tilde{\Psi}_i\rangle &= G_i \sum_j v_{ij} \int_{k<\Lambda} d^3k |\vec{k}|^l \langle \vec{k}|\tilde{\Psi}_j\rangle \,, \qquad i \neq 1 \,, \end{aligned} \tag{3.90}$$

with G_i defined as

$$G_i = \int_{p<\Lambda} d^3p \frac{|\vec{p}|^{2l}}{E - M_i - \frac{\vec{p}^{\,2}}{2\mu_i} + i\epsilon} \,. \tag{3.91}$$

As in the previous case we can define

$$\hat{\Psi}_i = \int_{p<\Lambda} d^3p |\vec{p}|^l \langle \vec{p}|\tilde{\Psi}_i\rangle \,, \tag{3.92}$$

which allows us to rewrite Eqs. (3.90) as

$$\begin{aligned} \hat{\Psi}_1 &= 1 + G_1 \sum_j v_{1j}\hat{\Psi}_j \,, \\ \hat{\Psi}_i &= G_i \sum_j v_{ij}\hat{\Psi}_j \,, \qquad\qquad i \neq 1 \,. \end{aligned} \tag{3.93}$$

In matrix form, we have

$$(1 - Gv)\hat{\Psi} = \begin{Bmatrix} 1 \\ 0 \\ \vdots \\ 0 \end{Bmatrix} \tag{3.94}$$

and hence we can write Eqs. (3.93) as

$$\hat{\Psi}_i = (1 - Gv)^{-1}_{i1} \,. \tag{3.95}$$

The $N \times N$ scattering matrix is still given by

$$t = (1 - vG)^{-1}v = (v^{-1} - G)^{-1} \,, \tag{3.96}$$

and by means of Eq. (3.95) we can write

$$\begin{aligned} v_{ij}\hat{\Psi}_j &= v_{ij}(1 - Gv)^{-1}_{j1} \\ &= (v^{-1} - G)^{-1}_{i1} = t_{i1} \,. \end{aligned} \tag{3.97}$$

Going back to Eq. (3.88), it follows

$$\begin{aligned} \langle \vec{p}|\Psi_1\rangle &= (4\pi)^{1/2} Y_{lm}(\hat{p}) \left(a(p) + \frac{\Theta(\Lambda - p)|\vec{p}|^l}{E - M_1 - \frac{\vec{p}^2}{2\mu_1} + i\epsilon} t_{11} \right) \,, \\ \langle \vec{p}|\Psi_i\rangle &= (4\pi)^{1/2} Y_{lm}(\hat{p}) \frac{\Theta(\Lambda - p)|\vec{p}|^l}{E - M_i - \frac{\vec{p}^2}{2\mu_i} + i\epsilon} t_{i1} \,, \qquad\qquad i \neq 1 \,. \end{aligned} \tag{3.98}$$

In coordinate space, the wave functions can be written as

$$\begin{aligned} \langle \vec{x}|\Psi_1\rangle &= (4\pi)^{1/2}\ i^l\ Y_{lm}(\hat{r}) \int \frac{d^3p}{(2\pi)^{3/2}}\ j_l(pr) \left(a(p) + \frac{\Theta(\Lambda - p)|\vec{p}|^l}{E - M_1 - \frac{\vec{p}^2}{2\mu_1} + i\epsilon} t_{11} \right) \,, \\ \langle \vec{x}|\Psi_i\rangle &= (4\pi)^{1/2}\ i^l\ Y_{lm}(\hat{r}) \int \frac{d^3p}{(2\pi)^{3/2}}\ j_l(pr) \frac{\Theta(\Lambda - p)|\vec{p}|^l}{E - M_i - \frac{\vec{p}^2}{2\mu_i} + i\epsilon} t_{i1} \qquad\qquad i \neq 1 \,. \end{aligned} \tag{3.99}$$

We take again the limit of small argument for the Bessel's functions (Eq. (3.46)) obtaining

$$\begin{aligned}\langle \vec{x} \to 0|\Psi_1\rangle &= \frac{(4\pi)^{1/2} Y_{lm}(\hat{r}) i^l |\vec{r}|^l}{(2\pi)^{3/2}(2l+1)!!} \left[1 + G_1 t_{11}\right] \\ &= \frac{(4\pi)^{1/2} Y_{lm}(\hat{r}) i^l |\vec{r}|^l}{(2\pi)^{3/2}(2l+1)!!} \left[1 + G_1 \sum_j v_{ij} \hat{\Psi}_j\right] \\ &= \frac{(4\pi)^{1/2} Y_{lm}(\hat{r}) i^l |\vec{r}|^l}{(2\pi)^{3/2}(2l+1)!!} \hat{\Psi}_1 \,,\end{aligned} \tag{3.100}$$

and, similarly

$$\langle \vec{x} \to 0|\Psi_i\rangle = \frac{(4\pi)^{1/2} Y_{lm}(\hat{r}) i^l |\vec{r}|^l}{(2\pi)^{3/2}(2l+1)!!} \hat{\Psi}_i \,, \qquad i \neq 1 \,. \tag{3.101}$$

In the vicinity of a resonance the scattering amplitude can be written as

$$t_{ij} \simeq \frac{g_i g_j}{E - E_R + i\frac{\Gamma}{2}} \,. \tag{3.102}$$

Hence

$$\frac{t_{i1}}{t_{11}} = \frac{g_i}{g_1} = \frac{\hat{\Psi}_i G_i^{-1}}{\hat{\Psi}_1 G_1^{-1}} \,. \tag{3.103}$$

We can also use Eq. (3.3) for the Lippmann-Schwinger equation, repeat the steps of section (3.35) and find, analogously, that

$$g_i = \hat{\Psi}_i G_i^{-1} \,. \tag{3.104}$$

3.3.2 The compositeness condition

In the case of resonances we cannot directly derive the sum rule in Eq. (3.80), since it follows from the normalization condition of the wave function in coordinate space, which is not finite any more. However, it still holds at the pole in the complex plane (see Ref. [95] for a different derivation), where again we have

$$\sum_i g_i^2 \left[\frac{dG_i}{dE}\right]_{E=E_P} = -1 \,, \tag{3.105}$$

with E_P the position of the complex pole and g_i is the coupling to the channel i defined as

$$g_i g_j = \lim_{E \to E_P} (E - E_P) t_{ij} \,. \tag{3.106}$$

Note that this definition leads to complex couplings and the sum rule that we derive is obtained in terms of them.

In **Chapter 4** we shall rewrite Eq. (3.105) for complex energies and discuss the meaning of each term. We anticipate here that each term represents the integral of the wave function squared (not the modulus squared) of each component, but this occurs only in a certain phase convention for the wave function that we shall then discuss. The terms of Eq. (3.105) are complex, which means that the imaginary parts cancel and then one has

$$\sum_i \mathrm{Re}\left(g_i^2\left[\frac{dG_i}{dE}\right]_{E=E_R}\right) = -1\,. \tag{3.107}$$

Knowing the meaning of these terms, we can consider each one of them as a measure of the relevance or weight of a given channel in the wave function of the state, but not a probability, which for open channels is not a useful concept since it will diverge.

As we already briefly mentioned in **Section 3.2.2**, sometimes, our knowledge of all needed coupled channels will be incomplete and we shall only have information on hadron-hadron scattering. There can be a genuine component different to the hadron-hadron one that we study. In order to take into account the weight of this genuine component, Eq. (3.105) can be rewritten as

$$-\sum_i \mathrm{Re}\left(g_i^2\left[\frac{dG_i}{dE}\right]_{E=E_P}\right) = 1-Z\,, \qquad Z = \mathrm{Re}\int d^3p\,(\Psi_\beta(p))^2\,, \tag{3.108}$$

where $\Psi_\beta(p)$ is the genuine component in the wave function of the state, when it is omitted from the coupled channels.

Note that the fixing of a phase in the wave function of one channel will determine the phase of the other wave functions in a coupled set of Lippman-Schwinger equations (see Eqs. (3.82) and (3.83)).

The left-hand side of Eq. (3.108) is the measure of this weight of hadron-hadron component, while its diversion from unity measures the weight of something different in the wave function. The interpretation of Z as a probability for the non meson-baryon component is rigorous for bound states. For poles in the complex plane we have to reinterpret these numbers, as we have mentioned here, and this will be thoroughly discussed in **Chapter 4**.

3.4 Application to meson resonances: the ρ and the K^*

The formalism developed is now used to investigate the nature of resonant states. In Refs. [97] and [98], we use this tool to analyse two meson resonances,

the ρ and the K^*. It is known that the ρ is not dynamically generated by the p-waves interaction of two π mesons, but it is generally considered as a genuine resonance [103]. Thus, we expect the sumrule of Eq. (3.105) not to be satisfied. On the other hand, the K^* particle shows up as a resonance in πK scattering, also in p-waves.

In order to quantify the compositeness of these two particles and identify their nature, we perform two tests: the first one, in **Section 3.4.1**, relying on a model based on chiral unitary theory, suitable for the description of the two states; in **Section 3.4.2** we propose a second one, purely phenomenological, where only scattering data are used.

3.4.1 The chiral unitary model

The first ingredient we need in order to apply the sum rule we found to specific cases is an appropriate potential describing the hadron-hadron interaction, v. As we saw in the previous sections, the formalism developed requires this potential to be independent of the momentum, since the factor $|\vec{p}|^{2l}$ (with $l = 1$) which takes into account the p-wave character of the processes, is now absorbed in the loop function.

We use the tree level potentials of Refs. [99] and [41], where the $\pi\pi$ and πK interactions in p-waves are respectively studied. These potentials are slightly modified in order to remove the dependence on the momentum and they read

$$\begin{aligned} v_\rho &= -\frac{2}{3f^2}\left(1+\frac{2G_V^2}{f^2}\frac{s}{M_\rho^2-s}\right), \\ v_{K^*} &= -\frac{1}{2f^2}\left(1+\frac{2G_V^2}{f^2}\frac{s}{M_{K^*}^2-s}\right), \end{aligned} \tag{3.109}$$

where M_ρ and M_{K^*} are the bare ρ and K^* masses, f is the π decay constant and G_V the coupling to $\pi\pi$ in the formalism of Ref. [25], where $G_V \simeq f/\sqrt{2}$.

In Ref. [104] this model for the ρ meson, still including the momentum dependence, was fitted to $\pi\pi$ data for the phase-shift in $I = 1$ and the values $f = 87.4$ MeV, $G_V = 53$ MeV and $M_\rho = 837.3$ MeV were obtained (very similar to those used in Ref. [99]). Now we must use a different potential and, as explained in the discussion after Eq. (3.11), the $|\vec{p}|^{2l}$ factor is included in the loop function. This means we have to redo the fit to the data using

$$t = \frac{1}{v^{-1} - G}, \tag{3.110}$$

with our new loop function

$$G(s) = \int \frac{d^3q}{(2\pi)^3}\frac{q^2}{s-(\omega_1+\omega_2)^2+i\epsilon}\left(\frac{\omega_1+\omega_2}{2\omega_1\omega_2}\right), \tag{3.111}$$

	f [MeV]	G_V [MeV]	M [MeV]	q_{max} [MeV]
ρ	93	53	855.36	661.52
K^*	86	54	995.76	724.70

Table 3.1: Values obtained from the best fit to the data for the parameters f, G_V, M and q_{max} for both $\pi\pi$ and πK scattering.

where $\omega_i = \sqrt{m_i^2 + q^2}$ and a relativistic reformulation is assumed [30]. In the case of the ρ, $m_1 = m_2 = m_\pi$, while for the K^* we have $m_1 = m_\pi$ and $m_2 = m_K$. The loop function of Eq. (3.111) is regularized by means of the cutoff $\theta(\Lambda - |\vec{q}|)$ contained in the potential (see Eq. (3.51)). Hence Λ plays the role of q_{max} in the integral of Eq. (3.111).

The p-wave phase shift is given by (see [99, 104])

$$T = p^2 t = \frac{-8\pi\sqrt{s}}{p\cot\delta(p) - ip}\,, \tag{3.112}$$

with p the three-momentum of the particles in the center of mass reference frame. The best fit to the data produces, for the four parameters f, G_v, M and q_{max}, the values listed in **Table 3.1**. The results can be seen in **Figure 3.1**.

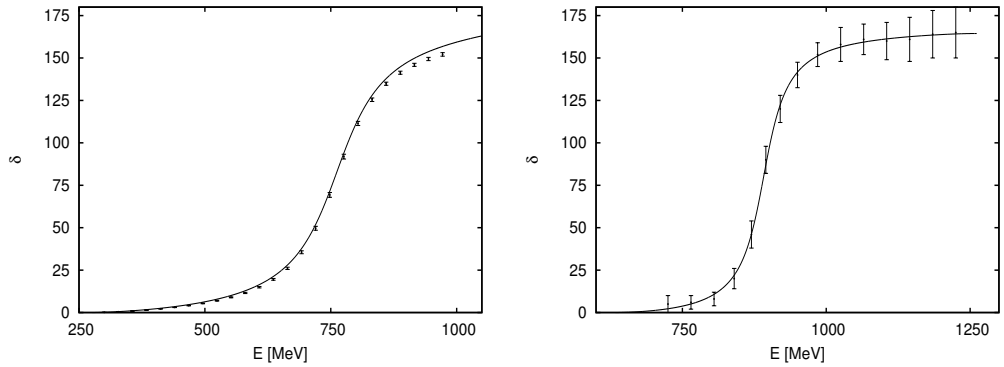

Figure 3.1: In the left panel, the solid curve represents the best fit to the phase shift data for $\pi\pi$ scattering in p-wave obtained with the new approach. The data are taken from Ref. [105], obtained using the Roy equations. In the right panel, we show the same for the case of πK scattering, with data taken from Refs. [41, 106, 107].

In order to apply the sum rule to the case of a resonance, we need to extrapolate the amplitude to the complex plane and look for the complex pole s_0 in the second Riemann sheet. This is done by changing G to G^{II} in Eq. (3.110) to obtain t^{II}.

$G^{II}(s)$ is the analytic continuation to the complex plane of the loop function

in p-wave for the two pions,

$$G^{II}(s) = G^{I}(s) + i\frac{p^3}{4\pi\sqrt{s}}\,, \qquad Im(p) > 0\,, \tag{3.113}$$

G^I and G^{II} are the loop functions in the first and second Riemann sheet and G^I is given by Eq. (3.111).

We are now able to determine the coupling to the hadron-hadron state, $\tilde{g}_R$, with $R = \rho, K^*$, as the residue at the pole of the amplitude,

$$\tilde{g}_R^2 = \lim_{s\to s_0}(s - s_0)t^{II}\,. \tag{3.114}$$

For the best fit to the data, we find the pole in

$$\sqrt{s_0^\rho} = (761.7 + i\ 71.4)\ MeV\,, \tag{3.115}$$

in the case of $\pi\pi$ scattering, in good agreement with what was obtained in Ref. [104], and in

$$\sqrt{s_0^{K^*}} = (891.0 + i\ 31.3)\ MeV\,, \tag{3.116}$$

in the case of πK scattering, in good agreement with the results of Refs. [108, 109]. For the couplings we get

$$\tilde{g}_\rho = (6.86 + i\ 0.41) \tag{3.117}$$

and

$$\tilde{g}_{K^*} = (7.19 + i\ 0.67)\,. \tag{3.118}$$

As anticipated in **Section 3.3**, we get complex values for the couplings when dealing with resonances and their complex energies.

We can use the sum rule of Eq. (3.108) for one single channel in order to evaluate its contribution to the production of the resonance,

$$-\,Re\left(\tilde{g}_R^2\left[\frac{dG^{II}(s)}{ds}\right]_{s=s_0}\right) = 1 - Z\,, \tag{3.119}$$

where Z represents the probability that the resonance considered is not a molecular state but something else.

We find that in the case of the ρ meson

$$1 - Z = 0.004\,, \tag{3.120}$$

while, for the K^*,

$$1 - Z = 0.122\,. \tag{3.121}$$

These two last results indicate that the amount of $\pi\pi$ in the wave function of the ρ and the amount of πK in the wave function of the K^* are both small.

3.4.2 The phenomenological approach

The exercise done before requires a theoretical model. Now we want to verify if it is possible to reach similar conclusions using only data with a pure phenomenological analysis.

The value of the coupling g can be obtained experimentally but in order to apply the sum rule we also need the derivative of the loop function. In the case of s-wave this is straightforward since $\frac{dG}{dE}$ is a convergent magnitude, even when $q_{max} \to \infty$. This is, however, not the case for a p-wave resonance, such that extra work is required.

The ρ and K^* amplitudes in a relativistic form can be written as

$$t_R = \frac{g_R^2}{s - m_R^2 + i m_R \Gamma_R \left(\frac{p}{p_{on}}\right)^3} , \tag{3.122}$$

where

$$p_{on} = p(\sqrt{s} = m_R) . \tag{3.123}$$

On the other hand, the coupling is related to the width through the equation

$$g_R^2 = \frac{8\pi m_R^2 \Gamma_{on}}{p_{on}^3} , \tag{3.124}$$

with values of the mass m_R and the width Γ_{on} of the ρ and K^* given by experiment.

We obtain t_R in the second Riemann sheet from Eq. (3.122) by taking s as complex, $s = a + i\ b$, and $p \to -p$ in the width term. Then we proceed as in the former subsection to get the pole and the coupling. We obtain

$$\begin{aligned} \sqrt{s_0^\rho} &= (751.1 + i\ 68.4)\ \mathrm{M}eV , \\ g_\rho &= (6.58 + i\ 1.01) , \end{aligned} \tag{3.125}$$

in the case of the ρ, while for the K^* we find

$$\begin{aligned} \sqrt{s_0^{K^*}} &= (892.0 + i\ 22.4)\ \mathrm{M}eV , \\ g_{K^*} &= (6.08 + i\ 0.50) . \end{aligned} \tag{3.126}$$

In both cases the values are very similar to those obtained in the previous section with chiral unitary approach.

However, when doing the $1 - Z$ test one does not know which value of the cutoff q_{max} should be used to regularize the G function. Hence, the best one can do is to use natural values of the cutoff and hope that the results are stable for a certain range of q_{max}, since $\frac{dG}{ds}$ is only logarithmically divergent.

	q_{max} $[GeV]$	$1-Z$
ρ	0.7	0.07
	0.8	0.09
	0.9	0.12
	1.0	0.13
	1.1	0.15
	1.2	0.16
K^*	0.7	0.08
	0.8	0.09
	0.9	0.11
	1.0	0.12
	1.1	0.14
	1.2	0.15

Table 3.2: Values of $1-Z$ for different cutoffs q_{max} and for the ρ and K^* cases.

The values of the strength $1-Z$ obtained changing the cutoff q_{max} are shown in **Table 3.2** for both the ρ and the K^*. As we can see, the results are rather stable and similar to those obtained in the former subsection with the same conclusion.

Note that since $1-Z$ is a small number, even relatively large uncertainties in this quantity are small errors on Z, which measures the amount by which the ρ and the K^* are not a $\pi\pi$ and a πK composite state.

3.5 Results and Conclusions

In this Chapter, we have made an analytical study of the scattering matrix and wave function for the case of the interaction of a pair of hadrons. For this purpose we have followed closely the formalism developed in the framework of chiral unitary theory but using quantum mechanics and making detailed derivations of the relations of interest. The novelty of the work is the extension of this formalism to the case of any partial waves.

We started with the case of bound states, for both single channel and coupled channels production, and then we repeated the analysis for open channels. We found interesting relations between the couplings of bound states and resonances to the hadron-hadron channels and the wave functions at the origin. Of particular value are the sum rules obtained.

In the case of bound states, the sum rule has an unambiguous interpretation that follows directly from the normalization of the wave function. It allows to determine the probability to find a certain hadron-hadron component in the

wave function. In particular, when the sum of these probabilities is unity, we can say that this state is a composite hadron-hadron state. When the sum is different from unity, this difference gives us a measure of the probability to find a genuine component in the wave function of non hadron-hadron molecular nature. In this sense we say that we extended the compositeness condition derived by Weinberg in the case of bound states and limited to s-waves to any partial waves. The case of open channels is more controversial, since the sum rule cannot be simply derived from the normalization of the wave function as in the previous case. However, it still holds at the pole.

As anticipated in **Section 3.3.2** a more complete analysis of the meaning of the sum rule in the case of open channels will be given in **Chapter 4**. We will see how, due to the complex character of the quantities involved, it is the real part of each term of the sum what can, in the end, be associated to the weight of the hadron-hadron component in the wave function.

The sum rule can be used to extract important information on the nature of resonances using experimental data. In particular, we applied it to two concrete cases, the ρ and the K^* meson, to check the amount of $\pi\pi$ and $K\pi$ character in their wave functions, respectively. We first calculated their couplings to the hadron-hadron component using the tree level chiral potentials. The poles corresponding to the position of the resonances in the complex plane have been obtained fitting our model to the data for the phase shifts and, together with the couplings, they are used to evaluate the amount of compositeness in the wave function of the states, which turned out to be very small in both cases. We also applied a phenomenological method to corroborate these results, relying only on the relation between the couplings and the mass and width of the particles. We obtained for the couplings and for the pole in the scattering matrix values consistent with the former ones and also in this case, the amount of hadron-hadron character in the resonance turned out to be very small, in agreement with the commonly accepted idea that the ρ and the K^* are genuine resonances and not dynamically generated by the interaction of two mesons.

CHAPTER 4

APPLICATION TO BARYONS AND INTERPRETATION

4.1 Introduction

In the previous chapter we have shown how the sum rule of Eq. (3.108) has been successfully used to investigate the nature of two meson resonances, the ρ and K^*. This Chapter is devoted to the analysis of some relevant baryonic states.

Thus, in complete analogy with the previous chapter, in **Section 4.2** and **Section 4.3**, the extended compositeness condition is used to determine the weight of the meson-baryon component in the $\Delta(1232)$ resonance and in the other members of the $J^P = \frac{3}{2}^+$ baryon decuplet respectively. The results presented here, have already been published in Ref. [110] and they represent the first attempt to describe the nature of baryons by means of the compositeness condition. Follow-ups of this idea can be found in Refs. [111, 112].

Section 4.4 is dedicated to the interpretation of the sum rule when dealing with resonances, which implies the appearance of complex values of energies and couplings, while in **Section 4.5** we analyse the effect of having an energy dependent potential in a single channel problem and how this is tied to the possibility of having something different from the hadron-hadron component in the wave function of the state under study.

Later, in **Section 4.6.1**, also the nature of the $\Lambda(1520)$ is investigated. The $\Lambda(1520)$ belongs to the $J^P = \frac{3}{2}^-$ resonances that in the last few years have been interpreted as being dynamically generated from the interaction of the octet of the pseudoscalar mesons with the decuplet of the baryons [113, 114]. It has been studied theoretically in Refs. [113, 114] and it is considered to be generated from the interaction of the coupled channels $\pi\Sigma(1385)$ and $K\Xi(1530)$

in s-wave. In this picture, it couples mostly to the first channel, qualifying as a quasibound state of $\pi\Sigma^*$, with a nominal mass of a few MeV below the $\pi\Sigma^*$ threshold. However, the large branching ratios to $\bar{K}N$ and $\pi\Sigma$ indicate that these two channels must play a remarkable role in the building up of the resonance in spite of the fact that they couple in d-wave.

In Ref. [115] a coupled channels analysis of the $\Lambda(1520)$ data using $\pi\Sigma^*$, $K\Xi^*$, $\bar{K}N$ and $\pi\Sigma$ has been performed. In this work, the $\pi\Sigma^*$ channel is still the one with the largest coupling, but its strength is reduced with respect to the quasibound $\pi\Sigma^*$ picture. At the same time, the couplings to $\bar{K}N$ and $\pi\Sigma$ are remarkable, making these two channels relevant for the interpretation of different reactions involving the $\Lambda(1520)$. The model provided in Ref. [115] has been tested in Ref. [116] through the study of the two reactions $pp \to pK^+K^-p$ and $pp \to pK^+\pi^0\pi^0\Lambda$ close to the $\Lambda(1520)$ threshold, giving important information about the couplings of the $\Lambda(1520)$ to $\bar{K}N$ and $\pi\Sigma^*$. Here we make an estimate of the relevance of the different channels in the wave function of the $\Lambda(1520)$, starting from the coupled channel study of Refs. [115] and [116]. This section relates to Ref. [117].

4.2 πN scattering and the $\Delta(1232)$ resonance

In this section we investigate the amount of πN in the wave function of the $\Delta(1232)$. We follow the same steps of **Section 3.4**, performing a first test based on chiral unitary theory and then a phenomenological one.

4.2.1 The chiral unitary model

The tree level potential we use is of the type

$$v = -\alpha \left(1 + \frac{\beta}{M^2 - s}\right) , \tag{4.1}$$

where M is the bare mass of the Δ resonance and α and β are two constant factors. It is important to notice that, in order to accommodate a possible genuine component of the $\Delta(1232)$ in its wave function, we are putting explicitly a CDD pole in v [102]. As already stressed in the previous chapter, we also need to account for the p-wave character of the process and this means that the potential v must be independent of the momenta of the particles.

Now, we fit the πN data for the phase shifts using Eq. (3.110) for the scattering amplitude. Since the pion is relativistic in the decay of the $\Delta(1232)$, we generalize the equations as already done for the case of $\rho \to \pi\pi$ in Ref. [97]. We take only the positive energy part of the relativistic generalization

M [MeV]	q_{max} [MeV]	α [MeV]	β [MeV]
1313.8	452.6	$698.0 \cdot 10^3$	112.5

Table 4.1: Values obtained from the best fit to the phase shift data for the parameters M, q_{max}, α and β for the πN scattering.

of the loop function, modified to contain the $|\vec{q}|^2$ factor, that in the case of meson-baryon intermediate states reads

$$G(s) = \int \frac{d^3q}{(2\pi)^3} \frac{1}{2\omega(q)} \frac{M_N}{E_N(q)} \frac{q^2}{\sqrt{s} - \omega(q) - E_N(q) + i\epsilon}\,, \tag{4.2}$$

with M_N the mass of the nucleon, m_π the mass of the pion, $E_N(q) = \sqrt{\vec{q}^2 + M_N^2}$ and $\omega(q) = \sqrt{\vec{q}^2 + m_\pi^2}$ the energies of the two particles respectively. Once again, the loop function in Eq. (4.2) is regularized by means of a cutoff coming from the potential, which we call q_{max}.

To be more in agreement with a propagator having a denominator linear in the energy, we slightly modify Eq. (4.1) as

$$v = -\frac{\alpha}{M_\Delta^4} \left(1 + \frac{\beta}{M - \sqrt{s}}\right)\,, \tag{4.3}$$

where the factor $1/M_\Delta^4$ is introduced in order to have both parameters, α and β, in units of MeV.

The πN phase shift is given by the formula [118]

$$T = p^2 t = \frac{-4\pi\sqrt{s}}{M_N} \frac{1}{p\cot\delta(p) - ip}\,, \tag{4.4}$$

with p the momentum of the particles in the center of mass reference frame.

From the best fit to the πN data we obtain, for the four parameters M, q_{max}, α and β, the values reported in **Table 4.1**. The results of the fit are shown in **Figure 4.1**.

Now we want to apply the sum rule of Eq. (3.108) to our case. Like in **Chapter 3**, we need to extrapolate the amplitude to the complex plane. In order to look for the complex pole $\sqrt{s_0}$ in the second Riemann sheet, we change again G to G^{II} in Eq. (3.110), to obtain t^{II}. In the case of baryons, G^{II} reads

$$G^{II}(s) = G^I + \frac{i}{2\pi} \frac{M_N}{\sqrt{s}} p^3\,, \qquad Im(p) > 0\,, \tag{4.5}$$

with G^I and G^{II} the loop functions in the first and second Riemann sheet, and G^I given by Eq. (4.2).

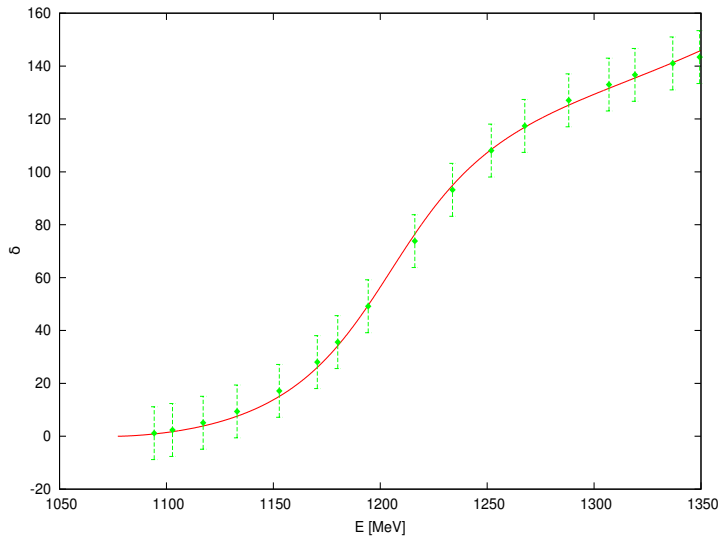

Figure 4.1: The solid curve represents the πN scattering p-wave phase shifts obtained with the new approach. The data are taken from [119].

We are now able to obtain the coupling $\tilde{g}_\Delta$ as the residue at the pole of the amplitude and to apply the sum rule of Eq. (3.108) to evaluate the πN contribution to the Δ resonance as

$$-\,Re\left[\tilde{g}_\Delta^2\left[\frac{dG^{II}(s)}{d\sqrt{s}}\right]_{\sqrt{s}=\sqrt{s_0}}\right]=1-Z\,, \tag{4.6}$$

with Z the weight of something different from a πN state in the Δ.

The value of the pole that we get for the best fit is

$$\sqrt{s_0}=(1204.6+i\,44.4)\ MeV\,, \tag{4.7}$$

while for the coupling we find

$$\tilde{g}_\Delta=(8.53+i\,1.85)\cdot 10^{-3}\ MeV^{-1}\,. \tag{4.8}$$

From these values we finally obtain

$$-\,\tilde{g}_\Delta^2\left[\frac{dG^{II}(s)}{d\sqrt{s}}\right]_{\sqrt{s}=\sqrt{s_0}}=(0.62-i\,0.41)\,, \tag{4.9}$$

and

$$1-Z=0.62\ , \tag{4.10}$$

which indicates a sizeable weight of πN in the resonance.

q_{max} $[GeV]$	$-g^2\frac{dG^{II}}{d\sqrt{s}}$	$1-Z$
0.4	$0.47-i0.38$	0.47
0.5	$0.57-i0.29$	0.57
0.6	$0.65-i0.22$	0.65

Table 4.2: Values of $-g^2\frac{dG^{II}}{d\sqrt{s}}$ and $1-Z$ for different cutoffs q_{max}.

4.2.2 The phenomenological approach

Now we repeat the phenomenological analysis of **Section 3.4.2** to test the sum rule by means only of experimental data.

The Δ amplitude in a relativistic form is given by

$$t_\Delta = \frac{g_\Delta^2}{\sqrt{s}-M_\Delta+i\frac{\Gamma_{on}}{2}\left(\frac{p}{p_{on}}\right)^3}\,, \tag{4.11}$$

where

$$g_\Delta^2 = \frac{2\pi M_\Delta \Gamma_{on}}{p_{on}^3 M_N}\,. \tag{4.12}$$

The values of M_Δ and Γ_{on} are known from the experiment.

Defining $\sqrt{s}=a+ib$ and making the substitution $p\to -p$ in the width term, we obtain the amplitude t_Δ in the second Riemann sheet. Then, we proceed as before to get the pole and the coupling.

The values we obtain,

$$\begin{aligned}\sqrt{s_0} &= (1208.0+i\,40.9)\ MeV\,,\\ g_\Delta &= (7.78+i\,1.86)\cdot 10^{-3}\ MeV^{-1}\,,\end{aligned} \tag{4.13}$$

are very similar to those obtained with the procedure of the former subsection.

In this case we do not know the size of the cutoff q_{max} needed to regularize the loop function, but the derivative of G^{II} in Eq. (4.6) is logarithmically divergent in the case of p-waves. Then, using natural values for the cutoff, as done in the previous chapter for the ρ and K^* mesons, we can establish if the results are stable in a certain range of q_{max}.

The values of $1-Z$ for three different values of q_{max} are shown in **Table 4.2**. They are rather stable and consistent with the result obtained in the previous section.

4.3 Application to the other $J^P=\frac{3}{2}^+$ resonances

Now we extend the study of the hadron-hadron content of resonances to the whole $J^P=\frac{3}{2}^+$ baryons decuplet, applying the phenomenological test of **Sec-**

tion 4.2.2 to the $\Sigma(1385)$, $\Xi(1530)$ and Ω^-.

We first investigate the $\pi\Lambda$ and $\pi\Sigma$ content of the $\Sigma(1385)$ wave function. It is known from the PDG [17] that the $\Sigma(1385)$ couples to these two channels with different branching ratios: 87% and 11.7%, respectively. In order to evaluate the couplings of the resonance to the single channel, the branching ratios must be taken into account, modifying Eq. (4.12) as follows:

$$g^2_{\Sigma^*,i} = \frac{2\pi M_{\Sigma^*}\Gamma_{on}}{p^3_{(i)on} M_i} \cdot BR^{(i)} \,, \tag{4.14}$$

where $BR^{(i)}$ is the branching ratio to the channel i, with $i = \pi\Lambda, \pi\Sigma$ and

$$p^{(i)}_{on} = p^{(i)}(\sqrt{s} = M_{\Sigma^*}) \,, \tag{4.15}$$

where

$$p^{(i)} = \frac{\lambda^{1/2}(s, M_i^2, m_\pi^2)}{2\sqrt{s}} \,. \tag{4.16}$$

The case of the $\Xi(1530)$ is completely analogous to the one of the $\Delta(1232)$, since, according to the PDG [17] it couples to the $\pi\Xi$ channel with a branching ratio of 100%. Hence, the coupling $g_{\Xi^*,\pi\Xi}$ is simply given by Eq. (4.12), doing the substitutions $M_\Delta \to M_{\Xi^*}$ and $M_N \to M_\Xi$.

On the other hand, the case of the Ω^- is different since this resonance is stable to strong decays. This means that the on shell amplitude Γ_{on} is zero and this prevents us from evaluating the coupling of the resonance to the $\bar{K}\Xi$ channel using Eq. (4.12). However, from $SU(3)$ symmetry considerations we can relate the $g_{\Omega^-,\bar{K}\Xi}$ coupling to $g_{\Delta,\pi N}$, since their ratios are simply ratios of Clebsch-Gordan coefficients. We find that

$$g^2_{\Omega^-,\bar{K}\Xi^0} = 2g^2_{\Delta,\pi N} \,. \tag{4.17}$$

The amplitude in relativistic form is again given by Eq. (4.11) and, in the case of the $\Sigma(1385)$ and $\Xi(1530)$, it is extrapolated to the second Riemann sheet in order to evaluate the pole and the new couplings. Since, as already said, the Ω^- does not decay through the strong interaction, the pole of the amplitude is found on the real axis, with no need to go to the second Riemann sheet. It is then possible to apply the sum rule, evaluating the derivative of the G function in the position of the pole. To do it we use a cutoff of the same order of magnitude as the one found doing the best fit for the $\Delta(1232)$, $q_{max} \simeq 450$ MeV. The results obtained for the three resonances are shown in **Table 4.3**. We also show the cutoff dependence of $1 - Z$, analogously to **Table 4.2**, in **Table 4.4**. We can see that the amount of meson-baryon component is smaller than for the case of the $\Delta(1230)$.

	Channel	$\sqrt{s_0}$ $[MeV]$	g $[MeV]^{-1}$	$1-Z$
$\Sigma(1385)$	$\pi\Lambda$	$1380.4 + i17.3$	$(5.11 + i0.60) \cdot 10^{-3}$	0.16
	$\pi\Sigma$	$1377.4 + i16.0$	$(3.63 + i0.81) \cdot 10^{-3}$	0.10
$\Xi(1530)$	$\pi\Xi$	$1532.9 + i4.7$	$(4.36 + i0.23) \cdot 10^{-3}$	0.11
Ω^-	$\bar{K}\Xi$	1672.4	$(1.56 + i0.37) \cdot 10^{-2}$	0.26

Table 4.3: Values of poles, couplings and $1-Z$ for the three baryons of the decuplet $J^P = \frac{3}{2}^+$, $\Sigma(1385)$, $\Xi(1530)$ and Ω^-, for a cutoff $q_{max} = 450\ MeV$.

	Channel	q_{max} [GeV]	$1-Z$
$\Sigma(1385)$	$\pi\Lambda$	0.4	0.13
		0.5	0.19
		0.6	0.24
$\Sigma(1385)$	$\pi\Sigma$	0.4	0.09
		0.5	0.10
		0.6	0.12
$\Xi(1530)$	$\pi\Xi$	0.4	0.09
		0.5	0.12
		0.6	0.15
Ω^-	$\bar{K}\Xi$	0.4	0.18
		0.5	0.34
		0.6	0.53

Table 4.4: Values of $1-Z$ for different cutoffs q_{max} for the three baryons of the decuplet $J^P = \frac{3}{2}^+$, $\Sigma(1385)$, $\Xi(1530)$ and Ω^-.

4.4 Interpretation of the sum rule for resonances

In the previous sections we have obtained values of $-g^2 \frac{dG^{II}}{d\sqrt{s}}$ which are complex and, thus, the probabilistic interpretation of the different terms of the sum rule in Eq. (3.107) presents some difficulties. The aim of this section is to clarify the meaning of these terms.

Before we give a general formulation of the sum rule for complex energies based on the results of Refs. [94, 96, 97], let us visualize it in a particular case with two channels, one of them closed and the other one open. Let us also assume, for simplicity, that the interaction in the closed channel is strong and attractive and let us neglect the diagonal interaction in the open channel. Thus, we have a potential like the one of Eq. (3.81) but now

$$v = \begin{pmatrix} v_{11} & v_{12} \\ v_{12} & 0 \end{pmatrix} . \tag{4.18}$$

The results that we get are general and the inclusion of v_{22} is straightforward though it does not add any important information to the discussion. We shall also assume for simplicity that $|v_{12}| \ll |v_{11}|$ only to relate, later on in this section, the imaginary part of the pole position to the width.

The t matrix is given by Eq. (3.110), that for the simple case of two channels means

$$t = \begin{pmatrix} v_{11} + v_{12}^2 G_2 & v_{12} \\ v_{12} & v_{12}^2 G_1 \end{pmatrix} \cdot \frac{1}{1 - v_{11} G_1 - v_{12}^2 G_1 G_2} . \tag{4.19}$$

Let us now assume that we have a pole in the bound region of channel 1 and open region of channel 2. Then, the denominator of t in Eq. (4.19) will be zero,

$$1 - v_{11} G_1 - v_{12}^2 G_1 G_2 = 0 \, , \tag{4.20}$$

but G_2 is complex in the first Riemann sheet and, in particular, for p-waves,

$$\mathrm{Im} G_2^I = -i 4\pi^2 \mu_2 \, k_2^3 \tag{4.21}$$

in the non-relativistic formulation and

$$\mathrm{Im} G_2^I = -i \frac{1}{4\pi} \frac{M_N}{\sqrt{s}} \, k_2^3 \tag{4.22}$$

in the relativistic one of **Section 4.2**, with $k_i = \sqrt{2\mu_i (E - m_{1i} - m_{2i})}$ or $k_i = \lambda^{1/2}(s, m_{1i}^2, m_{2i}^2)/2\sqrt{s}$ respectively, for $i = 2$.

Let us assume that the attractive v_{11} interaction is strong enough to produce a bound state in channel 1 with energy E_1, when only this channel is considered. Then, we would have

$$1 - v_{11} G_1(E_1) = 0 \ . \tag{4.23}$$

The addition of the interaction v_{12} will change this energy and Eq. (4.20) can be rewritten, taking Eq. (4.23) into account and remembering that v_{ij} is taken independent of the energy, as

$$- v_{11} \frac{\partial G_1}{\partial E}(E_R - E_1) - v_{12}^2 G_1 G_2 = 0 \, , \tag{4.24}$$

where E_R will be the new energy of the system.

Since $v_{11} < 0$ and $\frac{\partial G_1}{\partial E} < 0$ in the bound region, we have

$$E_R - E_1 = -\alpha \, v_{12}^2 G_1 G_2 \ , \qquad\qquad \alpha > 0 \, , \quad G_1 < 0 \tag{4.25}$$

where $\alpha = \left(v_{11} \frac{\partial G_1}{\partial E}\right)^{-1}$.

The complex value of G_2, see Eqs. (4.21) and (4.22), was obtained for an energy $E + i\epsilon$. We gradually continue along the complex plane making the $i\epsilon$ finite, $i\frac{\Gamma}{2}$, and Eq. (4.25) gives

$$\tilde{E}_R + i\frac{\Gamma}{2} = -\alpha \, v_{12}^2 G_1 G_2 \ , \tag{4.26}$$

$$\frac{\Gamma}{2} \simeq -\alpha \, v_{12}^2 G_1 \mathrm{Im} G_2 \ , \tag{4.27}$$

which is impossible to fulfill in the first Riemann sheet since $G_1 < 0$, $\alpha > 0$ and $\mathrm{Im}G_2^I$, given by Eqs. (4.21) and (4.22), is negative. This gives us a perspective of why one has to go to the second Riemann sheet, where $k_2 \to -k_2$ in G_2, in which case one finds a solution, with $\tilde{E}_R = E_1 - m_{1i} - m_{2i}$ $(i = 2)$ and

$$\Gamma = 2 \frac{v_{12}^2 G_1}{-v_{11} \frac{\partial G_1}{\partial E}} \mathrm{Im} G_2^{II} \, . \tag{4.28}$$

Next, let us calculate the couplings g_i, where $g_i g_j$ is the residue of the t_{ij} matrix element at the pole. Applying l'Hôpital rule, we have

$$\begin{aligned} g_1^2 &= \lim(E - E_R) t_{11} = \frac{v_{11} + v_{12}^2 G_2}{-v_{11} \frac{\partial G_1}{\partial E} - v_{12}^2 \frac{\partial G_1}{\partial E} G_2 - v_{12}^2 \frac{\partial G_2}{\partial E} G_1} \, , \\ g_2^2 &= \lim(E - E_R) t_{22} = \frac{v_{12}^2 G_1}{-v_{11} \frac{\partial G_1}{\partial E} - v_{12}^2 \frac{\partial G_1}{\partial E} G_2 - v_{12}^2 \frac{\partial G_2}{\partial E} G_1} \, . \end{aligned} \tag{4.29}$$

Let us now see that the sum rule of Eq. (3.107) is exactly fulfilled, since we have

$$g_1^2\frac{\partial G_1}{\partial E}+g_2^2\frac{\partial G_2}{\partial E}=\frac{(v_{11}+v_{12}^2G_2)\frac{\partial G_1}{\partial E}+v_{12}^2G_1\frac{\partial G_2}{\partial E}}{-v_{11}\frac{\partial G_1}{\partial E}-v_{12}^2\frac{\partial G_1}{\partial E}G_2-v_{12}^2\frac{\partial G_2}{\partial E}G_1}=-1\,. \tag{4.30}$$

However, this occurs only at the complex pole $\tilde{E}_R+i\frac{\Gamma}{2}$ using G_2^{II}, since we have made use of the fact that the denominator in g_1^2 and g_2^2 of Eqs. (4.29) vanishes for $E=\tilde{E}_R+i\frac{\Gamma}{2}$ to apply l'Hôpital rule, which only occurs in the second Riemann sheet.

Note that the sum rule has appeared with the definition of the couplings of Eq. (3.106). The explicit form obtained for the couplings in Eqs. (4.29) shows clearly that they are complex, since both G_1 and G_2 are now complex.

Now that we have obtained the couplings, let us rewrite Γ of Eq. (4.28), derived assuming $|v_{12}|\ll|v_{11}|$ and neglecting again v_{12} versus v_{11}, as

$$g_2^2\simeq\frac{v_{12}^2G_1}{-v_{11}\frac{\partial G_1}{\partial E}}\,, \tag{4.31}$$

from which follows

$$\Gamma=2g_2^2\frac{M}{4\pi\sqrt{s}}p^3\,, \tag{4.32}$$

where we have used the relativistic formula for $\mathrm{Im}G_2$ of Eq. (4.22) and Eq. (4.5). As we can see, we reproduce the formula for the width given by Eq. (4.12).

Now we want to interpret the meaning of the sum rule. Eq. (4.30) is a generalization to complex energies of the sum rule obtained in Eq. (119) of Ref. [94] and Eq. (3.105) for real energies. There it was interpreted as a consequence of the sum of probabilities of each channel to be unity. For complex values of the energies this interpretation is not possible and this is related to the fact that the eigenstates of a complex Hamiltonian are not generally orthogonal[1].

Formally the problem is solved using, in this case, a biorthogonal basis. Indeed, let λ_n be a complex eigenvalue of H and $|\lambda_n\rangle$ the corresponding eigenvector. It satisfies

$$\det(H-\lambda_nI)=0\,. \tag{4.33}$$

Then

$$\det(H^\dagger-\lambda_n^*I)=0\,, \tag{4.34}$$

[1] Although our Hamiltonian was given in terms of v_{ij} in coupled channels, only for formal purposes one could think of a complex Hamiltonian whose eigenvalues would be these complex energies.

which means that λ_n^* is an eigenvalue of $H^\dagger$. Let now $|\bar{\lambda}_n\rangle$ be the eigenvector of $H^\dagger$ associated to λ_n^*. The eigenvectors $|\lambda_n\rangle$ and $|\bar{\lambda}_n\rangle$ are not equal, but we can see that

$$\langle\bar{\lambda}_n|H|\lambda_m\rangle = \lambda_m\langle\bar{\lambda}_n|\lambda_m\rangle = \lambda_n\langle\bar{\lambda}_n|\lambda_m\rangle\,, \tag{4.35}$$

where to get the last term we have applied H as $H^\dagger$ to the bra state. Thus

$$(\lambda_n - \lambda_m)\langle\bar{\lambda}_n|\lambda_m\rangle = 0\,, \tag{4.36}$$

which means that $|\lambda_m\rangle$ and $|\bar{\lambda}_n\rangle$ are orthogonal for $n \neq m$. For the case of $n = m$, $\langle\bar{\lambda}_n|\lambda_n\rangle \neq 0$ and we can choose a normalization and a phase for $|\bar{\lambda}_n\rangle$ and $|\lambda_n\rangle$ such that $\langle\bar{\lambda}_n|\lambda_n\rangle = 1$.

The resolution of the identity is now given by $\sum_n |\lambda_n\rangle\langle\bar{\lambda}_n|$. Furthermore, if we have a symmetric but not hermitian Hamiltonian, as it is our case, then it is trivial to see that $|\bar{\lambda}_n\rangle = |\lambda_n^*\rangle$ for its wave function.

Then, the relationship

$$\langle\Psi_i|\Psi_i\rangle = \sum_i \int d^3p|\Psi_i(p)|^2 = 1 \tag{4.37}$$

used to derive the sum rule in Ref. [94] and in **Chapter 3**, must be substituted by

$$\langle\bar{\Psi}_i|\Psi_i\rangle = \sum_i \int d^3p\,(\bar{\Psi}_i(p))^*\Psi_i(p) = \int d^3p\,\Psi_i^2(p) = 1\,. \tag{4.38}$$

Hence, for complex values, the modulus squared of the wave function has to be substituted by its square. The integral of Eq. (4.38) depends on the prescription used for the phase of Ψ_i. Below we show that, with the standard phase convention used in **Chapter 3**, Eq. (4.38) is fulfilled.

The wave function for us is given by Eq. (3.84). However we can assume that in our formalism (exactly as in the formalism of Ref. [96], see Eqs. (46) and (47)) the asymptotic scattering state used to create the resonance couples extremely weakly to it, such that, for the sum rule, one only has to worry about the bound state and the relevant decaying states. Thus, omitting the spherical harmonics for simplicity, the wave function for a decaying channel of the resonance (that means that it does not contain the $|\Phi\rangle$ term in the wave function in Eq. (3.84)) is given by

$$\Psi_i(p) = g_i\frac{\Theta(\Lambda - |\vec{p}|)p}{E - m_{1i} - m_{2i} - p^2/2\mu_i}\,, \tag{4.39}$$

where we have used Eq. (3.98) and (3.103). Thus, we can write

$$\int d^3p\,(\Psi_i(p))^2 = g_i^2\int_{|\vec{p}|<\Lambda} d^3p\frac{p^2}{(E - m_{1i} - m_{2i} - p^2/2\mu_i)^2} = -g_i^2\frac{\partial G_i^{II}}{\partial E}\,, \tag{4.40}$$

but we saw in Eq. (4.30) that

$$\sum_i g_i^2 \frac{\partial G_i^{II}}{\partial E} = -1\,, \tag{4.41}$$

and, hence, we can conclude that

$$\sum_i \int d^3p\, \Psi_i^2(p) = 1\,, \tag{4.42}$$

with the phase and normalization chosen for the wave function in Eq. (4.39).

Note that for the case of bound states we can use the same formulation and the prescription taken for the phase is the one where the wave function is real. In general g_i can be complex and $\Psi_i(p)$ will be complex, but the prescription for the interpretation given is to take the phase convention with the wave function in momentum space given by Eq. (4.39).

This clarifies the meaning of the sum rule. It is the demanded extrapolation to complex energies of the sum of probabilities equal unity for real energies. The modulus square of the wave function is substituted by the square of the wave function with a given prescription for the phase, which in the case of bound states would be having the wave function real. Thus we should interpret $-g_i^2 \frac{\partial G_i^{II}}{\partial E}$ as the extrapolation of a probability into the complex plane, but it is not a probability. Yet, once we have interpreted it as the integrated strength of the wave function squared, we still can think of it as a magnitude providing the weight, or relevance, of one given channel in the wave function of a state.

As we can see, the integral $\int d^3p\,(\Psi(p))^2$, given in terms of the coupling g_i and $\frac{\partial G_i^{II}}{\partial E}$, is a finite but complex quantity.

Since the two terms in Eq. (4.30) will now be complex, the sum of the imaginary parts will vanish and the sum of real parts will be equal to -1. Thus we have

$$\mathrm{Re}(g_1^2 \frac{\partial G_1^{II}}{\partial E}) + \mathrm{Re}(g_2^2 \frac{\partial G_2^{II}}{\partial E}) = -1 \tag{4.43}$$

and the sum rule is fulfilled for the real part of the squares of the wave functions.

The evaluation of the integral of $(\Psi_i(p))^2$ is most easily done in momentum space and concretely in terms of G^{II}. Yet, one would like to have a feeling of what happens in terms of wave functions in coordinate space, even if the integration of $(\Psi_i(r))^2$ in coordinate space requires extra work and is not convenient. We calculate the wave function in coordinate space in Appendix **A** and we recall only the basic results that we use here for qualitative purposes.

For $r \to \infty$ one obtains for the open channel, in the non relativistic formulation of **Section 3.3** and in the first Riemann sheet

$$\Psi_2(r) \sim \frac{e^{ikr}}{r} \ , \qquad k = \sqrt{2\mu_2(\tilde{E}_R + i\frac{\Gamma}{2})} \, . \tag{4.44}$$

Defining $k_R = \sqrt{2\mu_2 \tilde{E}_R}$ and $k_I = \sqrt{2\mu_2 \tilde{E}_R} \frac{\Gamma}{4\tilde{E}_R}$, we can write

$$\Psi_2(r) \sim \frac{1}{r} e^{ik_R r} e^{-k_I r} \, . \tag{4.45}$$

In the second Riemann sheet, we would substitute k by $-k$ and then

$$\Psi_2^{II}(r) \sim \frac{1}{r} e^{-ik_R r} e^{k_I r} \, . \tag{4.46}$$

Hence the wave function in coordinate space in the second Riemann sheet would even blow up and we would find an infinite probability. This is actually also the case even if $k_I = 0$. Thus the concept of probability is not useful once we have open channels.

Yet,

$$(\Psi_2^{II}(r))^2 \sim \frac{1}{r^2} e^{-2ik_R r} e^{2k_I r} \, , \tag{4.47}$$

and it has an oscillatory behaviour that makes the integral for large values of r vanish in the sense of a distribution, like $\int d^3r \, e^{i\vec{p}\vec{r}}$ for $p \neq 0$. Of course, the finiteness of the integral is better seen integrating in the space of momenta, as we have seen.

4.5 Interpretation of the sum rule for energy dependent potentials

The sum rule of Eq. (3.105) holds for states that are generated in coupled channels with potentials which are independent of the energy and, in the case of bound states, we saw that $-g^2 \frac{\partial G}{\partial E}$ can be interpreted as the probability of having a certain state. Yet, we have been using a potential containing a CDD pole (Eq. (4.3)) to take into account the possible genuine component and, even in the presence of this energy dependent potential, we would still associate $-g^2 \frac{\partial G}{\partial E}$ to the possibility of finding channel 1 in a certain state, for bound states. This requires a justification. One can in principle go back to the work done in Ref. [94] and re-derive the formulas with an energy dependent potential. However, this meets with serious problems, because the eigenstates of the Hamiltonian are now not orthogonal and $\sum |\alpha\rangle\langle\alpha|$ is not the resolution

of the identity. These problems and possible solutions are studied in Refs. [120, 121].

A suggestion to interpret the results of the sum rule in the case of an energy dependent potential is given in Section 4.2 of Ref. [122]. There it was found that, for a state generated with an energy dependent potential in coupled channels, the sum rule has the form

$$-\sum_{i,j} g_i g_j \left[\frac{\partial G_i^{II}(E)}{\partial E}\delta_{ij} + G_i^{II}(E)\frac{\partial V_{ij}(E)}{\partial E}G_j^{II}(E)\right]_{E\to E_R} = 1\,, \tag{4.48}$$

with $V_{ij}(E)$ the interaction kernel, and then the compositeness (the probability of the state to be in either of the channels considered, for the case of bound states) is defined as

$$X = -\sum_i g_i^2 \left[\frac{\partial G_i^{II}(E)}{\partial E}\right]_{E\to E_R}\,, \tag{4.49}$$

while the elementariness (the part of the state that does not belong to the considered channels) is then

$$Z = -\sum_{ij} \left[g_i G_i^{II}(E)\frac{\partial V_{ij}(E)}{\partial E}G_j^{II}(E) g_j\right]_{E\to E_R}\,. \tag{4.50}$$

A different derivation of Eq. (4.48) can be found in Ref. [112].

We take advantage here to justify this in the case that we have discussed above with two channels, and we study the problem with a single channel and an effective energy dependent single channel potential. The effective potential method is also discussed in Ref. [122] in Section 3.2, using the Feshbach projection method [123]. Here we follow a different approach.

The idea is the following: we start with a two channel case with an energy independent potential that generates a certain bound state, and evaluate T_{ij}. Then we use just channel 1 with an effective potential, such that T_{11} is the same in both approaches. As a consequence, and for bound states, $-g_1^2\frac{\partial G_1}{\partial E}$, which is the same in both approaches, gives the probability to find channel 1 in the state that we study, which is smaller than one. The difference from unity of this quantity, in our approach, is Z, which gives the probability that the state that we find is not in channel 1. This latter probability is related to $\frac{\partial V_{eff}}{\partial E}$ as we see below.

Indeed, using the simplified case of Eq. (4.18) in two channels we have

$$T_{11} = \frac{v_{11} + v_{12}^2 G_2}{1 - (v_{11} + v_{12}^2 G_2)G_1}\,, \tag{4.51}$$

while in one channel with V_{eff}, we will have

$$T_{eff} = \frac{V_{eff}}{1 - V_{eff} G_1} \,. \tag{4.52}$$

It is clear that taking

$$V_{eff} = v_{11} + v_{12}^2 G_2 \tag{4.53}$$

the two amplitudes T_{11} and T_{eff} are identical and the residue at the pole, g_1^2, will also be the same as g_{eff}^2.

On the other hand, we have from Eq. (3.106)

$$g_{eff}^2 = \lim_{E \to E_0} \frac{(E - E_0) V_{eff}}{1 - V_{eff} G_1} = \frac{V_{eff}}{-\frac{\partial V_{eff}}{\partial E} G_1 - V_{eff} \frac{\partial G_1}{\partial E}} \,, \tag{4.54}$$

which, using the pole condition $1 - V_{eff} G_1 = 0$, can be rewritten as

$$g_{eff}^2 = \frac{1}{-G_1^2 \frac{\partial V_{eff}}{\partial E} - \frac{\partial G_1}{\partial E}} \,. \tag{4.55}$$

Hence,

$$- g_{eff}^2 G_1^2 \frac{\partial V_{eff}}{\partial E} - g_{eff}^2 \frac{\partial G_1}{\partial E} = 1 \,. \tag{4.56}$$

Since

$$X \equiv -g_{eff}^2 \frac{\partial G_1}{\partial E} = -g_1^2 \frac{\partial G_1}{\partial E} \tag{4.57}$$

is the probability to find the state in channel 1 (for bound states), then

$$- g_{eff}^2 G_1^2 \frac{\partial V_{eff}}{\partial E} \equiv Z \tag{4.58}$$

gives the probability to find the state somewhere else (originally channel 2). This is the result of Ref. [122] which we wrote in Eq. (4.50).

Note that to study the possibility to have a genuine (non πN) state in the resonance that we study, we have used a CDD pole term in the potential. We can use this also to account for missing channels. Coming back to our example, if we have (we change a bit the notation for convenience)

$$V_{eff} = a + \frac{b}{E - E_R} \tag{4.59}$$

we should equate it to the potential of Eq. (4.53), which is not possible in all the range of energies. But the minimum requirement is that they are the same

at the pole and give the same residue, for which it suffices to equate the two values of V_{eff} and $\frac{\partial V_{eff}}{\partial E}$. Thus,

$$\begin{aligned} a + \frac{b}{E_0 - E_R} &= v_{11} + v_{12}^2 G_2(E_0) \ , \\ -\frac{b}{(E_0 - E_R)^2} &= v_{12}^2 \left[\frac{\partial G_2}{\partial E}\right]_{E=E_0} \ . \end{aligned} \tag{4.60}$$

This is always possible and shall leave us still one parameter to make a fit for an optimal agreement of the two expressions in a certain range of energies around the pole.

Finally, we want to make a small remark in the sense that the use of the CDD pole is, to all purposes, a suited way to take into account the genuine states in a problem. If we take only the CDD pole term in V_{eff} with a small coupling b to channel 1, then we should expect to get $Z \simeq 1$. This is just the case and indeed we find

$$\begin{aligned} T_{eff} &= \frac{1}{\frac{E-E_R}{b} - G_1} \ , \\ g_{eff}^2 &= \frac{1}{\frac{1}{b} - \frac{\partial G_1}{\partial E}} \ , \end{aligned} \tag{4.61}$$

and when $b \to 0$ then $g_{eff}^2 \simeq b$. Hence

$$\begin{aligned} X &= -g_{eff}^2 \frac{\partial G_1}{\partial E} \to 0 \, , \\ Z &= -g_{eff}^2 G_1^2 \frac{\partial V_{eff}}{\partial E} \to -b G_1^2(E_0) \frac{-b}{(E_0 - E_R)^2} = \left(\frac{b}{E_0 - E_R} G_1\right)^2 = 1 \, , \end{aligned} \tag{4.62}$$

the last equation holding because of the pole in the denominator of T_{eff}, Eq. (4.61).

4.6 Composite nature of the $\Lambda(1520)$

As anticipated in the introduction to the chapter, our starting point for the investigation of the $\Lambda(1520)$'s nature is the analysis of Ref. [115]. The $\Lambda(1520)$ is studied in the framework of a coupled channels formalism including the channels $\pi\Sigma(1385)$ and $K\Xi(1530)$ in s-waves and $\bar{K}N$ and $\pi\Sigma$ in d-waves.

4.6.1 The chiral unitary model

The matrix containing the tree-level amplitudes can be written as

$$V = \begin{pmatrix} \mathcal{C}_{11}(k_1^0 + k_1^0) & \mathcal{C}_{12}(k_1^0 + k_2^0) & \gamma_{13}\, q_3^2 & \gamma_{14}\, q_4^2 \\ \mathcal{C}_{21}(k_1^0 + k_2^0) & \mathcal{C}_{22}(k_2^0 + k_2^0) & 0 & 0 \\ \gamma_{13}\, q_3^2 & 0 & \gamma_{33}\, q_3^4 & \gamma_{34}\, q_3^2\, q_4^2 \\ \gamma_{14}\, q_4^2 & 0 & \gamma_{34}\, q_3^2\, q_4^2 & \gamma_{44}\, q_4^4 \end{pmatrix}, \tag{4.63}$$

where $q_i = \sqrt{(s-(m_i-M_i)^2)(s-(m_i+M_i)^2)}/2\sqrt{s}$ and $k_i^0 = (s - M_i^2 + m_i^2)/2\sqrt{s}$, with m_i and M_i the masses of the meson and baryon in channel i ($i = 1, 4$), respectively.

The s- and d-waves character of the transitions is taken into account by means of the dependence of the potentials on the incoming and outgoing squared momenta. The s-wave transition elements are obtained from the lowest order chiral Lagrangian involving the interaction of the decuplet of baryons and the octet of pseudoscalar mesons, which gives $\mathcal{C}_{11} = -1/f^2$, $\mathcal{C}_{12} = \mathcal{C}_{21} = -\sqrt{6}/4f^2$ and $\mathcal{C}_{22} = -3/4f^2$, with $f = 1.15\ f_\pi$ and $f_\pi = 93$ MeV. The factor 1.15 in f represents the average between f_π and f_K [22].

Since we need a momenta independent potential, we define a new potential as

$$V' = \begin{pmatrix} \mathcal{C}_{11}(k_1^0 + k_1^0) & \mathcal{C}_{12}(k_1^0 + k_2^0) & \gamma_{13} & \gamma_{14} \\ \mathcal{C}_{21}(k_1^0 + k_2^0) & \mathcal{C}_{22}(k_2^0 + k_2^0) & 0 & 0 \\ \gamma_{13} & 0 & \gamma_{33} & \gamma_{34} \\ \gamma_{14} & 0 & \gamma_{34} & \gamma_{44} \end{pmatrix} \tag{4.64}$$

independent of the q^2 factors coming from the d-waves and, according to **Chapter 3**, we include this dependence in the new loop functions, that will now have the form

$$G_i^{(s)} = 2M_i \int \frac{d^3p}{(2\pi)^3} \frac{\omega_i(p) + E_i(p)}{2\omega_i(p)E_i(p)} \frac{1}{P^{02} - (\omega_i(p) + E_i(p))^2 + i\epsilon}, \tag{4.65}$$

$$G_i^{(d)} = 2M_i \int \frac{d^3p}{(2\pi)^3} \frac{\omega_i(p) + E_i(p)}{2\omega_i(p)E_i(p)} \frac{p^4}{P^{02} - (\omega_i(p) + E_i(p))^2 + i\epsilon}, \tag{4.66}$$

where $\omega_i(p) = \sqrt{p^2 + m_i^2}$ and $E_i(p) = \sqrt{p^2 + M_i^2}$ are the energies of the meson and the baryon involved in the loop, respectively. This modification concerns only the loop function for the d-wave channels, $G_i^{(d)}$ ($i = 3, 4$), which now contains the factor $p^{2l} = p^4$. Note that we are taking the relativistic propagator [30].

Note that the s-wave elements of the V' matrix (V'_{11}, V'_{12}, V'_{21} and V'_{22}) still contain an energy dependence through the k_i^0 factors. However this dependence is very smooth and it will play a role in the diversion from unity in the sum rule of Eq. (3.108), as will be further explained.

The loop functions in Eqs. (4.65) and (4.66) are regularized by means of two different cutoffs in momentum space, $p_{max}^{(s)}$ and $p_{max}^{(d)}$ for the s- and d-waves channels respectively. These two cutoffs, together with the coefficients γ_{13}, γ_{14}, γ_{44}, γ_{44} and γ_{34} of Eq. (4.64), constitute the set of free parameters in the theory.

However, this procedure presents a problem due to the different dimensions of the magnitudes involved. The elements of V' in Eq. (4.64) concerning the transitions involving the d-waves channels, after removing the dependence on the momenta, will have different dimension with respect to the other ones. The same happens to the loop functions, that now have different dimensions in the cases of s- or d-waves.

In order to render the dimensions homogeneous and evaluate the scattering amplitudes by means of the Bethe-Salpeter equation, which is a matrix equation, we define

$$\tilde{V} = \begin{pmatrix} \mathcal{C}_{11}(k_1^0 + k_1^0) & \mathcal{C}_{12}(k_1^0 + k_2^0) & \gamma_{13}\, q_3^{*2} & \gamma_{14}\, q_4^{*2} \\ \mathcal{C}_{21}(k_1^0 + k_2^0) & \mathcal{C}_{22}(k_2^0 + k_2^0) & 0 & 0 \\ \gamma_{13}\, q_3^{*2} & 0 & \gamma_{33}\, q_3^{*4} & \gamma_{34}\, q_3^{*2}\, q_4^{*2} \\ \gamma_{14}\, q_4^{*2} & 0 & \gamma_{34}\, q_3^{*2}\, q_4^{*2} & \gamma_{44}\, q_4^{*4} \end{pmatrix}, \quad (4.67)$$

with $q_i^* = q_i(m_{\Lambda^*}) = \sqrt{(m_{\Lambda^*}^2 - (m_i - M_i)^2)(m_{\Lambda^*}^2 - (m_i + M_i)^2)}/2m_{\Lambda^*}$, where we choose for m_{Λ^*} the $\Lambda(1520)$ mass. Nevertheless, this specific choice is obviously irrelevant for the final results. The dimensions of γ_{ij} are chosen such that all the elements of the matrix $\tilde{V}$ have the same dimensions.

Now, we can write

$$\tilde{G}_i^{(d)} = 2M_i \int \frac{d^3p}{(2\pi)^3} \frac{\omega_i(p) + E_i(p)}{2\omega_i(p)E_i(p)} \frac{p^4/q_i^4(m_{\Lambda^*})}{P^{02} - (\omega_i(p) + E_i(p))^2 + i\epsilon}\,. \quad (4.68)$$

This new loop function for the d-waves cases has the same dimension as $G_i^{(s)}$, and now the Bethe-Salpeter equation reads

$$\tilde{T} = \frac{1}{\tilde{V}^{-1} - \tilde{G}}\,, \quad (4.69)$$

with

$$\tilde{G} = \begin{pmatrix} G_1^{(s)} & 0 & 0 & 0 \\ 0 & G_2^{(s)} & 0 & 0 \\ 0 & 0 & \tilde{G}_3^{(d)} & 0 \\ 0 & 0 & 0 & \tilde{G}_4^{(d)} \end{pmatrix}. \quad (4.70)$$

Since the q_i momentum in Eq. (4.67) is relatively small, the $\tilde{G}_i^{(d)}$ of Eq. (4.68) can be large with respect to $G_i^{(s)}$ due to the p^4/q_i^4 factor in the integrand.

Set	$p_{max}^{(s)}$ [MeV]	$p_{max}^{(d)}$ [MeV]
1)	1797.960	868.265
2)	1427.119	865.693
3)	1324.125	904.062
4)	1438.782	897.246
5)	1747.956	911.004

Table 4.5: Values of the parameters $p_{max}^{(s)}$ and $p_{max}^{(d)}$ resulting from a sample of five best fits to the scattering data for the $\bar{K}N$ and $\pi\Sigma$ amplitudes.

Obviously, this depends on the cutoff for the d-wave loops, which is taken to be different from the s-wave one in the fit to the data. Whether $\tilde{G}_i^{(d)}$ will be large or not in the end compared to $G_i^{(s)}$ depends on this cutoff, but this is determined by the data.

4.6.2 Results and discussion

The scattering amplitudes derived using Eq. (4.69) contain, as we already mentioned, seven free parameters: $p_{max}^{(s)}$, $p_{max}^{(d)}$, γ_{13}, γ_{14}, γ_{44}, γ_{44} and γ_{34}. In order to obtain their values, we fit the model to the experimental scattering amplitudes for $\bar{K}N$ and $\pi\Sigma$ in d-wave and for $I = 0$ [124, 125]. The relation between the experimental and the theoretical amplitudes is given by

$$T_{ij}^{exp}(\sqrt{s}) = -\sqrt{\frac{M_i q_i}{4\pi\sqrt{s}}}\sqrt{\frac{M_j q_j}{4\pi\sqrt{s}}}\, T_{ij}(\sqrt{s})\,, \tag{4.71}$$

with i and j the channels involved in the transition.

We obtain several equivalent best fits to the experimental data and the values of the parameters obtained from a sample of five sets are listed in **Table 4.5** and **Table 4.6**. In **Figure 4.2** we show the results of the fit for the first set of **Table 4.5** and **Table 4.6**, but, in any case, the results are consistent for all the sets. The fact that we get approximately the same solutions with different sets of parameters indicates that there are strong correlations between them. The final results are also very similar independently of the set of parameters chosen (see **Table 4.8**).

At this point, we apply the sum rule extrapolating the amplitudes to the complex plane and changing $G_i^{(s)}$ and $G_i^{(d)}$ to $G_i^{II(s)}$ and $G_i^{II(d)}$ in Eqs. (4.65)

Set	γ_{13} [MeV^{-3}]	γ_{14} [MeV^{-3}]	γ_{33} [MeV^{-5}]	γ_{44} [MeV^{-5}]	γ_{34} [MeV^{-5}]
1)	$-0.875 \cdot 10^{-7}$	$1.169 \cdot 10^{-7}$	$-0.030 \cdot 10^{-11}$	$-0.055 \cdot 10^{-11}$	$0.003 \cdot 10^{-11}$
2)	$3.938 \cdot 10^{-7}$	$-5.028 \cdot 10^{-7}$	$-0.748 \cdot 10^{-11}$	$-1.345 \cdot 10^{-11}$	$0.966 \cdot 10^{-11}$
3)	$-0.695 \cdot 10^{-7}$	$0.840 \cdot 10^{-7}$	$-0.025 \cdot 10^{-11}$	$-0.033 \cdot 10^{-11}$	$-0.002 \cdot 10^{-11}$
4)	$2.799 \cdot 10^{-7}$	$-3.502 \cdot 10^{-7}$	$-0.037 \cdot 10^{-11}$	$0.048 \cdot 10^{-11}$	$-0.028 \cdot 10^{-11}$
5)	$2.248 \cdot 10^{-7}$	$-2.873 \cdot 10^{-7}$	$0.126 \cdot 10^{-11}$	$0.162 \cdot 10^{-11}$	$-0.174 \cdot 10^{-11}$

Table 4.6: Values of the parameters γ_{13}, γ_{14}, γ_{33}, γ_{44} and γ_{34} resulting from a sample of five best fits to the scattering data for the $\bar{K}N$ and $\pi\Sigma$ amplitudes.

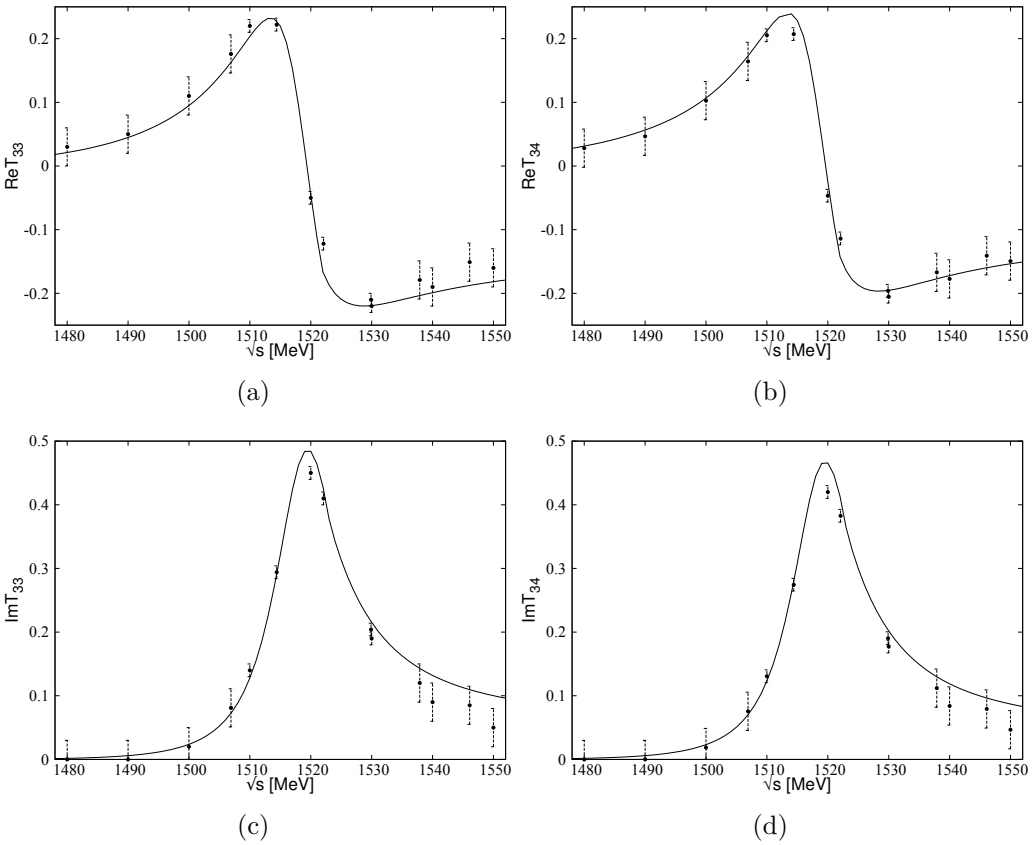

Figure 4.2: Fit to experimental amplitudes for $\bar{K}N \to \bar{K}N$ and $\bar{K}N \to \pi\Sigma$.

Set	$\sqrt{s_0}$ [MeV]	$g_{\pi\Sigma^*}$	$g_{K\Xi^*}$	$g_{\bar{K}N}$	$g_{\pi\Sigma}$
1)	$1518.7 - i6.4$	$0.70 - i0.01$	$-0.40 + i0.05$	$0.54 - i0.06$	$0.43 - i0.05$
2)	$1519.1 - i6.7$	$0.78 - i0.07$	$-0.35 + i0.07$	$-0.56 + i0.05$	$-0.45 + i0.03$
3)	$1518.3 - i6.5$	$0.73 + i0.01$	$-0.31 + i0.03$	$0.53 - i0.06$	$0.44 - i0.06$
4)	$1519.9 - i6.5$	$0.74 + i0.00$	$-0.34 + i0.04$	$0.53 - i0.07$	$0.44 - i0.04$
5)	$1518.5 - i6.4$	$0.63 + i0.02$	$-0.35 + i0.03$	$-0.53 + i0.07$	$-0.43 + i0.05$

Table 4.7: Pole positions and values of the couplings of the $\Lambda(1520)$ to the four different channels of the model.

and (4.68), in the channels which are open:

$$\begin{aligned} G_i^{II(s)}(\sqrt{s}) &= G_i^{I(s)} + \frac{i}{2\pi}\frac{M_i}{\sqrt{s}}\, q_i\,, \\ G_i^{II(d)}(\sqrt{s}) &= G_i^{I(d)} + \frac{i}{2\pi}\frac{M_i}{\sqrt{s}}\,\frac{q_i^5}{q_i^4(m_{\Lambda^*})}\,, \qquad Im(q_i) > 0\,, \end{aligned} \tag{4.72}$$

where $G_i^{I(s)}$ and $G_i^{I(d)}$ are the loop functions in the first Riemann sheet given by Eqs. (4.65) and (4.68).

The values of the poles that we get from the five sets are listed in the first column of **Table 4.7**.

Now we can evaluate the couplings of the resonance to the different channels as the residues at the pole of the amplitudes and apply the sum rule to evaluate the contribution of a single channel to the $\Lambda(1520)$:

$$(1 - Z)_i = -Re\left[g_i^2\left[\frac{dG_i^{II}(s)}{d\sqrt{s}}\right]_{\sqrt{s}=\sqrt{s_0}}\right]. \tag{4.73}$$

The couplings that we find are shown in **Table 4.7**. Note that there is an ambiguity in the sign of $g_{\bar{K}N}$ and $g_{\pi\Sigma}$ among the different sets but the product $g_{\bar{K}N}g_{\pi\Sigma}$ has the same sign. This is because we fit the transition $\bar{K}N \to \pi\Sigma$ which determines the relative sign but not the overall one referred to the $\pi\Sigma^*$ channel.

From these values we can obtain the relevance of the different channels in the wave function of the $\Lambda(1520)$ resonance, using Eq. (4.73). The values of the different weights are shown in **Table 4.8**.

We can now estimate the composite character of the $\Lambda(1520)$ resonance since, according to Eq. (3.108)

$$\sum_i (1 - Z)_i = 1 - Z\,, \tag{4.74}$$

Set	$(1-Z)_{\pi\Sigma^*}$	$(1-Z)_{K\Xi^*}$	$(1-Z)_{\bar{K}N}$	$(1-Z)_{\pi\Sigma}$	$1-Z$
1)	0.084	0.002	0.494	0.214	0.79
2)	0.089	0.001	0.526	0.225	0.84
3)	0.093	0.001	0.541	0.239	0.99
4)	0.093	0.001	0.518	0.237	0.87
5)	0.072	0.002	0.531	0.237	0.84

Table 4.8: Values of the weights X_i of the different channels in the wave function of the $\Lambda(1520)$ and the total $1-Z=\sum_i(1-Z)_i$.

and Z is a measure of the presence in the state of something different from the meson-baryon components considered (genuine components). We obtain for $1-Z$ the values shown in the last column of **Table 4.8**. Taking the average of the last column we have $1-Z=0.87\pm0.10$, which indicates an appreciable weight of meson-baryon character in the resonance with less than 15% weight for other genuine components.

It is worth noting that numerically, according to Eq. (4.50) [122], the value of Z corresponds to

$$Z=-\sum_{ij}\left[g_i G_i^{II}(\sqrt{s})\frac{\partial V_{ij}(\sqrt{s})}{\partial\sqrt{s}}G_j^{II}(\sqrt{s})g_j\right]_{\sqrt{s}=\sqrt{s_0}}. \tag{4.75}$$

Therefore, the diversion from unity of the compositeness $\sum_i X_i$ is due to the smooth energy dependence of the s-wave elements of the potential (see Eq. (4.67)). In **Section 4.5** we have shown that in cases where there is an explicit CDD pole in the potential accounting for a genuine state, which has a specific energy dependence, or when one channel has been eliminated introducing an equivalent effective potential, Eq. (4.75) indeed accounts for the probability, or weight, of the missing channels. On the other hand, it is not clear if the small magnitude obtained from the smooth energy dependence of the Weinberg Tomozawa interaction can be attributed to missing channels, and one could think of this amount simply as an uncertainty in the method used to determine Z. Specifically in the present case, we also see that it is of the same order of magnitude as the statistical uncertainties. Anyway, the fact that we get a good fit without needing to include a CDD pole is an indication of the low weight of genuine components in the building up of the $\Lambda(1520)$ resonance.

However, we can see in **Table 4.7** that the coupling of the resonance to the $\pi\Sigma^*$ channel is the largest one. Yet, in terms of weight (or, if it was a bound state, probability of the state) it represents only about 10%. This small probability can be deceiving, because the relevance of each channel is usually tied to the values of the wave function at the origin, more than to the

probability. This is why in each particular process one has to find out the relevance of each channel. For instance, from the study of the radiative decays $\Lambda(1520) \to \gamma\Lambda$, $\gamma\Sigma^0$ emerged that the $\pi\Sigma$, $\pi\Sigma^*$ channels did not contribute to the $\gamma\Lambda$ decay but this d-wave component gave the largest contribution to the decay width in the case of the $\gamma\Sigma^0$ decay channel [48] .

We should then stress that one must be careful asserting the relevance of the channels from the weight obtained. Indeed, for the open channels $\pi\Sigma$ and $\bar{K}N$, the value of X_i corresponds to the integral of the wave function squared, which goes as e^{-iqr}/r for large r. While the integral of the modulus squared of the wave function diverges, this is not the case for the wave function squared, where the oscillations of the e^{-2iqr} factor lead to large cancellations at large r. Yet, it is clear that for the open channels one is getting contributions to X_i from larger values of r than in the bound channels $\pi\Sigma^*$ and $K\Xi^*$. However, the wave function at large values of r will not have relevance in most processes involving short distances. In this sense, the couplings in the normalization that we have, or the relative values of X_i in the s-waves or d-waves channels, are the magnitudes that more fairly indicate the relevance of the different channels, but ultimately it is the specific dynamics of a given process that will determine the relevance of the channels, as seen in Ref. [48].

One example that helps put in perspective the former discussion is the case of the $X(3872)$ resonance, which from the molecular point of view corresponds to a $D\bar{D}^*$ molecule. In this case the $D^0\bar{D}^{*0}$ component is bound by barely 0.2 MeV while the charged component D^+D^{*-} is bound by about 7 MeV. It was found in Refs. [126, 127], and it will be shown in detail in **Chapter 7**, that the X_i is about 0.86 and 0.124 for the $D^0\bar{D}^{*0}$ and the D^+D^{*-} components, respectively. Thus, to the neutral component corresponds a very large probability, about seven times larger than for the charged one, a ratio even bigger than the ratio found here for $X_{\bar{K}N}$ and $X_{\pi\Sigma^*}$. Yet, this big difference does not mean that the neutral component is the most important in physical reactions, since in processes involving short distances it is the wave function at the origin what matters (g_iG_i for s-waves) [94] and this magnitude has about the same strength in the neutral and charged channels [126]. In view of this, one might get tempted to compare wave functions at the origin in the present case. However this is not possible, because we are dealing with s-wave and d-wave components simultaneously and the d-wave function is zero at the origin.

This discussion serves us as a warning not to interpret the X_i values obtained as the relevance of each channel in physical reactions. The large probability in the $D^0\bar{D}^{*0}$ case in the $X(3872)$ state came because the wave function in this channel extended to large distances, and in the case of an open channel, as $\bar{K}N$, $\pi\Sigma$ in the $\Lambda(1520)$, the distances to where the $\bar{K}N$, $\pi\Sigma$ can extend

are even larger.

Anyway, one can state that the sum rule is nearly saturated with the channels that we have considered, indicating that there is no much room for other channels. However, the relevance of each channel in particular reactions can only be asserted when explicit evaluations are done.

We should also note that the d-waves have not been included as a mean to obtain the $\Lambda(1520)$ resonance, parametrize short range physics or mimic possible genuine components. The d-waves are included because the $\Lambda(1520)$ is clearly visible in the $\bar{K}N \to \bar{K}N$ and $\bar{K}N \to \pi\Sigma$ d-wave amplitudes, as shown in **Figure 4.2**. This is a clear proof that the resonance couples to these components and they should be taken into account for a more accurate description of the resonance properties.

In early papers [113, 114] the $\Lambda(1520)$ was claimed to come from the $\pi\Sigma^*$ and $K\Xi^*$ channels in s-wave. However, in Ref. [115] the importance of the d-wave channels $\pi\Sigma$, $\bar{K}N$ was established in order to obtain the $\bar{K}N \to \bar{K}N$ and $\bar{K}N \to \pi\Sigma$ amplitudes around the $\Lambda(1520)$ resonance. In this perspective we have performed the following exercises: we first eliminated the d-wave channels and, with the same parameters, we were able to obtain a $\pi\Sigma^*$ bound state at $\sqrt{s} = 1508$ MeV. This means that the $\pi\Sigma^*$ interaction has sufficient strength to bind a system by itself. This is in line with the findings of Refs. [113, 114], where, however, other cutoffs were used leading to an energy displacement with respect to the 1508 MeV that we find in the present work. Then, we turned-off the s-wave channels, keeping only the $\pi\Sigma$, $\bar{K}N$ channels. With the same parameters, we find again a resonance at $\sqrt{s} = (1615 - i\,36)$ MeV. When all channels are considered together, a pole at $\sqrt{s} = (1519 - i7)$ MeV is found and our interpretation is that the consideration of the d-wave channels on top of the s-wave ones only shifts the pole by about 10 MeV, while the inclusion of s-wave channels on top of the d-wave ones reduces the energy of the pole by about 100 MeV. This seems to suggest a large relative importance of the s-wave channels but, as discussed above, the study of different physical processes is what allows one to claim the importance of a given channel with respect to another one.

4.7 Summary and Conclusions

In this Chapter we have applied the generalized compositeness condition, previously derived, to the decuplet of the $\Delta(1232)$ in order to quantify the weight of the meson-baryon cloud and genuine (presumably three quark) components. It is interesting to see that, with both the tests we use, we find the pole position for the $\Delta(1232)$ in very good agreement with the PDG [17] values and we ob-

tain a sizeable composite character, around 60%, as reported in Eq. (4.10) and in **Table 4.2**. Then, we extended the compositeness test to the other members of the decuplet and, as shown in **Table 4.3**, we found a decreasing size of the meson-baryon components when we go to the $\Sigma(1385)$ and $\Xi(1530)$, indicating that the higher energy members of the decuplet are better represented by a genuine (in principle three quark) component. For the $\Sigma(1385)$ and $\Xi(1530)$ there are also bound components of $\bar{K}N$ and $\bar{K}\Lambda$, $\bar{K}\Sigma$, respectively, which we estimate small compared to the open ones in the limited space allowed due to the decay into the open channels. In the case of the Ω^-, where only the bound component $\bar{K}\Xi$ is present, we estimate the weight of meson-baryon to be small, of the order of 25 %.

We also clarified the meaning of the extension of the Weinberg sum rule to the case of resonances, formulating an interpretation for the case of complex energies. We saw how $-g^2\frac{\partial G_{II}}{\partial E}$ measures $\int d^3p\ \langle\vec{p}\,|\Psi\rangle^2$ and not $\int d^3p\ |\langle\vec{p}\,|\Psi\rangle|^2$ as for bound states. So, the concept of probability is changed to the square of the wave function. Taking the integral of its real part we obtain a natural quantity to provide a measurement of the relevance of an open channel in the wave function, since the integral of the modulus squared diverges (even more in the second Riemann sheet). On the other hand, $\int d^3p\ \langle\vec{p}\,|\Psi\rangle^2$ is finite and the sum of these quantities for the different coupled channels is unity, within a certain phase convention, as shown by the generalization of the Weinberg sum rule.

The values we found for the weight of the πN component in the $\Delta(1232)$ wave function are relatively high, of the order of 60 %. This number could sound a bit large when one thinks of the $\Delta(1232)$ as just a spin flip on the quark spins of the nucleon. Yet, the result seems reasonable when one recalls that from Drell-Yan and deep inelastic scattering one induces a probability of about 34 % for the πN component in the nucleon [128, 129]. Once this is realized, it also looks less surprising that, unlike the case of the ρ where the analysis in terms of just the $\pi\pi$ component requires large counterterms beyond the lowest order contribution from the chiral Lagrangians [32, 99], in the case of the πN scattering in the $\Delta(1232)$ region a description was possible with moderate size of the counterterms [130, 131].

The large pion nucleon cloud in the $\Delta(1232)$ indicates that realistic calculations of its properties should take this cloud into account. Even before the present test was done to estimate the weight of πN component in the $\Delta(1232)$ wave function, the importance of the meson cloud has been often advocated and one example of it can be seen in the early works on the cloudy bag model [101] or chiral quark model [132]. The work presented here offers a new perspective on this interesting subject and the possibility to become more quantitative than in early works.

We have also given an interpretation of the terms of the sum rule for the case of an energy dependent potential. In the case that we have a complete set of coupled channels that generates a certain bound state, we can truncate the space and define an energy dependent potential in a space of lower dimension. The sum rule is now rewritten and a physical interpretation is given to the different terms. The probability Z that the state overlaps with the eliminated part of the space is related to the derivative of the potential with respect to the energy.

We have also tried to quantify the weight of the meson-baryon components (s-waves $\pi\Sigma^*$, $K\Xi^*$ and d-waves $\bar{K}N$, $\pi\Sigma$) into the $\Lambda(1520)$ wave function. The meson-baryon scattering amplitudes are obtained implementing the techniques of the chiral unitary approach where some unknown parameters (five d-wave coefficients and two cutoffs) are fitted to $\bar{K}N$ and $\pi\Sigma$ experimental scattering data. The momentum dependence coming from the d-wave channels is incorporated into the loop function, leaving a smooth energy dependent potential for which we can apply our techniques. The adding terms in the sum rule of Eq. (4.73), which are a measure of the weight of the different channels into the $\Lambda(1520)$ wave function, and the total sum rule itself can be evaluated.

While the largest coupling obtained is to $\pi\Sigma^*$ (see **Table 4.7**), the largest weight X_i is for $\bar{K}N$ (see **Table 4.8**). This is not contradictory since they represent different concepts. The coupling (actually the product of the coupling times the loop function, $g_i G_i$) accounts for the wave function at the origin, as we saw in **Chapter 3** for s-waves while, as already explained, $X_i = -g_i \frac{\partial G_i}{\partial E}$ is a measure of the probability to find that channel.

We also explained that the large weight obtained for the open channels was a consequence of the contribution to the integral of the wave function squared from larger values of r than for the bound channels, and not a measure of the contribution of the channel in different processes, most of which are sensible to short distances. The values of the couplings and the specific dynamics of those processes are what finally determines the relevance of each single channel.

CHAPTER **5**

TRIANGULAR $K\bar{K}$ LOOPS AND ISOSPIN BREAKING

5.1 Introduction

The $a_0(980)$ and $f_0(980)$ resonances classify among those states whose nature has opened an intense debate in the past years. After their discovery [133, 134] many attempts were made to characterize their nature: a $q\bar{q}$ picture [135–140], although no quark model proved capable to describe both states simultaneously [141], multiquark states [142, 143] or $K\bar{K}$ molecules [144–147].

In Refs. [30–32, 148–151] they appear as composite hadron states, dynamically generated by the interaction of mesons provided by the chiral Lagrangians [25, 26]. The basic building blocks are $\pi\pi$ and $K\bar{K}$ for the $f_0(980)$ and $\pi\eta$ and $K\bar{K}$ for the $a_0(980)$ [30–32, 148–151]. These resonances do not couple directly to external sources but it is the constituent meson pairs what couples directly to them. Then, upon unitarization (multiple scattering of mesons), the resonances are formed.

According to this idea, a series of reactions involving the $f_0(980)$ and $a_0(980)$ were studied and, with no extra parameters than those needed in the study of meson-meson scattering, predictions were made for cross sections or other observables, supporting the dynamically generated picture. Examples of it are the reactions $\phi \to \pi^0\pi^0\gamma$, $\pi^0\eta\gamma$ [152], $J/\psi \to \phi(\omega)f_0$ [153–156], $J/\psi \to p\bar{p}\pi\pi$ [157] and the photoproduction of $f_0(980)$ on nucleons [158].

Since, due to the different masses of charged and neutral kaons, isospin symmetry is broken in meson rescattering, the $a_0(980)$ and $f_0(980)$ can mix and quantifying this mixing can help understanding the nature of these two resonances, as early discussed in Ref. [159]. More recently, the subject was thoroughly studied in Refs. [160, 161], where the reaction $J/\psi \to \phi\pi^0\eta$ was

suggested as a test. The same reaction was also theoretically studied in Ref. [162] using chiral unitary approach, as in Ref. [161], showing that not only the shape of the experiment, but also the absolute rate can be reproduced. In Ref. [163] the reaction $\chi_{c1} \to \pi^0\pi\eta$ was also proposed as a test to measure the amount of $a_0(980)$-$f_0(980)$ mixing.

The reaction $J/\psi \to \phi\pi^0\eta$ was then experimentally studied by the BES collaboration [164] and a narrow signal was found, with width of the order of the difference of the kaon masses and in agreement with the predictions of Refs. [160, 161]. The signal showed an intensity of half percent of the one of $J/\psi \to \phi\pi^+\pi^-$ in the region of the $f_0(980)$ peak in the $\pi\pi$ distribution. Following the suggestion of Wu and Zou [163], the same experimental work of Ref. [164] also reports on the $\chi_{c1} \to \pi^0\pi\pi$ in the region of the $f_0(980)$ peak of the $\pi\pi$ mass distribution. Once again one finds a narrow signal, with an intensity with respect to $\chi_{c1} \to \pi^0\pi^0\eta$ in the $a_0(980)$ region of the $\pi^0\eta$ mass distribution also of the order of half per cent. These numbers are within expected values for isospin violation. The narrowness of the isospin forbidden signal reflects the fact that the isospin violation is tied to the difference of the loop functions of intermediate kaons in the rescattering of mesons that leads to the $f_0(980)$ and $a_0(980)$ resonances. This provides support [161] to the chiral dynamical picture of these resonances.

However, a recent work by the BES team on the $\eta(1405) \to \pi^0 f_0(980)$ and $\eta(1405) \to \pi^0 a_0(980)$ reactions [165] has brought a surprise. Since the $\eta(1405)$ is an $I = 0$ object, it can naturally decay to $\pi^0 a_0(980)$, while the decay into $\pi^0 f_0(980)$ violates isospin. The signal for the isospin violating channel $\eta(1405) \to \pi^0 f_0(980)$ is also very narrow, in agreement with previous findings in analogous reactions, but the reported ratio of the partial decay widths of the two channels is abnormally large, 18% for $\eta(1405) \to \pi^0\pi^+\pi^-$ to $\eta(1405) \to \pi^0 a_0(980)$ or, summing the $\pi^0\pi^0$ channel to the $\pi^+\pi^-$, 27% for the ratio of rates of $\eta(1405) \to \pi^0 f_0(980)$ to $\eta(1405) \to \pi^0 a_0(980)$. Such a large rate is difficult to explain in a theoretical description, unless the same $\eta(1405)$ state already contains a large mixture of $I = 0$ and $I = 1$. However, if this were the case, the production of the $f_0(980)$ would proceed unhindered, showing its natural width of about 50 MeV instead of the 9 MeV observed in the BES experiment [165].

In order to provide an explanation to this experimental result, Wu *et al.* proposed a particular mechanism in Ref. [166], consisting in the $\eta(1405)$ decay into $K^*\bar{K}$, the following K^* decay into $\pi^0 K$ and the rescattering of the $K\bar{K}$ to produce either the $f_0(980)$ and the $a_0(980)$ resonances. This leads to a triangular loop diagram that has two cuts (singularities in the integrand), which make it different from the standard G loop function from $K\bar{K}$, that only has the $K\bar{K}$ on shell singularity. The final loop function that appeared

in the calculation of Ref. [166] containing the three propagators was divergent and needed to be regularized. The authors used an unknown cutoff or form factor to implement convergence, but then the decay rates were dependent on this undetermined parameter. We will see in **Section 5.2.3** that the problem is automatically solved in the framework of chiral unitary approach, and that the triangular loop can be regularized with the same cutoff used in the meson-meson interaction problem, which is a parameter fitted to the scattering data that naturally appears in the calculation. This made possible to evaluate the ratio of the decay rates for $\eta(1405) \to \pi^0\pi^0\eta$ and $\eta(1405) \to \pi^0\pi^+\pi^-$ and the shapes of the invariant mass distributions, which are in good agreement with experiment.

In **Section 5.2**, we make first a thorough discussion of the issue assuming a contact (or contact like) $\eta(1405) \to \pi^0 K\bar{K}$ vertex. Under this assumption one can make a quite model independent study, and the conclusion is that the results obtained are in line with those of other reactions, like the $J/\psi \to \phi\pi^0\eta(\pi\pi)$. A second part is devoted to the explicit study of the triangular mechanism of Ref. [166]. Using the chiral unitary approach we shall see that we are able to evaluate the ratio for isospin violation, beyond the reach of the method of Ref. [166], where the ratio of widths for $\eta(1405) \to \pi^0\pi^+\pi^-$ and $\eta(1405) \to \pi^0\pi^0\eta$ was dependent on an unknown cutoff.

In **Section 5.3**, we apply the same mechanism of Refs. [166] to the reactions $f_1(1285) \to \pi^0\pi^0\eta$ and $f_1(1285) \to \pi^0\pi^+\pi^-$. We evaluate the branching ratio for the decay of the $f_1(1285)$ to $a_0\pi$, excluding the $a_0(980)$ decay to $K\bar{K}$, in order to compare our result with the value of about 36% reported in the PDG, with the aim to give further support to the basic idea about the nature of the $f_1(1285)$, $a_0(980)$ and $f_0(980)$ resonances.

Indeed, the $f_1(1285)$ is one of the cleanest example of these dynamically generated resonances and, with quantum numbers $I^G(J^P) = 0^+(1^{++})$, it appears in Ref. [51] from the single channel $K^*\bar{K} - cc$. An extension of the work of Ref. [51], including higher order terms in the Lagrangian, has shown that the effect of the higher order terms is negligible [167]. Using these theoretical tools, predictions for lattice simulations in finite volume have been done in Ref. [168]. The width of the $f_1(1285)$ is 24 MeV, much smaller than what expected for resonances of its mass. However, it is naturally explained within the molecular picture, since it cannot decay into two pseudoscalar mesons (in principle $K\bar{K}$ in this case) for parity and angular momentum conservation reasons.

There is another large channel, apart from the $a_0\pi$, which is the $K\bar{K}\pi$, accounting for about 9% of the width of the $f_1(1285)$. This decay mode is tied to the $K\bar{K}^* - cc$ nature of the state and we study it in **Section 5.4**. The channel $K\bar{K}^*$ is bound for the energy of the $f_1(1285)$ by about 100 MeV, hence

this decay is not observed experimentally [17]. However, the decay of the K^* off shell can produce the $K\pi$ pair leading to $K\bar{K}\pi$ in the final decay channel. Definitely, this decay channel is related to the coupling of the $f_1(1285)$ to the $K\bar{K}^* - cc$, and consequently to the nature of this state. Our aim is to study quantitatively this process from this perspective.

In doing so we also have to face the final state interaction (FSI) of the $K\bar{K}$ and the πK, which we do using the chiral unitary approach [30, 32, 59]. The FSIs lead to triangular loops analogous to the ones of **Section 5.2** and **Section 5.3**. We follow the same approach to complement the tree level contribution with the FSI of two mesons.

Here we present an unusual picture for the $f_1(1285)$, which in the Literature is mostly considered as a simple $q\bar{q}$ state [19, 169–173]. In Ref. [169] the quark pair creation model is used to account for decays of this resonance in two mesons and the $\pi a_0(980)$ decay is addressed from this perspective. In Refs. [19, 170] the $f_1(1285)$ is assumed to belong to a nonet of $q\bar{q}$ mesons. In Ref. [174] the B^0 and B_s^0 decays into J/ψ and $f_1(1285)$ are investigated and the results are interpreted in terms of a $q\bar{q}$ state, mostly made of u and d quarks. Yet, in none of the works quoted, or others, have we found an evaluation of the decay of this resonance into $K\bar{K}\pi$. We show that we obtain results compatible with experiment, hence supporting the molecular picture of the $f_1(1285)$.

The results we show make reference to three published works, [175–177].

5.2 The $\eta(1405) \to \pi^0 f_0(980)$ decay

As we mentioned in the introduction, the starting point in the following discussion is the acceptance that the $f_0(980)$ and $a_0(980)$ qualify as composite meson-meson states which are dynamically generated by the meson-meson interaction provided by the chiral Lagrangians.

5.2.1 Standard formalism assuming local primary $\eta(1405) \to \pi^0 PP$ vertices

We consider the vertex $\eta(1405) \to \pi^0 PP$ (where P stands for pseudoscalar) well described by a contact (or contact like) interaction and we also accept that the $\eta(1405)$ is an isospin zero state. Then, the mechanism for production of either $\pi^+\pi^-$ or $\pi^0\eta$ in the final state, together with an extra π^0, is given by **Figure 5.1**.

Implicit in the picture of **Figure 5.1** is the fact that the π^0 of the upper line, when the $f_0(980)$ or $a_0(980)$ are produced by the other pair of mesons, has an energy which does not match with the energy of the other mesons to

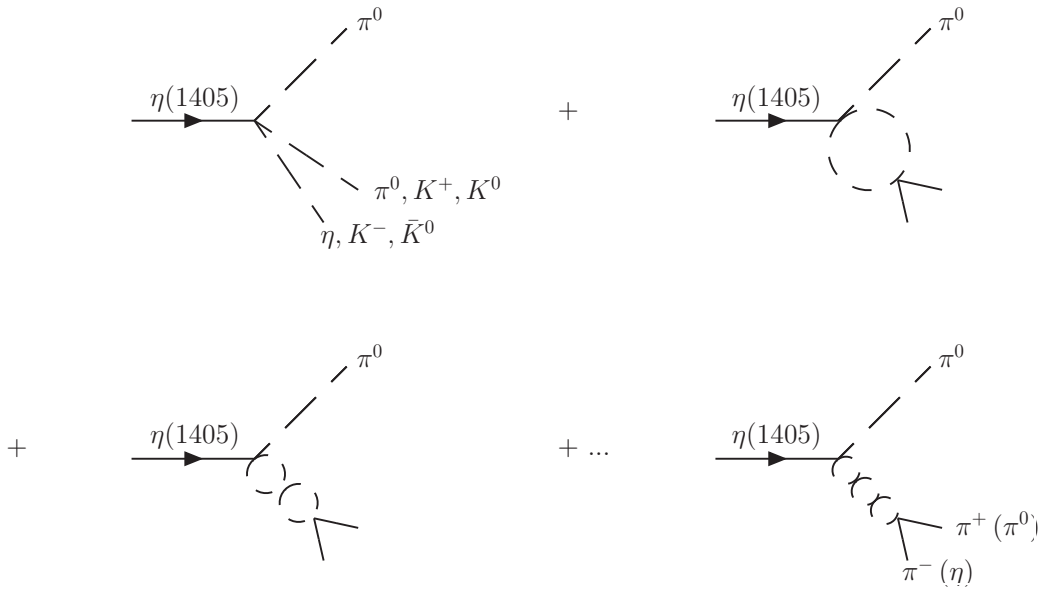

Figure 5.1: Diagrammatic representation of the $\pi^0\pi^+\pi^-$, $\pi^0\pi^0\eta$ production in the $\eta(1405)$ decay.

generate the $f_0(980)$ or the $a_0(980)$ in the case of $\pi^0\eta$ production. In the case of $\pi^+\pi^-$ production, the π^0 would not generate either the $f_0(980)$, that has zero charge, nor the $a_0(980)$ which does not couple to two pions. But even if it had, it would not play a role in the reaction as we shall discuss below.

If we invoke exact $I = 0$ for the $\eta(1405)$, the pair of interacting mesons in **Figure 5.1** must have $I = 1$. Then the $K\bar{K}$ pair appears in the $I = 1$ combination

$$\frac{1}{\sqrt{2}}(K^+K^- - K^0\bar{K}^0)\,, \tag{5.1}$$

where we take the convention that $|K^-\rangle \equiv -|1/2, -1/2\rangle$. If charged and neutral kaons had the same masses, the loop functions in the figure would be the same in the two cases. The relative minus sign in Eq. (5.1) guarantees the exact cancellation of the K^+K^- and $K^0\bar{K}^0$ contributions, preventing the production of the $\pi^+\pi^-$ pair in the final state (the $\pi^0\eta \to \pi^+\pi^-$ would also not proceed). However, when the physical masses are considered, the exact cancellation turns into a partial cancellation, leading to an isospin breaking effect that we study in detail below.

So far we have only advocated isospin conservation in the $\eta \to \pi^0 PP$ vertex. Now we can go one step further and put some constraints on the $\pi^0\eta$ primary production using arguments of $SU(3)$.

The η and η' are members of a nonet, with the η largely an octet and the

η' basically a singlet with a small mixing [178–180]. By analogy, we can also assume that in the next pair of η states, the $\eta(1235)$ is largely an octet and the $\eta(1405)$ is mostly a singlet (later on this constraint will be released to quantify uncertainties). This means that if we want a singlet to be produced with the octet of the spectator π^0, we have to place the interacting meson pair into an octet. Then, up to an undetermined reduced matrix element, the weight of K^+K^-, $K^0\bar{K}^0$ and $\pi^0\eta$ is determined by the $SU(3)$ Clebsch-Gordan coefficients of the $8 \otimes 8 \to 1$ decomposition. We have up to a global factor,

$$M_{K^+K^-} = \sqrt{\frac{3}{5}}\,, \qquad M_{K^0\bar{K}^0} = -\sqrt{\frac{3}{5}}\,, \qquad M_{\pi^0\eta} = \sqrt{\frac{4}{5}}\,. \tag{5.2}$$

Then, the scattering matrix for the production of the final state is given by

$$T_f = M_f + \sum_{i=1}^{3} M_i G_i\, t_{if}\,, \tag{5.3}$$

where t_{if} is the 5×5 scattering matrix for the channels K^+K^- (1), $K^0\bar{K}^0$ (2), $\pi^0\eta$ (3), $\pi^+\pi^-$ (4), $\pi^0\pi^0$ (5) and M_i in the same basis is given by

$$M_i = A\left(\sqrt{\frac{3}{5}}, -\sqrt{\frac{3}{5}}, \sqrt{\frac{4}{5}}, 0, 0\right)\,, \tag{5.4}$$

with A a reduced matrix element.

The t matrix is obtained using the Bethe-Salpeter equation in the five coupled channels with V taken from Ref. [30] (care is taken to multiply by $1/\sqrt{2}$ the matrix elements in the case of $\pi^0\pi^0$ states, thus implementing the unitary normalization which is suited for the sum over intermediate states of identical particles).

The G function is the diagonal loop matrix for the propagators of the intermediate particles of Eq. (2.57). By using a cutoff $q_{max} = 900$ MeV we obtain a good description of the $f_0(980)$ and $a_0(980)$ resonances, as in Ref. [30]. As explained in **Chapter 2**, in a certain range of energy one could use equivalently a dimensionally regularized G function. In the present case we deliberately use the cutoff method because the knowledge of this cutoff will serve to regularize the loop function we find in the next sections.

Note that in Eq. (5.3) we have two sources of isospin violation: the one due to the G_i functions, which now are different for K^+K^- and $K^0\bar{K}^0$, and the t_{if} matrix elements, which are evaluated using the Bethe-Salpeter equation in the charge basis of the states and that also break isospin symmetry since the G_i functions are different for different members of the same isospin multiplets.

Now we would like to release the assumption of the $\eta(1405)$ being an $SU(3)$ singlet. Let us accept that it could be a mixture of an octet and a singlet. In

the case of a pure octet for the $\eta(1405)$, the interacting pair can belong to the 8, 10 and 27 representations. Defining

$$R = \frac{M(\pi^0\eta)}{M(K^+K^-)}\,, \tag{5.5}$$

we find that the values of this quantity are $R = \sqrt{4/3}$ for the octet, $R = 0$ for the decuplet and $R = -\sqrt{3}$ for the 27. If the $\eta(1405)$ were a pure octet, the interacting pair would only couple to the 27 representation. However, this possibility is quite unlikely. This leads us to values of R preferably positive. Note that with negative values of R (we have seen that this can happen for values around $R \simeq -1.5$) there is a destructive interference between $\pi^0\eta$ and $K\bar{K}$ induced $a_0(980)$ production such that the $\pi^0 a_0(980)$ production would disappear in the $\eta(1405)$ decay, which is not the case experimentally [181]. The order of magnitude for R is determined with these simple arguments, but we can get help from experiment since from Refs. [181] and [182] we know the ratio

$$R_\Gamma = \frac{\Gamma(\pi\pi\eta)}{\Gamma(\pi K\bar{K})} = 1.09 \pm 0.48\,. \tag{5.6}$$

Assuming the ratio to hold for the rates to $\pi^0\pi^0\eta$ and $\pi^0(K^+K^- + K^0\bar{K}^0)$ we get

$$R_\Gamma = \frac{1}{2}\; R^2\; \frac{PS(\pi^0\pi^0\eta)}{PS(\pi^0 K\bar{K})}\,, \tag{5.7}$$

where PS stands for the phase space of each final state, which is obtained integrating $\frac{d\Gamma}{dm_f}$ of Eq. (5.9) over m_f (taking $\beta = |T_f| = 1$). By doing this we obtain

$$|R| = 0.75 \pm 0.17\,. \tag{5.8}$$

This result with positive sign would be in agreement with the prediction based on the assumption of the $\eta(1405)$ being an $SU(3)$ singlet, $R = \sqrt{4/3} = 1.15$. Yet, in the next Section we will explore the results within the range $R \in [-1, 1.2]$.

5.2.2 Results with the local vertices

We need to evaluate $\frac{d\Gamma}{dm_f}$, where m_f is the invariant mass of the final interacting pair ($\pi^+\pi^-$ or $\pi^0\eta$), to compare it with the experimental results. Since the meson-meson interaction that leads to the $f_0(980)$ and $a_0(980)$ resonances is s-wave, there is no angular dependence in the T_f matrix and, since we are only interested in the region around $m_f = 980$ MeV, the magnitude A in Eq. (5.4)

can be considered as a constant. In this case we have [183]

$$\frac{d\Gamma}{dm_f} = \beta\ p_1\ \tilde{p}_2\ |T_f|^2\,, \tag{5.9}$$

with β a constant factor and where

$$p_1 = \frac{\lambda^{1/2}(m_{\eta'}^2, m_{\pi^0}^2, m_f^2)}{2m_\eta} \tag{5.10}$$

is the momentum of the spectator π^0 in the $\eta(1405)$ rest frame and

$$\tilde{p}_2 = \frac{\lambda^{1/2}(m_f^2, m_2^2, m_3^2)}{2m_f} \tag{5.11}$$

the momentum of the interacting pair in the rest frame of the pair. In Eqs. (5.10) and (5.11), m_2, m_3 are the masses of the mesons of the interacting pair.

In **Figure 5.2** and **Figure 5.3**, we plot $\frac{d\Gamma}{dm_f}$ for f equal to $\pi^+\pi^-$ and $\pi^0\eta$, taking A in Eq. (5.4) equal to 1. We can rightly say that the unitarization from the meson-meson pairs should be implemented in other pairs too. Think for instance of the case of primary production of $\pi^0 K\bar{K}$ and then the successive $\pi^0 K$ interaction, producing an effective $\eta(1405)K\bar{K}\pi^0$ vertex that will depend on $m_{\pi^0 K}$. After this, the $K\bar{K}$ will interact again to finally produce the f_0 or a_0. The isospin or $SU(3)$ argument used before should also hold, but the coefficient A would now be dependent on $m_{\pi^0 K}$, which also introduces an angular dependence on this coefficient. However, upon projection over s-wave, needed to generate the f_0 or a_0 resonances, and the selection of a narrow window for $m_{K\bar{K}}$ around 980 MeV, the coefficient A turns again into a constant. Similar arguments can be used with respect to the symmetrization of the two pions in the $\pi^0\pi^0\eta$ channel.

What we can see in **Figure 5.2** and **Figure 5.3** is that in the case of the $\pi^+\pi^-$ production we obtain a very narrow peak around 980 MeV, like observed in the experiment [165]. The width of this peak is about 10 MeV, also in agreement with experimental observations. As we discussed above, the peak appears in the $f_0(980)$ region, between the thresholds of K^+K^- and $K^0\bar{K}^0$, because now the quantity $G_{K^+K^-} - G_{K^0\bar{K}^0}$ is different from zero. However, this difference, which is due to the different kaon masses, is only significant in a region of energies around the $K\bar{K}$ thresholds, where $\Delta(\sqrt{s})$ is of the order of $m_{K^+} - m_{K^0}$, as it can be clearly seen in **Figure 5.4**. Far away from the thresholds the difference of the two G functions, due to the mass difference, becomes gradually smaller and this leads to the peculiar narrow shape of the $f_0(980)$ excitation in the $\pi^+\pi^-$ channel, already anticipated in Refs. [159–161].

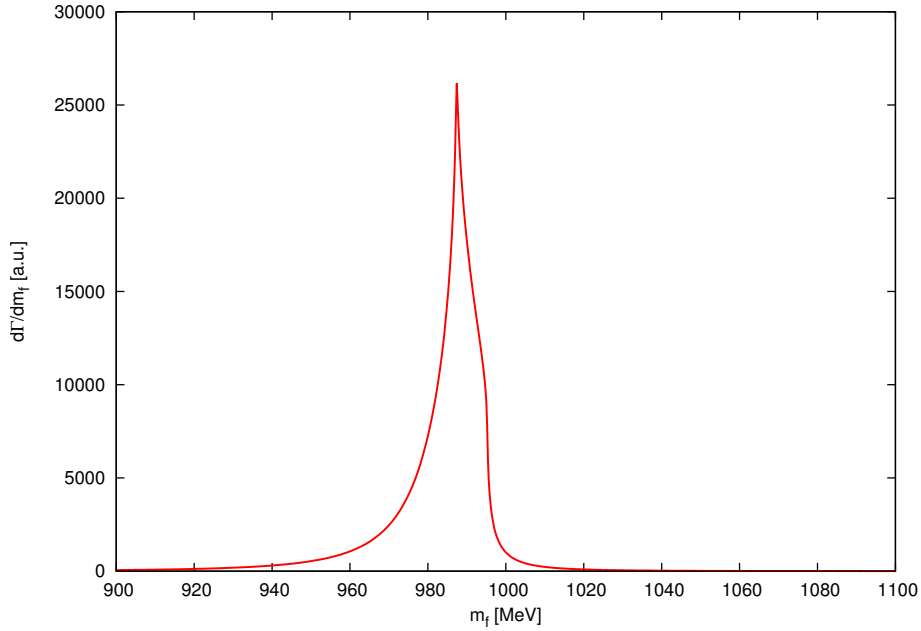

Figure 5.2: $\frac{d\Gamma}{dm_f}$ for $\eta' \to \pi^0\pi^+\pi^-$ decay in the $f_0(980)$ region.

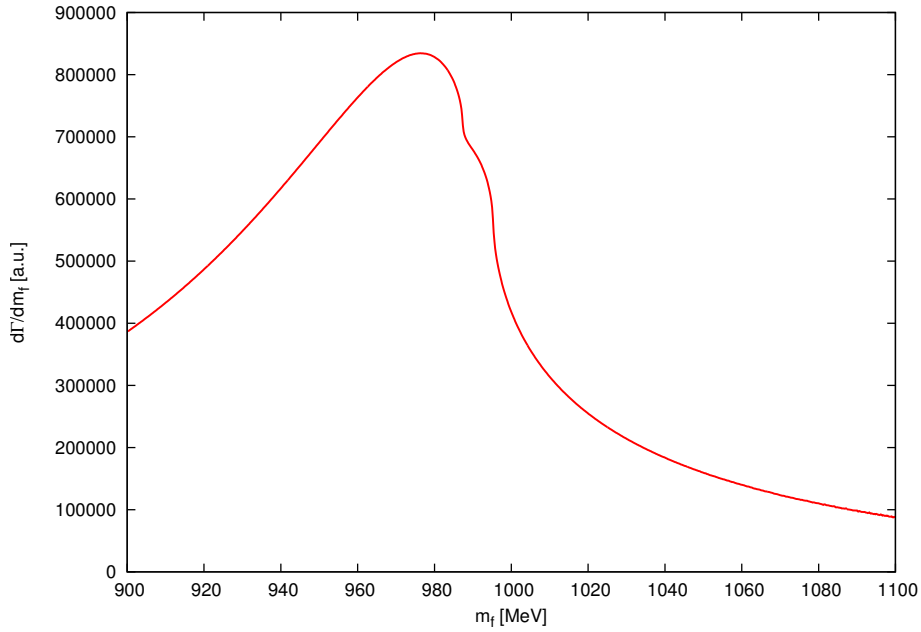

Figure 5.3: $\frac{d\Gamma}{dm_f}$ for $\eta' \to \pi^0\pi^0\eta$ decay in the $a_0(980)$ region.

One should stress here that the shape of **Figure 5.2** is not the standard one of the $f_0(980)$ seen in isospin allowed reactions and the width is tied to the mass difference $m_{K^+} - m_{K^0}$. This comment is very relevant in view of what

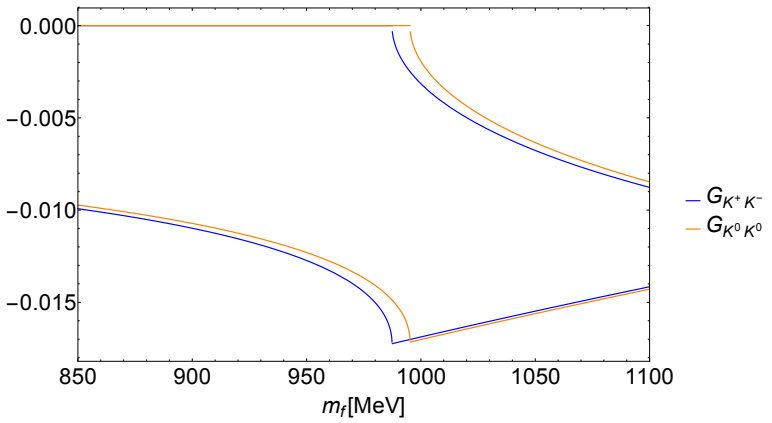

Figure 5.4: Real and imaginary part of $G_{K^+K^-}$ and $G_{K^0\bar{K}^0}$ as functions of the energy.

quoted in Ref. [165]: "The measured width of the $f_0(980)$ is much narrower than the world average". It is clear that the shape of $\pi^+\pi^-$ production here is not the usual shape of the $f_0(980)$.

In **Figure 5.3** we see the signal for the $a_0(980)$ excitation, which is isospin allowed. The width is much larger, and also is the strength at the peak. If we compare the strength of the peak for $\pi^+\pi^-$ of f_0 and $\pi^0\eta$ of a_0 production, we find that the ratio is of the order of 3%.

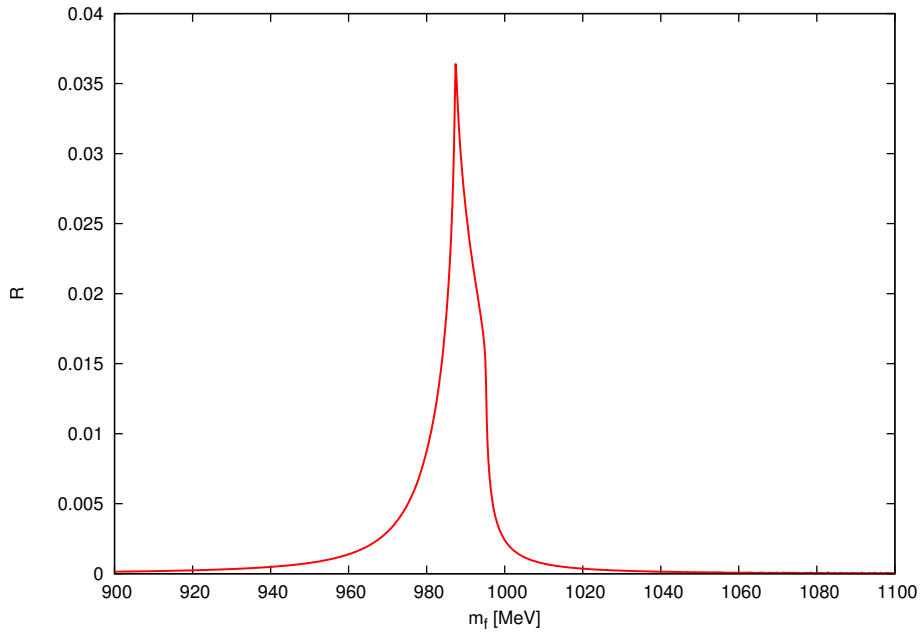

Figure 5.5: Ratio $\left(\frac{d\Gamma}{dm_f}\right)_{\pi^+\pi^-} / \left(\frac{d\Gamma}{dm_f}\right)_{\pi^0\eta}$ as a function of m_f.

However, if we integrate the strength over m_f in the region of the peaks for the two cases, we find a smaller ratio

$$\frac{\Gamma(\pi^0, \pi^+\pi^-)}{\Gamma(\pi^0, \pi^0\eta)} = 0.015\,, \tag{5.12}$$

of the order of 1.5%, which is along the lines of the 0.6% observed in the two reactions $J/\psi \to \phi\pi^0\eta(\pi^+\pi^-)$ or $\chi_{c1} \to \pi^0(\pi^+\pi^-)(\pi^0\eta)$ [164]. In **Figure 5.5**, we show the ratio $d\Gamma(\pi^+\pi^-)/d\Gamma(\pi^0\eta)$ as a function of the energy. We observe a peculiar structure, where the K^+K^-, $K^0\bar{K}^0$ thresholds show up as cusps, as predicted in Refs. [160, 161] and also shown in Ref. [162].

We come now to the analysis of the uncertainties due to the diversion from the $SU(3)$ hypothesis assumed. We allow R of Eq. (5.5) to vary between -1 and 1.2, as anticipated in the previous section. In **Figure 5.6** we can see that

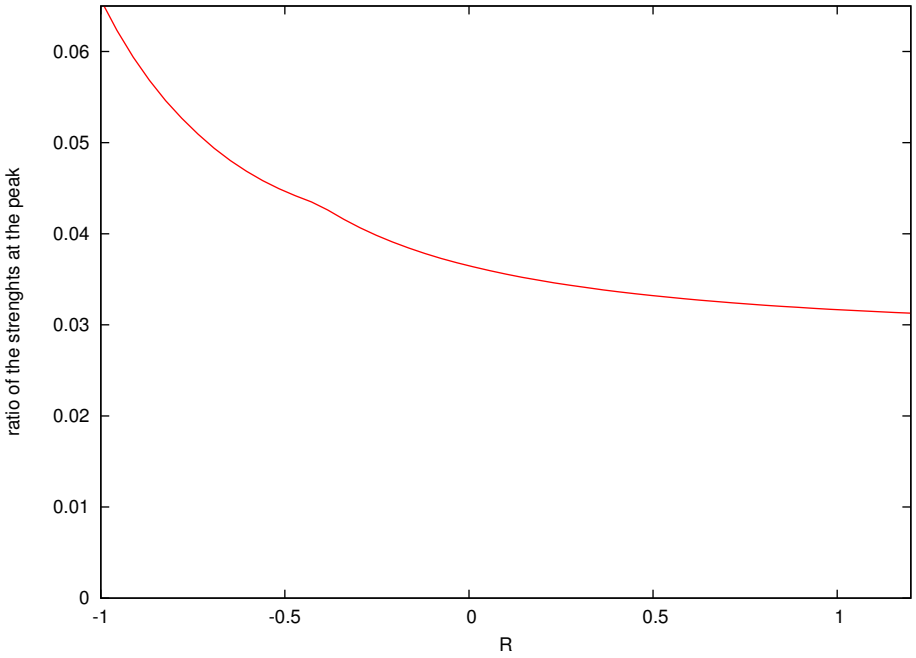

Figure 5.6: Ratio of strengths at the peak as a function of R.

the ratio of strengths at the peak of each resonance changes within a factor two in such a large range. In terms of the m_f integrated over the peak, removing background, the range is

$$\frac{\Gamma(\pi^0, \pi^+\pi^-)}{\Gamma(\pi^0, \pi^0\eta)} \in [0.01 - 0.04]\,. \tag{5.13}$$

The results are shown in **Figure 5.7**. At the extreme negative value of R, not preferred by the theory, the ratio reaches the value of 0.042. In the range

from $R = 0$ (the value implicitly taken in Ref. [166]) to $R = 1.2$ ($R = 1.15$ corresponds to the $SU(3)$ singlet for the $\eta(1405)$) the value of the ratio of Γ's ranges from 1% to 1.5%. This means that, even with this theoretical uncertainty, it is clear that we cannot obtain a ratio as big as the 18% reported in the experiment of Ablikim *et al.* [165].

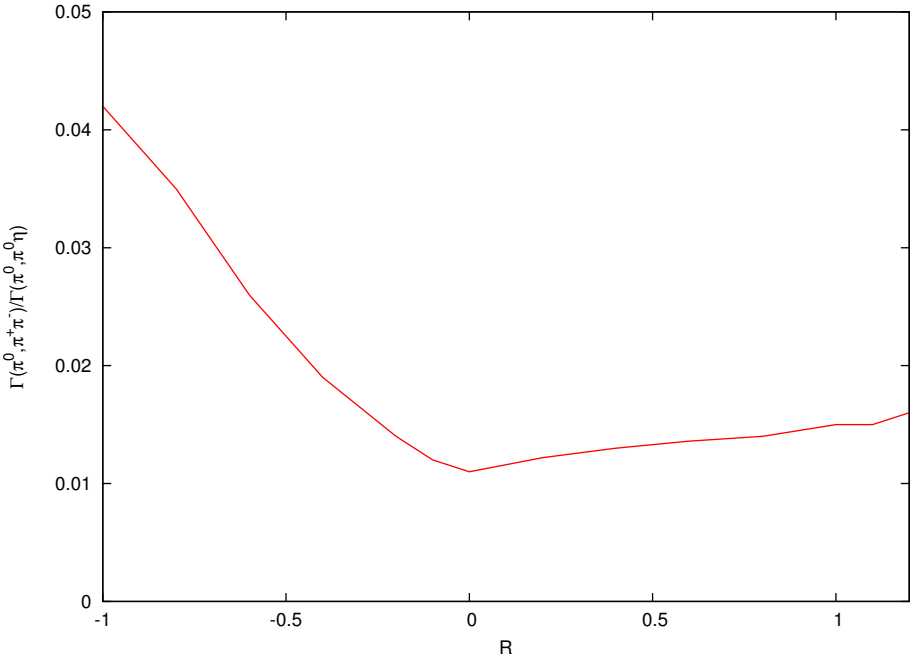

Figure 5.7: Ratio $\frac{\Gamma(\pi^0,\pi^+\pi^-)}{\Gamma(\pi^0,\pi^0\eta)}$ as a function of R.

However, so far we have always assumed the $\eta(1405)$ to be a pure $I = 0$ state. Let us now assume that we have a mixture of $I = 0$ and $I = 1$ in that state (the same conclusions would hold if we say instead that there is isospin violation in the production of mesons of the first step, something that is very unusual in chiral theories [161]). In the case of $I = 1$ for the $\eta(1405)$, the interacting meson pair can have $I = 0$, which we assume in the $SU(3)$ octet to magnify the $f_0(980)$ production. Then the channels involved are $\pi\pi$ and $K\bar{K}$, but the $\pi\pi$ channel is weak in this process and for the exercise that we do can be safely ignored in the production vertices, but not in the t_{if} matrix of Eq. (5.3). The $K\bar{K}$ $I = 0$ combination is

$$\frac{1}{\sqrt{2}}(K^+K^- + K^0\bar{K}^0)\,. \tag{5.14}$$

Taking into account the isospin mixture and a different reduced matrix element for $I = 0$ pair production, and putting the product in a coefficient α,

we have now $M_i \to \tilde{M}_i$, with $\tilde{M}_i$ given by

$$\tilde{M}_i = A\left((1+\alpha)\sqrt{\frac{3}{5}}, (\alpha-1)\sqrt{\frac{3}{5}}, \sqrt{\frac{4}{5}}, 0, 0\right) . \tag{5.15}$$

We vary the parameter α until we find a ratio $\Gamma(\pi^0,\pi^+\pi^-)/\Gamma(\pi^0,\pi^0\eta) = 0.18$. Such a ratio corresponds to a value of 0.54 for the parameter α, which implies a massive isospin violation in a physical state. This would be difficult to accept in physical terms, but there is one stronger reason to reject this solution. Indeed, as seen in **Figure 5.8**, once we have an $I = 0$ pair to begin with, the $f_0(980)$ production can proceed unhindered and, then, with its natural width. The combination of Eq. (5.15) leads to an effective width of about 20 MeV, much bigger than the experimentally observed 9 MeV of Ref. [165]. In **Figure 5.9** we can see that the $a_0(980)$ resonance is also produced in this case with a shape like the ordinary one.

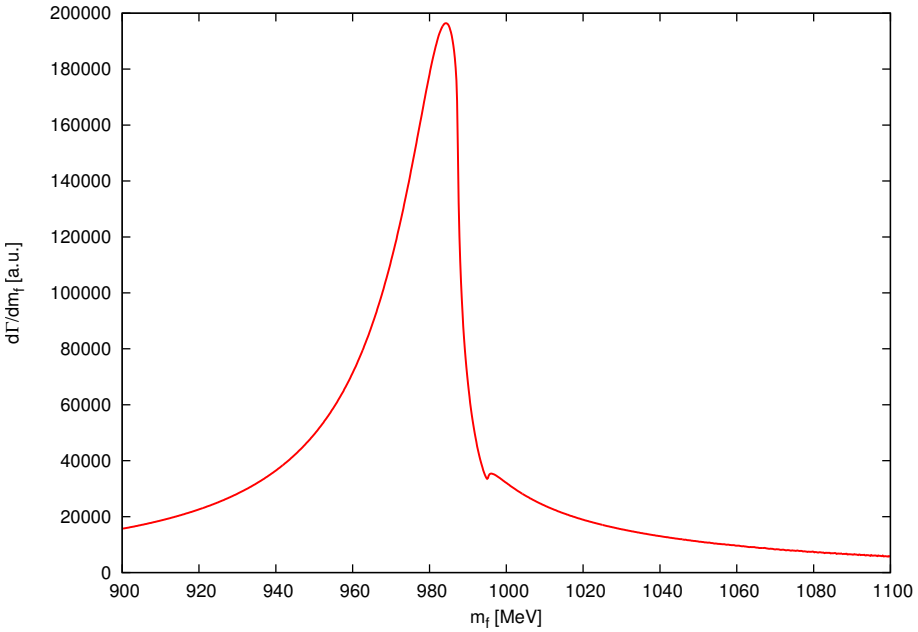

Figure 5.8: $\frac{d\Gamma}{dm_f}$ for $\eta \to \pi^0\pi^+\pi^-$ decay in the $f_0(980)$ region, for $\alpha = 0.54$.

5.2.3 The primary production vertex with the $K^*\bar{K}$ singularity

In the former section we have proved that it is not possible to get such a large isospin violation as found in Ref. [165] assuming a local vertex production.

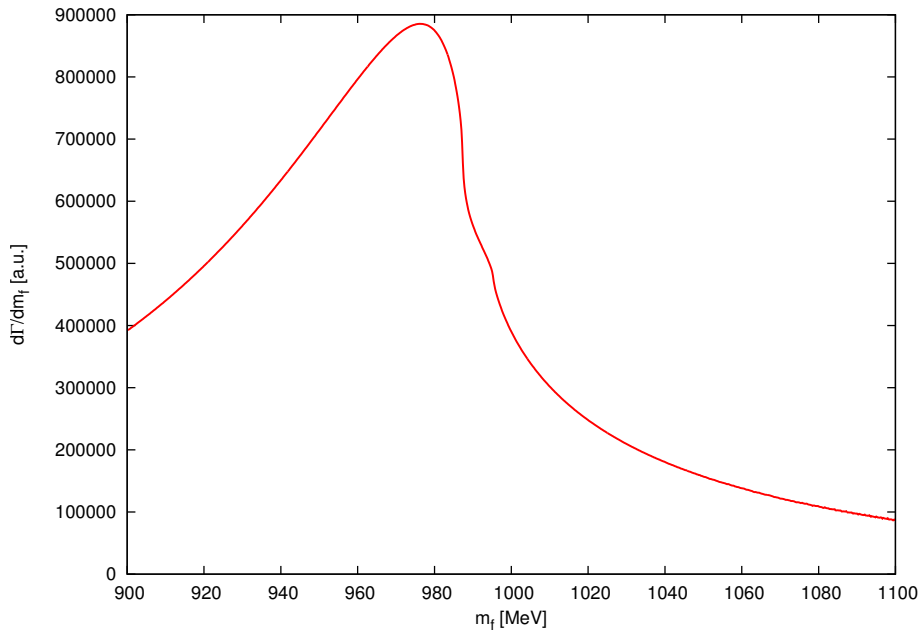

Figure 5.9: $\frac{d\Gamma}{dm_f}$ for $\eta \to \pi^0\pi^0\eta$ decay in the $a_0(980)$ region, for $\alpha = 0.54$.

In the work of Ref. [166] it was shown that using the $\eta(1405)$ decay mode to $K^*\bar{K}$ and the successive decay of the K^* into $K\pi$ one obtains a mechanism for $K\bar{K}\pi$ production at tree level leading to a good agreement with experimental data on this channel. This production mechanism is depicted in **Figure 5.10**

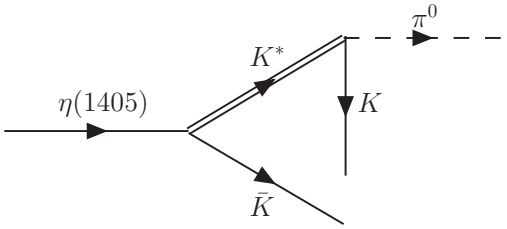

Figure 5.10: Singular mechanism for $\pi^0 K\bar{K}$ production.

After rescattering of the $K\bar{K}$ pair, as shown in **Figure 5.11**, the f_0 and a_0 resonances will be produced in our approach. The novelty now is that the first loop depicted in **Figure 5.11** is rather different than the one of the ordinary G function for $K\bar{K}$ propagation shown in the second diagram of **Figure 5.1**. The difference is substantial because the structure of the loop function (through dispersion relations) is determined by the singularities (pairs of intermediate particles that can be simultaneously placed on shell in the loop integration).

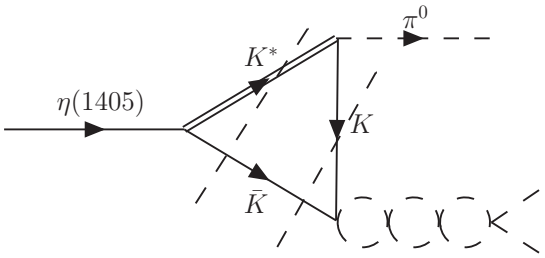

Figure 5.11: Rescattering mechanism for the production of the f_0 and a_0.

The loop in **Figure 5.11** has two singularity cuts, indicated by the dashed lines, one for the $K^*\bar{K}$ on shell and the other one for the $K\bar{K}$ on shell. The kinematics of the two cuts are not too far away, which magnifies the difference in the loop functions in the charged and neutral cases due to the different masses amongst the kaons and the K^*.

Note that the situation is completely different for the $J/\psi \to \phi f_0$ reaction. Indeed, even if the highly suppressed $J/\psi \to K^*\bar{K}$ decay were followed by the $K^* \to \phi K$ vertex, this latter process is kinematically forbidden, which means that the K^* is produced highly off shell. So, this mechanism for $J/\psi \to \phi K\bar{K}$ qualifies as a contact term for $\phi K\bar{K}$ production. Thus, the approach followed in the former section is the most appropriate for this case and it is in essence the one followed in Refs. [161, 162]. The experimental ratio for the J/ψ decay widths in this reaction are in line with the results obtained in the former section.

On the other hand, the mechanism depicted in **Figure 5.10** reminds one of the $\phi \to \pi^0\pi^0\gamma$ decay which has the same structure with $\phi \to K\bar{K}$, the K (or $\bar{K}$) radiating a photon and the resulting $K\bar{K}$ pair interacting to give $\pi^0\pi^0$ or $\pi^0\eta$ (same diagram as **Figure 5.11** substituting the π^0 by γ and the K^* by K). One has there two cuts for $K\bar{K}$ before and after the radiation of the photon. The mechanism outlined above revealed very successful [152, 184–186] reproducing the experimental data for $\phi \to \pi^0\pi^0\gamma, \pi^0\eta\gamma$.

Let us now proceed to the explicit evaluation of the amplitude for the mechanism of **Figure 5.11**. The loop function is evaluated using the momenta assignment shown in **Figure 5.12**. For convenience we make the evaluation in the frame where $\vec{P} = 0$ and thus $\vec{p}_{\eta'} = \vec{p}_\pi$, with the symbol η' is adopted in the formulas for simplicity and stands for $\eta(1405)$.

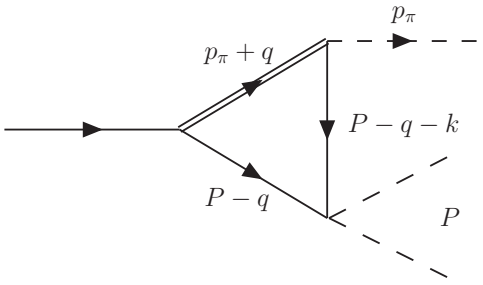

Figure 5.12: Loop for the function $\tilde{G}$.

Given the structure of the $V \to PP$ vertices, $\epsilon^\mu (p_1 - p_2)_\mu$, we obtain

$$\tilde{G}(P, p_\pi, m_K, m_{K^*}) = i \int \frac{d^4q}{(2\pi)^4} \epsilon^\mu (P + p_\pi + P - q)_\mu \, \epsilon^\nu (p_\pi - q)_\nu \times \frac{1}{(p_\pi + q)^2 - m_{K^*}^2 + i\epsilon} \, \frac{1}{q^2 - m_K^2 + i\epsilon} \, \frac{1}{(P - q)^2 - m_K^2 + i\epsilon} \,. \tag{5.16}$$

By summing over the polarizations,

$$\sum \epsilon_\mu \epsilon_\nu \to -g_{\mu\nu} + \frac{(p_\pi + q)_\mu (p_\pi + q)_\nu}{m_{K^*}^2} \,, \tag{5.17}$$

we get

$$\tilde{G}(P, p_\pi, m_K, m_{K^*}) = i \int \frac{d^4q}{(2\pi)^4} \frac{F_{num}}{(p_\pi + q)^2 - m_{K^*}^2 + i\epsilon} \, \frac{1}{q^2 - m_K^2 + i\epsilon} \times \frac{1}{(P - q)^2 - m_K^2 + i\epsilon} \,, \tag{5.18}$$

where

$$\begin{aligned} F_{num} &= -(2P(p_\pi - q) + m_\pi^2 + q^2 - 2p_\pi q) + \frac{(m_\pi^2 - q^2)}{m_{K^*}^2} [2P(p_\pi + q) + m_\pi^2 - q^2] \\ &= 2p_{\eta'}(p_\pi - q) + \frac{(m_\pi^2 - q^2)}{m_{K^*}^2} [2P(p_\pi + q) + m_\pi^2 + m_{K^*}^2 - q^2] \,. \end{aligned} \tag{5.19}$$

The integral in Eq. (5.18) led the authors of Ref. [166] to face a technical problem, consisting in the fact that, since it is highly superficially divergent (d^4q/q^2), some form factor or cutoff had to be used to implement convergence. However, we shall see below that the integral is only logarithmically divergent.

When performing the evaluation of the $\eta(1405) \to \pi^0\pi^+\pi^-$ amplitude one has the difference of $\tilde{G}$ for the charged K^-K^+ and the neutral ones and the results are convergent, but the ratio to the $\eta(1405) \to \pi^0\pi^0\eta$ is still tied to an unknown form factor.

Our approach solves naturally the former problem. To see this recall that, in the Bethe-Salpeter equation for the scattering, the G function is also formally divergent and is regularized by means of a cutoff, fitted to the experimental meson-meson scattering data. The natural choice is to use this same cutoff in the new loop, but this becomes a necessity if one recalls that the results of the chiral unitary approach with the G function implementing a cutoff $\theta(q_{max} - |\vec{q}|)$ in the integration are obtained, in a Quantum Mechanical formulation, with a potential (for s-waves)

$$V(\vec{q}, \vec{q}\,') = v\ \theta(q_{max} - |\vec{q}\,|)\ \theta(q_{max} - |\vec{q}\,'|)\,, \tag{5.20}$$

which leads to an amplitude

$$t(\vec{q}, \vec{q}\,') = t\,\theta(q_{max} - |\vec{q}|)\,\theta(q_{max} - |\vec{q}\,'|)\,. \tag{5.21}$$

Then in **Figure 5.11** the cutoff $\theta(q_{max} - |\vec{q}|)$ appears automatically in the loop function from the first $K\bar{K} \to PP$ potential in the sum of the diagrams implicit in the figure. Observe that the cutoff is in three-momentum. The q^0 integration must be done analytically and it is convergent.

The expressions are simplified and equally accurate if we just take the positive energy part of the relativistic K^* propagator

$$\frac{1}{2\omega_{K^*}(\vec{p}_\pi + \vec{q}\,)}\ \frac{1}{p_\pi^0 + q^0 - \omega_{K^*}(\vec{p}_\pi + \vec{q}\,) + i\epsilon}\,, \tag{5.22}$$

where $\omega_{K^*}(\vec{p}\,) = \sqrt{\vec{p}^{\,2} + m_{K^*}^2}$. Using Cauchy's theorem for the q^0 integration, we obtain then

$$\begin{aligned}\tilde{G}(P, p_\pi, m_K, m_{K^*}) = \int_{|\vec{q}|<q_{max}} \frac{d^3q}{(2\pi)^3}\ \frac{1}{2\omega}\ \frac{1}{P^0}\ \frac{1}{2\omega_{K^*}}\Big[\frac{F'_{num}}{P^0 + 2\omega}\ \frac{1}{p_\pi^0 - \omega - \omega_{K^*}} \\ + \frac{F''_{num}}{P^0 - 2\omega + i\epsilon}\ \frac{1}{P^0 + p_\pi^0 - \omega - \omega_{K^*} + i\epsilon}\Big]\,,\end{aligned} \tag{5.23}$$

where $F'_{num} = F_{num}(q^0 = -\omega)$, $F''_{num} = F_{num}(q^0 = P^0 - \omega)$, $\omega = \sqrt{\vec{q}^{\,2} + m_K^2}$ and $\omega_{K^*} = \sqrt{\vec{q}^{\,2} + m_{K^*}^2}$. Eq. (5.23) shows explicitly in the second term the two singularities corresponding to the cuts depicted in **Figure 5.11**. One can show from Eq. (5.23) that $\tilde{G}$ is only logarithmically divergent. The apparent two extra powers of q introduced by the K^* polarization sum of Eq. (5.17)

result fictitious once the value of q^0 at the poles is substituted in Eq. (5.19) in the Wick rotation leading to Eq. (5.23).

Taking into account that the $\eta(1405)$ is an $I = 0$ object and that the K^+K^- and $K^0\bar{K}^0$ vertices appear with different sign, the amplitude of Eq. (5.3) is substituted now by

$$T_f = \tilde{G}(P, p_\pi, m_{K^+}, m_{K^{*+}})\; t_{K^+K^-,f} - \tilde{G}(P, p_\pi, m_{K^0}, m_{K^{*0}})\; t_{K^0\bar{K}^0,f}\,, \quad (5.24)$$

where f stands for $\pi^+\pi^-$ or $\pi^0\eta$, as before.

5.2.4 Results with the triangular diagram

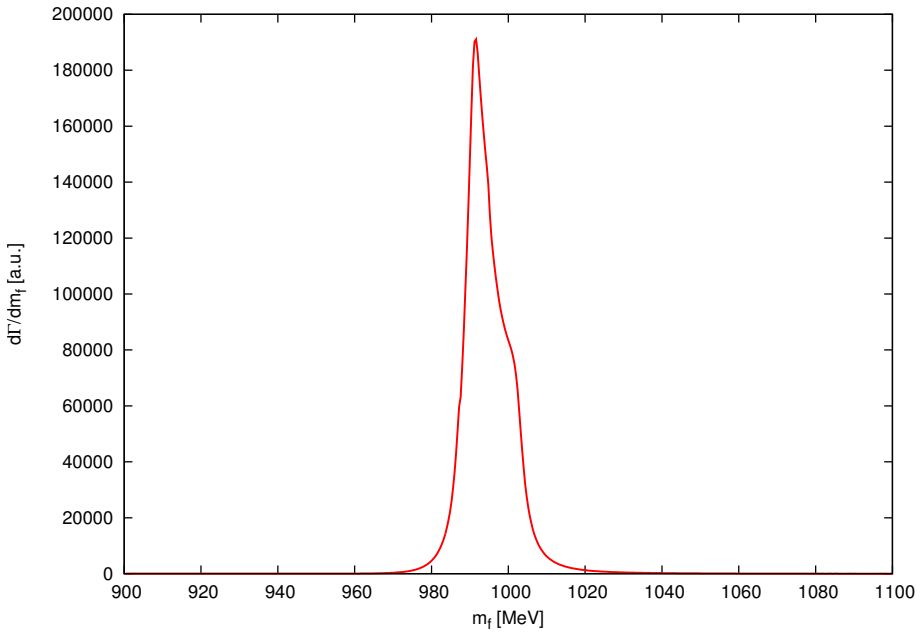

Figure 5.13: $\frac{d\Gamma}{dm_f}$ for $\eta' \to \pi^0\pi^+\pi^-$ decay in the $f_0(980)$ region.

In **Figure 5.13** we show the result for $d\Gamma/dm_f$ for $\eta(1405) \to \pi^0\pi^+\pi^-$ and in **Figure 5.14** for $\eta(1405) \to \pi^0\pi^o\eta$. The shapes are very similar to those in **Figure 5.2** and **Figure 5.3** but we can already observe that the ratio, depicted in **Figure 5.15**, is much bigger than what we had in **Figure 5.5** for the contact vertex, and about a factor nine bigger. From these spectra we find that the ratio of integrated decay widths is now

$$\frac{\Gamma(\pi^0, \pi^+\pi^-)}{\Gamma(\pi^0, \pi^0\eta)} \simeq 0.13\,. \quad (5.25)$$

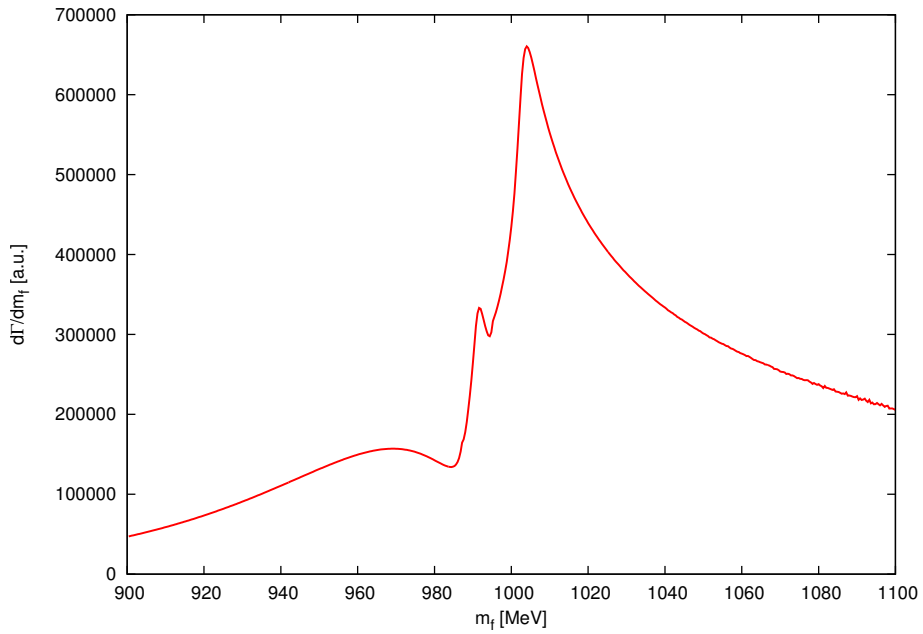

Figure 5.14: $\frac{d\Gamma}{dm_f}$ for $\eta' \to \pi^0\pi^0\eta$ decay in the $a_0(980)$ region.

This 13% is much closer to the experimental value of $(17.9 \pm 4.2)\%$, which has a lower limit of 13.7%. Assuming similar theoretical uncertainties the results are compatible.

We have made some estimates of the errors by changing the cutoff q_{max} by ± 20 MeV, which moves the $f_0(980)$ and $a_0(980)$ peaks in $\pi\pi$ and $\pi\eta$ scattering by about 8 MeV. We find that this change induces a variation in the ratio of Eq. (5.25) of 0.01. However, an uncertainty of 0.02 is more indicated to account also for the uncertainties in the background subtraction. So we would be obtaining (0.13 ± 0.02) for the fraction of decay rates. This increase by about one order of magnitude with respect to the standard calculation is a consequence of the two neighbouring singularities in the triangle diagram.

We can now estimate the effect of having also $\pi^0\pi^0\eta$ in the primary production process. A triangular diagram of the type used for $\pi^0 K\bar{K}$ production is not possible now. Indeed, one would have to substitute the K^* by a ρ, but this is dynamically forbidden (no $\rho\pi^0\eta$ coupling). Then we must rely upon a contact term. By recalling the exercise done in **Section 5.2.1** (Eqs. (5.6)-(5.8)) and the conclusion that positive values of R (with respect to an equivalent local $\pi^0 K\bar{K}$ production mechanism) were preferred, the inspection of **Figure 5.7** can give us a qualitative estimate of what adding this new primary $\pi^0\pi^0\eta$ production vertex can do to the widths, which is a moderate increase of the ratio $\Gamma(\pi^0, \pi^+\pi^-)/\Gamma(\pi^0, \pi^0\eta)$ by about 26%. This would provide a ratio around 16.4% with an uncertainty of 2.5% or, rounding errors, a

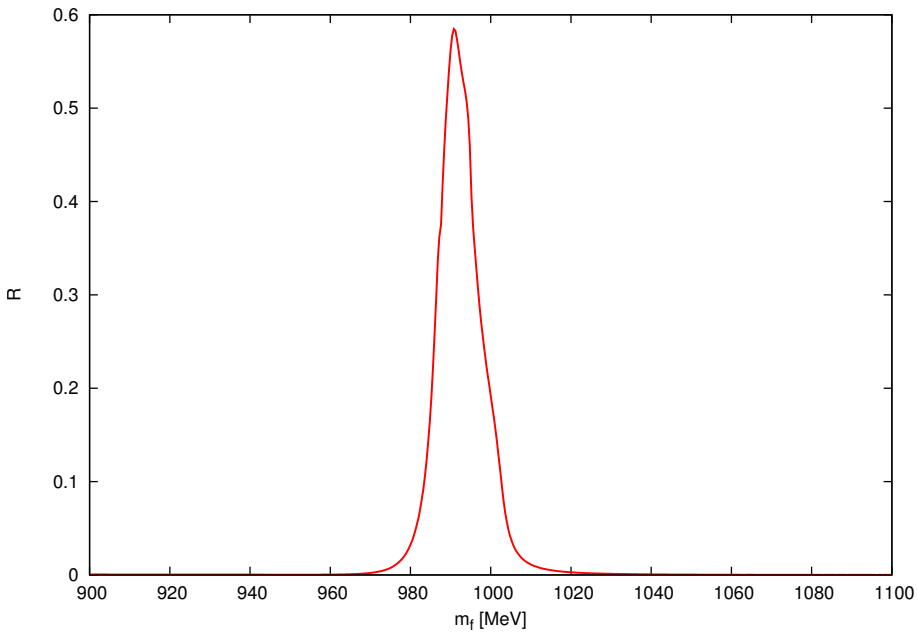

Figure 5.15: Ratio $\left(\frac{d\Gamma}{dm_f}\right)_{\pi^+\pi^-} / \left(\frac{d\Gamma}{dm_f}\right)_{\pi^0\eta}$ as a function of m_f.

ratio of (0.16 ± 0.03), in good agreement with the experimental values.

Now we come back to the BES experiment [166]. In this experiment the authors cannot distinguish whether they have the $\eta(1405)$ or the $\eta(1475)$ resonance, so we must assume that they have a mixture of both. In order to account for this possibility, we have evaluated the same ratio of rates as before assuming that we have now the $\eta(1475)$ resonance. The result that we obtain is

$$\left.\frac{\Gamma(\pi^0, \pi^+\pi^-)}{\Gamma(\pi^0, \pi^0\eta)}\right|_{\eta(1475)} \simeq 0.16\,. \tag{5.26}$$

This coincides with the centroid of our result of (0.16 ± 0.03). We might also think about the possibility of having a contribution from the original $\pi\pi\eta$ channel. However, the same collaboration team reports for the mixture of the resonances in the $J/\psi \to \gamma\pi^+\pi^-\eta$, $J/\psi \to \gamma K\bar{K}\eta$ a large dominance of the second process by nearly one order of magnitude [187, 188], which means we can neglect the primary $\pi\pi\eta$ channel in this case. Hence, assuming the same uncertainties as before, our final results for the $\eta(1405)$, the $\eta(1475)$, or a mixture of both, are given by

$$\frac{\Gamma(\pi^0, \pi^+\pi^-)}{\Gamma(\pi^0, \pi^0\eta)} = 0.16 \pm 0.03\,. \tag{5.27}$$

We discuss here also the case of the $\eta(1295)$. Little is known about the

coupling of this resonance to different channels. One might intuitively think that, by complementarity and orthogonality, if the $\eta(1405)$ couples strongly to $K^*\bar{K}$ it indicates that it has a large $s\bar{s}$ component, in which case the $\eta(1295)$ would mostly account for $u\bar{u}$ ($d\bar{d}$). In this case the coupling to $K^*\bar{K}$ would be highly suppressed.

We have evaluated the ratio $\Gamma(\pi^0,\pi^+\pi^-)/\Gamma(\pi^0,\pi^0\eta)$ at the peak of the f_0, a_0 for the two situations as before: (a) contact primary vertex, (b) triangular mechanism via $K^+\bar{K}$ production. In case (a) we found

$$\frac{\Gamma(\pi^0,\pi^+\pi^-)}{\Gamma(\pi^0,\pi^0\eta)} = 0.017\,, \tag{5.28}$$

while in the case (b) we found

$$\frac{\Gamma(\pi^0,\pi^+\pi^-)}{\Gamma(\pi^0,\pi^0\eta)} = 0.12\,. \tag{5.29}$$

In this latter case the channel $\eta(1295)\to K^*\bar{K}$ is not open, but close by, such that its near singularity still has an effect on the ratio similar to the one of Eq. (5.25). In the former case, Eq. (5.28), the results are also similar to all other cases where we have assumed dominance by primary contact production vertices.

Given the argumentation above, where we expect the $\eta(1295)$ to have small $s\bar{s}$ component, and hence small couplings to $K^*\bar{K}$, we would expect rates of the order of 0.017 for $\Gamma(\pi^0,\pi^+\pi^-)/\Gamma(\pi^0,\pi^0\eta)$. Should the experiment find a large value of this ratio, comparable with the one of the $\eta(1405)$, we would face an unexpected situation that could bring new light into the quest for the nature of the $\eta(1295)$ and $\eta(1405)$ resonances, which has stimulated much work [189–192].

5.3 The $f_1(1285)\to a_0(980)\pi^0$, $f_0(980)\pi^0$ decays

Now we want to study the decay of the $f_1(1285)$ to $a_0\pi$, excluding the $a_0(980)$ decay to $K\bar{K}$. According to the PDG [17], it makes up for a sizeable fraction of the total $f_1(1285)$ decay width, $(36\pm7)\%$. In addition, we will simultaneously study the reactions $f_1(1285)\to a_0(980)\pi^0$ and $f_1(1285)\to f_0(980)\pi^0$ to make an estimate of the amount of $a_0(980)-f_0(980)$ mixing.

Once the dynamically generated picture for the $f_1(1285)$, $a_0(980)$ and $f_0(980)$ is assumed, the process can be described resorting to the triangular mechanism already used in **Section 5.2.3**, and it consists in the four diagrams

depicted in **Figure 5.16**: we have the $f_1(1285)$ decaying to $K^*\bar{K}$, the decay of the K^* into $K\pi$ and the rescattering of the $K\bar{K}$ pair leading to $\pi^0\eta$ or $\pi^+\pi^-$ in the final state, which will proceed via the $a_0(980)$ or $f_0(980)$ resonances accounted for by the $K\bar{K} \to \pi^0\eta$ and $K\bar{K} \to \pi^+\pi^-$ amplitudes, respectively.

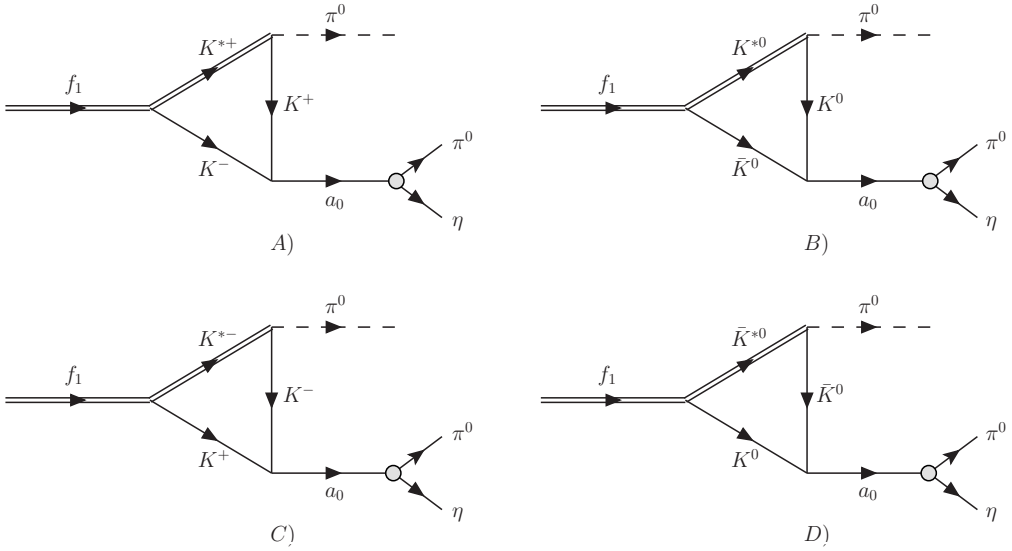

Figure 5.16: Diagrams representing the process $f_1(1285) \to \pi^0\eta$.

5.3.1 The structure of the vertices

In order to evaluate the amplitudes of the diagrams in **Figure 5.16**, we need the structure of the two vertices involved plus the $K\bar{K} \to \pi^-\pi^+(\pi^0\eta)$ amplitude, shown in **Figure 5.17**.

As mentioned before the $f_1(1285)$ results as dynamically generated from the interaction of $K^*\bar{K} - cc$ in Ref. [51]. We can write the vertex 1) of **Figure 5.17** as

$$-it_1 = -i\, g_{f_1}\, C_1 \epsilon^\mu \epsilon'_\mu\,, \tag{5.30}$$

where ϵ is the polarization vector of the f_1 and ϵ' is the polarization vector of the K^* ($\bar{K}^*$).

The coupling g_{f_1} of the f_1 to the $K^*\bar{K}$ channel is evaluated as the residue at the pole of the scattering amplitude for $K^*\bar{K} - cc$ in $I = 0$. The scattering amplitude is obtained using the Bethe-Salpeter equation (Eq. (2.59)) with the potential V taken from Ref. [51]. The loop function G is given by Eq. (2.57), with $\omega_i = \sqrt{\vec{q}^2 + m_i^2}$. We obtain a good description of the $f_1(1285)$ using a cutoff of about 1 Gev, as in Ref. [51]. We get $g_{f_1} = 7555$ MeV and we will use this value in the present calculation. This result is a bit bigger than the

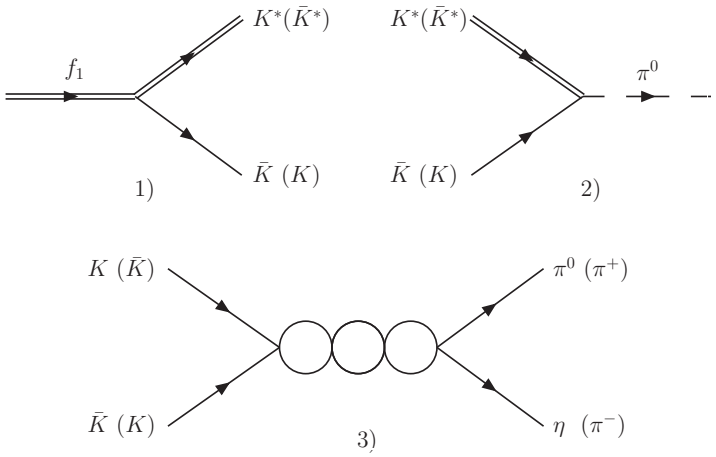

Figure 5.17: Vertices involved in the decay of the $f_1(1285)$ to $\pi^0\eta$ or $\pi^+\pi^-$, the $f_1(1285) \to K^*\bar{K}$ 1) and the VPP vertex 2), and amplitude for $a_0(980)$ and $f_0(980)$ production 3).

value of 7230 MeV found in Ref. [51], where a global fit to the axial vectors was conducted.

The factors C_1 in Eq. (5.30) are due to the fact that the $f_1(1285)$ couples to the $I = 0, C = +, G = +$ combination of $K^*\bar{K}$ mesons, which is represented by the state

$$\frac{1}{\sqrt{2}}(K^*\bar{K} - \bar{K}^*K) = -\frac{1}{2}(K^{*+}K^- + K^{*0}\bar{K}^0 - K^{*-}K^+ - \bar{K}^{*0}K^0)\,, \quad (5.31)$$

where the convention $CK^* = -K^*$ is taken, consistently with the standard chiral Lagrangians. The different values of C_1 for each diagram of **Figure 5.16**, corresponding to the weights of the charged and neutral components in the wave function of Eq. (5.31), are listed in the second column of **Table 5.1**.

The structure of the vertices of type 2) can be derived using the hidden gauge symmetry Lagrangian describing the VPP interaction of Eq. (2.92). Thus, the amplitude of the vertex can be written as

$$-it_2 = i\,g\,C_2\,(2k - P + q)_\mu \epsilon'^\mu\,, \quad (5.32)$$

where the factors C_2 for each diagram in **Figure 5.16** are shown in the third column of **Table 5.1**. The momenta in Eq. (5.32) are assigned as shown in **Figure 5.18**.

The $K\bar{K} \to \pi^0\eta(\pi^+\pi^-)$ amplitude in **Figure 5.17** corresponds to the mechanism for the production of either $\pi^0\eta$ or $\pi^+\,\pi^-$ in the final state after the rescattering of the $K\bar{K}$ pair that dynamically generates in coupled channels the $a_0(980)$ and $f_0(980)$ resonances [30], as in **Section 5.2.3**. However, we

Diagram	C_1	C_2	C
A)	$-\frac{1}{2}$	$\frac{1}{\sqrt{2}}$	$-\frac{1}{2\sqrt{2}}$
B)	$-\frac{1}{2}$	$-\frac{1}{\sqrt{2}}$	$\frac{1}{2\sqrt{2}}$
C)	$\frac{1}{2}$	$-\frac{1}{\sqrt{2}}$	$-\frac{1}{2\sqrt{2}}$
D)	$\frac{1}{2}$	$\frac{1}{\sqrt{2}}$	$\frac{1}{2\sqrt{2}}$

Table 5.1: Factors C_1 and C_2 for the vertices 1) and 2) in **Figure 5.17** and for the four diagrams in **Figure 5.16** in the second and third column, respectively. The values of their product, C, for the four different diagrams are listed in the fourth column.

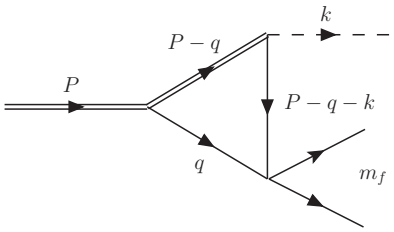

Figure 5.18: Momenta assignment for the $f_1(1285) \to a_0(980)\pi^0$, $f_0(980)\pi^0$ decays.

must keep in mind that the $f_1(1285)$ is an $I = 0$ object. If isospin symmetry were an exact symmetry (or if the kaons had the same mass), the process would only go via a_0 production, which is $I = 1$, and this would prevent finding the $\pi^+\pi^-$ pair in the final state in s-wave (the ρ^0 in p-wave is forbidden by C-parity conservation). Again, analogously to the case of the $\eta(1405)$, when the physical masses of the kaons are considered, we have an isospin breaking effect that leads to the production of the f_0 and then of the $\pi^+\pi^-$ pair.

We will write, for simplicity, this vertex as

$$-it_3 = -it_{if} \ , \tag{5.33}$$

where t_{if} is the if element of the same scattering matrix t appearing in Eq. (5.3). We have $i = 1$ for the diagrams A) and C) and $i = 2$ for the diagrams B) and D) of **Figure 5.16**, while the index f stands for channel 3 or 4 depending on the meson pair in the final state. The loop function G in the Bethe-Salpeter equation is given by Eq. (2.57) and it is regularized again using a cutoff around 900 MeV, which well reproduces the a_0 and f_0. This parameter enters the evaluation of the loop integral in the diagrams of **Figure 5.16**, as in the decay of the $\eta(1405)$.

5.3.2 The triangular loop

Putting together Eqs. (5.30), (5.32) and (5.33), we can explicitly write the total amplitude for each one of the diagrams in **Figure 5.16** as

$$\begin{aligned} -it = -i\,C_1\,g_{f_1}\,i\,C_2\,g \int \frac{d^4q}{(2\pi)^4}(2k-P+q)_\mu \epsilon'^{\mu}\,\epsilon_\alpha \epsilon'^{\alpha} \frac{i}{q^2-m_K^2+i\epsilon} \\ \times \frac{i}{(P-k-q)^2-m_K^2+i\epsilon}\,\frac{1}{2\omega^*(q)}\,\frac{i}{P^0-q^0-\omega^*(q)+i\epsilon}\,(-it_{if})\,, \end{aligned} \tag{5.34}$$

where $\omega^*(q) = \sqrt{\vec{q}^{\,2}+m_{K^*}^2}$ is the K^* energy. Again, in Eq. (5.34) only the positive energy part of the K^* propagator $i[(P^0-q^0-\omega^*)2\omega^*]^{-1}$ is taken, which is a good approximation given the large mass of the K^*.

We assume we are dealing with small three-momenta compared to the masses of the particles involved. This means that only the spatial components of the polarization vector of the K^* are non vanishing,

$$\epsilon'^0 = \frac{|\vec{P}-\vec{q}|}{m_{K^*}} = \frac{|\vec{q}|}{m_{K^*}} \sim 0\,, \tag{5.35}$$

and that the completeness relation of Eq. (5.17) can now be written as

$$\sum_{pol} \epsilon'_\mu \epsilon'_\alpha \simeq \sum_{pol} \epsilon'_i \epsilon'_j = \delta_{ij}\ ; \qquad \mu = i,\quad \alpha = j;\quad i,j = 1,2,3\,. \tag{5.36}$$

Using Eq. (5.36), the amplitude reduces to

$$\begin{aligned} t = -i\,C_1\,C_2\,g_{f_1}\,g \int \frac{d^4q}{(2\pi)^4}(2\vec{k}+\vec{q})\cdot\vec{\epsilon}\,\frac{1}{q^2-m_K^2+i\epsilon} \\ \times \frac{1}{(P-k-q)^2-m_K^2+i\epsilon}\,\frac{1}{2\omega^*(q)}\,\frac{1}{P^0-q^0-\omega^*(q)+i\epsilon}\,t_{if}\,. \end{aligned} \tag{5.37}$$

We can further simplify Eq. (5.37) writing it as

$$t = C\,g_{f_1}\,g\,\vec{\epsilon}\cdot\vec{k}\,(2I_1+I_2)\,t_{if} = \tilde{t}\,\vec{\epsilon}\cdot\vec{k}\,t_{if}\,, \tag{5.38}$$

where I_1 and I_2 are defined as

$$\begin{aligned} I_1 &= -i \int \frac{d^4q}{(2\pi)^4}\frac{1}{q^2-m_K^2+i\epsilon}\,\frac{1}{(P-k-q)^2-m_K^2+i\epsilon}\,\frac{1}{2\omega^*(q)}\,\frac{1}{P^0-q^0-\omega^*(q)+i\epsilon}\,, \\ I_2 &= -i \int \frac{d^4q}{(2\pi)^4}\frac{1}{q^2-m_K^2+i\epsilon}\,\frac{\vec{k}\cdot\vec{q}/|\vec{k}\,|^2}{(P-k-q)^2-m_K^2+i\epsilon}\,\frac{1}{2\omega^*(q)}\,\frac{1}{P^0-q^0-\omega^*(q)+i\epsilon}\,. \end{aligned} \tag{5.39}$$

The constant C is the product of C_1 and C_2 and its value depends on the diagram that we are considering, as shown in the last column of **Table 5.1**.

After analytically integrating Eqs. (5.39) in dq^0 using Cauchy's theorem, we obtain

$$I_1 = -\int \frac{d^3q}{(2\pi)^3} \frac{1}{8\,\omega(q)\omega'(q)\omega^*(q)} \frac{1}{k^0-\omega'(q)-\omega^*(q)+i\epsilon} \frac{1}{P^0-\omega^*(q)-\omega(q)+i\epsilon} \times \frac{2P^0\omega(q)+2k^0\omega'(q)-2(\omega(q)+\omega'(q))(\omega(q)+\omega'(q)+\omega^*(q))}{(P^0-\omega(q)-\omega'(q)-k^0+i\epsilon)(P^0+\omega(q)+\omega'(q)-k^0-i\epsilon)}\,, \tag{5.40}$$

$$I_2 = -\int \frac{d^3q}{(2\pi)^3} \frac{\vec{k}\cdot\vec{q}/|\vec{k}\,|^2}{8\,\omega(q)\omega'(q)\omega^*(q)} \frac{1}{k^0-\omega'(q)-\omega^*(q)+i\epsilon} \frac{1}{P^0-\omega^*(q)-\omega(q)+i\epsilon} \times \frac{2P^0\omega(q)+2k^0\omega'(q)-2(\omega(q)+\omega'(q))(\omega(q)+\omega'(q)+\omega^*(q))}{(P^0-\omega(q)-\omega'(q)-k^0+i\epsilon)(P^0+\omega(q)+\omega'(q)-k^0-i\epsilon)}\,, \tag{5.41}$$

where $\omega(q) = \sqrt{\vec{q}^{\,2}+m_K^2}$ and $\omega'(q) = \sqrt{(\vec{q}+\vec{k})^2+m_K^2}$ are the energies of the K ($\bar{K}$) and $\bar{K}$ (K) in the loop respectively.

Exactly as in the case of the loop integral of Eq. (5.18), when performing numerically the integrations in d^3q of Eqs. (5.40) and (5.41), we have to consider that the upper limit is naturally provided by chiral unitary approach. This means that the cutoff $q_{max} = 900$ MeV appears automatically as the upper limit of the integrals of Eqs. (5.40) and (5.41) thanks to the $K\bar{K} \to PP$ potential used to dynamically generate the a_0 and f_0. Note, however, that the integrals in Eqs. (5.40) and (5.41) are already convergent without implementing q_{max}. The loop also should implement the cutoff used in the evaluation of the $f_1(1285)$, which was $q_{max} = 1000$ MeV. Hence, the use of $q_{max} = 900$ MeV accounts for both cutoffs.

Proceeding with the evaluation of the total amplitude of the reactions $f_1(1285) \to \pi^0\pi^0\eta$ and $f_1(1285) \to \pi^0\pi^+\pi^-$, we have to take into account that the neutral and charged kaons have different physical masses. Thus, we define $\tilde{t}^{(+)}$ and $\tilde{t}^{(0)}$, corresponding to the quantity $\tilde{t}$ of Eq. (5.38) evaluated for the masses of K^+, K^-, K^{*+}, K^{*-} (summing A and C of **Figure 5.16**) and K^0, $\bar{K}^0$, K^{*0}, $\bar{K}^{*0}$ (summing B and D of **Figure 5.16**) respectively. This allows us to write the total amplitudes of the processes as

$$\begin{aligned} T_{\pi^0\eta} &= (2\tilde{t}^{(+)}\,t_{K^+K^-,\pi^0\eta} + 2\tilde{t}^{(0)}\,t_{K^0\bar{K}^0,\pi^0\eta})\,\vec{\epsilon}\cdot\vec{k}\,, \\ T_{\pi^+\pi^-} &= (2\tilde{t}^{(+)}\,t_{K^+K^-,\pi^+\pi^-} + 2\tilde{t}^{(0)}\,t_{K^0\bar{K}^0,\pi^+\pi^-})\,\vec{\epsilon}\cdot\vec{k}\,. \end{aligned} \tag{5.42}$$

From these last two equations, the role of the mass difference between neutral and charged kaons in the isospin symmetry breaking can be clearly

understood. When equal masses for the kaons are taken, due to the fact that the global factor C in $\tilde{t}$ has opposite sign in the charged and in the neutral case (see **Table 5.1**), we have that $\tilde{t}^{(0)} = -\tilde{t}^{(+)}$. Moreover, from Ref. [30] we know that

$$\begin{aligned} t_{K^+K^-\to\pi^0\eta} &= -t_{K^0\bar{K}^0,\pi^0\eta}\,, \\ t_{K^+K^-\to\pi^+\pi^-} &= t_{K^0\bar{K}^0,\pi^+\pi^-}\,. \end{aligned} \tag{5.43}$$

This means that if the masses of the neutral and charged kaons were equal, the amplitude $T_{\pi^+\pi^-}$ would vanish, preventing the production of the $f_0(980)$ as intermediate state, which indeed is isospin forbidden. Since the isospin symmetry is not an exact symmetry, due to the mass difference, the decay can go via both a_0 and f_0 production, leading to the $\pi^0\eta$ and $\pi^+\pi^-$ pairs in the final state.

Given the structure of Eq. (5.42) we define $T_{\pi^0\eta}$ and $T_{\pi^+\pi^-}$ as

$$\begin{aligned} T_{\pi^0\eta} &= \tilde{T}_{\pi^0\eta}\,\vec{\epsilon}\cdot\vec{k}\,, \\ T_{\pi^+\pi^-} &= \tilde{T}_{\pi^+\pi^-}\,\vec{\epsilon}\cdot\vec{k}\,. \end{aligned} \tag{5.44}$$

5.3.3 Results

The invariant mass distribution is given by the formula [193]

$$\frac{d\Gamma}{dm_f} = \frac{1}{(2\pi)^3}\,\frac{p_\pi\,|\vec{k}\,|}{4M_{f_1}^2}\,\frac{1}{2}\int_{-1}^{1} d\cos\theta\;\overline{\Sigma}|T|^2\,, \tag{5.45}$$

where the symbol $\overline{\Sigma}$ stands for the average over the polarizations of the $f_1(1285)$, θ is the angle between $\vec{k}$ and $\vec{\epsilon}$ and m_f is the invariant mass of the final interacting pair (see **Figure 5.18**). The momenta in Eq. (5.45) are defined as

$$p_\pi = \frac{\lambda^{1/2}(m_f^2, m_{\pi^0}^2, m_\eta^2)}{2m_f} \tag{5.46}$$

in the case of $\pi^0\eta$ in the final state (π^0 momentum un the $\pi^0\eta$ rest frame) and

$$p_\pi = \frac{\lambda^{1/2}(m_f^2, m_{\pi^+}^2, m_{\pi^-}^2)}{2m_f} \tag{5.47}$$

in the case of $\pi^+\pi^-$ (π^+ momentum un the $\pi^+\pi^-$ rest frame), while

$$|\vec{k}\,| = \frac{\lambda^{1/2}(M_{f_1}^2, m_{\pi^0}^2, m_f^2)}{2M_{f_1}} \tag{5.48}$$

is the momentum of the spectator π^0 in the reference frame in which the $f_1(1285)$ is at rest.

Eq. (5.45) can be rewritten, after performing the integration in $d\cos\theta$, as

$$\frac{d\Gamma}{dm_f} = \frac{1}{(2\pi)^3} \frac{p_\pi |\vec{k}|^3}{4M_{f_1}^2} \frac{1}{3} |\tilde{T}|^2 . \tag{5.49}$$

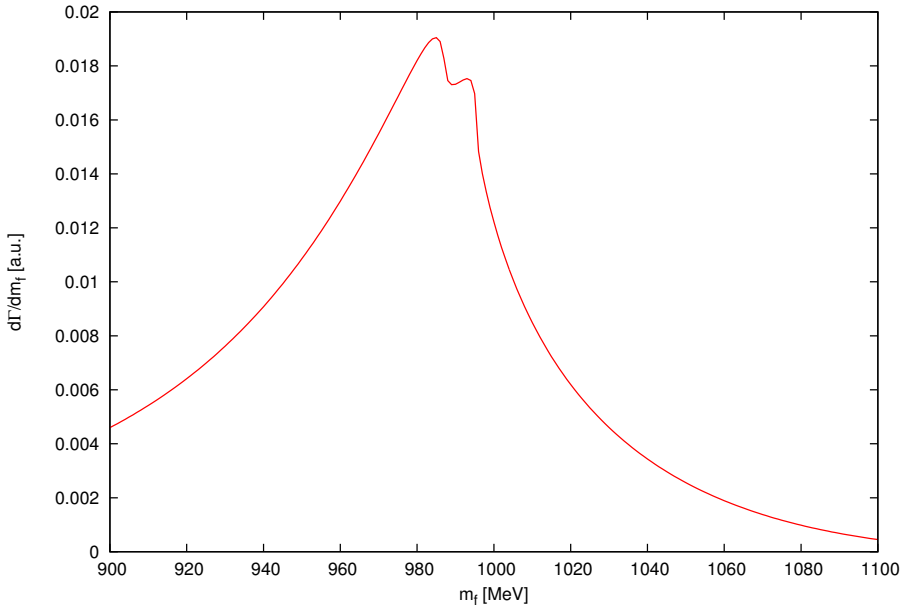

Figure 5.19: $d\Gamma/dm_f$ for $f_1(1285) \to \pi^0\pi^0\eta$ decay in the $a_0(980)$ region.

The result for $d\Gamma/dm_f$ for the $f_1(1285) \to \pi^0\pi^0\eta$ case is shown in **Figure 5.19** while in **Figure 5.20** we have the same plot for $f_1(1285) \to \pi^0\pi^+\pi^-$. For the same reason as in the case of the $\eta(1405)$, we do not symmetrize the two π^0 in the $\pi^0\pi^0\eta$ final state, since the a_0 resonance is relatively narrow and the two π^0 have very distinct kinematics.

For $\pi^+\pi^-$ in the final state we obtain, as in the previous section, an unusually narrow peak around 980 MeV, with a width around 10 MeV, in agreement with what was found experimentally in other reactions like the one studied by BES collaboration [165]. The peak shows up again in the $f_0(980)$ region between the two thresholds of K^+K^- and $K^0\bar{K}^0$ and its peculiar features can be attributed to the difference in the physical masses of neutral and charged kaons. Analogously to **Figure 5.4**, we plot in **Figure 5.21** the two loop integrals $\tilde{t}^{(0)}$ and $\tilde{t}^{(+)}$: once again, their difference is significant only in the region of energies around the two $K\bar{K}$ thresholds, leading to the narrow shape of the

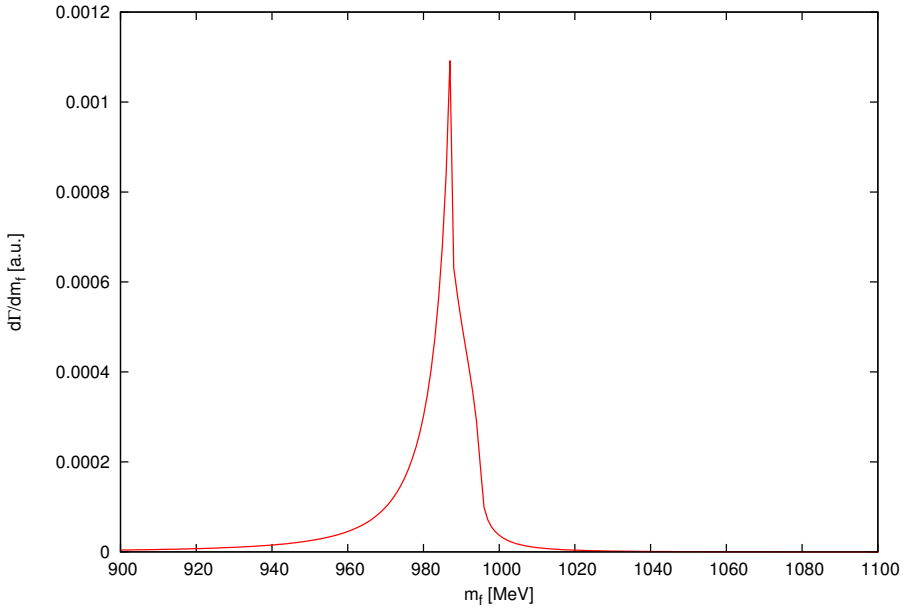

Figure 5.20: $d\Gamma/dm_f$ for $f_1(1285) \to \pi^0\pi^+\pi^-$ decay in the $f_0(980)$ region.

invariant mass distribution for the $f_0(980)$, already observed in the case of the reaction $\eta(1405) \to \pi^0 f_0(980)$. The shape of the peak that we predict has been later confirmed by the BES collaboration and the results they obtained are published in Ref. [194]. As expected, the signal is much wider in the

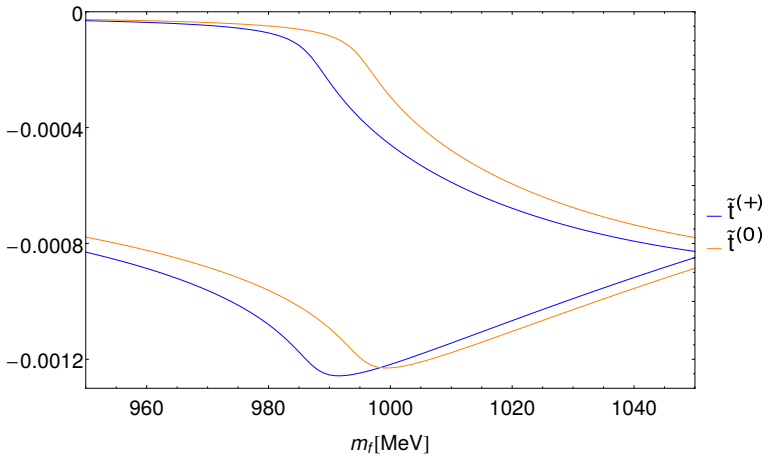

Figure 5.21: $\mathrm{Im}[\tilde{t}^{(0)}]$, $\mathrm{Im}[\tilde{t}^{(+)}]$, $\mathrm{Re}[\tilde{t}^{(0)}]$, $\mathrm{Re}[\tilde{t}^{(+)}]$ as functions of m_f.

case of the $\pi^0\eta$ channel, **Figure 5.19**. The a_0 is produced with its normal width, since the reaction is isospin allowed, and with a bigger strength at the peak. In **Figure 5.22** we show the ratio $(\frac{d\Gamma}{dm_f})_{\pi^+\pi^-}/(\frac{d\Gamma}{dm_f})_{\pi^0\eta}$ as a function of

the invariant mass and we can see that the ratio of strength at the peak is of the order of 6%, ten times smaller than for the decay of the $\eta(1405)$. We find another different value for isospin mixing, indicating that there is not an absolute value for this magnitude. It depends on the particular reaction but provides extra information about the nature of the resonances and the reaction mechanism.

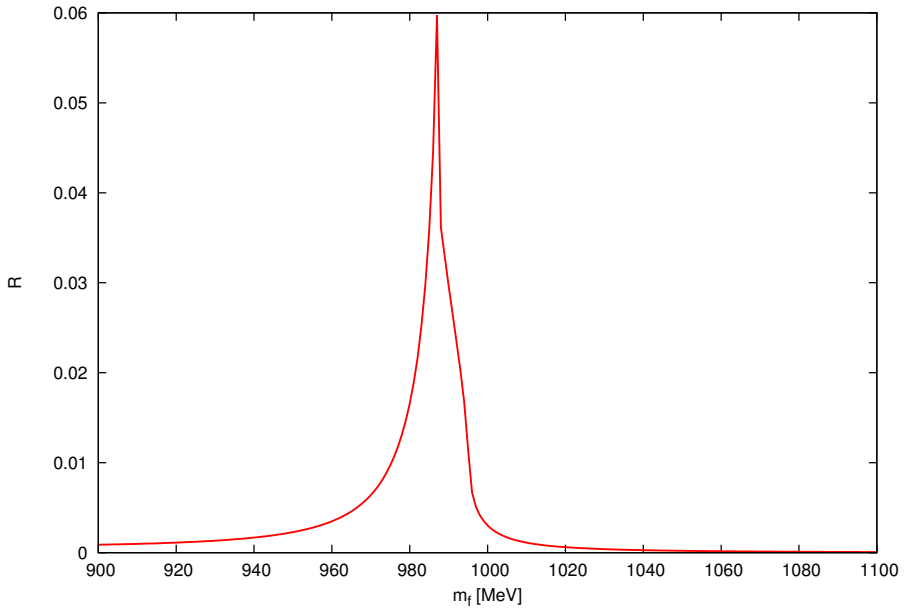

Figure 5.22: Ratio $(\frac{d\Gamma}{dm_f})_{\pi^+\pi^-}/(\frac{d\Gamma}{dm_f})_{\pi^0\eta}$ as a function of m_f.

Now we proceed to the evaluation of the partial width for the decay mode of the $f_1(1285)$ to $a_0(980)\pi$. We want to compare our result with the experimental one reported in the PDG [17]

$$BR(f_1 \to a_0\pi)|_{exp} = (36 \ \pm \ 7)\% \,, \tag{5.50}$$

ignoring the $a_0(989) \to K\bar{K}$ decay.

In order to do it, we need to take into account all the three possible final states, $a_0^+\pi^-$, $a_0^0\pi^0$, $a_0^-\pi^+$. However, the state of $I = 0$ coming from the interaction of two $I = 1$ particles is given by

$$|I = 0, I_3 = 0\rangle = \frac{1}{\sqrt{3}}|1,1\rangle - \frac{1}{\sqrt{3}}|1,0\rangle + \frac{1}{\sqrt{3}}|1,-1\rangle \,, \tag{5.51}$$

which means that the three final states appear with the same weight. Thus, we can restrict the calculation to the diagrams in **Figure 5.16** and then multiply

the result by a factor three to take into account the three charges. We find

$$\Gamma_{a_0\pi} = 3 \int dm_f \left(\frac{d\Gamma}{dm_f}\right)_{\pi^0\eta} = 4.5 \text{ MeV}\,, \tag{5.52}$$

with $\left(\frac{d\Gamma}{dm_f}\right)_{\pi^0\eta}$ given by Eq. (5.49), which corresponds to a branching ratio

$$BR(f_1 \to a_0\pi)|_{th} \simeq \ 19\% \ , \tag{5.53}$$

in good agreement with the experimental value.

We have made an estimate of the error on this result considering two possible sources of uncertainties. The first one is the cutoff in the meson-meson loop function used in the Bethe-Salpeter equation to generate the $f_1(1285)$, that we have taken around 1000 MeV. The value of the coupling g_{f_1} used in the decay amplitude of Eq. (5.38) depends slightly on this cutoff. Changing its value by ± 50 MeV, the resonance is still well reproduced and its position moved by only 20 MeV. This changes the value of the coupling g_{f_1} by 1%, leading to the same uncertainty on the final result for $\Gamma_{a_0\pi}$. The other source of uncertainty is the cutoff q_{max} used as upper limit in the loop integral of the decay. We make again a variation of ± 50 MeV, which moves the $a_0(980)$ and $f_0(980)$ peak in the scattering amplitude of 10 MeV. This induces a change in the value of $\Gamma_{a_0\pi}$, which gives, summed to the uncertainty coming from the other source,

$$\begin{cases} \Gamma^{th}_{a_0\pi} = (4.5 \pm 0.3) \text{ MeV}\,, \\ \\ BR(f_1 \to a_0\pi)|_{th} = (18.7 \pm \ 1.5)\%\,. \end{cases} \tag{5.54}$$

The ratio of integrated strengths over the invariant mass in the region of the $a_0(980)$ and $f_0(980)$ for the reactions $f_1(1285) \to \pi^0\pi^0\eta$ and $f_1(1285) \to \pi^0\pi^+\pi^-$ gives

$$\frac{\Gamma(\pi^0\pi^+\pi^-)}{\Gamma(\pi^0\pi^0\eta)} = 0.82 \times 10^{-2}\,, \tag{5.55}$$

$$\frac{\Gamma(\pi^0 f_0(980))}{\Gamma(\pi^0 a_0(980))} = 1.28 \times 10^{-2}\,, \tag{5.56}$$

where we have taken into account that the rate of $f_1(1285) \to \pi^0\pi^+\pi^-$ is twice the amount of $f_1(1285) \to \pi^0\pi^0\pi^0$.

This is much smaller than what was found for the $\eta(1405)$ decay, as we saw in **Section 5.2.3**, and twice as big as found for the J/ψ decay, $\frac{\Gamma(J/\psi\to\phi f_0(980))}{\Gamma(J/\psi\to\phi a_0(980))} = 0.6 \times 10^{-2}$ [164]. However, the result we obtain for the amount of isospin breaking (Eq. (5.55)) is compatible with the value reported by BES in Ref. [194], $(3.6 \pm 1.4)\%$.

5.4 The $f_1(1285) \to K\bar{K}\pi$ decay

In this Section we want to study the decay $f_1(1285) \to \pi K\bar{K}$ resorting again to the assumption that the $f_1(1285)$ is dynamically generated from the $K^*\bar{K} - cc$ interaction. Thus, the decay proceeds via $f_1(1285) \to K^*\bar{K} - cc$ followed by $K^* \to K\pi$ and the tree level diagrams are shown in **Figure 5.23**.

5.4.1 Decay amplitude at tree level

In order to evaluate the partial decay width of $f_1(1285) \to \pi K\bar{K}$, we need the decay amplitudes of the tree level diagrams shown in **Figure 5.23**.

The vertices we need to evaluate them are 1) and 2) in **Figure 5.17**. In particular, the $f_1(1285)K^*\bar{K}$ vertex is given by Eq. (5.30) and we take again $g_{f_1} = 7555$ MeV as in **Section 5.3**. Later, we will account for the difference with the value found in another work to measure the theoretical uncertainties. The factors C_1 that account for the weight of each $K^*\bar{K}$ ($\bar{K}^*K$) component in the $I = 0$ and $C = +$ combination of $K^*\bar{K}$ mesons Eq. (5.31), are listed in the first column of **Table 5.1** and reported here for convenience:

$$C_1^{A,B} = -\frac{1}{2}; \quad C_1^{C,D} = -\frac{1}{2}; \quad C_1^{E,F} = \frac{1}{2}; \quad C_1^{G,H} = \frac{1}{2}\,. \tag{5.57}$$

The vertex of $K^*K\pi$ can be written as

$$-it_2 = igC_2(k-p)^\mu \epsilon'_\mu\,. \tag{5.58}$$

We use here a different momenta assignment with respect to **Section 5.3.1**. Now k and p are the momenta of the π and K mesons respectively. From Eq. (2.92) and from the explicit expressions of the P and V matrices (Eqs. (2.29) and (2.83)), the factors C_2 for each diagram shown in Fig. (5.23) can be obtained,

$$C_2^{A,H} = \frac{1}{\sqrt{2}}; \quad C_2^{B,C} = 1; \quad C_2^{D,E} = -\frac{1}{\sqrt{2}}; \quad C_2^{F,G} = -1. \tag{5.59}$$

We can now sum the amplitudes of the diagrams that have same final state. By means of Eqs. (5.30) and (5.58) and taking into account the values of C_1 and C_2, the decay amplitude is obtained straightforwardly:

$$\begin{aligned} M_{\text{tree}}^{A+E} &= M_{\text{tree}}^{D+H} = M_{\text{tree}}\,, \\ M_{\text{tree}}^{B+G} &= M_{\text{tree}}^{C+F} = \sqrt{2}M_{\text{tree}}\,, \end{aligned} \tag{5.60}$$

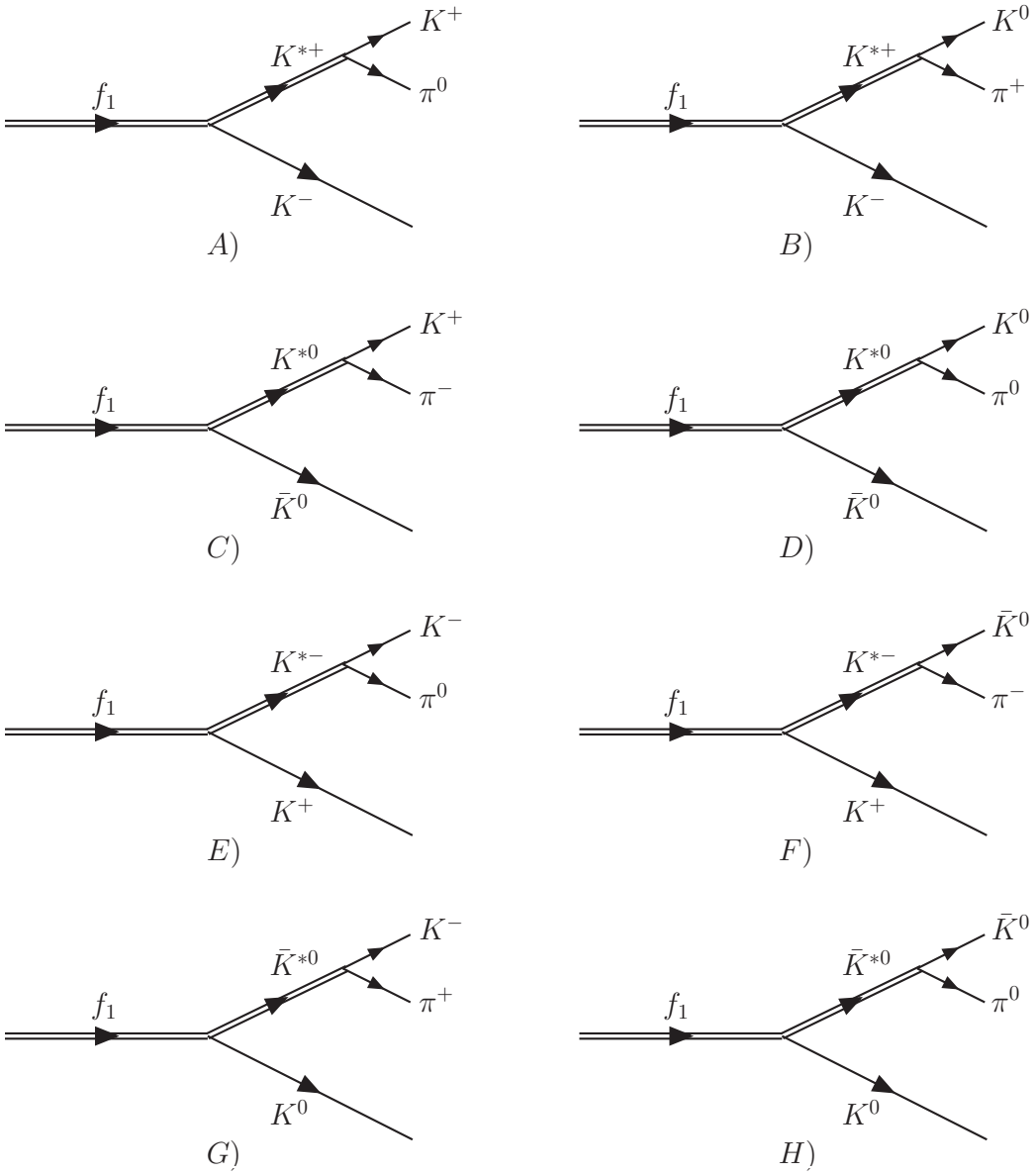

Figure 5.23: Tree level diagrams for the process $f_1(1285) \to \pi K \bar{K}$.

with

$$\begin{aligned} M_{\text{tree}} &= \frac{g g_{f_1}}{2\sqrt{2}}\big([-(k-p)_\mu + \frac{m_\pi^2 - m_K^2}{m_{K^*}^2}(k+p)_\mu]D_1 \\ &+ [-(k-p')_\mu + \frac{m_\pi^2 - m_K^2}{m_{K^*}^2}(k+p')_\mu]D_2\big)\epsilon^\mu \\ &= \frac{g g_{f_1}}{2\sqrt{2}}\big([(\vec{k}-\vec{p}) - \frac{m_\pi^2 - m_K^2}{m_{K^*}^2}(\vec{k}+\vec{p})]D_1 \\ &+ [(\vec{k}-\vec{p'}) + \frac{m_\pi^2 - m_K^2}{m_{K^*}^2}(\vec{k}+\vec{p'})]D_2\big)\cdot\vec{\epsilon}, \end{aligned} \tag{5.61}$$

where

$$D_1 = \frac{1}{(k+p)^2 - m_{K^*}^2 + i m_{K^*}\Gamma_{K^*}}, \tag{5.62}$$

$$D_2 = \frac{1}{(k+p')^2 - m_{K^*}^2 + i m_{K^*}\Gamma_{K^*}} \tag{5.63}$$

are the propagators of the K^* ($\bar{K}^*$). Taking diagrams A) and E) for reference to calculate M_{tree}, the variables p, p' and k refer to the K^+, K^- and π^0, and Γ_{K^*} is the total decay width of the K^* meson.

Since the dominant decay channel of K^* is $K\pi$, we can take

$$\Gamma_{K^*} = \Gamma_{\text{on}}\left(\frac{q_{\text{on}}}{q_{\text{off}}}\right)^3 \tag{5.64}$$

in the K^* propagators D_1 and D_2, with $\Gamma_{\text{on}} = 49.1$ MeV and

$$\begin{aligned} q_{\text{on}} &= \frac{\lambda^{1/2}(M_{K^*}^2, m_K^2, m_\pi^2)}{2M_{K^*}}, \\ q_{\text{off}} &= \frac{\lambda^{1/2}(M_{\text{inv}}^2, m_K^2, m_\pi^2)}{2M_{\text{inv}}}\theta(M_{\text{inv}} - m_K - m_\pi), \end{aligned} \tag{5.65}$$

In Eqs. (5.65), M_{inv} is the invariant mass of the πK system, which is $\sqrt{(k+p)^2}$ for the D_1 propagator and $\sqrt{(k+p')^2}$ for D_2.

5.4.2 Decay amplitude for the triangular loop

In addition to the tree level diagrams, we also study the contributions of the $K\bar{K}$ and πK final state interactions (FSIs). We use again the triangular mechanism of the previous decays, which allows us to describe the process by means of the diagrams shown in **Figure 5.24**, consisting in the rescattering of the $K\bar{K}$ and πK pairs.

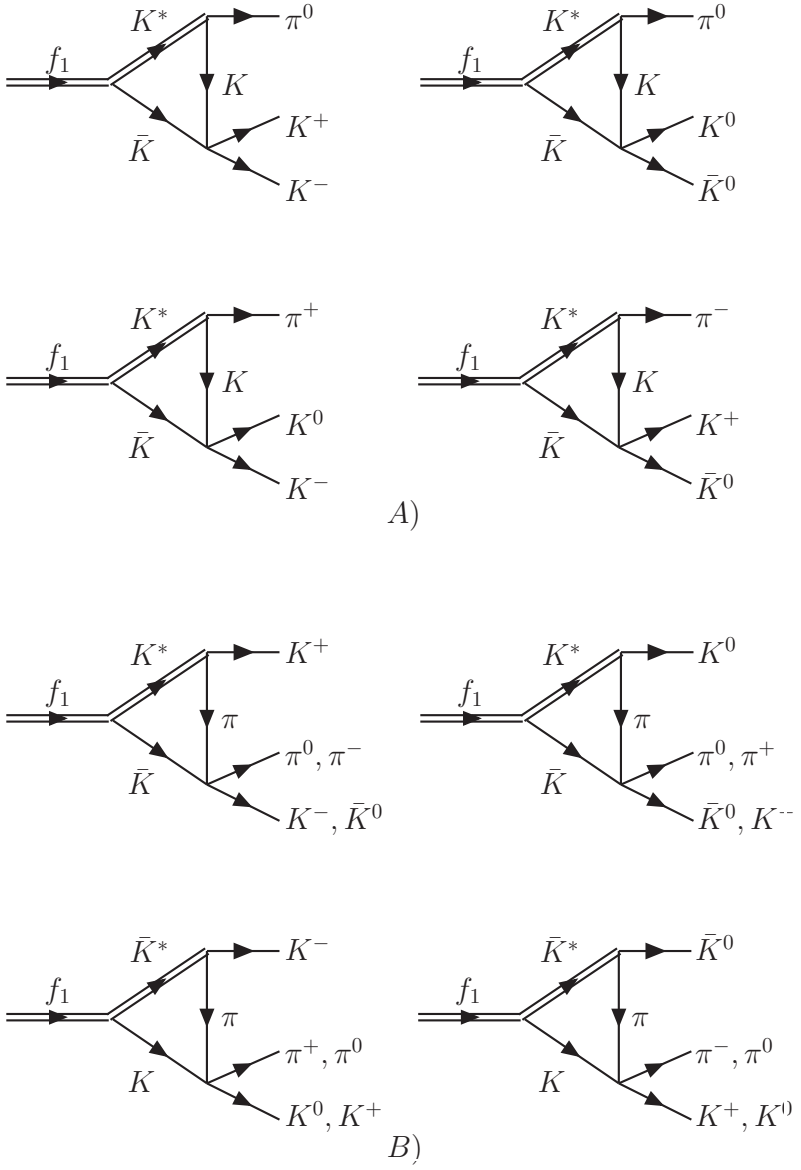

Figure 5.24: Triangular loop contributions to the $f_1(1285) \to \pi K \bar{K}$ decay.

Since the $f_1(1285)$ has $I = 0$, considering only isospin conserving terms, the $K\bar{K}$ will be in $I = 1$ and the πK in $I = 1/2$. The rescattering of the $K\bar{K}$ and πK pairs with this isospin dynamically generates in coupled channels the $a_0(980)$ and $\kappa(800)$ resonances respectively. We write for simplicity the $K\bar{K} \to K\bar{K}$ and $\pi K \to \pi K$ rescattering amplitudes as,

$$t^{K\bar{K}}_{\rm FSI}(M_{K\bar{K}}) = t^{I=1}_{K\bar{K}\to K\bar{K}}(M_{K\bar{K}})\,, \tag{5.66}$$

$$t^{\pi K}_{\rm FSI}(M_{\pi K}) = t^{I=1/2}_{\pi K\to \pi K}(M_{\pi K})\,, \tag{5.67}$$

where $M_{K\bar{K}}$ and $M_{\pi K}$ are the invariant masses for the $K\bar{K}$ and πK systems. The quantities $t^{I=1}_{K\bar{K}\to K\bar{K}}$ and $t^{I=1/2}_{\pi K\to \pi K}$ stand for the scattering amplitudes of $K\bar{K} \to K\bar{K}$ in $I = 1$ and $\pi K \to \pi K$ in $I = 1/2$, and they can be obtained using the Bethe-Salpeter equation with the potential V taken from Ref. [30]. The Bethe-Salpeter equation will contain the loop function for the propagators of the intermediate particles. We take the $K\bar{K}$ and $\pi\eta$ channels for the case of $K\bar{K}$ FSI, while for πK FSI, we take πK and ηK. For a good description of the $a_0(980)$ and $\kappa(800)$ we take again a cutoff $q_{\rm max} = 900$ MeV, for both $K\bar{K}$ and πK FSIs.

With the ingredients given above, we can explicitly write the decay amplitude for the diagrams in **Figure 5.24**. As for the tree level case, we sum the diagrams with the same final state. In **Figure 5.24** A), we show the four possible final states for the $K\bar{K}$ FSI. The amplitude corresponding to the first diagram, that is the $\pi^0 K^+ K^-$ final state which we take as reference, is then given by

$$M^{K\bar{K}}_{\rm FSI} = -\frac{g g_{f_1}}{2\sqrt{2}}(2I_1 + I_2) 2 t^{I=1}_{K\bar{K}\to K\bar{K}}(M_{K\bar{K}})\vec{\epsilon}\cdot\vec{k}\,, \tag{5.68}$$

with $M_{K\bar{K}} = \sqrt{(p+p')^2}$. Here we have summed explicitly the contributions of four diagrams corresponding to the intermediate states $K^* K\bar{K}$: $K^{*+}K^-K^+$, $K^{*0}\bar{K}^0K^0$, $K^{*-}K^+K^-$ and $\bar{K}^{*0}K^0\bar{K}^0$, easily done taking into account the C_1 and C_2 coefficients and the fact that

$$\begin{aligned} t^{I=1}_{K\bar{K}\to K\bar{K}} &= t_{K^+K^-\to K^+K^-} - t_{K^+K^-\to K^0\bar{K}^0} \\ &= t_{K^0\bar{K}^0\to K^0\bar{K}^0} - t_{K^+K^-\to K^0\bar{K}^0}\,, \end{aligned} \tag{5.69}$$

with the phase convention $|K^-\rangle = -|1/2, -1/2\rangle$. The quantities I_1 and I_2 for the case of $M^{K\bar{K}}_{\rm FSI}$ are given by Eqs. (5.40) and (5.41). It is worth mentioning that after performing the integrations, the I_1 and I_2 integrals in the above equations depend only on the modulus of the momentum of the π^0, which can be easily related to the invariant mass of the $K\bar{K}$ system via $M^2_{K\bar{K}} = M^2_{f_1} + m^2_\pi - 2M_{f_1}\sqrt{|\vec{k}|^2 + m^2_\pi}$. The d^3q integrations are done with a cutoff $q_{\rm max} = 900$ MeV.

In the group B) of diagrams in **Figure 5.24**, we show the possible final states corresponding to the πK FSI. Each one of the diagrams has two possible $\pi\bar{K}$ or πK final states. In addition, each one of the diagrams has two possible $K^*\bar{K}$ or $\bar{K}^*K$ intermediate states: in the first diagram we can have $K^{*+}K^-$ or $K^{*0}\bar{K}^0$ and this leads, after considering the C_1 and C_2 coefficients, to the combination $t_{\pi^0K^-\to\pi^0K^-} + \sqrt{2}t_{\pi^-K^0\to\pi^0K^-}$, proportional to $t^{I=1/2}_{\pi K\to\pi K}$. The sum of the first and third diagram with $\pi^0K^+K^-$ in the final state is then easily done and can be cast as

$$\begin{aligned} M^{\pi K}_{\rm FSI} = &\frac{gg_{f_1}}{2\sqrt{2}}(2I_1' + I_2')t^{I=1/2}_{\pi K\to\pi K}(M^{(1)}_{\pi K})\vec{\epsilon}\cdot\vec{p} \\ &+ \frac{gg_{f_1}}{2\sqrt{2}}(2I_1'' + I_2'')t^{I=1/2}_{\pi K\to\pi K}(M^{(2)}_{\pi K})\vec{\epsilon}\cdot\vec{p}\,'\,, \end{aligned} \tag{5.70}$$

where I_1', I_2' are evaluated again with Eqs. (5.40) and (5.41) but replacing one kaon propagator by a pion, putting $\omega'(q) = \sqrt{(\vec{q}+\vec{p})^2 + m_\pi^2}$ and substituting k^0 by p^0. Similarly I_1'' and I_2'' are also evaluated with the same equations putting $\omega'(q) = \sqrt{(\vec{q}+\vec{p}\,')^2 + m_\pi^2}$ and substituting k^0 by p'^0. The integrals I_1', I_2' are functions of $|\vec{p}|$ and I_1'', I_2'' of $|\vec{p}\,'|$, which can be written in terms of the invariant masses $M^{(1)}_{\pi K} = \sqrt{(k+p')^2}$ and $M^{(2)}_{\pi K} = \sqrt{(k+p)^2}$ respectively, similarly to what done before for the $K\bar{K}$ interaction terms.

The relative minus sign between Eqs. (5.68) and (5.70) is easily traced back to the sign of the $K^* \to K\pi$ when we have either the K or the π in the loop.

5.5 Results

With the decay amplitudes obtained above, we can easily get the total decay width of $f_1(1285) \to \pi K\bar{K}$ which is

$$\begin{aligned} \Gamma = 6\,\frac{1}{64\pi^3 M_{f_1}}\int\int d\omega_{K^+}d\omega_{K^-}\overline{\sum}|M|^2 \\ \times\,\theta(1-\cos^2\theta_{K\bar{K}})\theta(M_{f_1}-\omega_{K^+}-\omega_{K^-}-m_\pi)\,, \end{aligned} \tag{5.71}$$

where M is the full amplitude of the process $f_1(1285) \to \pi^0K^+K^-$ including the FSIs,

$$M = M_{\rm tree} + M^{K\bar{K}}_{\rm FSI} + M^{\pi K}_{\rm FSI}\,, \tag{5.72}$$

with $\omega_{K^+} = \sqrt{m_K^2 + \vec{p}^{\,2}}$ and $\omega_{K^-} = \sqrt{m_K^2 + \vec{p}'^{\,2}}$ the energies of the K^+ and K^- mesons. The symbol $\overline{\sum}$ stands for the average over the polarizations of the initial $f_1(1285)$ state. The factor 6 in the formula of Γ accounts for the different final charges for $\pi K\bar{K}$: $\pi^0K^+K^-$, $\pi^+K^0K^-$, $\pi^-K^+\bar{K}^0$, and $\pi^0K^0\bar{K}^0$, having

weights 1, 2, 2, and 1, respectively, easily obtained using simple Clebsch-Gordan coefficients. Besides, the $\cos\theta_{K\bar{K}}$ is defined by energy conservation as

$$\begin{aligned}\cos\theta_{K\bar{K}} &= \frac{1}{2|\vec{p}||\vec{p}\,'|}[M_{f_1}^2 + 2m_K^2 - 2M_{f_1}(\omega_{K^+} + \omega_{K^-}) \\ &\quad +2\omega_{K^+}\omega_{K^-} - m_\pi^2]\,. \end{aligned} \tag{5.73}$$

With the full amplitude of Eq. (5.72), the numerical result for the partial decay width is, using $g_{f1} = 7555$ MeV, $\Gamma = 1.9$ MeV, which corresponds to a branching ratio

$$B.R.[f_1(1285) \to \pi K\bar{K}] = 7.8\%\,, \tag{5.74}$$

If we use the coupling of Ref. [51], $g_{f1} = 7230$ MeV, then we get $\Gamma = 1.74$ MeV, corresponding to a branching ratio

$$B.R.[f_1(1285) \to \pi K\bar{K}] = 7.2\%\,, \tag{5.75}$$

This gives a band of theoretical results of

$$B.R.[f_1(1285) \to \pi K\bar{K}] = (7.2 - 7.8)\%\,, \tag{5.76}$$

which is in agreement with the experimental value $(9.0 \pm 0.4)\%$ [17, 195, 196]. The result would be 9%, with the higher value for the g_{f1} coupling, if we considered only the tree level diagrams. This indicates that the contribution from the FSIs is small. This occurs because of the relative minus sign in Eqs. (5.68) and (5.70), which makes the effects of the FSIs for $K\bar{K}$ and πK go in opposite directions bringing a partial cancelation in Γ.

As done for the previous decay, we can see the variation of our results by changing the values of the two cutoffs in a range such that the masses of the $f_1(1285)$ and $a_0(980)$ do not significantly differ from the experimental values. As already mentioned in **Section 5.3**, changes of $q_{\max}$ from 950 MeV to 1050 MeV bring changes in the coupling g_{f1} of only 1%. These changes are smaller than the range of couplings accepted in Eq. (5.76). Similarly, changes in $q_{\max}$ for $a_0(980)$ from 860 MeV to 940 MeV change the mass of the $a_0(980)$ in about 10 MeV. Re-evaluating the branching ratios with values of $q_{\max}$ within the range $(850 - 950)$ MeV, we obtain for the branching ratio

$$B.R.[f_1(1285) \to \pi K\bar{K}] = (7.2 - 8.3)\%, \tag{5.77}$$

with the upper limit a little closer to the experimental value.

Next, we study the invariant mass distribution of the $f_1(1285) \to \pi^0 K^+ K^-$ decay to see the effect of the K^* propagator in the tree level and of the $K\bar{K}$ and πK FSIs.

The invariant mass distributions are given by the formulas

$$\frac{d\Gamma}{dM_{K^+K^-}} = \frac{M_{K^+K^-}}{64\pi^3 M_{f_1}^2}\int d\omega_{K^+}\overline{\sum}|M|^2\theta(1-\cos^2\theta_{K\bar{K}})\times \theta(M_{f_1}-\omega_{K^+}-\omega_{K^-}-m_\pi)\theta(\omega_{K^-}-m_K)\,, \tag{5.78}$$

$$\frac{d\Gamma}{dM_{\pi^0K^+}} = \frac{M_{\pi^0K^+}}{64\pi^3 M_{f_1}^2}\int d\omega_{K^+}\overline{\sum}|M|^2\theta(1-\cos^2\theta_{K\bar{K}})\times \theta(M_{f_1}-\omega_{K^+}-\omega_{K^-}-m_\pi)\theta(\omega_{K^-}-m_K)\,, \tag{5.79}$$

where

$$\omega_{K^-} = \frac{1}{2M_{f_1}}(M_{K^+K^-}^2 + M_{f_1}^2 - m_\pi^2) - \omega_{K^+}\,, \tag{5.80}$$

for $\frac{d\Gamma}{dM_{K^+K^-}}$, while

$$\omega_{K^-} = \frac{1}{2M_{f_1}}(M_{f_1}^2 + m_K^2 - M_{\pi^0K^+}^2)\,, \tag{5.81}$$

for $\frac{d\Gamma}{dM_{\pi^0K^+}}$.

The results for $\frac{d\Gamma}{dM_{K^+K^-}}$ and $\frac{d\Gamma}{dM_{\pi^0K^+}}$ are shown in **Figure 5.25** and **Figure 5.26**, respectively and it is very interesting to compare the different curves. We show there the results assuming just a phase space distribution ($\overline{\sum}|M|^2$ in Eqs. (5.78) and (5.79) is set to a constant), and with the tree level or tree level plus final state interaction of $K\bar{K}$ and πK. For the sake of comparison, the curves are normalized to the same Γ. In **Figure 5.25** we see that the tree level alone shows a distinct shape, very different from phase space, with a peak at low $M_{K^+K^-}$. This must be attributed to the effect of the K^* off shell propagator. The implementation of FSI, particularly the $K\bar{K}$ in this case, is responsible for a further shift of the mass distribution to lower invariant masses, closer to the $K\bar{K}$ threshold, where the $a_0(980)$ resonance appears.

In **Figure 5.26**, where the πK invariant mass distribution is plotted, we see a similar behaviour. The tree level alone already produces a shape quite different from phase space, with a peak at high values of $M_{\pi K}$, to be attributed once again to the off shell K^* propagator. The implementation of FSI, particularly the πK in this case, pushes the peak of the mass distributions to higher $M_{\pi K}$, closer to the region where the $\kappa(800)$ resonance appears.

The two figures show how the most drastic change in the shape of the two mass distributions is already caused by the tree level alone and, as mentioned before, this is tied to the K^* propagators, which appear at tree level because of the $\bar{K}^*K - cc$ nature of the $f_1(1285)$ state that we have assumed. These mass distributions have not been measured yet and it is clear from the present

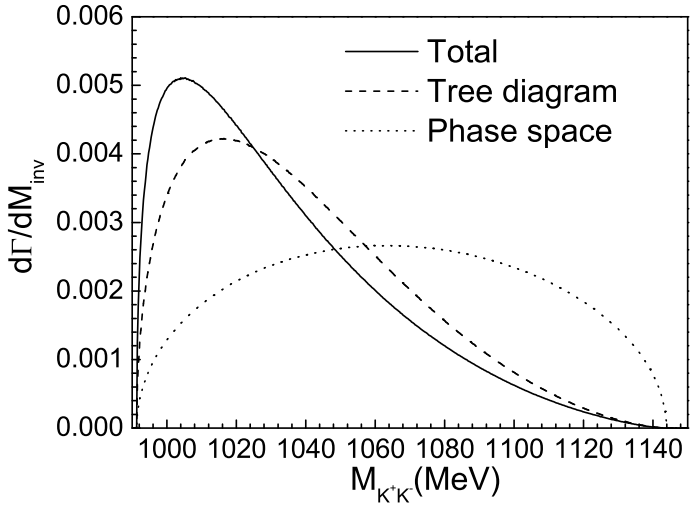

Figure 5.25: The mass distribution $\frac{d\Gamma}{dM_{K^+K^-}}$ as a function of the invariant mass of K^+K^- system.

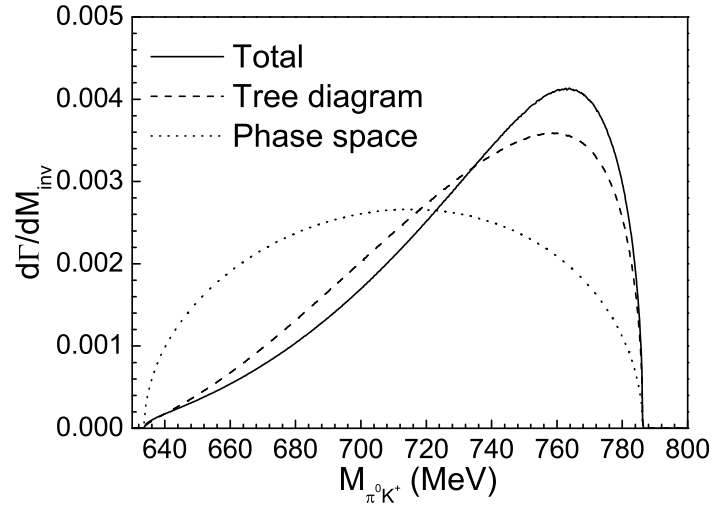

Figure 5.26: The mass distribution $\frac{d\Gamma}{dM_{\pi^0 K^+}}$ as a function of the invariant mass of $\pi^0 K^+$ system.

study that their observation would be very important to determine the nature of this resonance.

So far we have assumed that the $f_1(1285)$ resonance is fully made from $K\bar{K}^*$. There are hints that the resonance could have also other components. Indeed, in the study of this resonance in finite volume [168] it was shown that applying the compositeness sum rule [95, 122, 197] to this case with the chiral potential, the $K\bar{K}^*$ molecular component accounts for about 50% of the probability of the wave function, but there could still be a sizeable fraction for other non $K\bar{K}^*$ components. The size of these components is uncertain because it relies on the energy dependence contained in the chiral potential but, though it is unclear if this accounts for missing channels (see **Chapter 4**), it really hints at the possibility of having some non negligible non $K\bar{K}^*$ molecular component in the $f_1(1285)$ wave function. This might seem to be in conflict with our claim of a basically molecular state for this resonance and requires some explanation. Different parts of the wave function revert in different ways to certain observables. The easiest such case is the nucleon form factor, which at low momentum transfer is dominated by the meson-baryon components of the nucleon, while at high momentum transfers it is the core of quarks that is responsible for it [28, 198].

In this sense, it is logical that the decay of the $f_1(1285)$ into $K\bar{K}\pi$ and related channels is mostly due to the $K\bar{K}^*$ molecular component of the wave function, and other components would show up in other reactions. In this sense it is interesting to note that in Ref. [174] the B^0 and B_s^0 decays into J/ψ and $f_1(1285)$ are investigated and the interpretation in terms of a $q\bar{q}$ state leads to an $f_1(1285)$ state mostly made of u and d quarks. In our case we have four quarks to start with and a sizeable fraction of strange quarks in our $K\bar{K}^*$ molecular component, so the models seem to be contradictory. Yet, one must recall that in this latter case we have the production of the resonance in B decays and the resonance must be formed starting from a $q\bar{q}$ component. The investigation done in Refs. [199, 200] of the B decays, together with the ratio of the rates of $\bar{B}^0 \to J/\psi f_0(500)$ [201] and $\bar{B}^0 \to J/\psi\rho$ [17], show that the hadronization of the primary $q\bar{q}$ component to give two mesons has a penalty factor that reverts into a factor of 0.37 decrease in the partial decay width. In this sense, the decays of heavy mesons leading to light ones might reveal themselves into a source of information on the non molecular components of states like the present one. Further research considering both the molecular and $q\bar{q}$ components for this resonance in the B decays would be most welcome after the discussion made here.

5.6 Summary and Conclusions

In this chapter we have carried out a calculation of the decay rates of the $\eta(1405) \to \pi^0 f_0(980)(\pi^+\pi^-)$ and $\eta(1405) \to \pi^0 a_0(980)(\pi^0\eta)$ reactions. The aim was an investigation of the isospin violation in the first reaction, which is tied to the $f_0(980)$-$a_0(980)$ mixing, using the terminology of other works. We have abstained from talking about a measure of the mixing since in our formalism there is no transition of one resonance to the other. We have, instead, a simultaneous production of both once the problem is tackled with meson states in charge basis with different masses, and then a small violation of isospin is immediately obtained.

Since the two resonances are produced from the interaction of meson pairs, the process proceeds via a first step in which a π^0 and a pair of mesons are produced and a second step in which the pair of mesons interacts. Isospin violation has then two sources, the first loop after the production and the scattering matrices of meson-meson interaction. In both cases, the violation is tied to the difference of masses between charged and neutral kaons. The consequence is that the shape of the peak obtained for the $\pi^+\pi^-$ production in the first reaction has a very narrow width, of the size of this mass difference, of the order of 9 MeV. This comes naturally in the approach and is in perfect agreement with the observation in the experiment.

In the first part of **Section 5.2**, we avoided making an explicit model for the reaction, but we assumed the primary production of $\pi^0 PP$ to be given by a contact term. We could see that, invoking general principles and admitting large uncertainties in the input, we obtain a rather small rate of $\pi^+\pi^-$ production versus $\pi^0\eta$ production, of the order of one percent. This result is in good agreement with the $f_0(980)$ and $a_0(980)$ mixing of the two BES experiments on $J/\psi \to \phi\pi\eta$ and $\chi_{c1} \to \pi^0\pi\pi$, with respect to the isospin allowed counterparts [164] and also with the rates obtained in theoretical papers [161, 162]. However, it is very small compared to the experimental result [165], for $\eta(1405) \to \pi^0 f_0(980)(\pi^+\pi^-)$, about one order of magnitude smaller. We tried to understand the situation by admitting a large admixture of $I = 1$ in the $\eta(1405)$ wave function, but it required a very large I=1 component, not easily acceptable and, worse, it gave a signal for the $f_0(980)$ production with a width of the order of 20 MeV, much larger than the experimental one.

In the second part we followed the approach of Ref. [166] using the dominant primary production mechanism given by $\eta' \to K^*\bar{K}$ followed by $K^* \to K\pi$. The first loop now was quite different than for the contact interactions, since the new singularity associated to $\eta' \to K^*\bar{K}$ played a very important role in the reaction. We found that with this new mechanism of production, the ratio of $\Gamma(\pi^0, \pi^+\pi^-)/\Gamma(\pi^0, \pi^0\eta)$ was increased by about one

order of magnitude, providing results very close to those in the experiment. These results confirm the claims of Ref. [166] where, however, a precise determination of that ratio could not be given, due to unknown form factors needed to regularize the divergent loops. The use of the chiral unitary approach in the present work solved this problem, since one could associate the regularizing cutoff in the new loops to the one used in meson-meson scattering to generate the $f_0(980)$ and $a_0(980)$ resonances dynamically. This allowed us to make quantitative predictions for the $\Gamma(\pi^0,\pi^+\pi^-)/\Gamma(\pi^0,\pi^0\eta)$ ratio, with a value (0.16 ± 0.03), in basic agreement with experimental one, of (0.179 ± 0.04). We also showed that the results obtained for that ratio were the same if we had the $\eta(1475)$ resonance instead of the $\eta(1405)$, or a mixture of the two, as seems to be the case in the BES experiment.

Later, we have evaluated the decay width of the $f_1(1285)\to\pi^0\pi^0\eta$, which shows a prominent peak in the $a_0(980)$ resonance region. We use the picture in which the $f_1(1285)$ is dynamically generated from the vector-pseudoscalar interaction in the $K\bar{K}^*-cc$ channel. We take advantage of the same triangular decay mechanism used in the case of the $\eta(1405)$ and we found a branching fraction for the $f_1(1285)$ decay of about 20%, in qualitative agreement with experiment. At the same time, we evaluated the $f_1(1285)\to\pi^0\pi^+\pi^-$ decay rate through the same mechanism, but with the $K\bar{K}$ scattering to produce $\pi^+\pi^-$. This last process is isospin forbidden and gives zero in our approach if we consider equal masses for the charged and neutral kaons. When physical masses are used, then isospin is slightly violated and we find a prominent peak, albeit with small intensity, in the $f_0(980)$ region. Once again, the width of this peak is found narrow, like in the $\eta(1405)\to\pi\pi\eta$ decay. These predictions have been confirmed in a recent BESIII experiment [194] and, as in the previous decay, the mass distribution for the $\pi^0\pi^+\pi^-$ final state does not reflect the natural width of the $f_0(980)$ resonance but simply the region where the mass difference of the charged and neutral kaons is appreciable compared to the value of their masses. Also the shape obtained is similar to the one found in the $\eta(1405)\to\pi^0\pi^+\pi^-$ and $J/\psi\to\phi\pi^0\eta$ reactions, but the amount of isospin breaking is quite different to either processes. However, we obtain an isospin violation of about 1%, a value compatible with that reported by the BES collaboration in Ref. [194].

In view of this discussion, we consider the concept of $f_0(980)$-$a_0(980)$ mixing not appropriate: the apparent mixing is so different in different reactions that we prefer talking in terms of isospin violation, magnified due to the proximity of the $f_0(980)$ and $a_0(980)$ resonances, but which is very much tied to the nature of each one of the reactions considered. The ability of the chiral unitary approach to provide a fair description of all these processes certainly gives support to this method and to the underlying consequence, in this case, that

the $f_0(980)$, $a_0(980)$ and the $f_1(1285)$ resonances are basically molecular states of meson-meson, mostly $K\bar{K}$ in the first two cases and $K^*\bar{K} - cc$ in the last one.

The last section of the chapter was dedicated to the evaluation of the partial decay width of the $f_1(1285) \to \pi K\bar{K}$. The tree level diagrams, that proceed via $f_1(1285) \to K^*\bar{K} - cc \to \pi K\bar{K}$, were first considered but, at a later stage, we also took into account the final state interactions of $K\bar{K} \to K\bar{K}$ and $\pi K \to \pi K$, in which the triangular loop plays again a fundamental role. The result that we obtained for the decay width is compatible with experiment within errors.

The contributions to the partial decay width from the FSIs, compared to the tree level diagrams, are very small but we saw that they change the mass distributions of the $f_1(1285) \to \pi K\bar{K}$ decay. These mass distributions possess a relevant feature: their shape is, indeed, very different from the one of the phase space alone and, since the tree level is dominant, only in small proportion due to the FSIs. This change in the shape must be attributed to the off shell K^* propagator appearing in the process under the assumption that the $f_1(1285)$ is a $K^*\bar{K} - cc$ molecule. Their experimental observation would then provide very valuable information on the nature of this resonance.

CHAPTER 6

HIDDEN CHARM AND HIDDEN BOTTOM STATES

6.1 Introduction

In 2003 the Belle collaboration observed the first new charmoniumlike state called $X(3872)$ in the $B^+ \to X(3872)K^+ \to J/\psi\,\pi^+\pi^-K^+$ process [202], which was later confirmed by BaBar, CDF and $D0$ collaborations [203–205]. After its discovery, many other new states have been experimentally found, with masses placed in the charmonium mass region. Most of them are above the meson-meson threshold and, if they were conventional charmonium states, they would decay into a pair of open charm mesons. However, this is not seen in the experiment and what it is observed, instead, is their decay into J/ψ plus pions, an unusual property for a simple $c\bar{c}$ state. Furthermore, the predictions from potential models for masses and decay channels do not fit with the experimental results. For all these reasons, a strong experimental and theoretical effort has been made in order to understand the quark configuration of these new states as well as their production mechanisms, decay widths, masses and spin-parity assignments. In Refs. [206–211] a detailed discussion about the current status of those states, commonly called X, Y and Z, can be found.

Their masses are relatively simple to reproduce using the models mentioned above. This is the reason why it is fundamental to evaluate other properties, like widths and partial decay widths of possible decay channels. Since the discovery of the X, Y and Z states, an enormous bulk of work has been done in an attempt to accommodate them in an exotic picture, like hybrid, tetraquark, hadrocharmonium and meson molecule. The exotic state idea is not new but before the recent discovery of $Z_c^+(3900)$ by BESIII and Belle collaborations no

exotic structure had been conclusively identified.

One of the last surprises has been the finding of Z states with isospin $I = 1$. In the hidden charm sector a state around 4020 MeV and a width of about 8 MeV, called $Z_c(4020)$, has been observed in the $e^+e^- \to \pi^+\pi^- h_c$ reaction, looking at the invariant mass of the $\pi^\pm h_c$ system [212]. Another BES experiment [213] has found a peak in the $(D^*\bar{D}^*)^\pm$ spectrum close to threshold, which was interpreted in terms of a new resonance with mass around 4025 MeV and width of about 25 MeV. It is unclear whether these two states can be the same, and the quantum numbers are, in any case, not well determined. The peak seen in the $(D^*\bar{D}^*)^\pm$ spectrum is appealing since in Ref. [214] the study of the $D^*\bar{D}^*$ interaction gave rise to a state with $I = 1$ in spin $J = 2$. The state appeared around 3920 MeV with uncertainties. Actually, we will claim here that it should be much less bound but that, most probably, it is related to the peak seen in the $(D^*\bar{D}^*)^\pm$ distribution in Ref. [213]. The threshold for $(D^*\bar{D}^*)^\pm$ is 4017 MeV, so a bound state of $D^*\bar{D}^*$ should have a smaller energy, while the energy of the state is claimed, in Ref. [213], to be at 4025 MeV. Yet, the interpretation of peaks around threshold is always problematic and a source of confusion. Indeed, most often, an enhancement of the invariant mass at threshold is an indication of a bound state or resonance below threshold.

There are multiple examples of it. In a similar reaction, $e^+e^- \to J/\psi D\bar{D}$ the Belle collaboration reported a bump close to the threshold in the $D\bar{D}$ invariant mass distribution [215], which was tentatively interpreted as a new resonance. However, this peak was considered in Ref. [216] in terms of a bound $D\bar{D}$ molecular state, called $X(3700)$, which had been already predicted in Ref. [59] and, later on, also reported in other works [217–222]. In a similar way, in Ref. [223], a peak seen in the $\phi\omega$ threshold in the $J/\psi \to \gamma\phi\omega$ reaction [224] was better interpreted as a manifestation below the $\phi\omega$ threshold of the $f_0(1710)$ resonance, which couples strongly to $\phi\omega$ [225]. More recently a bump close to threshold in the $K^0\bar{K}^0$ invariant mass distribution, seen in the $J/\psi \to \eta K^0\bar{K}^0$ decay in Ref. [226], is interpreted in Ref. [227] as a signal of the formation of an h_1 resonance, predicted in Ref. [225], which couples mostly to the $K^*\bar{K}^*$.

In the same direction as in the previous works, in Ref. [228] the experiment of [213] was reanalyzed and the enhancement in the $D^*\bar{D}^*$ invariant mass distribution was found compatible with a state with $J = 2$, mass around 3990 MeV and width around 160 MeV, although fits with other solutions were also found acceptable. Yet, resonances with mass bigger than the $D^*\bar{D}^*$ mass were discouraged based on the difficulty to have single channel resonances with energy above threshold. Indeed, it was shown in Ref. [96] that an energy independent potential, smooth in momentum space, could not generate a resonance above the mass of the interacting particles. In this sense, any energy below threshold

is preferred, and the $J = 2$ solution with mass around 3990 was proposed as a good candidate to explain the experimental peak. Another reason in favour of this interpretation was that if the state were a $J^P = 1^+$ produced in s-wave, as assumed in the experimental work [213], it would easily decay into $\pi J/\psi$. This decay channel is the same of the $Z_c(3900)$ [229]. However, while a peak is clearly visible in the $\pi J/\psi$ invariant mass distribution for the $Z_c(3900)$, no peak is seen around 4025 MeV (see Fig. 4 of Ref. [229]).

Stimulated by the large impact that the X(3872) state [204] had in this field [56, 206, 230–238], the $D\bar{D}^*$ systems have been the most studied. Much at the origin, this state was assumed to be a $D^0\bar{D}^{*0}$ [239, 240]. However, subsequent works have stressed the relevance of the charged component $D^+\bar{D}^{*-}$, thus forming a quite good $I = 0$ state [94, 126, 231]. More recently, the radiative decay of the $X(3872)$ into $\gamma J/\psi$ has shown that the charged components are essential to obtain the right rates [241, 242]. We will go back to this subject in **Chapter 7**, where some relevant decays of the $X(3872)$ will be widely discussed.

Once again, it was surprising to find $D\bar{D}^*$ $I = 1$ states, since the interaction in this channel is weaker than for $I = 0$. Yet, experimental work has been conducted and the BESIII collaboration reported a state $Z_c(3900)$ found in the invariant mass distribution of $\pi J/\psi$ in the $e^+e^- \to \pi^+\pi^- J/\psi$ reaction [229], with a width of $46 \pm 10 \pm 20$ MeV. The Belle Collaboration has reconfirmed the finding and, using different energies for the electron beam, a peak is also seen in $\pi J/\psi$ around 3894 MeV and a width of about $63 \pm 24 \pm 26$ MeV [243]. CLEO has followed with more precision and reported a peak at 3886 MeV and a width of $37 \pm 4 \pm 8$ MeV [244]. The state observed has $I = 1$ and $J^P = 1^+$.

Theoretical work has followed: in Ref. [245] a discussion is done on possible structures of this state and suggestions of new experiments are made to get a further insight on its nature. A $D\bar{D}^*$ molecular structure is suggested in Refs. [246–249]. Work has also been done using QCD sum rules, suggesting a tetraquark structure. In particular, the authors of Ref. [250] use a tetraquark interpolating current in order to estimate the decay width of the $Z_c(3900)$, while in Ref. [251] the same tetraquark current is used to estimate the mass.

The same challenges also concern the bottomoniumlike states and in this Chapter we will focus in particular on the $Z_b(10650)$ and $Z_b(10610)$. They were observed by the Belle collaboration in $\pi^\pm h_b(nP)$ and $\pi^\pm \Upsilon(mS)$, with $n = 1, 2$ and $m = 1, 2, 3$, invariant mass distribution of the $\Upsilon(5S)$ decay channel [252]. As a result of the measurements, Belle reported: $M_{Z_b(10610)} = (10608.4 \pm 2.0)$ MeV, $\Gamma_{Z_b(10610)} = (15.6 \pm 2.5)$ MeV and, for the $Z_b(10650)$, $M_{Z_b(10650)} = (10653.2 \pm 1.5)$ MeV and $\Gamma_{Z_b(10650)} = (14.4 \pm 3.2)$ MeV. The quantum numbers are reported as $J^P = 1^+$ and positive G-parity. The neutral partner has also been observed in the $\Upsilon(5S) \to \Upsilon(nS)\pi\pi$ decay by the Belle

Colaboration [253].

In an attempt to understand the $Z_b(10610)$ and $Z_b(10650)$ configuration, some interpretations were considered. We will try to summarize here the huge amount of work that has been done.

The authors of Ref. [254] treated the $Z_b(10610)$ and $Z_b(10650)$ as molecular states of $B\bar{B}^*$ and $B^*\bar{B}^*$ using heavy quark spin symmetry (HQSS), but the strength of the interaction was unknown. The proximity of the masses of these states to the $B\bar{B}^*$ and $B^*\bar{B}^*$ thresholds prompted the authors of Ref. [255] to suggest that these peaks could be a consequence of cusps originated at these thresholds. This idea has been made more quantitative in a recent paper [256]. Again from the molecular perspective, in Refs. [230, 257] the authors consider the states driven by the one pion exchange interaction, while in Ref. [258] the $\Upsilon(5S) \to \Upsilon(nS)\pi^+\pi^-$ decays are analysed. In Ref. [259], several decay channels are investigated in order to give support for the molecular picture and in Ref. [260], using phenomenological Lagrangians, the $Z \to \Upsilon(nS)\pi$ transition rates are evaluated. A molecular interpretation was used once again in Ref. [261], extending the work of Refs. [230, 257], in order to explain the states as $B^*\bar{B}$ and $B^*\bar{B}^*$ assuming a s- and d-waves mixture. In Ref. [262] the molecular option is also supported by sum rules, but with an uncertainty in the mass of about 220 MeV.

In Ref. [263] the dynamics of hadro-quarkonium system was formulated, based on the channel coupling of a light hadron (h) and heavy quarkonium $(Q\,\bar{Q})$ to intermediate open-flavor heavy-light mesons (Qq, Qq).

In Ref. [264] the authors used QCD sum rules assuming tetraquarks or molecules, and in all cases they could obtain good results, though the errors in the masses were of the order of 200 to 300 MeV. In the same line, in Ref. [265] the states are also assumed to be tetraquarks, as in Refs. [266, 267], where the authors, using the framework of QCD sum rules, calculated the Z_b's mass. However, the masses obtained were lower than those of the Z_b states. Also in Refs. [268] and [269] a tetraquark nature is invoked. Pion exchange is considered in Ref. [270] and limits for the strength to produce binding are discussed. In Ref. [271] a tetraquark is preferred, since meson exchange binds in $I = 0$ but not in $I = 1$. In Ref. [272] the $B\bar{B}^*$ and $B^*\bar{B}^*$ systems (in s-wave) are investigated in the framework of chiral quark models using the Gaussian expansion method. The bound states of $B\bar{B}^*$ and $B^*\bar{B}^*$ with quantum numbers $I(J^P) = 1(1^+)$, which are good candidates for the $Z_b(10610)$ and $Z_b(10650)$, are obtained. Another $B\bar{B}^*$ bound state with $I(J^{PC}) = 0(1^{++})$, and other two $B^*\bar{B}^*$ with $I(J^{PC}) = 1(0^{++})$, $I(J^{PC}) = 0(2^{++})$ are predicted in that work. In Ref. [265] $I^G = 1^+$ tetraquarks are invoked again and possible $J^{PC} = 1^{++}$, 2^{++} states from charge conjugation are investigated.

In Ref. [273] HQSS is used, analysing the power counting of the loops, and concluding that the molecular nature of the states can account for the observed features. In Ref. [274] the authors mention that using HQSS and the molecular picture, states with $I^G = 1^-$ should exist in addition to the reported states with 1^+. In [275] the authors make arguments of HQSS starting from the $X(3872)$ extrapolated to the beauty sector, and find a plausible molecular interpretation for the $Z_b(10610)$ state. In Ref. [276] once again the molecular structure is supported within HQSS. A different interpretation is given in Ref. [277], where the initial pion emission mechanism is invoked to reproduce the $\Upsilon(5S) \to \Upsilon(nS)\pi\pi$, with the second pion and the resonance produced from the loop diagram involving three B^* states. By using HQSS and assuming the states to be molecular, different modes of production are evaluated in Ref. [278]. In Ref. [279] the authors use HQSS to relate these states, which are assumed to be molecular, to the $X(3872)$. Finally, using the chiral quark models, the authors of Ref. [280] interpret the states as loosely bound states of $B\bar{B}^*$, $B^*\bar{B}^*$.

In this chapter we do a thorough investigation of $D\bar{D}^*$, $D\bar{D}^*$, $B\bar{B}^*$ and $B^*\bar{B}^*$ taking into account the possible sources of interaction, in order to compare them and identify the most relevant processes. We start analysing the contribution coming from the exchange of vector mesons. Then, we proceed to the evaluation of the interaction coming from the single light pseudoscalar (π, η or η') exchange, followed by the two pseudoscalars exchange. We also treat the case of the crossed-two-pion exchange and two interacting pions, leading to a "σ" exchange.

6.2 Formalism

We want to study the states of $I = 1$ generated by the $D\bar{D}^*$, $D^*\bar{D}^*$, $B\bar{B}^*$ and $B^*\bar{B}^*$ interactions. The starting point is the observation that the interactions proceeding via the exchange of one light meson are not allowed by the Okubo-Zweig-Iizuka (OZI) rule.

In **Figure 6.1** we show as an example a diagram illustrating the $D^{*+}\bar{D}^{*0}$ case: in order for the process to occur, a $d\bar{d}$ state must be converted in a $u\bar{u}$ state, which means that the reaction is OZI forbidden. In terms of physical mesons, this implies that the contributions coming from the ρ and ω meson exchange cancel when equal masses are taken (as it is indeed the case in the hidden gauge approach [214]). The same argument holds for the exchange of pseudoscalars and an exact cancellation of the π, η and η' exchange is found in the limit of equal masses. When considering different masses for the pseudoscalar mesons, the cancellation is only partial at low momenta,

becoming quite drastic for momentum transfers of the order of the mass of the η'. We shall show this in detail in **Section 6.2.5**.

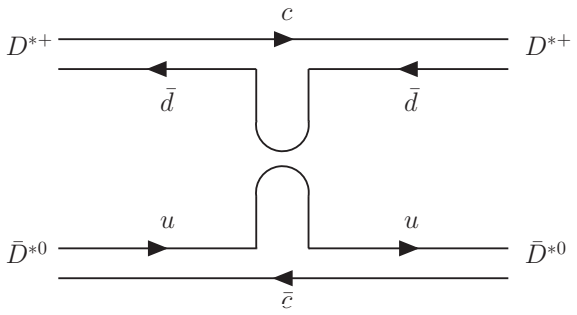

Figure 6.1: Feynman diagram depicting the exchange of a light $q\bar{q}$ pair in the $D^*\bar{D}^*$ interaction. A $d\bar{d}$ from the upper vertex is forced to convert into a $u\bar{u}$ pair in the lower one, evidencing an OZI forbidden mechanism.

Due to these cancellations, we shall consider also processes in which the OZI restriction no longer holds, starting, in this same section, from the exchange of one heavy vector meson. We study the $VV \to V'V'$ and $PV \to P'V'$ interactions via vector exchange in the framework of the hidden gauge formalism but using its extension to the heavy quark sector [214]. This means that we are going to use the Langrangians describing the VPP and VVV vertices given by Eqs. (2.92) and (2.96), with the matrices P and V in Eqs. (2.29) and (2.83) substituted by their $SU(4)$ extensions. We have, for the charm sector

$$P = \begin{pmatrix} \frac{\eta}{\sqrt{3}} + \frac{\eta'}{\sqrt{6}} + \frac{\pi^0}{\sqrt{2}} & \pi^+ & K^+ & \bar{D}^0 \\ \pi^- & \frac{\eta}{\sqrt{3}} + \frac{\eta'}{\sqrt{6}} - \frac{\pi^0}{\sqrt{2}} & K^0 & D^- \\ K^- & \bar{K}^0 & -\frac{\eta}{\sqrt{3}} + \sqrt{\frac{2}{3}}\eta' & D_s^- \\ D^0 & D^+ & D_s^+ & \eta_c \end{pmatrix} \tag{6.1}$$

and

$$V_\mu = \begin{pmatrix} \frac{\omega}{\sqrt{2}} + \frac{\rho^0}{\sqrt{2}} & \rho^+ & K^{*+} & \bar{D}^{*0} \\ \rho^- & \frac{\omega}{\sqrt{2}} - \frac{\rho^0}{\sqrt{2}} & K^{*0} & D^{*-} \\ K^{*-} & \bar{K}^{*0} & \phi & D_s^{*-} \\ D^{*0} & D^{*+} & D_s^{*+} & J/\psi \end{pmatrix}_\mu , \tag{6.2}$$

while, for the bottom sector,

$$P = \begin{pmatrix} \frac{\eta}{\sqrt{3}} + \frac{\eta'}{\sqrt{6}} + \frac{\pi^0}{\sqrt{2}} & \pi^+ & K^+ & B^+ \\ \pi^- & \frac{\eta}{\sqrt{3}} + \frac{\eta'}{\sqrt{6}} - \frac{\pi^0}{\sqrt{2}} & K^0 & B^0 \\ K^- & \bar{K}^0 & -\frac{\eta}{\sqrt{3}} + \sqrt{\frac{2}{3}}\eta' & B_s^0 \\ B^- & \bar{B}^0 & \bar{B}_s^0 & \eta_b \end{pmatrix} \tag{6.3}$$

and

$$V_\mu = \begin{pmatrix} \frac{\omega}{\sqrt{2}} + \frac{\rho^0}{\sqrt{2}} & \rho^+ & K^{*+} & B^{*+} \\ \rho^- & \frac{\omega}{\sqrt{2}} - \frac{\rho^0}{\sqrt{2}} & K^{*0} & B^{*0} \\ K^{*-} & \bar{K}^{*0} & \phi & B_s^{*0} \\ B^{*-} & \bar{B}^{*0} & \bar{B}_s^{*0} & \Upsilon \end{pmatrix}_\mu . \tag{6.4}$$

We are interested in channels with quantum numbers $I = 1$, strangeness $S = 0$ and $C = 0$ in the case of $D\bar{D}^*$ and $D^*\bar{D}^*$, and $I = 1$, $S = 0$ and $B = 0$ for $B\bar{B}^*$ and $B^*\bar{B}^*$. We will treat the four interactions separately.

6.2.1 The $D\bar{D}^*$ vector exchange interaction

In the sector with $I = 1$, $S = 0$ and $C = 0$ it is possible to distinguish channels with positive or negative G-parity combinations. In the case of positive G-parity $[I^G(J^{PC}) = 1^+(1^{+-})]$ there are six possible channels that can contribute to the process: $\pi\omega$, $\eta\rho$, $(\bar{K}K^* + c.c.)/\sqrt{2}$, $(\bar{D}D^* + c.c.)/\sqrt{2}$, $\eta_c\rho$ and $\pi J/\Psi$ [56][1]. However, we will only take into account the last three. Since we are investigating the energy region around 3900 MeV, the $\pi\omega$ and $\eta\rho$ channels, whose thresholds are at much smaller energies, will only slightly affect the results. Analogously, for negative G-parity $[I^G(J^{PC}) = 1^-(1^{++})]$ we will only include in the formalism the $(\bar{D}D^* - c.c.)/\sqrt{2}$ channel since the $(\bar{K}K^* - c.c.)/\sqrt{2}$ and $\pi\rho$ are too far from the energy values we are interested in.

We already mentioned that the tree level amplitudes of the interaction can be evaluated by means of the Lagrangians in Eqs. (2.92) and (2.96). However, they would result identical to those obtained with the chiral Lagrangian of Ref. [281] and, in Refs. [51, 56], they are explicitly evaluated and projected in s-wave, with the result

$$\begin{aligned} V_{ij}(s) = -\frac{\vec{\epsilon}\,\vec{\epsilon}\,'}{8f^2}\,\mathcal{C}_{ij}[3s - (M^2 + m^2 + M'^2 + m'^2) \\ - \frac{1}{s}(M^2 - m^2)(M'^2 - m'^2)] \,. \end{aligned} \tag{6.5}$$

[1]Note that we have $C\rho^0 = -\rho^0$, $C\rho^+ = -\rho^-$, $C\rho^- = -\rho^+$.

The masses M (M') and m (m') in Eq. (6.5) correspond to the initial (final) vector meson and pseudoscalar meson, respectively, while the indices i and j represent the initial and final VP channels.

In the case of positive G-parity, we will have a 3×3 matrix for the coefficients $\mathcal{C}_{ij}$, that we take from Ref. [56],

$$\mathcal{C}_{ij} = \begin{pmatrix} -\psi & 2\sqrt{\frac{2}{3}}\gamma & 2\sqrt{\frac{2}{3}}\gamma \\ 2\sqrt{\frac{2}{3}}\gamma & 0 & 0 \\ 2\sqrt{\frac{2}{3}}\gamma & 0 & 0 \end{pmatrix}, \tag{6.6}$$

with $\gamma = \left(\frac{m_L}{m_H}\right)^2$ and $\psi = -\frac{1}{3} + \frac{4}{3}\left(\frac{m_L}{m'_H}\right)^2$. The parameters m_L, m_H and m'_H are chosen of the order of magnitude of a light vector meson mass, of a charmed vector mass and of the J/ψ mass. We take $m_L = 800$, $m_H = 2050$ MeV, and $m'_H = 3000$ MeV as done in Ref. [56]. The factors γ and ψ are defined in this way in order to take into account the suppression due to the exchange of a heavy vector meson.

In the case of negative G-parity only one channel is present, whose corresponding coefficient in Eq. (6.5) is $\mathcal{C} = -\psi$. In the language of vector meson exchange this means that a J/ψ is exchanged.

The potential of Eq. (6.5) is derived by the combination of momenta $(p_1 + p'_1)(p_2 + p'_2)$, with p_i and p'_i the momenta of the initial and final particles ($i = 1, 2$), and which we can approximate with $({p_1}^0 + {p'_1}^0)({p_2}^0 + {p'_2}^0)$, since we assume that the three-momenta of the external particles are small. In Ref. [282] it was shown that this Weinberg-Tomozawa interaction should accommodate a factor $(p_1^0/m_{K^*})(p_2^0/m_{K^*})$ multiplying the $SU(3)$ value, that stems from the implementation of the $HQSS$. In this work, the authors relate the $D^*D\pi$ vertex to its analogous in the strange sector, $K^*K\pi$. The same exercise is repeated for the Weinberg-Tomozawa term that we consider now based on vector exchange, and they show how the rules of HQSS [283–285] can be obtained from the impulse approximation at the quark level assuming the s and c quarks as spectators. The conclusion is that the interaction used automatically incorporates this factor, so that no changes are needed with respect to what was done in Ref. [56], and we can safely use Eq. (6.5).

Eq. (6.5) provides the potential V that must be used to solve the Bethe-Salpeter equation in coupled channels (Eq. (2.59)) removing the $\vec{\epsilon}\,\vec{\epsilon}\,'$ factor that can also be factorized in T. These transition potentials V_{ij} are shown in **Figure 6.2** while the elements of the diagonal loop function matrix G are given by Eq. (2.57).

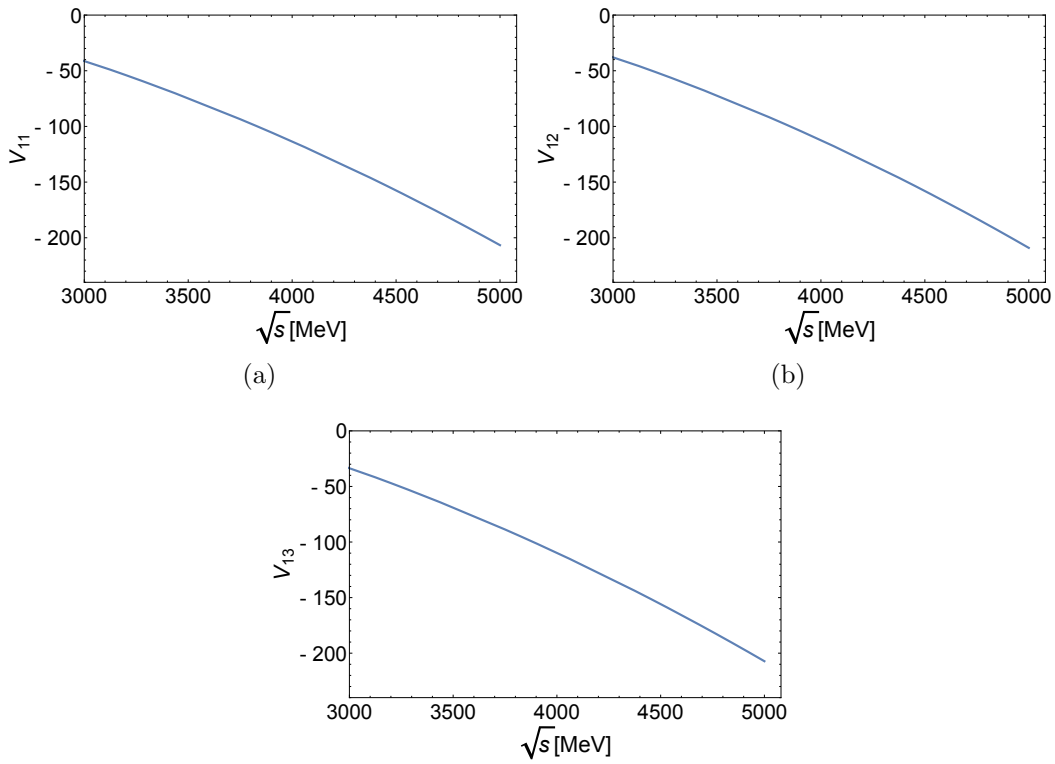

Figure 6.2: Potentials $V_{D\bar{D}^* \to D\bar{D}^*}$ (a), $V_{D\bar{D}^* \to \eta_C \rho}$ (b) and $V_{D\bar{D}^* \to \pi J/\psi}$ (c) as functions of the center of mass energy $\sqrt{s}$.

6.2.2 The $D^*\bar{D}^*$ vector exchange interaction

In this case, the channels with $I = 1$, charm $C = 0$ and strangeness $S = 0$ are $D^*\bar{D}^*, K^*\bar{K}^*, \rho\rho, \rho\omega, \rho J/\psi, \rho\phi$. The transition amplitudes that will be used as the kernel for the Bethe-Salpeter equation have already been evaluated by means of the Lagrangians of Eqs. (2.95) (giving the contact term) and (2.96) (giving the vector-exchange term) in Ref. [214], where all the details of the derivation can be found.

In Ref. [214], the $\rho\rho$, $\rho\omega$, $\rho\phi$ light vector channels were included in the calculation. However, their thresholds are situated at energies much smaller than the mass of the state we are looking for, such that the results would be only slightly affected by their inclusion. Moreover, we will only consider the case with $J = 2$ since this is the only spin channel where the interaction gives an attractive potential for $D^*\bar{D}^* \to D^*\bar{D}^*$.

The expressions of the potentials for the channels we are going to consider are given by the following equations, including both the contact and the vector-exchange term:

$$t^{I=1,J=2}_{D^*\bar{D}^*\to D^*\bar{D}^*} = -g_D^2 + g_D^2 \frac{(2m_\omega^2 m_\rho^2 + m_{J/\psi}^2(-m_\omega^2 + m_\rho^2))(4m_{D^*}^2 - 3s)}{4m_{J/\psi}^2 m_\omega^2 m_\rho^2}\,, \tag{6.7}$$

$$t^{I=1,J=2}_{D^*\bar{D}^*\to \rho J/\psi} = -2gg_D + gg_D \frac{2m_{D^*}^2 + m_{J/\psi}^2 + m_\rho^2 - 3s}{m_{D^*}^2}\,, \tag{6.8}$$

where m_ρ, m_ω and $m_{J/\psi}$ are the masses of the ρ, ω and J/ψ mesons respectively. The constant $g_D = m_{D^*}/(2f_D)$, which was used in Ref. [214], is analogous to the coupling g for light mesons, with $f_D = 206/\sqrt{2} = 145.66$ MeV, and it is the strong coupling of the D^* meson to $D\pi$, which in $SU(3)$ is equal to 4.16.

However, we can use again constrains of HQSS to provide a more accurate coupling. The $D^*\bar{D}^* \to D^*\bar{D}^*$ interaction is now mediated by J/ψ exchange ($c\bar{c}$) in analogy to the ϕ exchange in $K^*\bar{K}^* \to K^*\bar{K}^*$. As mentioned before, these constraints are deduced in the impulse approximation at the quark level assuming the s and c quarks as spectators. Then, given the $(2\omega)^{-1/2}$ normalization factors of the fields at the meson level, there is a factor $\omega_{D^*}/\omega_{K^*}$ between the D^*D^*J/ψ and the $K^*K^*\phi$ vertices. Since the $K^*K^*\phi$ vertex is proportional to ω_{K^*}, the D^*D^*J/ψ will have the same proportionality coefficient multiplied by ω_{D^*}, which is what the straight application of $SU(4)$ provides in this case. Note that the vector exchange term in Eq. (6.7) at the $D^*\bar{D}^*$ threshold, for simplicity, gives $g_D^2 \frac{m_{D^*}^2}{m_{J/\psi}^2}$ with $m_\omega = m_\rho$. There we see explicitly the energy of the m_{D^*} from the two vertices and $m_{J/\psi}^2$ from the J/ψ propagator but, according with the previous argument, we should get $g^2 \frac{m_{D^*}^2}{m_{J/\psi}^2}$. Therefore, we use

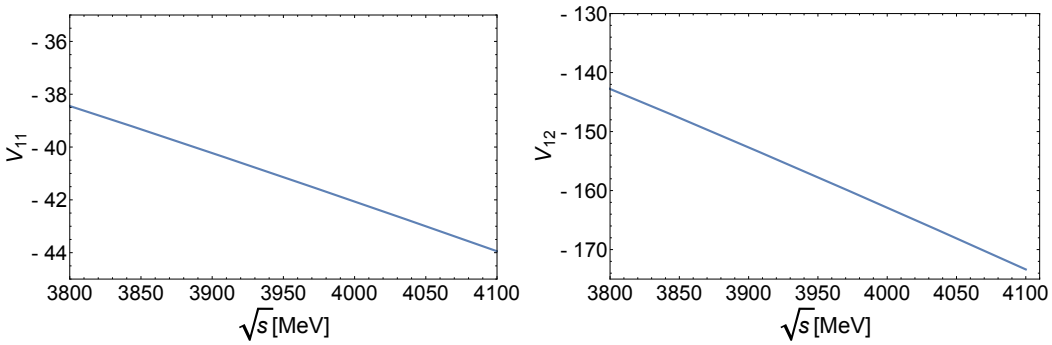

(a) (b)

Figure 6.3: Potentials $V_{D^*\bar{D}^*\to D^*\bar{D}^*}$ (a) and $V_{D^*\bar{D}^*\to\rho J/\psi}$ (b) as functions of the center of mass energy $\sqrt{s}$.

here the normal g coupling which is in agreement with HQSS. For consistency, we also take g^2 in the contact term, which is smaller than the J/ψ exchange one, and in the transition potential of Eq. (6.8). The use of the new coupling will have as a consequence the reduction of the binding of the $I = 1$ state with respect to the one found in Ref. [214].

The two potentials, which are the elements of the 2×2 matrix potential V in the Bethe-Salpeter equation, with $V_{11} = V_{D^*\bar{D}^*\to D^*\bar{D}^*}$, $V_{12} = V_{21} = V_{D^*\bar{D}^*\to\rho J/\psi}$, and $V_{22} = 0$, are plotted in **Figure 6.3** as functions of the centre of mass energy $\sqrt{s}$. As it is clear from the figure, the $\rho J/\psi$ channel plays an important role in this problem. Indeed, the transition potential of $D^*\bar{D}^* \to \rho J/\psi$ has a strength almost four times bigger than the $D^*\bar{D}^* \to D^*\bar{D}^*$ transition.

6.2.3 The $B\bar{B}^*$ vector exchange interaction

As in the case of $D\bar{D}^*$ interaction, the evaluation of the tree level scattering amplitudes leads to Eq. (6.5). This result can be obtained from the chiral Lagrangian of Ref. [281] but we show the derivation using the hidden gauge approach in Appendix **B**. In this case, the indices i and j represent the initial and final channels $(B\bar{B}^* + cc)/\sqrt{2}$, $\eta_b\,\rho$ and $\pi\,\Upsilon$.

The $\mathcal{C}_{ij}$ coefficients are the elements of a 3×3 matrix, which for the positive G-parity of the $B\bar{B}^*$ combination, is given by

$$\mathcal{C}_{ij} = \begin{pmatrix} -\psi & \sqrt{2}\gamma & \sqrt{2}\gamma \\ \sqrt{2}\gamma & 0 & 0 \\ \sqrt{2}\gamma & 0 & 0 \end{pmatrix} . \tag{6.9}$$

The factors γ and ψ, as in the $D\bar{D}^*$ case, take into account the suppression due to the exchange of a heavy vector meson. The values of the parameters

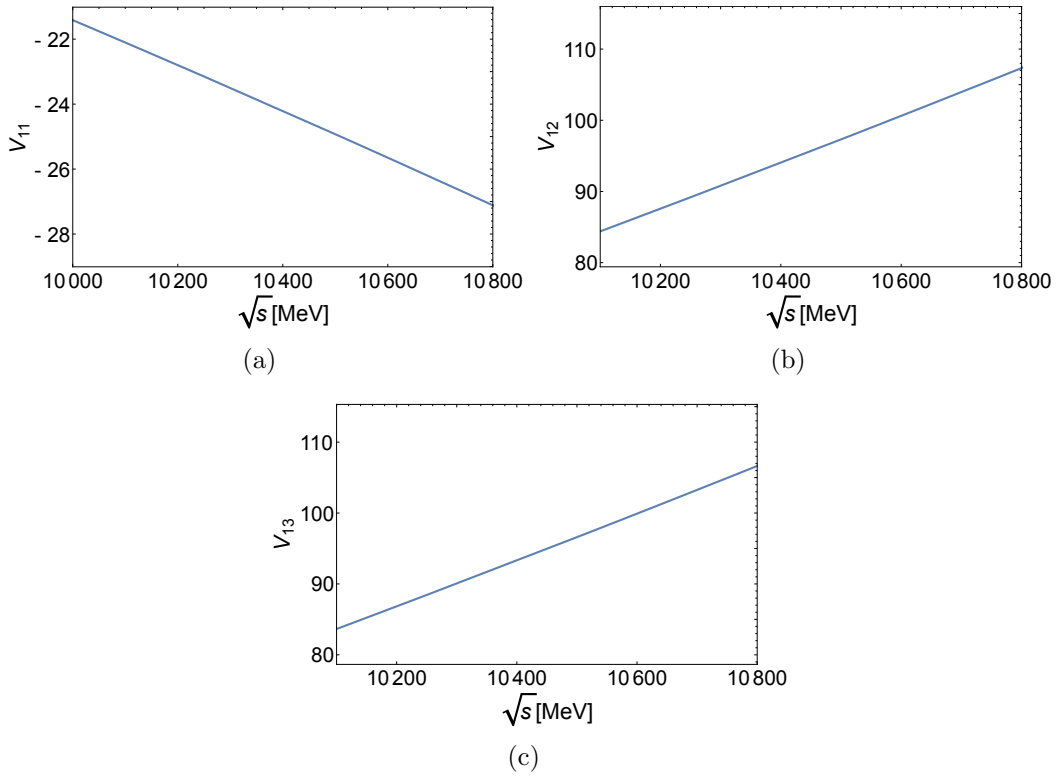

Figure 6.4: Potentials $V_{B\bar{B}^*\to B\bar{B}^*}$ (a), $V_{B\bar{B}^*\to\eta_b\rho}$ (b) and $V_{B\bar{B}^*\to\pi\Upsilon}$ (c) as functions of the center of mass energy $\sqrt{s}$.

m_L, m_H and $m_{H\prime}$ are chosen in order to have the same order of magnitude of the light and heavy vector meson masses: $m_L = 800$, $m_H = 5000$ MeV and $m_{H\prime} = 9000$ MeV. These masses stand for the ρ or ω, B^* and Υ respectively. We shall see how the results change by making some variation in the values of these parameters. The three potentials are shown in **Figure 6.4** as functions of the center of mass energy.

6.2.4 The $B^*\bar{B}^*$ vector exchange interaction

In this case, the channels contributing in the $S = 0$, $B = 0$ and $I = 1$ sector are $B^*\bar{B}^*$ and $\rho\Upsilon$. The tree level transition amplitudes are evaluated following the same steps as in Ref. [214] and the calculation for the exchange terms has been reproduced in detail, for this specific case, in Appendix **C**.

Putting together the exchange and the contact terms, already evaluated in Ref. [214], we get, for the case $J = 2$, which is the one that gives an attractive

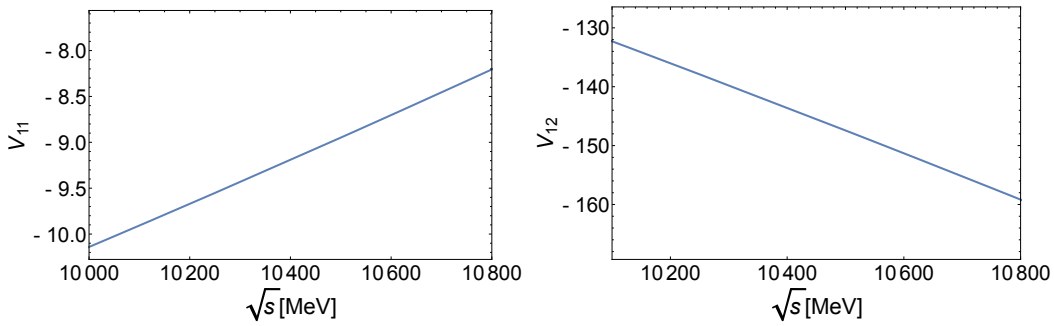

(a) (b)

Figure 6.5: Potentials $V_{B^*\bar{B}^*\to B^*\bar{B}^*}$ (a) and $V_{B^*\bar{B}^*\to\rho\Upsilon}$ (b) as functions of the center of mass energy $\sqrt{s}$ for $J = 2$.

interaction for the $B^*\bar{B}^* \to B^*\bar{B}^*$ transition,

$$
\begin{aligned}
t^{I=1,J=2}_{B^*\bar{B}^*\to B^*\bar{B}^*} &= -g^2 + g^2\left[\frac{2M_\rho^2 M_\omega^2 + M_\Upsilon^2(-M_\omega^2 + M_\rho^2)}{4M_\Upsilon^2 M_\omega^2 M_\rho^2}\right](4M_{B^*}^2 - 3s)\,, \\
t^{I=1,J=2}_{B^*\bar{B}^*\to\rho\Upsilon} &= -2g^2 + g^2\left[\frac{2M_{B^*}^2 + M_\Upsilon^2 + M_\rho^2 - 3s}{M_{B^*}^2}\right]\,,
\end{aligned}
\tag{6.10}
$$

where s is the square of the center of mass energy of the $B^*\bar{B}^*$ system. Again, as for the $D^*\bar{D}^*$ interaction, we can use the normal coupling g without entering into contradiction with the HQSS formalism.

In the case of the $B^*\bar{B}^* \to B^*\bar{B}^*$ transition, the exchange term is the same for every value of the spin $J = 0, 1, 2$ while, for the contact terms, one finds $2g^2$ and $3g^2$ for $J = 0$ and $J = 1$ respectively, as reported in in Ref. [214]. In the case of the non-diagonal transition, both the exchange and the contact terms vanish for $J = 1$. For $J = 0$ the contact terms $4g^2$ and the exchange one is the same as for $J = 2$.

Eqs. (6.10) will be used as a kernel of the Bethe-Salpeter equation. The two potentials are plotted in **Figure 6.5** as functions of the centre of mass energy $\sqrt{s}$ for $J = 2$.

6.2.5 Light pseudoscalar exchange

In this section we proceed with the evaluation of the amplitude for the exchange of a single light pseudoscalar mesons (π, η, η'). The diagrams describing the process are shown in **Figure 6.6** for the four cases under study: $D\bar{D}^*$ (a), $D^*\bar{D}^*$ (b), $B\bar{B}^*$ (c) and $B^*\bar{B}^*$ (d).

First we will take into consideration the cases of $D\bar{D}^*$ and $B\bar{B}^*$, since they

present identical formalism. Then, we will treat the case of the interaction between two vectors.

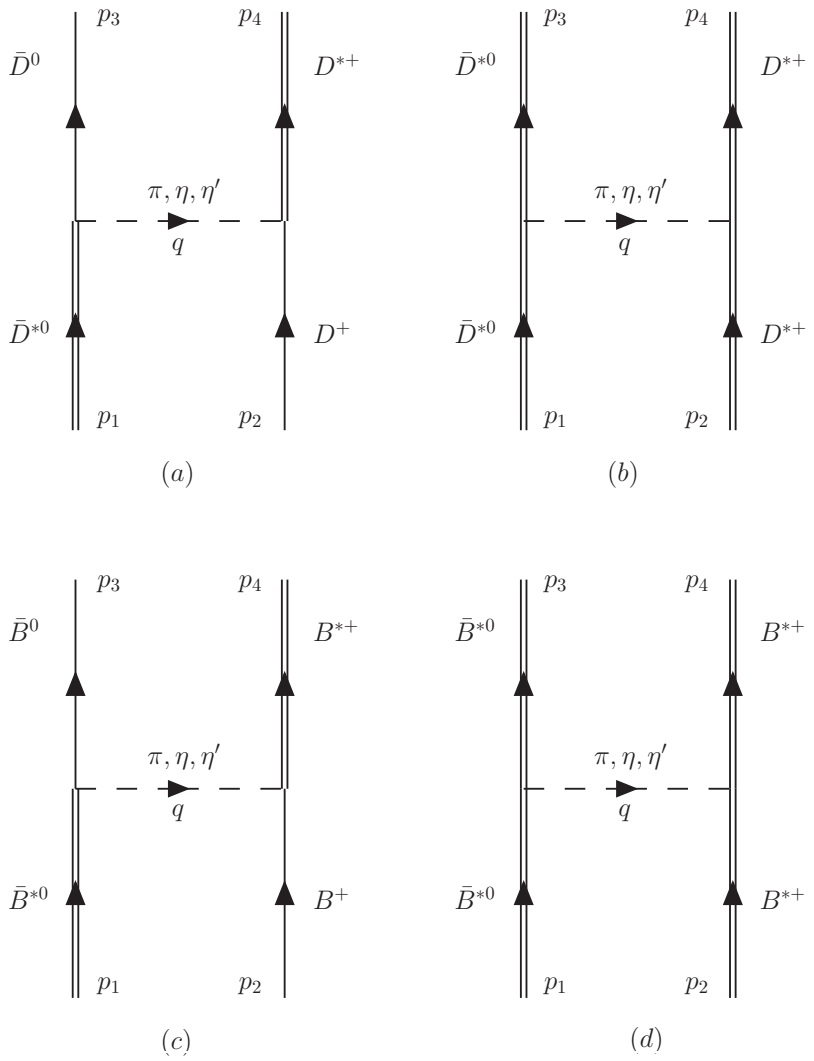

Figure 6.6: Diagrammatic representation of the $D\bar{D}^*$ (a), $D^*\bar{D}^*$ (b), $B\bar{B}^*$ (c) and $B^*\bar{B}^*$ (d) interaction via light pseudoscalar exchange.

THE $D\bar{D}^*$ AND $B\bar{B}^*$ CASES

In order to evaluate the amplitude of the diagrams in **Figure 6.6** (a) and (c) we need the Lagrangian for the PPV vertex of Eq.(2.92) but using the constant g_D, the strong coupling of the D^* meson to $D\pi$, which in $SU(3)$ is equal to 4.16. However this is in contradiction with the empirical value of

$g \simeq 9$ needed to get the $D^* \to D\pi$ width. This apparent contradiction is settled by looking at the $D^* \to D\pi$ decay using the impulse approximation at the quark level, assuming the heavy quarks as spectators. Once again, the standard normalization used for the meson fields at the macroscopic level (mesons, not quarks) demands that the $g\ \vec{\epsilon}\cdot\vec{q}$ operator that one has for the D^{*0} decay at rest is normalized by an extra m_{D^*}/m_{K^*} factor. This gives an effective g constant for D, D^* mesons, $\tilde{g}_D \simeq 9.40$. With this coupling we get a width of 71 KeV for the $D^{*+} \to D^0\pi^+$ decay, which is in agreement with the more recent result of (65 ± 15) KeV of [286]. The same argument holds in the case of the B and B^* meson, and the coupling is given by $\tilde{g}_B = m_{B^*}/m_{K^*}g$.

In isospin equal to 1, we have the states ψ_1, corresponding to

$$|\psi_1\rangle = \frac{1}{\sqrt{2}}\Big(|D^+\bar{D}^{*0}\rangle + |\bar{D}^0 D^{*+}\rangle\Big)\,, \tag{6.11}$$

and

$$|\psi_1\rangle = \frac{1}{\sqrt{2}}\Big(|B^+\bar{B}^{*0}\rangle + |\bar{B}^0 B*+\rangle\Big)\,. \tag{6.12}$$

We can see that the pseudoscalar meson exchange with the interaction of Eq. (2.92) mixes the first component of Eqs. (6.11) and (6.12) for the initial state with the second component of the same equation for the final state and vice-versa.

Using Eq. (2.92) to write explicitly the $P\bar{D}^{*0}\bar{D}^0$ ($P\bar{B}^{*0}\bar{B}^0$) and $PD^{*+}D^+$ ($PB^{*+}B^+$) vertices, with P the exchanged light pseudoscalar, we find for both cases

$$\begin{aligned} t_{\psi_1\to\psi_1} = -4\tilde{g}_V^2\Big(&-\frac{1}{2}\frac{1}{q^2 - m_\pi^2 + i\epsilon} + \frac{1}{6}\frac{1}{q^2 - m_\eta^2 + i\epsilon} \\ &+ \frac{1}{3}\frac{1}{q^2 - m_{\eta'}^2 + i\epsilon}\Big)(\epsilon_1\cdot p_3)(\epsilon_4\cdot p_2)F^2(\vec{q})\,, \end{aligned} \tag{6.13}$$

where m_π, m_η, $m_{\eta'}$ are the masses of the π, η and η' respectively, ϵ_1 and ϵ_4 are the polarization vectors for the $\bar{D}^{*0}$ ($\bar{B}^{*0}$) and D^{*+} (B^{*+}) vector mesons respectively, $F(\vec{q})$ is a form factor of the type

$$F(\vec{q}) = \frac{\Lambda^2}{\Lambda^2 + \vec{q}^{\,2}}\,, \tag{6.14}$$

with $\Lambda = 1$ GeV, which will be also used later for the other interactions, and $\vec{q}$ the three-momentum transferred in the process. We called the coupling, generically, $\tilde{g}_V$, with $V = D, B$.

Considering that the masses of the vectors are heavy compared to the external momenta, the following approximations occur: $\epsilon_1\cdot p_3 = -\vec{\epsilon_1}\cdot\vec{p_3}$ and

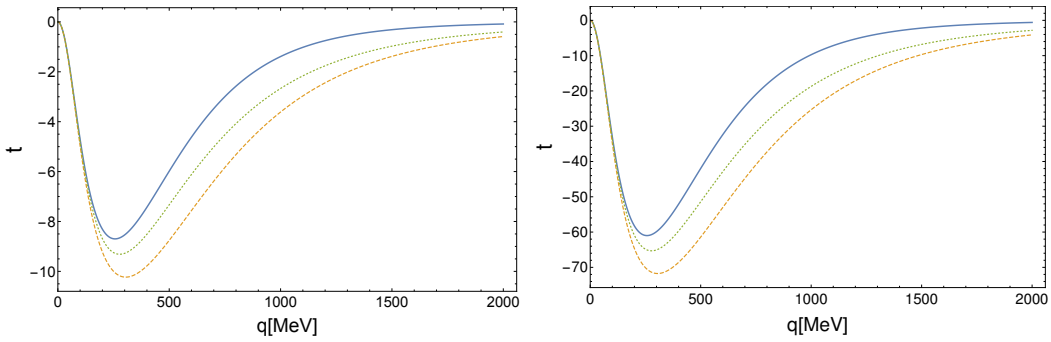

(a) (b)

Figure 6.7: $D\bar{D}^*$ (a) and $B\bar{B}^*$ (b) one pseudoscalar exchange potential for the exchange of one pion (dashed line), π plus η (dotted line) and π plus η plus η' (thick line) as functions of the transferred momentum q.

$\epsilon_4 \cdot p_2 = -\vec{\epsilon_4} \cdot \vec{p_2}$. Moreover, we can use for simplicity the Breit frame where

$$\begin{aligned} p_1 &\equiv (p_1^0, \vec{q}/2) \ , \\ p_2 &\equiv (p_2^0, -\vec{q}/2) \ , \\ p_3 &\equiv (p_3^0, -\vec{q}/2) \ , \\ p_4 &\equiv (p_4^0, \vec{q}/2) \, . \end{aligned} \tag{6.15}$$

Since we are doing an estimate, we have chosen $q^0 \equiv 0$. We are dealing with s-waves and this allows us to use $q_i q_j \to \frac{1}{3}\vec{q}^{\,2}\delta_{ij}$ and, then, to rewrite the amplitude of Eq. (6.13) as

$$\begin{aligned} t_{\psi_1 \to \psi_1} = \frac{\tilde{g}_V^2}{3}\vec{q}^{\,2}\Big(&- \frac{1}{2}\frac{1}{\vec{q}^{\,2} + m_\pi^2 + i\epsilon} + \frac{1}{6}\frac{1}{\vec{q}^{\,2} + m_\eta^2 + i\epsilon} \\ &+ \frac{1}{3}\frac{1}{\vec{q}^{\,2} + m_{\eta'}^2 + i\epsilon}\Big) F^2(\vec{q}) \, . \end{aligned} \tag{6.16}$$

In **Figures 6.7(a)** and **6.7(b)** we show the contributions coming from Eq. (6.16) for the exchange of one pion (dashed line), π plus η (dotted line) and π plus η plus η' (thick line) as functions of the transferred momentum q for the $D\bar{D}^*$ and $B\bar{B}^*$ case respectively. We can see, in both cases, a partial cancellation between the three contributions, which becomes very effective at large momenta and exact in the limit of equal masses for the light pseudoscalars.

It is interesting to compare the contributions of **Figures 6.7(a)** and **6.7(b)** with the ones due to vector exchange, which we plot in **Figures 6.8(a)** and **6.8(b)**. Recall that the use of the vector exchange potential as V in the Bethe-Salpeter equation (Eq. (2.59)), together with a G function regularized with a

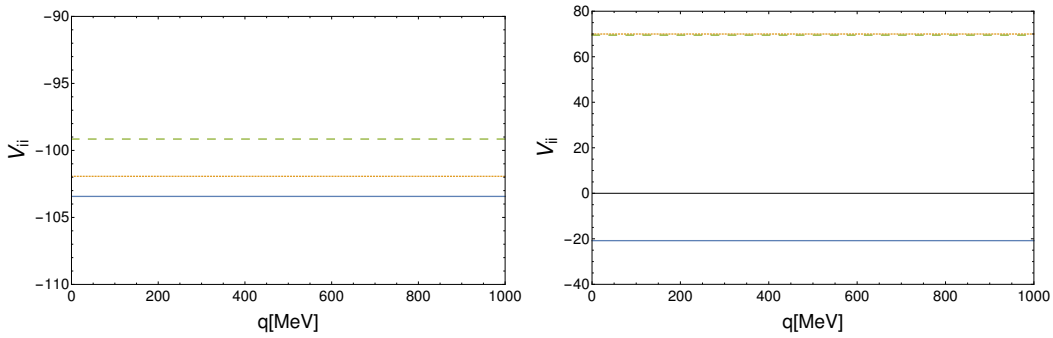

(a) (b)

Figure 6.8: In Fig. (a): vector exchange potentials $V_{D\bar{D}^*\to D\bar{D}^*}$ (thick line), $V_{D\bar{D}^*\to\eta_C\rho}$ (dotted line) and $V_{D\bar{D}^*\to\pi J/\psi}$ (dashed line) as functions of the transferred momentum q. In Fig. (b): vector exchange potentials $V_{B\bar{B}^*\to B\bar{B}^*}$ (thick line), $V_{B\bar{B}^*\to\eta_b\rho}$ (dashed line) and $V_{B\bar{B}^*\to\pi\Upsilon}$ (dotted line) as functions of the transferred momentum q.

cutoff q_{max}, is equivalent to using a potential of the type [94]

$$V(\vec{p},\vec{p}\,') = V\theta(q_{max}-\vec{p})\theta(q_{max}-\vec{p}\,') \ , \tag{6.17}$$

Assuming $\vec{p}\simeq 0$, $\vec{p}\,'$ takes the place of $\vec{q}$, and this allows a proper comparison keeping in mind that q_{max}, to be used later, is of the order of 770 MeV in the $D\bar{D}^*$ case and 700 MeV in the $B\bar{B}^*$. While in the case of D mesons the exchange of one pseudoscalar is very small compared to the vector exchange and can be safely neglected, this is not the case for the B mesons. We will see later that this contribution can be included in the theoretical uncertainties considered.

THE $D^*\bar{D}^*$ AND $B^*\bar{B}^*$ CASE

The light pseudoscalar exchange between vector mesons, shown in **Figure 6.6** (b) and (d), proceeds via the anomalous vector-vector-pseudoscalar (PVV) coupling. Using the Lagrangian of Eq. (2.97) for the vertices involved, its contribution can be easily evaluated and, close to threshold, it reads

$$t \simeq -\frac{G^2}{2}m_V^2\ \vec{q}\cdot(\vec{\epsilon}_1\times\vec{\epsilon}_3)\ \vec{q}\cdot(\vec{\epsilon}_2\times\vec{\epsilon}_4)\Big(-\frac{1}{2}\frac{1}{q^2-m_\pi^2}+\frac{1}{3}\frac{1}{q^2-m_\eta^2} + \frac{1}{6}\frac{1}{q^2-m_{\eta'}^2}\Big)\ , \tag{6.18}$$

where $\vec{\epsilon}_1$ and $\vec{\epsilon}_2$ stand for the initial polarizations of the vector mesons, $\vec{\epsilon}_1$ and $\vec{\epsilon}_3$ for the final ones and q is the momentum transfer. The symbol m_V stands

for the mass of the heavy vector, D^* or B^*. Once again, to derive Eq. (6.18) we used the approximation of small three-momenta of the vectors.

Note that t in Eq. (6.18) is already proportional to ω_V^2 (m_V^2 at threshold) and the factor proportional to ω_V in each vertex demanded by HQSS is automatically included in Eq. (6.18) as it was also the case in the Weinberg-Tomozawa terms.

Since we are concerned in s-waves, we can take again $\vec{q}_i\vec{q}_j \to \frac{1}{3}\vec{q}^{\,2}\delta_{ij}$, which leads to the spin structure

$$(\vec{\epsilon_1}\times\vec{\epsilon_3})(\vec{\epsilon_2}\times\vec{\epsilon_4}) = \epsilon_i\epsilon_i\epsilon_j\epsilon_j - \epsilon_i\epsilon_j\epsilon_j\epsilon_i \ , \tag{6.19}$$

where the order of the polarization vectors in the right-hand side of Eq. (6.19) is 1, 2, 3 and 4. By recalling the form of the spin projector operators in Eqs. (C.5) of Appendix **C**, we see that

$$(\vec{\epsilon_1}\times\vec{\epsilon_3})(\vec{\epsilon_2}\times\vec{\epsilon_4}) = 2\mathcal{P}^{(0)} + \mathcal{P}^{(1)} - \mathcal{P}^{(2)} \, . \tag{6.20}$$

Thus we have

$$t \simeq -A\,\frac{G^2}{2}m_V^2\ \vec{q}^{\,2}\Big(\frac{1}{2}\frac{1}{\vec{q}^{\,2}+m_\pi^2} - \frac{1}{3}\frac{1}{\vec{q}^{\,2}+m_\eta^2} - \frac{1}{6}\frac{1}{\vec{q}^{\,2}+m_{\eta'}^2}\Big)F^2(\vec{q}\,) \, , \tag{6.21}$$

with $A = 2, 1, -1$ when $J = 0, 1, 2$. In Eq. (6.21) we have taken into account that $q^0 = 0$ and we have introduced again the convergence form factor $F(\vec{q}\,) = \frac{\Lambda^2}{\Lambda^2+\vec{q}^{\,2}}$, with $\Lambda = 1000$ MeV [287].

In Eq. (6.21) we observe the cancellation of the exchange of π, η, η' in the limit of equal masses. In **Figures 6.9(a)** and **6.9(b)** we plot t as a function of $\vec{q}$ for $D^*\bar{D}^*$ and $B^*\bar{B}^*$ respectively and for $J = 2$, and this cancellation can be seen explicitly. We compare the amplitude with the vector exchange potentials, exactly as we did in the previous section, shown in **Figures 6.10(a)** and **6.10(b)**.

Again, for the charm sector the strength of the vector exchange interaction is bigger, but this is not the case of the bottom sector.

6.2.6 Iterated two meson exchange

In this section we discuss the case of the exchange of two light pseudoscalar mesons. The transition needs a box diagram to accommodate the two intermediate pseudoscalar states and it is shown in **Figure 6.11** for the four cases under consideration. As we did in **Section 6.2.5**, we will first treat the $PV \to PV$ cases (**Figure 6.11** (a) and **Figure 6.11** (c)) and then the $VV \to VV$ ones (**Figure 6.11** (b) and **Figure 6.11** (d)).

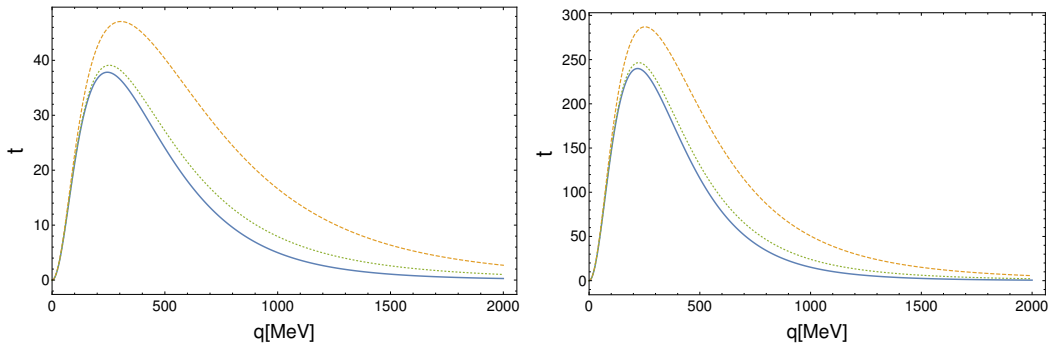

(a) (b)

Figure 6.9: $D^*\bar{D}^*$ (a) and $B^*\bar{B}^*$ (b) one pseudoscalar exchange potential for the exchange of one pion (dashed line), π plus η (dotted line) and π plus η plus η' (thick line) as functions of the transferred momentum q and for $J = 2$.

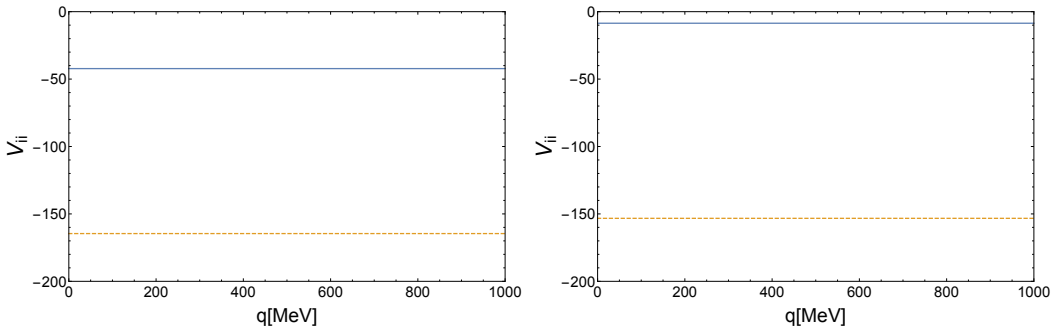

(a) (b)

Figure 6.10: In Fig. (a): vector exchange potentials $V_{D^*\bar{D}^*\to D^*\bar{D}^*}$ (thick line) and $V_{D^*\bar{D}^*\to\rho J/\psi}$ (dotted line) as functions of the transferred momentum q. In Fig. (b): vector exchange potentials $V_{B^*\bar{B}^*\to B^*\bar{B}^*}$ (thick line) and $V_{B^*\bar{B}^*\to\rho\Upsilon}$ (dotted line) as functions of the transferred momentum q.

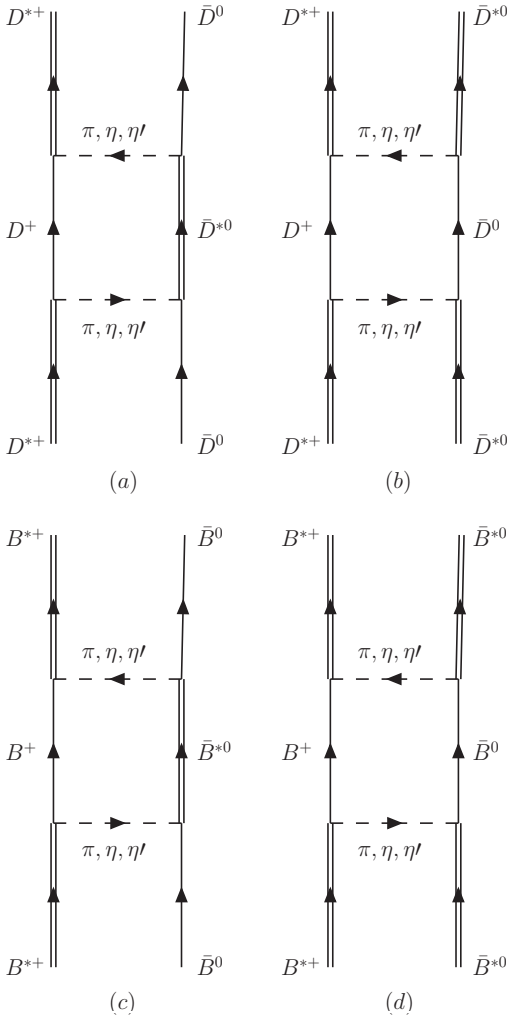

Figure 6.11: Diagrammatic representation of the $D\bar{D}^*$ (a), $D^*\bar{D}^*$ (b), $B\bar{B}^*$ (c) and $B^*\bar{B}^*$ (d) interaction via iterated two pseudoscalar exchange.

THE $D\bar{D}^*$ AND $B\bar{B}^*$ CASES

In this case, in order to evaluate the transition amplitude we only need the four VPP vertices, derived using Eq. (2.92), with the couplings constants imposed by HQSS, $\tilde{g}_D$ and $\tilde{g}_B$. We use the $D\bar{D}^*$ case as an example. The amplitude for the $B\bar{B}^*$ interaction can be obtained following exactly the same steps. We get the expression

$$\begin{aligned} t = i\tilde{g}_D^4 \frac{1}{3}\,\vec{\epsilon}\cdot\vec{\epsilon}\,' \int \frac{d^4p}{(2\pi)^4}\,\vec{p}^{\,4}\Big(-\frac{1}{2}\frac{1}{p^2-m_\pi^2+i\epsilon} + \frac{1}{3}\frac{1}{p^2-m_\eta^2+i\epsilon} \\ + \frac{1}{6}\frac{1}{p^2-m_{\eta'}^2+i\epsilon}\Big)^2 \frac{1}{E_D(\vec{p})}\,\frac{1}{E_{D^*}(\vec{p})}\,\frac{1}{m_D-q^0-E_{D^*}(\vec{p})+i\epsilon} \\ \times \frac{1}{m_{D^*}+q^0-E_D(\vec{p})+i\epsilon}\,, \end{aligned} \tag{6.22}$$

where $\vec{\epsilon}$ and $\vec{\epsilon}\,'$ are the polarization vectors of the two external vector mesons, $E_{D^*}=\sqrt{\vec{p}^{\,2}+m_{D^*}^2}$ is the energy of the intermediate heavy vector meson and $E_D=\sqrt{\vec{p}^{\,2}+m_D^2}$ the energy of the intermediate D meson. We have taken only the positive part of the D and D^* propagators, $[(p^0-E_D)2E_D]^{-1}$ and $[(p^0-E_{D^*})2E_{D^*}]^{-1}$, which is a good approximation given the large masses of the particles. To derive Eq. (6.22) we have used, as in the previous section, the approximation of small external three-momenta and the fact that, by symmetry, $p_ip_j\to\frac{1}{3}\vec{p}^{\,2}\delta_{ij}$.

Once we perform analytically the integration in p^0 in Eq. (6.22), we obtain

$$t=\frac{1}{4}t_{\pi\pi}^{box}+\frac{1}{9}t_{\eta\eta}^{box}+\frac{1}{36}t_{\eta'\eta'}^{box}-\frac{1}{3}t_{\pi\eta}^{box}-\frac{1}{6}t_{\pi\eta'}^{box}+\frac{1}{9}t_{\eta\eta'}^{box}\,, \tag{6.23}$$

where

$$\begin{aligned} t_{ij}^{box} &= \tilde{g}_D^4\frac{1}{3}\,\vec{\epsilon}\cdot\vec{\epsilon}\,'\int\frac{d^3p}{(2\pi)^3}\,\vec{p}^{\,4}\,F(\vec{p})^2\,\frac{1}{E_{D^*}(\vec{p})}\,\frac{1}{E_D(\vec{p})}\,\frac{1}{E_{D^*}(\vec{p})+\omega_1-E_D(\vec{p})\pm i\epsilon} \\ &\times \frac{1}{E_{D^*}(\vec{p})+\omega_1-E_D(\vec{p})\pm i\epsilon}\,\frac{1}{E_{D^*}(\vec{p})+\omega_2-E_D(\vec{p})\pm i\epsilon}\Big(\frac{1}{2\omega_1\omega_2} \\ &\times \frac{1}{\omega_1+\omega_2}\,\frac{1}{E_D(\vec{p})-\omega_1-E_{D^*}(\vec{p})+i\epsilon}\,\frac{\text{Num}}{E_D(\vec{p})-\omega_2-E_{D^*}(\vec{p})+i\epsilon} \\ &+ \frac{1}{E_D(\vec{p})+\omega_1-E_{D^*}(\vec{p})-i\epsilon}\,\frac{1}{E_D(\vec{p})+\omega_2-E_{D^*}(\vec{p})-i\epsilon} \\ &\times \frac{1}{M_D-E_D(\vec{p})+M_{D^*}-E_{D^*}(\vec{p})+i\epsilon}\Big)\,, \end{aligned} \tag{6.24}$$

with $i,j=\pi,\eta,\eta'$. The numerator Num in Eq. (6.23) is given by

$$\begin{aligned} \text{Num} = -(\omega_1^2+\omega_2^2+\omega_1\omega_2)+(\omega_1+\omega_2)(M_D+E_D-M_{D^*}-E_{D^*}) \\ \times(M_D-E_{D^*})(M_{D^*}-E_D)\,, \end{aligned} \tag{6.25}$$

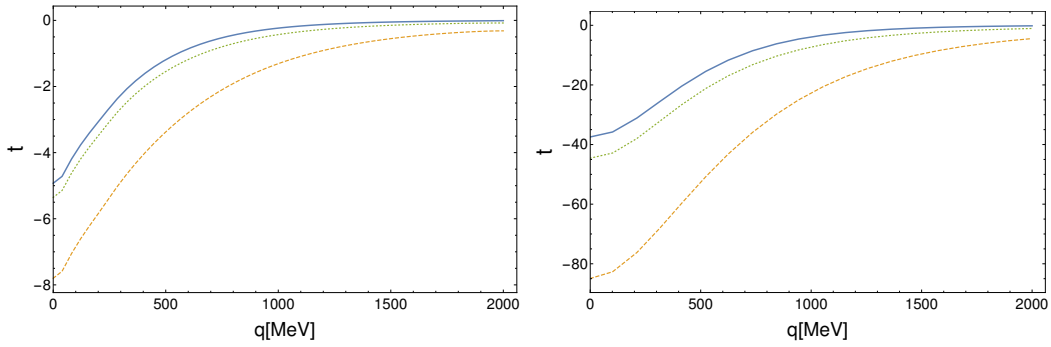

(a) (b)

Figure 6.12: $D\bar{D}^*$ (a) and $B\bar{B}^*$ (b) two pseudoscalar exchange potential. The thick line accounts for π plus η plus η' exchange, the dashed line only for pion exchange $(\frac{t^{box}_{\pi\pi}}{4})$ and the dotted line for π plus η exchange $(\frac{t^{box}_{\pi\pi}}{4} + \frac{t^{box}_{\eta\eta}}{9} - \frac{t^{box}_{\pi\eta}}{6})$.

where ω_1 and ω_2 are the energies of the two mesons exchanged. In the case of the $B\bar{B}^*$ interaction the calculation leads exactly to the same result with the substitutions $D \to B$, $D^* \to B^*$.

The calculation is done at threshold but the dependence on the momentum transfer $\vec{q}$ can be easily obtained using again the Breit reference frame, that corresponds to taking for the initial (1, 2) and final (3, 4) four-momenta the values of Eqs. (6.15). In **Figures 6.12(a)** and **6.12(b)** the amplitude of Eq. (6.23) is plotted as a function of the transferred momentum $\vec{q}$ for the $D\bar{D}^*$ and $B\bar{B}^*$ case respectively (thick line), and it is compared with the pion exchange $\frac{t^{box}_{\pi\pi}}{4}$ (dashed line) and with the exchange of π plus η, given by $\frac{t^{box}_{\pi\pi}}{4} + \frac{t^{box}_{\eta\eta}}{9} - \frac{t^{box}_{\pi\eta}}{6}$ (dotted line). Analogously to the case of one light pseudoscalar exchange of **Section 6.2.5**, we can notice a partial cancellation between π, η and η', which becomes exact in the limit of equal masses.

THE $D^*\bar{D}^*$ AND $B^*\bar{B}^*$ CASE

The amplitude for the processes depicted in **Figure 6.11** (b) and (d) can be derived in a very similar way, leading, in the case of $D^*\bar{D}^*$, to the expression

$$\begin{aligned} t = i\tilde{g}_D^4 \int \frac{d^4p}{(2\pi)^4}\, 2\vec{p}\cdot\vec{\epsilon}_1\, 2\vec{p}\cdot\vec{\epsilon}_2\, 2\vec{p}\cdot\vec{\epsilon}_3\, 2\vec{p}\cdot\vec{\epsilon}_4 \Big(-\frac{1}{2}\frac{1}{p^2 - m_\pi^2 + i\epsilon} \\ + \frac{1}{3}\frac{1}{p^2 - m_\eta^2 + i\epsilon} + \frac{1}{6}\frac{1}{p^2 - m_{\eta'}^2 + i\epsilon}\Big)^2 \frac{1}{(2E_D(\vec{p}))^2} \\ \times \frac{1}{m_{D^*} - p^0 - E_D(\vec{p}) + i\epsilon}\, \frac{1}{m_{D^*} - p^0 - E_D(\vec{p}) + i\epsilon}\,, \end{aligned} \tag{6.26}$$

where $E_D(\vec{p}) = \sqrt{\vec{p}^{\,2} + m_D^2}$ is the energy of the intermediate D meson.

By symmetry reasons we can substitute

$$p_i p_j p_k p_m \;\to\; \frac{1}{15}(\delta_{ij}\delta_{km} + \delta_{ik}\delta_{jm} + \delta_{im}\delta_{jk})\,\vec{p}^{\,4}\,, \tag{6.27}$$

which renders the spin combination into

$$\frac{1}{15}(\epsilon_{1i}\epsilon_{2i}\epsilon_{3m}\epsilon_{4m} + \epsilon_{1i}\epsilon_{2j}\epsilon_{3i}\epsilon_{4i} + \epsilon_{1i}\epsilon_{2j}\epsilon_{3j}\epsilon_{4i})\,. \tag{6.28}$$

Taking into account the spin projections of Eqs. (C.5), the combination of spin that we have in Eq. (6.28) is

$$\frac{1}{15}(5\mathcal{P}^{(0)} + 2\mathcal{P}^{(2)})\,. \tag{6.29}$$

Then, performing analytically the p^0 integration in Eq. (6.26), we obtain

$$t = \frac{1}{4}\tilde{t}^{box}_{\pi\pi} + \frac{1}{9}\tilde{t}^{box}_{\eta\eta} + \frac{1}{36}\tilde{t}^{box}_{\eta'\eta'} - \frac{1}{3}\tilde{t}^{box}_{\pi\eta} - \frac{1}{6}\tilde{t}^{box}_{\pi\eta'} + \frac{1}{9}\tilde{t}^{box}_{\eta\eta'}\,, \tag{6.30}$$

where

$$\begin{aligned}\tilde{t}^{box}_{ij} = \tilde{g}_D^4 S_J \int \frac{d^3p}{(2\pi)^3}\,\vec{p}^{\,4} F(\vec{p})^4 \frac{1}{m_{D^*} + \omega_1 - E_D(\vec{p}) \pm i\epsilon}\,\frac{1}{m_{D^*} + \omega_2 - E_D(\vec{p}) \pm i\epsilon} \\ \times \frac{1}{(E_D(\vec{p}))^2}\Big(\frac{1}{2\omega_1\omega_2}\,\frac{1}{\omega_1+\omega_2}\,\frac{\mathrm{Num}'}{m_{D^*} - \omega_1 - E_D(\vec{p}) + i\epsilon}\,\frac{1}{m_{D^*} - \omega_2 - E_D(\vec{p}) + i\epsilon} \\ + \frac{1}{E_D(\vec{p}) - m_{D^*} + \omega_1 + i\epsilon}\,\frac{1}{E_D(\vec{p}) - m_{D^*} + \omega_2 + i\epsilon}\,\frac{1}{2m_{D^*} - 2E_D(\vec{p}) + i\epsilon}\Big)\,.\end{aligned} \tag{6.31}$$

In this last equation, the subscript ij stands for the two light mesons exchanged, ω_1 and ω_2 are their energies,

$$S_J = \begin{cases} \frac{4}{3} & J = 0\,, \\ \\ \frac{8}{15} & J = 2\,, \end{cases} \tag{6.32}$$

and

$$\mathrm{Num}' = -(\omega_1^2 + \omega_2^2 + \omega_1\omega_2) + (m_{D^*} - E_D(\vec{p}))^2\,. \tag{6.33}$$

The discussion still holds in the case of $B^*\bar{B}^*$ with the substitutions $m_{D^*} \to m_{B^*}$, $m_D \to m_B$ and $\tilde{g}_D \to \tilde{g}_B$.

Introducing the dependence on the transferred momentum $\vec{q}$ like done in the previous section, we can plot the amplitude of Eq. (6.23) for both $D^*\bar{D}^*$ and $B^*\bar{B}^*$ interactions, **Figures Figure 6.13** (a) and (b) respectively, and for both angular momenta, $J = 0$ (thick line) and $J = 2$ (dashed line). For both interactions this process is negligible when compared to the heavy vector exchange of **Figures 6.10(a)** and **6.10(b)**.

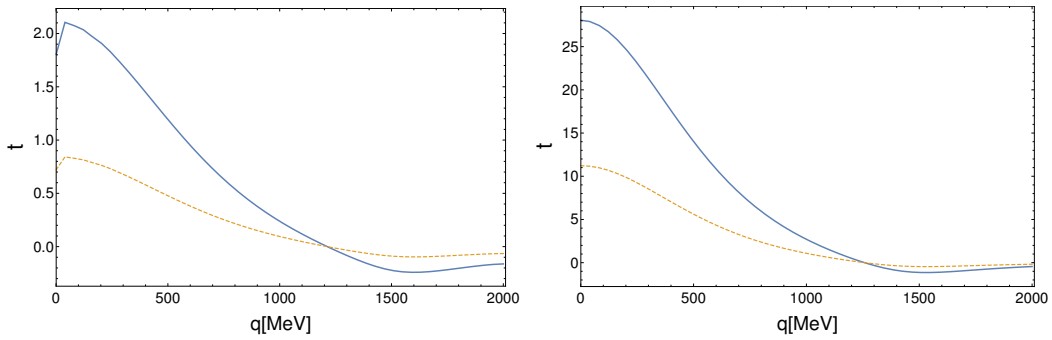

(a) (b)

Figure 6.13: $D^*\bar{D}^*$ (a) and $B^*\bar{B}^*$ (b) two pseudoscalar exchange potential. The thick line is for the $J = 0$ case while the dashed line for the $J = 2$.

6.2.7 The σ exchange

The nucleon-nucleon interaction calls for an intermediate range attraction which was traditionally taken into account by means of "σ" exchange. With ups and downs the σ resonance is now listed in the PDG [17] as the $f_0(500)$. This resonance appears unavoidably in a study of the $\pi\pi$ interaction with a unitary approach using as input the kernel from the chiral Lagrangians [30, 31, 150]. The analysis of $\pi\pi$ data with Roy equations allows one to establish the mass and width of this resonance with some precision [288, 289], compatible with the predictions of chiral unitary approach, of a mass around 460 MeV and half width of about 280 MeV. A recent thorough review on the σ properties and nature is given in Ref.[290]. From this point of view it was interesting to provide a microscopic picture for σ exchange, based on the nature of the σ resonance stemming from the interaction of two pions. This job was done in Ref. [287] considering the exchange of two correlated (interacting) pions for the NN interaction. In this section we extend these ideas to the interaction of $D\bar{D}^*$, $D^*\bar{D}^*$, $B\bar{B}^*$ and $B^*\bar{B}^*$.

$D\bar{D}^*$ AND $B\bar{B}^*$ CASES

The diagrams contributing are four for each interaction and they are shown in **Figure 6.14**. As it can be seen, each diagram has four VPP vertices involving a heavy vector meson, a pion and a heavy pseudoscalar meson. The grey circle in the crossing of the pion lines indicates that we have there the $\pi\pi$ scattering amplitude.We make the calculation for the $D\bar{D}^*$ case. The $B\bar{B}^*$ amplitude can be evaluated analogously. Using the Lagrangian of Eq. (2.92) we find vertices

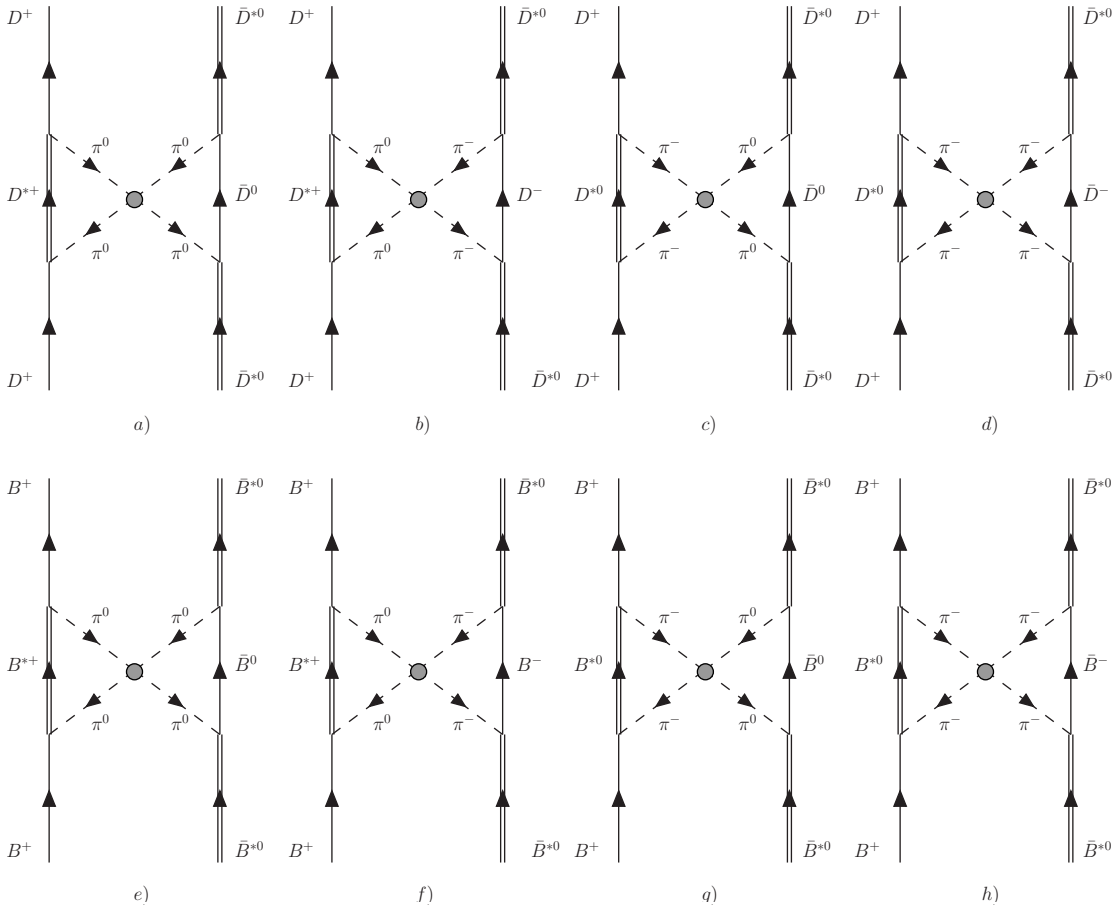

Figure 6.14: Lowest order $\pi\pi$ interaction in the $I = 1$ channel for $D\bar{D}^* \to D\bar{D}^*$ and $B\bar{B}^* \to B\bar{B}^*$.

of the form

$$-it_{VPP} = -ig\,C(p_D + p_\pi)_\mu \epsilon_V^\mu\,, \tag{6.34}$$

where p_D and p_π are the four-momenta of the D meson and of the pion respectively, and ϵ_V is the polarization vector of the D^* meson in the vertex.

The amplitude of the process can be written as

$$-it_\sigma = -i\;V_A\,V_B\,(\frac{1}{4}t_{\pi^0\pi^0\to\pi^0\pi^0} + \frac{1}{2}t_{\pi^0\pi^0\to\pi^+\pi^-} + \frac{1}{2}t_{\pi^+\pi^-\to\pi^0\pi^0} + t_{\pi^+\pi^-\to\pi^+\pi^-})\,, \tag{6.35}$$

where the factors V_A and V_B represent the contributions of the two triangular loops to the diagram, which we show in **Figure 6.15** and shall evaluate later. Note that, in order to write the amplitude, we must assume two initial pions and two final pions all pointing to the right in the diagrams of **Figure 6.14**, hence providing the amplitude of Eq. (6.35).

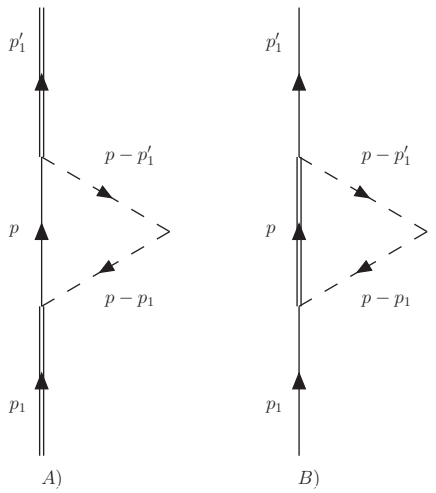

Figure 6.15: Two pion exchange triangle vertices, V_A in Fig. A) and V_B in Fig. B).

Considering the unitary normalization of the $\pi\pi$ states [30],

$$|\pi\pi, I = 0\rangle = -\frac{1}{\sqrt{6}}|\pi^0\pi^0 + \pi^+\pi^- + \pi^-\pi^+\rangle\,, \tag{6.36}$$

and writing explicitly the isoscalar amplitude

$$t^{I=0}_{\pi\pi\to\pi\pi} = \frac{1}{6}(t_{\pi^0\pi^0\to\pi^0\pi^0} + 2t_{\pi^0\pi^0\to\pi^+\pi^-} + 2t_{\pi^+\pi^-\to\pi^0\pi^0} + 4t_{\pi^+\pi^-\to\pi^+\pi^-})\,, \tag{6.37}$$

we can rewrite Eq. (6.35) as

$$-it_\sigma = -i\;V_A\,V_B\,\frac{3}{2}\;t^{I=0}_{\pi\pi\to\pi\pi}\,. \tag{6.38}$$

Since the pions in the diagrams in **Figure 6.14** are off shell, we need to use the off shell t-matrix obtained from the lowest order meson-meson Lagrangian [30]

$$t^{I=0}_{\pi\pi\to\pi\pi} = -\frac{1}{9f^2}\left(9s + \frac{15m_\pi^2}{2} - 3\sum_i p_i^2\right), \tag{6.39}$$

with s the Mandelstam variable and m_π and p_i the mass and momenta of the pions. As done in Ref. [287], we can obtain the on shell amplitude simply putting $p_i^2 = m_\pi^2$ and this allows us to rewrite Eq. (6.39) as

$$t^{I=0}_{\pi\pi\to\pi\pi} = t^{I=0,OS}_{\pi\pi\to\pi\pi} + \frac{1}{3f^2}\sum_i (p_i^2 - m_\pi^2), \tag{6.40}$$

where

$$t^{I=0,OS}_{\pi\pi\to\pi\pi} = -\frac{1}{f^2}(s - \frac{m_\pi^2}{2}). \tag{6.41}$$

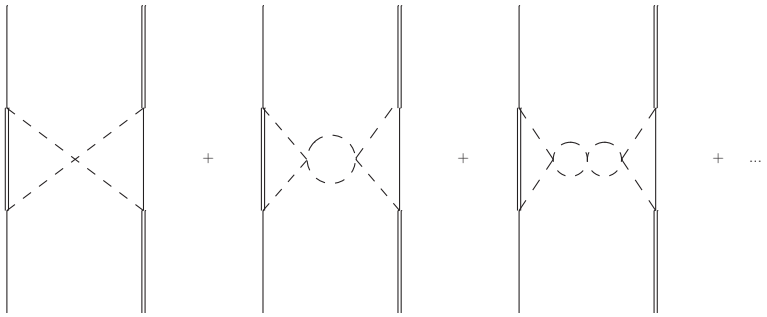

Figure 6.16: $D\bar{D}^*$ or $B\bar{B}^*$ interaction when the $\pi\pi$ scattering matrix is summed up to all orders in chiral unitary approach.

Following the approach of Ref. [287], it can be shown that the off shell part cancels exactly with other diagrams at the same order in the chiral counting. Thus, at lowest order, we can write

$$t_\sigma = V_A\, V_B\, \frac{3}{2}\, \frac{1}{f^2}(s - \frac{m_\pi^2}{2}). \tag{6.42}$$

In order to apply the unitary Bethe-Salpeter approach to the scalar mesons amplitude, we need to sum the set of diagrams in **Figure 6.16**. This is easily done substituting the on shell meson-meson amplitude of Eq. (6.41) by [30]

$$t^{I=0}_{\pi\pi\to\pi\pi} = -\frac{1}{f^2}\, \frac{s - \frac{m_\pi^2}{2}}{1 + \frac{1}{f^2}(s - \frac{m_\pi^2}{2})G(s)}, \tag{6.43}$$

where $G(s)$ is the two pions loop function, conveniently regularized [287].

In order to evaluate the two factors V_A and V_B we use again, for simplicity, the Breit reference frame which, with the specific momenta assignment of **Figure 6.15**, means

$$\begin{aligned} p_1 &\equiv (p_1^0, \vec{q}/2)\,, \\ p_1' &\equiv (p_1'^{\,0}, -\vec{q}/2)\,, \\ p &\equiv (p^0, \vec{p})\,. \end{aligned} \tag{6.44}$$

Since there is no energy exchange, $s = -\vec{q}^{\,2}$. It is also useful to define the variable $q \equiv (0, \vec{q})$. Thus, by means of Eq. (6.34) and keeping in mind that we already factorized outside V_A the coefficients C, we can write the expression of V_A as

$$\begin{aligned} V_A = i\tilde{g}_D^2 \int \frac{d^4p}{(2\pi)^4} \epsilon_\mu (2p - p_1)^\mu \epsilon'_\nu (2p - p_1')^\nu \frac{1}{p^2 - m_D^2 + i\epsilon} \\ \times \frac{1}{(p - p_1)^2 - m_\pi^2 + i\epsilon} \frac{1}{(p - p_1')^2 - m_\pi^2 + i\epsilon}\,, \end{aligned} \tag{6.45}$$

with m_D the mass of the D meson. Note that, as in **Section 6.2.6**, we are using the coupling $\tilde{g}_D$ that accounts for the factor m_{D^*}/m_{K^*} of HQSS.

The integral in Eq. (6.45) is logarithmically divergent. As in Ref. [287], the regularization is accomplished by means of a cutoff in the space of intermediate states ($p_{max} = 2$ GeV) and a form factor. In order to keep the integration in p^0 simple, we use the product of static form factors

$$F = F_1(\vec{p} + \frac{\vec{q}}{2})\, F_2(\vec{p} - \frac{\vec{q}}{2}) = \frac{\Lambda^2}{\Lambda^2 + (\vec{p} + \frac{\vec{q}}{2})^2} \frac{\Lambda^2}{\Lambda^2 + (\vec{p} - \frac{\vec{q}}{2})^2}\,, \tag{6.46}$$

with $\Lambda = 1$ GeV.

Since $\epsilon_\mu\, p_1^\mu = 0$ and $\epsilon'_\nu\, p_1'^\nu = 0$, Eq. (6.45) can be rewritten as

$$\begin{aligned} V_A = 4i\tilde{g}_D^2 \int \frac{d^4p}{(2\pi)^4} \epsilon_\mu\, p^\mu \epsilon'_\nu\, p^\nu \frac{1}{p^2 - m_D^2 + i\epsilon} \frac{1}{(p - p_1)^2 - m_\pi^2 + i\epsilon} \\ \times \frac{F}{(p - p_1')^2 - m_\pi^2 + i\epsilon}\,. \end{aligned} \tag{6.47}$$

The integral in Eq. (6.47) is symmetric with respect to p_1 and p_1' and this allows us to derive the structure of the result of the integration, which will be of the type

$$V_A = \epsilon_\mu \epsilon'_\nu (a g^{\mu\nu} + b(p_1^\mu p_1^\nu + p_1'^\mu p_1'^\nu) + c(p_1^\mu p_1'^\nu + p_1'^\mu p_1^\nu))\,. \tag{6.48}$$

In the last expression, due to the Lorentz condition, only the terms $ag^{\mu\nu}$ and $cp_1'^{\mu}p_1^{\nu}$ survive but we need the entire structure to evaluate them. This is done taking the trace of Eq. (6.47) and multiplying the equation by $(p_{1\mu}p_{1\nu}+p'_{1\mu}p'_{1\nu})$ and $(p_{1\mu}p'_{1\nu}+p'_{1\mu}p_{1\nu})$, in order to obtain a system of three equations. Solving the system, we find the expressions of the three coefficients in Eq. (6.48) but, as we already said, we are only interested in

$$\begin{aligned} a &= \frac{-Ym_{D^*}^2 + Z(p_1p_1') + X(m_{D^*}^4 - (p_1p_1')^2)}{2(m_{D^*}^4 - (p_1p_1')^2)}\,, \\ c &= \frac{-3Ym_{D^*}^2(p_1p_1') + X(m_{D^*}^4 - (p_1p_1')^2) + Z(m_{D^*}^4 + 2(p_1p_1')^2)}{2(m_{D^*}^4 - (p_1p_1')^2)^2}\,, \end{aligned} \tag{6.49}$$

where

$$\begin{aligned} X &= 4g_D^2 I_1 + 4\tilde{g_D}^2 m_D^2 I_2\,, \\ Y &= 8g_D^2 p_1^{0\,2} I_1 + 8\tilde{g_D}^2 I_3\,, \\ Z &= 8g_D^2 p_1^{0\,2} I_1 + 8\tilde{g_D}^2 I_4\,. \end{aligned} \tag{6.50}$$

The four integrals I_1, I_2, I_3 and I_4 in the equations above, have the following expressions:

$$\begin{aligned} I_1 &= \int \frac{d^4p}{(2\pi)^4} \frac{1}{(p-p_1)^2 - m_\pi^2 + i\epsilon} \frac{1}{(p-p_1')^2 - m_\pi^2 + i\epsilon} F\,, \\ I_2 &= \int \frac{d^4p}{(2\pi)^4} \frac{1}{p^2 - m_D^2 + i\epsilon} \frac{1}{(p-p_1)^2 - m_\pi^2 + i\epsilon} \frac{1}{(p-p_1')^2 - m_\pi^2 + i\epsilon} F\,, \\ I_3 &= \int \frac{d^4p}{(2\pi)^4} \frac{(\vec{p}^2 + m_D^2)p_1^{0\,2} + (\vec{p}\,\frac{\vec{q}}{2})^2}{p^2 - m_D^2 + i\epsilon} \frac{1}{(p-p_1)^2 - m_\pi^2 + i\epsilon} \frac{1}{(p-p_1')^2 - m_\pi^2 + i\epsilon} F\,, \\ I_4 &= \int \frac{d^4p}{(2\pi)^4} \frac{(\vec{p}^2 + m_D^2)p_1^{0\,2} - (\vec{p}\,\frac{\vec{q}}{2})^2}{p^2 - m_D^2 + i\epsilon} \frac{1}{(p-p_1)^2 - m_\pi^2 + i\epsilon} \frac{1}{(p-p_1')^2 - m_\pi^2 + i\epsilon} F\,. \end{aligned} \tag{6.51}$$

After performing the integration in dp^0, which can be done analytically using Cauchy's theorem, we obtain

$$\begin{aligned} I_1 &= \int \frac{d^3p}{(2\pi)^3} \frac{\omega_1+\omega_2}{2\omega_1\omega_2} \frac{1}{-\vec{q}^2 - (\omega_1+\omega_2)^2} F\,, \\ I_2 &= \int \frac{d^3p}{(2\pi)^3} \frac{1}{2E_D} \frac{1}{2\omega_1} \frac{1}{\omega_2} \frac{1}{\omega_1+\omega_2} \frac{\omega_1+\omega_2+E_D-m_{D^*}}{E_D+\omega_1-m_{D^*}-i\epsilon} \frac{1}{E_D+\omega_2-m_{D^*}-i\epsilon} F\,, \\ I_3 &= \int \frac{d^3p}{(2\pi)^3} \frac{1}{2E_D} \frac{1}{2\omega_1} \frac{1}{\omega_2} \frac{1}{\omega_1+\omega_2} \frac{\omega_1+\omega_2+E_D-m_{D^*}}{E_D+\omega_1-m_{D^*}-i\epsilon} \frac{(\vec{p}^2 + m_D^2)p_1^{0\,2} + (\vec{p}\,\frac{\vec{q}}{2})^2}{E_D+\omega_2-m_{D^*}-i\epsilon} F\,, \\ I_4 &= \int \frac{d^3p}{(2\pi)^3} \frac{1}{2E_D} \frac{1}{2\omega_1} \frac{1}{\omega_2} \frac{1}{\omega_1+\omega_2} \frac{\omega_1+\omega_2+E_D-m_{D^*}}{E_D+\omega_1-m_{D^*}-i\epsilon} \frac{(\vec{p}^2 + m_D^2)p_1^{0\,2} - (\vec{p}\,\frac{\vec{q}}{2})^2}{E_D+\omega_2-m_{D^*}-i\epsilon} F\,, \end{aligned} \tag{6.52}$$

where $\omega_1 = \sqrt{(\vec{p}+\vec{q}/2)^2 + m_\pi^2}$, $\omega_2 = \sqrt{(\vec{p}-\vec{q}/2)^2 + m_\pi^2}$ and $E_D = \sqrt{\vec{p}^{\,2} + m_D^2}$ are the energies of the two pions and of the D meson involved in the loop, respectively, and m_{D^*} is the mass of the $\bar{D}^*$ meson. Since the mass of the D meson is so large, we have taken the positive energy component of the propagator $[(p^0 - E_D)2E_D]^{-1}$, which simplifies the integration.

In the case of V_B, after some simple algebra, we obtain

$$\begin{aligned} V_B = {} & \tilde{g}_D^2 I_1 + \tilde{g}_D^2 \left[2(m_D^2 - m_\pi^2) - 4p_1 p_1' - \frac{(m_D^2 - m_\pi^2)^2}{m_{D^*}^2} + m_{D^*}^2 \right] I_5 \\ & - 2\tilde{g}_D^2 \left[1 + \frac{m_D^2 - m_\pi^2}{m_{D^*}^2} \right] I_6 + \tilde{g}_D^2 \frac{1}{m_{D^*}^2} I_7 \,, \end{aligned} \tag{6.53}$$

where

$$\begin{aligned} I_5 &= \int \frac{d^3p}{(2\pi)^3} \frac{1}{2E_V} \frac{1}{2\omega_1} \frac{1}{\omega_2} \frac{1}{\omega_1 + \omega_2} \frac{\omega_1 + \omega_2 + E_V - m_D}{E_V + \omega_1 - m_D} \frac{F}{E_V + \omega_2 - m_D} \,, \\ I_6 &= \int \frac{d^3p}{(2\pi)^3} \frac{1}{2E_V} \frac{F}{\omega_1} \frac{\omega_1 + E_V}{p_1^{0\,2} - (\omega_1 + E_V)^2} \,, \\ I_7 &= \int \frac{d^3p}{(2\pi)^3} \frac{F}{2E_V} \,, \end{aligned} \tag{6.54}$$

and $E_V = \sqrt{\vec{p}^{\,2} + m_{D^*}^2}$. Once again the non relativistic propagator for the intermediate D^* has been taken to get the former equations.

We can now go back to the $D\bar{D}^*$ potential in momentum space, whose final expression, according to Eqs. (6.35) and (6.43), is given by

$$t_\sigma(\vec{q}) = V_A \, V_B \, \frac{3}{2} \frac{1}{f^2} \frac{\vec{q}^{\,2} + \frac{m_\pi^2}{2}}{1 - G(-\vec{q}^{\,2}) \frac{1}{f^2} (\vec{q}^{\,2} + \frac{m_\pi^2}{2})} \,, \tag{6.55}$$

with

$$V_A = \epsilon_\mu \epsilon_\nu' (a g^{\mu\nu} + c p_1'^{\mu} p_1^{\nu}) \,, \tag{6.56}$$

a and c derived using Eqs. (6.49), (6.50) and (6.52), and V_B given by Eq. (6.53). Again, with the substitutions $\tilde{g}_D \to \tilde{g}_B$, $m_D \to m_B$ and $m_{D^*} \to m_{B^*}$ we get the amplitude for the $B\bar{B}^*$ case.

The potential t_σ is shown in **Figures 6.17(a)** and **6.17(b)** as a function of the momentum transfer $\vec{q}$ for both the $D\bar{D}^*$ and $B\bar{B}^*$ cases, respectively. In the case of the $B\bar{B}^*$ interaction the contribution is remarkable, while in the case of $D\bar{D}^*$ the vector meson exchange is still the more relevant process.

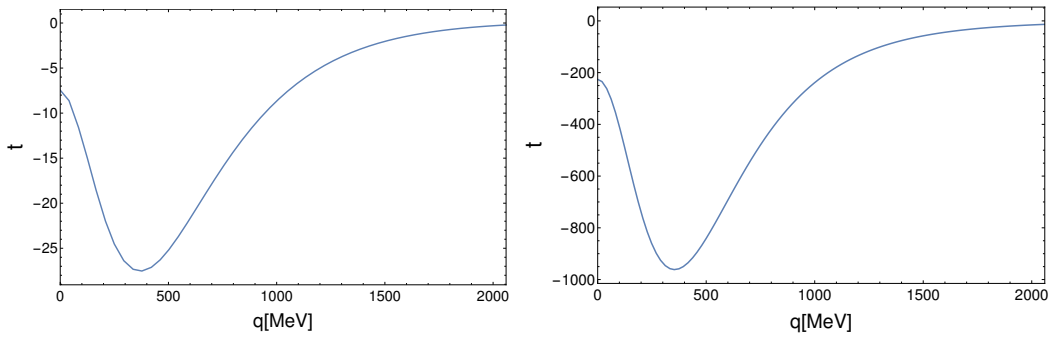

(a) (b)

Figure 6.17: Potential t_σ for $D\bar{D}^*$ (a) and $B\bar{B}^*$ (b) as a function of the momentum transfer $\vec{q}$.

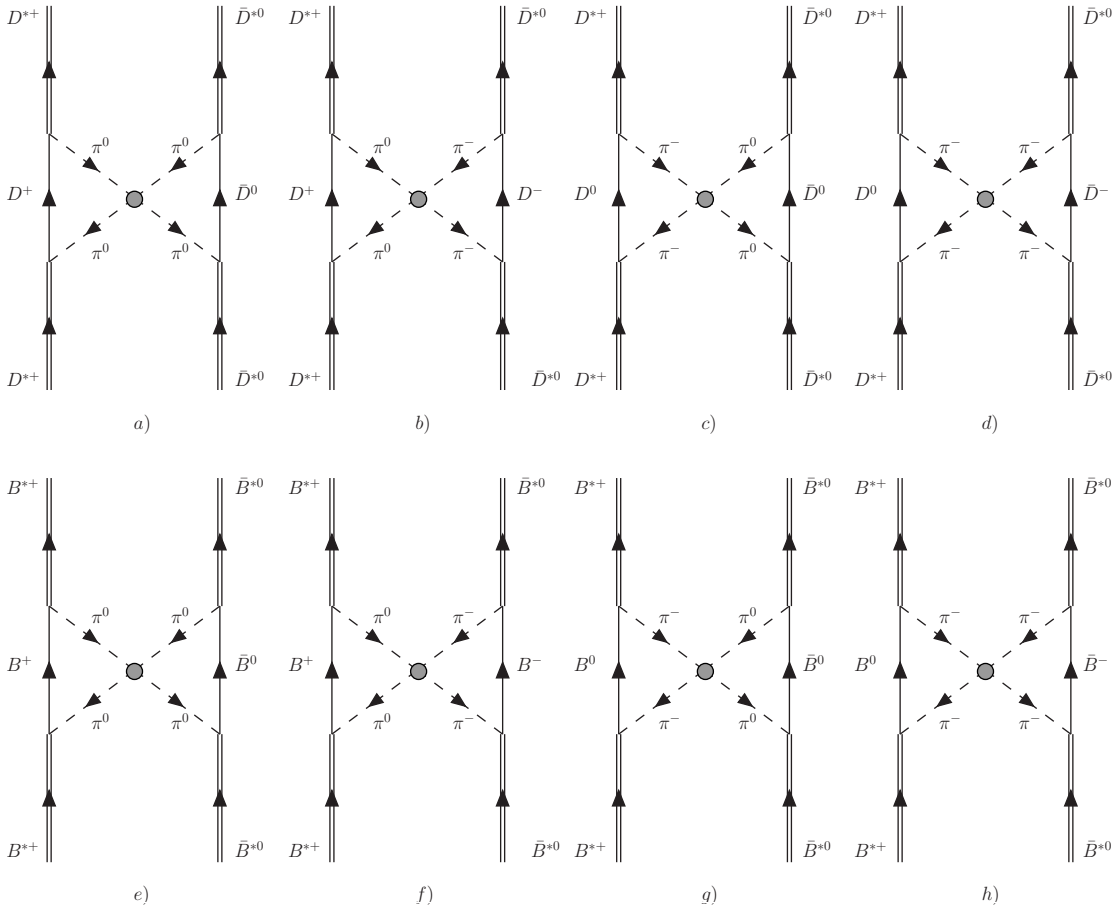

Figure 6.18: Lowest order $\pi\pi$ interaction in the $I = 1$ channel for $D^*\bar{D}^* \to D^*\bar{D}^*$ and $B^*\bar{B}^* \to B^*\bar{B}^*$.

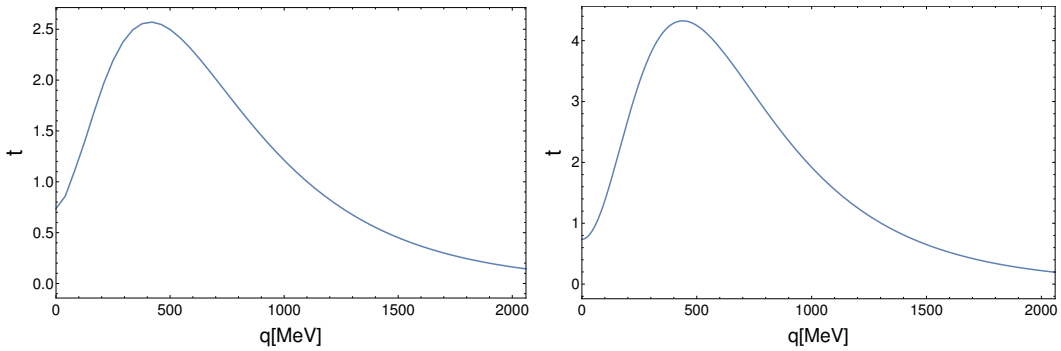

(a) (b)

Figure 6.19: Potential t_σ for $D^*\bar{D}^*$ (a) and $B^*\bar{B}^*$ (b) as a function of the momentum transfer $\vec{q}$.

$D^*\bar{D}^*$ AND $B^*\bar{B}^*$ CASES

The diagrams representing the process under study are shown in **Figure 6.18**. In this case, we only need the triangular vertex V_A in **Figure 6.15** (a) to evaluate the amplitude. We proceed in complete analogy to the previous section finding the expression

$$t_\sigma(\vec{q}) = V_A^2 \frac{3}{2} \frac{1}{f^2} \frac{\vec{q}^{\,2} + \frac{m_\pi^2}{2}}{1 - G(-\vec{q}^{\,2}) \frac{1}{f^2}(\vec{q}^{\,2} + \frac{m_\pi^2}{2})}\,, \tag{6.57}$$

with V_A given by Eq. (6.56).

Since we assume small initial momenta $\vec{p}_1$ and $\vec{p}_1{}'$ of the vectors compared to the vector mass, we can take $\epsilon^0 \equiv 0$ and only the $a\epsilon\epsilon'$ combination remains. The other vertex will provide a similar structure. Hence, we have the combination

$$\epsilon_i^{(1)}\epsilon_j^{(2)}\epsilon_i^{(3)}\epsilon_j^{(4)}\,, \tag{6.58}$$

with $1 + 2 \to 3 + 4$ that, resorting to the expressions of the spin projector operators of Eqs. (C.5), becomes

$$\epsilon_i^{(1)}\epsilon_j^{(2)}\epsilon_i^{(3)}\epsilon_j^{(4)} \equiv \mathcal{P}^{(0)} + \mathcal{P}^{(1)} + \mathcal{P}^{(2)}\,. \tag{6.59}$$

The strength of $t_\sigma(\vec{q})$, removing $g^{\mu\nu}\epsilon_\mu\epsilon_\nu$, gives already the strength of the two pion exchange potential in $J = 0, 1, 2$ since, according to Eq. (6.59) the three spins have the same weight. The potential t_σ as a function of the transferred momentum $\vec{q}$ is plotted in **Figures 6.19(a)** and **6.19(b)** for $D^*\bar{D}^*$ and $B^*\bar{B}^*$, respectively. In both cases the relevance of this process is rather small.

6.2.8 Uncorrelated crossed two pion exchange

Now we study the case of the exchange of two non interacting pions. For both the $PV \to PV$ and $VV \to VV$ interaction, only the crossed diagrams a), d) (for $D\bar{D}^*$ and $D^*\bar{D}^*$) and e) and h) (for $B\bar{B}^*$ and $B^*\bar{B}^*$) in **Figure 6.14** and **Figure 6.18**, respectively, contribute to the process. In both cases, for the evaluation of the amplitude we will use the momenta assignment shown in **Figure 6.20**. Note that we take only the crossed diagrams. The iterated one π exchange (together with η and η'), which we saw was OZI suppressed, was already evaluated in **Section 6.2.6** and we do not consider it here.

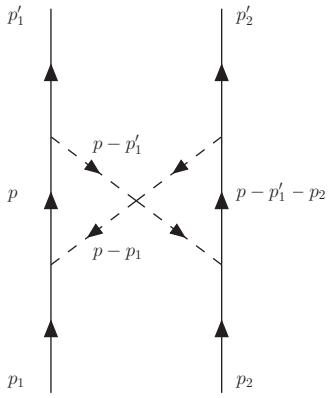

Figure 6.20: Momenta assignment for two pion exchange.

$D\bar{D}^*$ AND $B\bar{B}^*$ CASES

Using the vertices provided by the hidden gauge lagrangians, it is very easy to evaluate the amplitude that, for the charm sector, reads

$$\begin{aligned} t_{\pi\pi} = & \frac{5}{4} i \tilde{g}_D^4 \int \frac{d^4p}{(2\pi)^4} \epsilon_\mu (2p_1 - p)^\mu \epsilon_\nu (2p_1' - p)^\nu \epsilon'_\alpha (2p - 2p_1' + p_2)^\alpha \epsilon''_\beta \\ & \times (2p - p_1' - p_1 + p_2)^\beta \frac{F^2}{p^2 - m_{D^*}^2 + i\epsilon} \frac{1}{(p - p_1' + p_2)^2 - m_D^2 + i\epsilon} \\ & \times \frac{1}{(p - p_1)^2 - m_\pi^2 + i\epsilon} \frac{1}{(p - p_1')^2 - m_\pi^2 + i\epsilon} , \end{aligned} \tag{6.60}$$

where ϵ is the polarization four-vector corresponding to the vector meson in the triangular loop, while ϵ' and ϵ'' correspond to the vector mesons in the external legs of the diagram. Since only two of the diagrams depicted in **Figure 6.14** are contributing, the isospin factor given by the different vertices involved will be $\frac{5}{4}$. Also the $\pi\pi$ amplitude (see Eq. (6.40)) is missing since now the pions do not interact.

We assume again small three-momenta for the external vectors, hence $\epsilon^0 \equiv 0$, and also that $4\vec{p}^{\,2} \gg \vec{q}^{\,2}/4$. Thus, applying the completeness condition for the polarization vectors, that under our assumption becomes $\sum_{pol} \epsilon'_\mu \epsilon'_\alpha \simeq \sum_{pol} \epsilon'_i \epsilon'_j = \delta_{ij}$, with $i, j = 1, 2, 3$, we can rewrite Eq. (6.60) as

$$\begin{aligned} t_{\pi\pi} = & \frac{5}{4} i \tilde{g}_D^4 \frac{1}{2} \vec{\epsilon}\,' \, \vec{\epsilon}\,'' \int \frac{d^4p}{(2\pi)^4} (\vec{p}^{\,2} - \vec{q}^{\,2}) \left[(4\vec{p}^{\,2} - \frac{\vec{q}^{\,2}}{4}) - \frac{1}{\vec{q}^{\,2}} \left[(2\vec{p}\,\vec{q})^2 - \frac{\vec{q}^{\,4}}{4} \right] \right] \\ & \times F^2 \frac{1}{p^2 - m_{D^*}^2 + i\epsilon} \frac{1}{(p - p'_1 + p_2)^2 - m_D^2 + i\epsilon} \frac{1}{(p - p_1)^2 - m_\pi^2 + i\epsilon} \\ & \times \frac{1}{(p - p'_1)^2 - m_\pi^2 + i\epsilon} \,. \end{aligned} \tag{6.61}$$

Performing the analytical integration in dp^0, we obtain

$$\begin{aligned} t_{\pi\pi} = & -\frac{5}{4} \tilde{g}_D^4 \frac{1}{2} \vec{\epsilon}\,' \, \vec{\epsilon}\,'' \int \frac{d^3p}{(2\pi)^3} (\vec{p}^{\,2} - \vec{q}^{\,2}) \left[(4\vec{p}^{\,2} - \frac{\vec{q}^{\,2}}{4}) - \frac{1}{\vec{q}^{\,2}} \left[(2\vec{p}\,\vec{q})^2 - \frac{\vec{q}^{\,4}}{4} \right] \right] \\ & \times \frac{F^2}{\omega_1 + \omega_2} \frac{1}{2\omega_1\omega_2} \frac{1}{2E_D} \frac{1}{2E_V} [\omega_1^2 + \omega_2^2 + \omega_1\omega_2 - (\omega_1 + \omega_2)(2p_1^0 - E_V - E_D) \\ & + (p_1^0 - E_V)(p_1^0 - E_D)] \frac{1}{p_1^0 - \omega_1 - E_V + i\epsilon} \frac{1}{p_1^0 - \omega_1 - E_D + i\epsilon} \frac{1}{p_1^0 - \omega_2 - E_V + i\epsilon} \\ & \times \frac{1}{p_1^0 - \omega_2 - E_D + i\epsilon} \,. \end{aligned} \tag{6.62}$$

As before, the potential of Eq. (6.62) also holds in the case of $B\bar{B}^*$ with substitutions. We plot it as a function of the transferred momentum $\vec{q}$ for both cases in **Figures 6.21(a)** and **6.21(b)**. These contributions are rather small with respect to the heavy vector exchange of **Figures 6.8(a)** and **6.8(b)**.

$D^*\bar{D}^*$ AND $B^*\bar{B}^*$ CASES

Proceeding as in the previous case, with suitable substitution of the momenta involved and of the propagators, since now we have two intermediate pseudoscalars D or B, we can write the amplitude as

$$\begin{aligned} t_{\pi\pi} = & \frac{5}{4} i \tilde{g}_D^4 \int \frac{d^4p}{(2\pi)^4} \epsilon_\mu (2p - p_1)^\mu \epsilon_\nu (2p - p'_1)^\nu \epsilon_\alpha (2p - 2p'_1 + p_2)^\alpha \epsilon_\beta \\ & \times (2p - p'_1 - p_1 + p_2)^\beta \, F^2 \frac{1}{p^2 - m_D^2 + i\epsilon} \frac{1}{(p - p'_1 + p_2)^2 - m_D^2 + i\epsilon} \\ & \times \frac{1}{(p - p_1)^2 - m_\pi^2 + i\epsilon} \frac{1}{(p - p'_1)^2 - m_\pi^2 + i\epsilon} \,. \end{aligned} \tag{6.63}$$

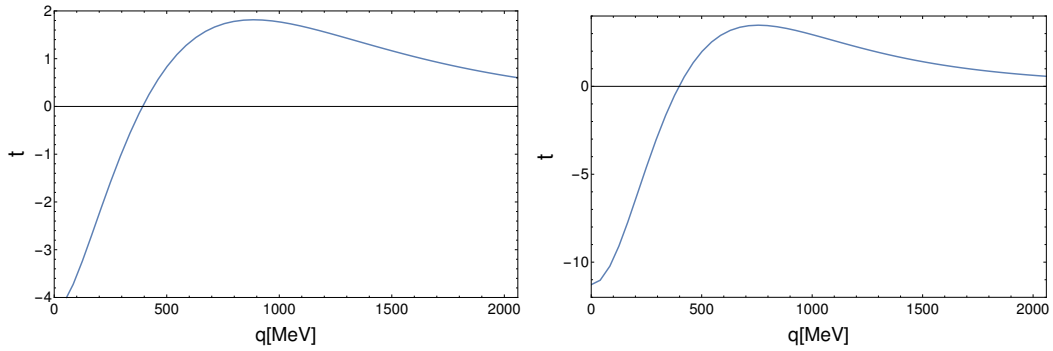

(a) (b)

Figure 6.21: Potential $t_{\pi\pi}$ for $D\bar{D}^*$ (left panel) and $B\bar{B}^*$ (right panel) as a function of the momentum transfer $\vec{q}$.

We use again the non-relativistic approximation rewriting Eq. (6.63) as

$$\begin{aligned} t_{\pi\pi} = \frac{5}{4} i\tilde{g}_D^4 \int \frac{d^4p}{(2\pi)^4} \, \epsilon_i(2p-p_1)_i\epsilon_j(2p-p_1')_j\epsilon_l(2p-2p_1'+p_2)_l\epsilon_m \\ \times (2p-p_1'-p_1+p_2)_m \, F^2 \frac{1}{p^2-m_D^2+i\epsilon} \, \frac{1}{(p-p_1'+p_2)^2-m_D^2+i\epsilon} \\ \times \frac{1}{(p-p_1)^2+m_\pi^2+i\epsilon} \, \frac{1}{(p-p_1')^2+m_\pi^2+i\epsilon} \, . \end{aligned} \tag{6.64}$$

Once we assume that $4\vec{p}^{\,2} \gg \vec{q}^{\,2}/4$, the dominant term in Eq. (6.64) is the one with the form $p_i p_j p_l p_m$. This means that the amplitude in Eq. (6.63) will have the same structure as in the case of **Section 6.2.6**:

$$\frac{1}{15} \left(\delta_{ij}\delta_{lm} + \delta_{il}\delta_{jm} + \delta_{im}\delta_{jl}\right) . \tag{6.65}$$

Thus, we can write

$$\begin{aligned} t_{\pi\pi} = \frac{5}{4} i\tilde{g}_D^4 \frac{1}{15} \int \frac{d^4p}{(2\pi)^4} (4\vec{p}^{\,2} - \frac{\vec{q}^{\,2}}{4})^2 \left(\epsilon_i\epsilon_l\epsilon_i\epsilon_l + \epsilon_i\epsilon_i\epsilon_l\epsilon_l + \epsilon_i\epsilon_l\epsilon_l\epsilon_i\right) F^2 \frac{1}{p^2-m_D^2+i\epsilon} \\ \times \frac{1}{(p-p_1'+p_2)^2-m_D^2+i\epsilon} \, \frac{1}{(p-p_1)^2+m_\pi^2+i\epsilon} \, \frac{1}{(p-p_1')^2+m_\pi^2+i\epsilon} \, , \end{aligned} \tag{6.66}$$

that, performing the analytical integration in dp^0, becomes

$$t_{\pi\pi} = \frac{5}{4}\tilde{g}_D^4 \frac{1}{15}\int \frac{d^3p}{(2\pi)^3}(4\vec{p}^{\,2} - \frac{\vec{q}^{\,2}}{4})^2 \left(\epsilon_i\epsilon_l\epsilon_i\epsilon_l + \epsilon_i\epsilon_i\epsilon_l\epsilon_l + \epsilon_i\epsilon_l\epsilon_l\epsilon_i\right) F^2 \frac{1}{\omega_1+\omega_2} \times \frac{1}{2\omega_1\omega_2}\frac{1}{E_D^2}\left(1 + \frac{E_D+\omega_1+\omega_2-p_1^0}{p_1^0-\omega_1-E_D+i\epsilon} + \frac{E_D+\omega_1+\omega_2-p_1^0}{p_1^0-\omega_2-E_D+i\epsilon}\right) \times \frac{1}{p_1^0-\omega_1-E_D+i\epsilon}\frac{1}{p_1^0-\omega_2-E_D+i\epsilon}\,. \tag{6.67}$$

The combination of polarization vectors appearing in Eq. (6.67) can be rewritten in terms of the spin projector operators of Eqs. (C.5) [214] as

$$\epsilon_i\epsilon_l\epsilon_i\epsilon_l + \epsilon_i\epsilon_i\epsilon_l\epsilon_l + \epsilon_i\epsilon_l\epsilon_l\epsilon_i = 5\mathcal{P}^{(0)} + 2\mathcal{P}^{(2)}\,. \tag{6.68}$$

Thus, the final expression of the amplitude reads

$$t_{\pi\pi} = \frac{5}{4}\tilde{g}_D^4 \frac{A}{15}\int \frac{d^3p}{(2\pi)^3}(4\vec{p}^{\,2} - \frac{\vec{q}^{\,2}}{4})^2 F^2 \frac{1}{\omega_1+\omega_2}\frac{1}{2\omega_1\omega_2}\frac{1}{4E_D^2}\frac{1}{p_1^0-\omega_1-E_D+i\epsilon} \times \frac{1}{p_1^0-\omega_2-E_D+i\epsilon}\left(1 + \frac{E_D+\omega_1+\omega_2-p_1^0}{p_1^0-\omega_1-E_D+i\epsilon} + \frac{E_D+\omega_1+\omega_2-p_1^0}{p_1^0-\omega_2-E_D+i\epsilon}\right), \tag{6.69}$$

where $A = 5$ for the $J = 0$ case and $A = 2$ for the $J = 2$ case.

In the case of $B^*\bar{B}^*$ the potential has exactly the same form and can be obtained with the substitution $D \to B$. The expression in Eq. (6.69) is plotted as a function of the transferred momentum $\vec{q}$ for both interactions in **Figures 6.22(a)** and **6.22(a)** and for both values of the spin, $J = 0$ (thick line) and $J = 1$ (dashed line). Also in this case the strength of the process is smaller than the one of the vector meson exchange of **Figures 6.10(a)** and **6.10(b)**.

6.3 Determination of the $D\bar{D}^*$ invariant mass distribution for the process $e^+e^- \to \pi^\pm(D\bar{D}^*)^\mp$

In Ref. [291] the $e^+e^- \to \pi^\pm(D\bar{D}^*)^\mp$ reaction is studied for a center of mass energy $\sqrt{s} = 4.26$ GeV and the $D\bar{D}^*$ invariant mass associated with this reaction is obtained, showing a signal around 3885 MeV with a width close to 30 MeV and which is interpreted as a $J^P = 1^+$ resonant state. Following Ref. [228], we can calculate the $D\bar{D}^*$ invariant mass spectrum for the reaction

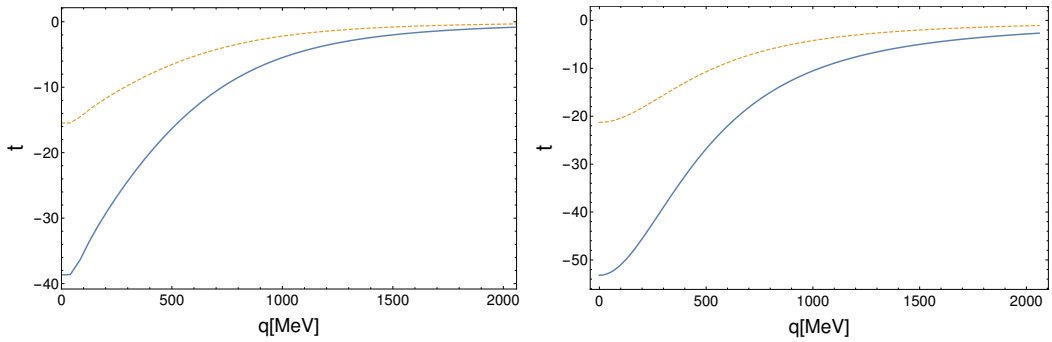

(a) (b)

Figure 6.22: Potential $t_{\pi\pi}$ for $D^*\bar{D}^*$ (a) and $B^*\bar{B}^*$ (b) as a function of the momentum transfer $\vec{q}$ for $J = 0$ (thick line) and $J = 2$ (dashed line).

studied in Ref. [291] as

$$\frac{d\sigma}{dM_{D^*\bar{D}^*}} \propto \frac{p\tilde{q}}{s\sqrt{s}} |T|^2 F_L \,, \tag{6.70}$$

where $\sqrt{s}$ is fixed to the value 4.26 GeV, p is the pion three-momentum in the e^+e^- center of mass frame, and $\tilde{q}$ is the center of mass momentum in the $D\bar{D}^*$ system:

$$p = \frac{\lambda^{1/2}(s, m_\pi^2, M_{D\bar{D}^*}^2)}{2\sqrt{s}} \,, \tag{6.71}$$

$$\tilde{q} = \frac{\lambda^{1/2}(M_{D\bar{D}^*}^2, m_D^2, m_{\bar{D}^*}^2)}{2M_{D\bar{D}^*}} \,. \tag{6.72}$$

The factor $F_L = p^{2L}$ in Eq. (6.70) is needed to account for the relative partial wave between the pion and the $D\bar{D}^*$ system produced in the reaction. In this case, we are going to consider the formation of a $J^P = 1^+$ state near threshold, thus the $D\bar{D}^*$ system is preferably produced in s-wave ($L = 0$). If a state with mass M_R and width Γ_R is formed in the $D\bar{D}^*$ system, the amplitude T of Eq. (6.70) can be parametrized as

$$T = \frac{A}{M_{D\bar{D}^*}^2 - M_R^2 + iM_R\Gamma_R} \,, \quad A \equiv \text{constant} \,. \tag{6.73}$$

In general, the $D\bar{D}^*$ invariant mass distribution can have contributions from a non resonant background. Following Ref. [291] we consider a background of the form

$$B = \alpha(M_{D\bar{D}^*} - M_{D\bar{D}^*}^{\min})^\beta (M_{D\bar{D}^*}^{\max} - M_{D\bar{D}^*})^\eta \,, \tag{6.74}$$

where $M^{\rm min}_{D\bar{D}^*}$ and $M^{\rm max}_{D\bar{D}^*}$ represent the minimum and maximum values of the $D\bar{D}^*$ invariant mass and α, β and η are unknown constants.

In this way, the $D\bar{D}^*$ invariant mass spectrum can be obtained as

$$\frac{d\sigma}{dM_{D\bar{D}^*}} = \frac{1}{s\sqrt{s}} p\tilde{q} \left(|T|^2 F_L + B \right) . \tag{6.75}$$

As can be seen from Eqs. (6.73) and (6.74), we have six unknown parameters to determine the $D\bar{D}^*$ spectrum (same number as in Ref. [291]): the magnitude of the resonant amplitude A, the mass and width of the state (M_R and Γ_R, respectively), the magnitude of the background amplitude, α, and the exponents β and η. To constrain these parameters we perform a fit to the data minimizing the χ^2 and consider a value of the χ^2 per degrees of freedom (d.o.f) around 1 as the criteria to establish the goodness of the fit. This is the same criteria as the one adopted by the authors in Ref. [291], in which a value of χ^2/d.o.f of 1 is found for the $D^0\bar{D}^{*-}$ mass spectrum and of 1.1 for the $D^+\bar{D}^{*0}$ case.

6.4 Results

Once all the contributions to the interactions are computed as functions of the momentum transfer $\vec{q}$, they can be compared looking at the plots. It is also possible to make a rough estimate of the strength of the different potentials evaluating the integral $\int V(q) d^3q$.

The study of the four interactions we are considering in this Chapter has been done in three different works. There, two different simple strategies have been used to deal with all the processes. The first one, that we used in Refs. [292, 293] for the case of $D\bar{D}^*$ and $D^*\bar{D}^*$, consists in simply neglecting the contributions coming from the exchange of light pseudoscalars, their strengths being much smaller than the one of the heavy vector exchange, that is dominant in both cases. However, the neglected processes are kept in mind when evaluating uncertainties.

On the other hand, in Ref. [294], where the cases of the BB^* and $B^*\bar{B}^*$ are studied, we adopted another method, due to the fact that the vector exchange is not the dominant process in the bottom sector. After the strengths of the potentials for the exchange of light mesons are evaluated, we use them to obtain an effective potential V_{eff}. We will get the strengths $\int d^3q\, V_i\,(q)$ for all the potentials exchanging light mesons and sum them. Then we convert the sum into an effective potential of the type of the vector exchange,

$$V_{eff}\, \theta(q_{max} - |\vec{q}\,|)\theta(q_{max} - |\vec{q}\,'|) . \tag{6.76}$$

In Eq. (6.76), q_{max} is the maximum momentum used in the loop functions, such that $\int_{q<q_{max}} d^3q\, V_{eff}$ is equal to the sum of $\int d^3q\, V_i\,(q)$. While solving the Bethe-Salpeter equation with an $\vec{r}$ dependent potential is feasible, as done for instance in Ref. [261] for the Schrödinger equation, the former separable form of the potential renders the Bethe-Salpeter equation an algebraic equation. The stability of the results with relative large changes in the value of V_{eff} makes the more elaborate procedure of solving it in the $\vec{r}$ space unnecessary. Then, we take as potential this effective potential plus the one coming from vector exchange. Both are of the type of Eq. (6.17) and can then be used in the Bethe-Salpeter equation, with the same G function regularized with the cutoff q_{max}.

In the following sections we study the shape of $|T|^2$ for the four $D\bar{D}^*$ and $D^*\bar{D}^*$, $B\bar{B}^*$ and $B^*\bar{B}^*$ interactions. As we will discuss in detail, the four amplitudes show a clear peak and the large uncertainties on the potentials that we will consider do not affect drastically their positions.

6.4.1 Results for $D\bar{D}^*$

It can be seen, by looking at the plots of **Figures 6.7(a)**, **6.8(a)**, **6.12(a)**, **6.17(a)** and **6.21(a)**, that the dominant contribution comes, as mentioned above, from the heavy vector exchange.

In particular, summing the contributions given by one meson exchange and two pion exchange, with and without interaction, we obtain a strength $\int V(q)d^3q \simeq -112$ GeV^3. In the case of vector exchange, the strength is $\int V(q)d^3q \simeq -433$ GeV^3. We can then safely neglect the light pseudoscalar exchange contributions, but we will keep them in mind when evaluating uncertainties. This means that, for the moment, we study the T-matrix coming from vector exchange for values of $\sqrt{s}$ around 3900 MeV, in particular the shape of $|T_{11}|^2$.

Although no bound state showed up in the $1^-(1^{++})$ case in the region under study, we found interesting results in the case with positive G-parity. In **Figure 6.23**, $|T_{11}|^2$ (where the subscript 11 means that we are considering the $D\bar{D}^* \to D\bar{D}^*$ transition) for the case $1^+(1^{+-})$ is shown as a function of the centre of mass energy. We used the dimensional regularization expression of Eq. (2.63) for the G function, using for the subtraction constants of the three different coupled channels $\alpha_{D\bar{D}^*} = -1.28$, $\alpha_{\eta_c\rho} = -1.57$ and $\alpha_{\pi J/\psi} = -1.86$ and choosing $\mu = 1500$ MeV, as suggested in Ref. [56]. This choice of the parameters is equivalent to using a cutoff $q_{max} = 770$ MeV. A clear peak, corresponding to $\sqrt{s} = 3872$ MeV and with a width of approximately $\Gamma \simeq 40$ MeV, is visible in **Figure 6.23**.

In **Figure 6.24** we show the dependence of the position of the peak on

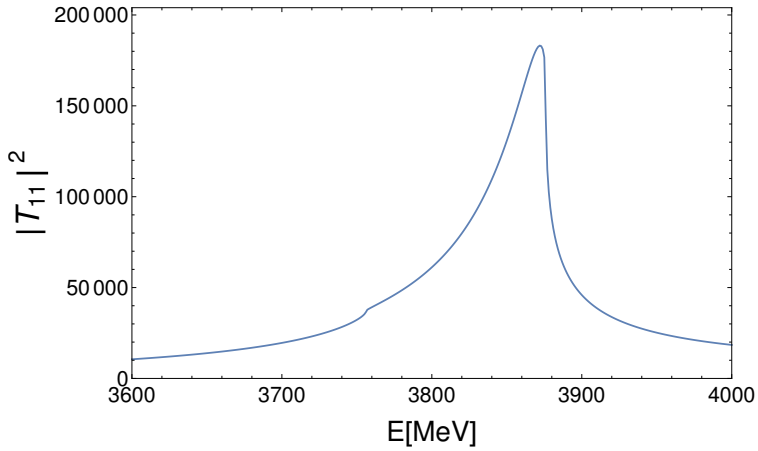

Figure 6.23: $|T_{11}|^2$ as a function of $\sqrt{s}$ for the $D\bar{D}^*$ interaction.

q_{max} [MeV]	$\sqrt{s}$ [MeV]
700	3875
750	3873
770	3872
800	3869
850	3867

Table 6.1: Position of the peak of $|T|^2$ corresponding to different values of q_{max} for the $D\bar{D}^*$ interaction.

the cutoff. The quantity $|T_{11}|^2$ is plotted as a function of $\sqrt{s}$ for values of the subtraction constants α_i corresponding to a cutoff equal to 700, 750, 770, 800 and 850 MeV. The corresponding values of the peak are shown in **Table 6.1**: going to higher values of the cutoff, the binding energy of the state increases. The width varies within $40 - 50$ MeV. These changes can serve to quantify our uncertainties from the neglected pseudoscalar exchanges or other possible sources. We have also changed the parameter Λ in the form factor of Eq. (6.46) in the range $700 - 1200$ MeV. We have checked that multiplying our potential by a factor within the range of $0.6 - 1.4$ gives us similar results as with these changes of the cutoff Λ. The calculations are done using average values of the masses of the D and $\bar{D}^*$. If we use the actual masses in the experiments quoted, the changes in the binding energy are of the order of 1 MeV.

It is interesting to note that the energies obtained all stick around threshold (3876 MeV). Next we discuss if there are poles associated to the peaks observed in **Figure 6.24**.

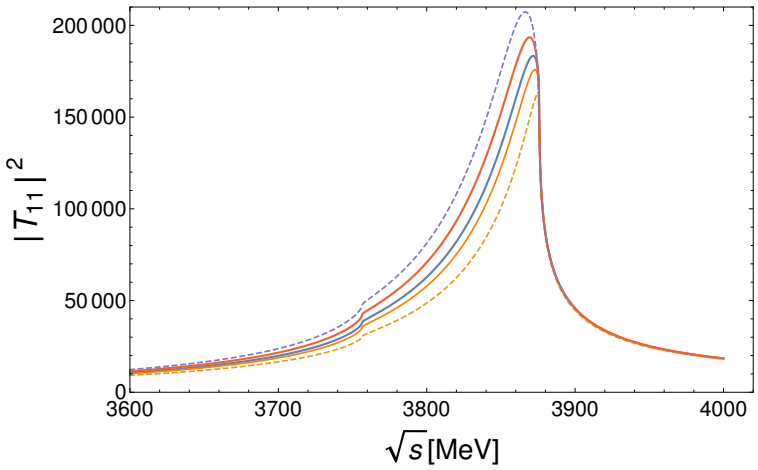

Figure 6.24: $|T_{11}|^2$ for $D\bar{D}^* \to D\bar{D}^*$ as a function of $\sqrt{s}$ for values of the cutoff q_{max} equal to 850, 800, 770, 750 and 700 MeV. The peak moves to the left as the cutoff increases.

We move to the complex plane, extrapolating the amplitude to complex values of the energy. To do this, for the channels which are open, we need the expression of the loop function in the second Riemann sheet (Eq. (2.78)). In **Figure 6.25** $|T_{11}|^2$ is plotted in the second Riemann sheet for the value of $q_{max} = 770$ MeV. A pole, corresponding to a state with $(\sqrt{s} + i\Gamma/2) = (3878 + i23)$ MeV is perfectly visible.

If we lower the cutoff, one still gets poles in the complex plane for a while, but for values of $q_{max} < 700$ MeV, the poles in $\sqrt{s}$ fade away although one still has a pronounced cusp effect of the amplitude, with experimental consequences in cross sections. This situation is usually referred as having a virtual pole.

Note that in all cases our states produce peaks around the $D\bar{D}^*$ threshold of 3876 MeV.

THE $D\bar{D}^*$ INVARIANT MASS DISTRIBUTION

As we have seen in the previous section, the dynamics involved in the $D\bar{D}^*$ system gives rise to the generation of a state with $I = 1$, quantum numbers $J^P = 1^+$, mass $3867 - 3875$ MeV and width around 40 MeV. The question which arises now is if a state below the $D\bar{D}^*$ threshold can be responsible for the signal reported in the $D\bar{D}^*$ spectrum when studying the reaction $e^+e^- \to \pi^\pm(D\bar{D}^*)^\mp$ [291].

Using Eq. (6.75) and the procedure explained in **Section 6.3**, we show in **Figure 6.26** the results found for the D^0D^{*-} (left panel) and $D^+\bar{D}^{*0}$ spectra (right panel) respectively, determined considering the formation of a state as the one obtained in our study of the $D\bar{D}^*$ system. As it can be seen, the data

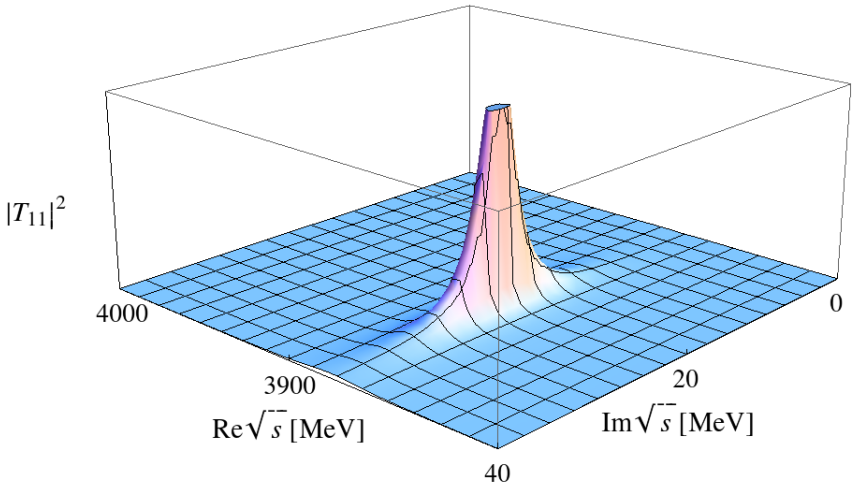

Figure 6.25: $|T_{11}|^2$ in the second Riemann sheet for the transition $D\bar{D}^* \to D\bar{D}^*$ for the $I^G(J^{PC}) = 1^+(1^{+-})$ sector.

can be perfectly explained with a state with a mass close to 3870 MeV and with a width around 30 MeV.

We have studied the range of masses that the fit can accommodate. We can have higher masses than 3870 MeV with still good values of the χ^2, but they gradually increase as the mass increases. We put the limit at 3884 MeV where the χ^2 values are no longer good. This gives a range $3862 - 3884$ MeV, by means of which we can give an acceptable fit to the data. The theory band of $3867 - 3875$ MeV given in the previous section is within the band allowed by the fit to the data.

6.4.2 Results for $D^*\bar{D}^*$

We proceed as in **Section 6.4.1** to compare the different contributions to the $D^*\bar{D}^* \to D^*\bar{D}^*$ interaction. We find that $\int V(q)d^3q \simeq -70$ GeV^3 for the sum of the potentials involving the exchange of pseudoscalars, while for the heavy vector exchange we get $\int V(q)d^3q \simeq -690$ GeV^3, implying that once again it is the dominant process in the interaction. However, we will change the value of the vector exchange potential by about 10% in order to take into account the contributions from the other terms in the evaluation of the uncertainties.

We want to study the T matrix for the two channels for values of $\sqrt{s}$ around 4000 MeV. **Figure 6.27** shows $|T_{11}|^2$, where the subscript 11 stands for the transition from the channel $D^*\bar{D}^*$ to itself, as a function of the centre of mass

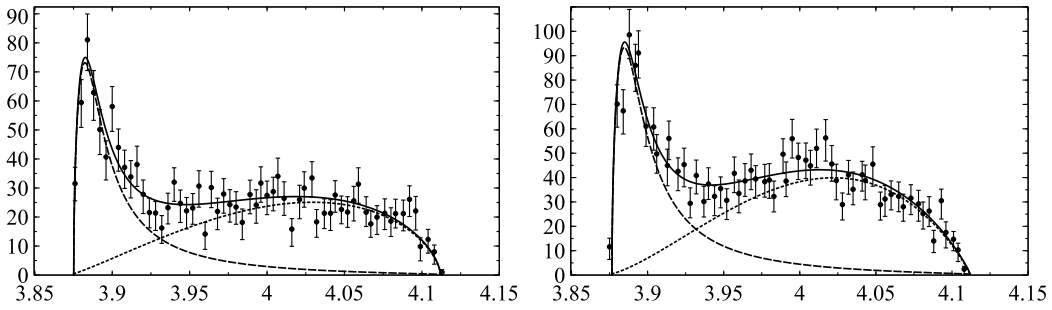

Figure 6.26: Invariant mass distribution for the D^0D^{*-} (left panel) and $D^+\bar{D}^{*0}$ (right panel) systems. The abscissa axis represents the corresponding $D\bar{D}^*$ invariant mass in units of GeV and the ordinate axis the spectrum in arbitrary units. The dashed line represents the bound state contribution: $M_R = 3874.15$ MeV, width $\Gamma_R = 27$ MeV (left panel) and $M_R = 3875.62$ MeV, width $\Gamma_R = 30$ MeV (right panel). The dotted line corresponds to the background and the solid line is the final result from the fit: $\chi^2/\text{d.o.f} = 1.3$ (left panel) and $\chi^2/\text{d.o.f} = 1.1$ (right panel).

energy. We use the dimensional regularization for the G function, as before, choosing as the subtraction constants $\alpha_{D^*\bar{D}^*} = -2.3$ and $\alpha_{J/\psi\rho} = -2.6$, while $\mu = 1000$ MeV. This is equivalent to using a cutoff $q_{max} = 960$ MeV. With this choice of the parameters we obtain a clear peak around $\sqrt{s} = 3998$ MeV, with a width $\Gamma \simeq 90$ MeV. This is about 19 MeV below the $D^*\bar{D}^*$ threshold. The binding is smaller than found in Ref. [214] because we use g for the coupling instead of g_D, which we justified from the findings of Ref. [282].

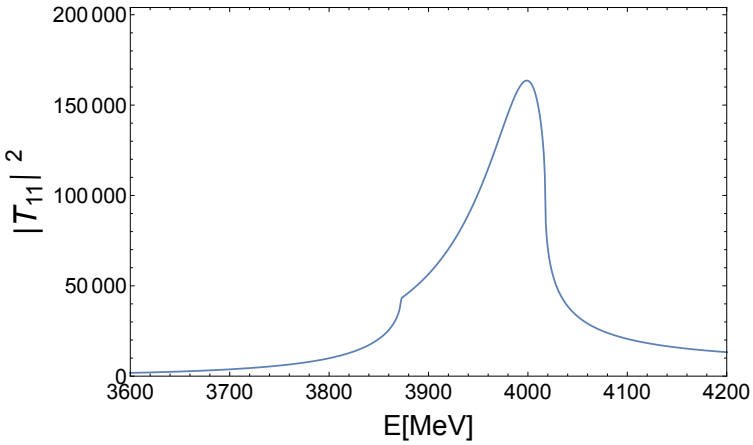

Figure 6.27: $|T_{11}|^2$ as a function of $\sqrt{s}$ for the $D^*\bar{D}^*$ interaction.

This result is very interesting. Indeed, as mentioned in the Introduction, the BESIII collaboration observed a peak in the $(D^*\bar{D}^{*0})^\pm$ invariant mass spectrum close to the $(D^*\bar{D}^{*0})^\pm$ threshold [213], which they interpreted as a

signal of a $J = 0$ resonance at 4025 MeV. However in Ref. [228] it was found that the spectrum could be equally reproduced assuming a $J = 2$ resonance below threshold, with a mass around 3990 MeV and a width of 160 MeV. A fit with about 8 MeV less binding and smaller width is also acceptable by looking at the different options discussed in Ref. [228]. Our choice of the parameters is motivated to get a binding similar to that suggested in this last work, but we discuss below our uncertainties. The finding of the present paper would give support to the interpretation of the results given by BESIII in Ref. [213] as a consequence of an $I = 1$ resonance coming from the $D^*\bar{D}^*$ interaction, with the option suggested in Ref. [228] of a bound $D^*\bar{D}^*$ state with relatively large width.

We have also evaluated the uncertainties in the results due to the possible contribution of the exchange of pseudoscalars. As we already mentioned in the beginning of this section, this contribution is small and attractive at small $\vec{q}$. In order to take it into account, we increase the magnitude of the vector exchange potential for $D^*\bar{D}^* \to D^*\bar{D}^*$ of Eq. (6.7) and see how the position of the peak changes. We find that, with an increase in the magnitude of the potential of 50%, the energy of the peak decreases by about 5 MeV. Then we did the same thing, but adjusting the cutoff used in the loop function G in order to maintain fixed at 3998 MeV the position of the peak. The results obtained are shown in **Figure 6.28**. Increasing the magnitude of $t_{D^*\bar{D}^*\to D^*\bar{D}^*}$, the peak in $|T_{11}|^2$ is maintained in the same position using a lower cutoff. In the case of an increase of 20% (the dotted line in **Figure 6.28**), we need a cutoff of $q_{max} \simeq 940$ MeV, while in the case of 50% (the dashed line in **Figure 6.28**), $q_{max} \simeq 930$ MeV. The shape of $|T_{11}|^2$ is slightly changed when going to higher magnitudes, giving a narrower peak and a higher strength.

We have taken natural values for α_i, or the cutoff, guided by the results of the analysis of Ref. [228]. Yet, it is interesting to see what happens if we reduce the cutoff. In **Figure 6.29** we show $|T_{11}|^2$ for different values of the cutoff. We can see that as q_{max} decreases, the peak of $|T_{11}|^2$ is moving closer to the threshold and its strength decreases. At $q_{max} = 700$ MeV we already have a clear cusp and, for lower values of q_{max}, the cusp remains but the strength of $|T_{11}|^2$ at the peak becomes very weak and we are no longer able to produce an enhancement of the $D^*\bar{D}^*$ invariant mass distribution as seen in the experiment of Ref. [213]. It is also interesting to see that even for values of $q_{max} \simeq 800$ MeV, as in [295–297], we still find a state bound by a few MeV. On the other hand, bigger values of q_{max} would produce a too large binding that would contradict the results of the analysis of Ref. [228]. Hence, considering uncertainties in our model, we can say that we are obtaining a bound $D^*\bar{D}^*$ state or barely bound or even a virtual state (decaying to $J/\psi\rho$) within $3990 - 4000$ MeV, with a width of about 100 MeV. Note that, even

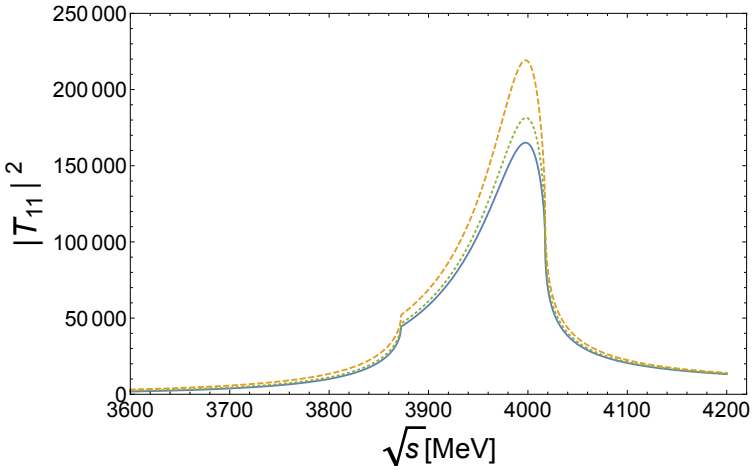

Figure 6.28: $|T_{11}|^2$ for the $D^*\bar{D}^* \to D^*\bar{D}^*$ transition as a function of $\sqrt{s}$ for the vector exchange potentials of Eq. (6.7) and (6.8) (thick line), for an increase of 20% in the vector exchange potential (dotted line) and for an increase of 50% (dashed line), for a peak at 3998 MeV.

when the pole in the bound region gets close to threshold and disappears, it can get converted into a virtual state with a clearly visible cusp that can be translated into a peak close to threshold in an experimental analysis.

As already mentioned in **Section 6.2.2**, in Ref. [214] also the $\rho\rho$, $\rho\omega$, $\rho\phi$ light vector channels were considered and the $\rho\omega$ and $\rho\phi$ also give some contribution to the width. A slight increase in the value of $\Gamma \simeq 100$ MeV, would be in agreement with the analysis of Ref. [228] where $\Gamma = 160$ MeV.

6.4.3 Results for $B\bar{B}^*$

In this case, we are interested in studying the transition matrix T for the channels $B\bar{B}^*$, $\eta_b\,\rho$ and $\pi\,\Upsilon$ and we evaluate it for values of $\sqrt{s}$ around 10600 MeV. In order to do this, we use again the dimensional regularization formula for the loop function G. We take a cutoff $q_{max} = 700$ MeV, for which we find $\alpha_{B\bar{B}^*} = -2.79$, $\alpha_{\eta_b\,\rho} = -3.56$ and $\alpha_{\pi\,\Upsilon} = -3.78$ for the subtraction constants.

In the previous cases we studied the changes in the position of the peak of $|T_{11}|^2$ due to the variation of q_{max}. However, the value of the strength of the different potentials depends on the value of the upper limit of the integral $\int d^3q\,V(q)$. For this reason, in the case of the $B\bar{B}^*$, we decided to calculate the effective potential V_{eff} using values of this limit for the light meson exchange potentials varying from 700 to 1100 MeV. Changing the upper limit in $\int d^3q\,V_i\,(q)$ introduces large uncertainties in the approach concerning the final potential. In this case, the strength of the final potential, summing V_{eff} and

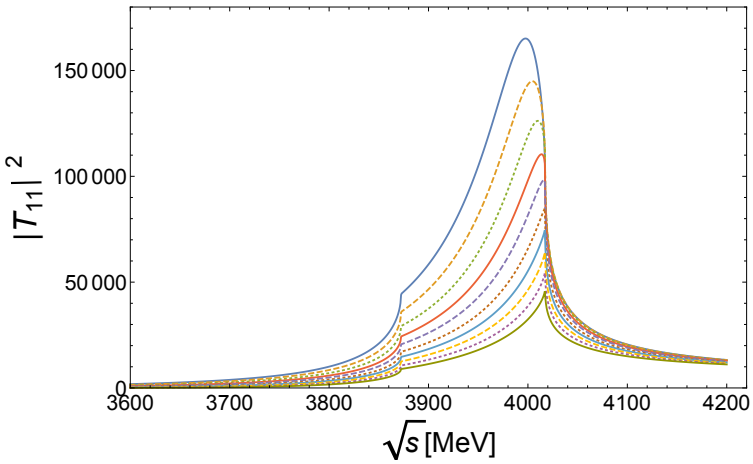

Figure 6.29: $|T_{11}|^2$ for the $D^*\bar{D}^* \to D^*\bar{D}^*$ transition as a function of $\sqrt{s}$, for different values of the cutoff q_{max}. From up down, q_{max} = 960, 900, 850, 800, 750, 700, 650, 600, 550, 500 MeV.

the vector exchange, is a factor between 30 and 64 the vector exchange alone. This means that the changes due to the variations of q_{max} are much smaller than the ones due to the variations of the upper limit of the integral $\int d^3q\, V(q)$ used to estimate V_{eff}.

In **Figure 6.30** the shape of $|T_{11}|^2$, the component of the T matrix that describes the transition $B\bar{B}^* \to B\bar{B}^*$, for different values of the integration limit, is depicted. As can be seen, even choosing values of the limit between 700 and 1100 MeV, the effect on the binding and the width is small. As a result, we find that the position of the peak moves slightly to higher energies for decreasing values of the upper limit and it is seen in the range of $10587 - 10601$ MeV. These values are very close to what was found by the Belle collaboration, $M_{Z_b(10610)} = (10608.4 \pm 2.0)$ MeV.

We have also studied the stability of the results with respect to variations of the m_H, $m_{H'}$ parameters (and related ψ and γ) in Eq. (6.9). We change m_H in the range $(4000 - 6000)$ MeV and $m_{H'}$ in the range $(8000 - 10000)$ MeV. The value of the binding energy from one extreme $(4000, 8000)$ to the other $(6000, 10000)$ changes in 1.2 MeV, which is a smaller change than those seen before.

It is worth noting that both the $\eta_b\,\rho$ and $\pi\,\Upsilon$ channels are open for decays, and this gives a width between 1.6 and 3 MeV, with bigger widths corresponding to lower values of the integration limit. The experimental value reported by Belle collaboration is $\Gamma_{Z_b(10610)} = (15.6 \pm 2.5)$ MeV. This difference might seem large to make claims of reproduction of this state. However, one should note that we do not include channels of VP type with two light mesons. These

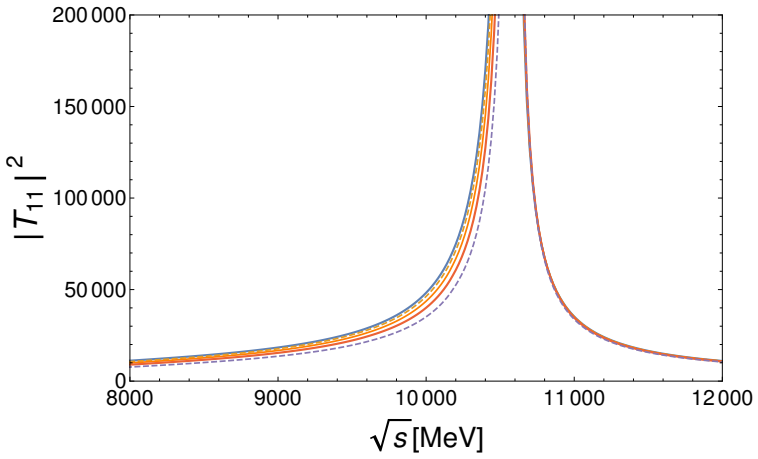

Figure 6.30: $|T_{11}|^2$ as a function of the $\sqrt{s}$ center of mass energy for the case of $B\bar{B}^*$. Each curve is associated with a value of the integration limit: 700 MeV, 800 MeV, 900 MeV, 1000 MeV, 1100 MeV. The peak moves from right to left as the integration limit increases.

light channels could be reached in our approach including them as coupled channels, but the large difference in the masses, together with the weak transition to these states, which requires the exchange of heavy vectors, makes them inoperative concerning the mass of the state found. However, even with very small couplings of the resonance to these channels, the large phase space available for the decay can produce a contribution to the width larger than the one estimated by us with the $\eta_b\rho$ and $\pi\Upsilon$ channels. Examples of this can be seen in the study of hidden charm baryons in Ref. [295] and hidden beauty baryons in Ref. [297].

6.4.4 Results for $B^*\bar{B}^*$

For this case we have two channels $B^*\bar{B}^*$ and $\rho\,\Upsilon$ and we use $\mu = 1500$ MeV and the subtraction constants $\alpha_{B^*\bar{B}^*} = -2.79$ and $\alpha_{\rho\Upsilon} = -3.56$, corresponding to a cutoff value equal to $q_{max} = 700$ MeV.

Figure 6.31 shows the shape of $|T_{11}|^2$, which means the component of the T matrix that describes the transition from $B^*\bar{B}^*$ to itself, for different values of the integration limit plotted as a function of the center of mass energy, $\sqrt{s}$, of the system. This peak corresponds to spin $J = 0$. In **Figure 6.32**, we show the shape of $|T_{11}|^2$ for the $J = 2$ case, again for different values of the integration limit. It is important to emphasize that, according to the second one of Eqs. (6.10), there is no contribution in the transition matrix T from $B^*\bar{B}^*$ to $\rho\,\Upsilon$ channel for spin $J = 1$. In this case, $B^*\bar{B}^*$ stands as a single

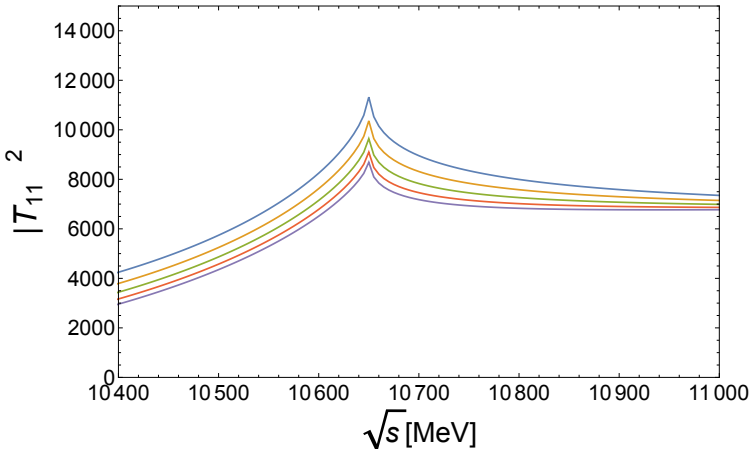

Figure 6.31: $|T_{11}|^2$ as a function of the $\sqrt{s}$ center of mass energy for the case of $B^*\bar{B}^*$ for $J = 0$. Each curve is associated with a value of the integration limit: 700 MeV, 800 MeV, 900 MeV, 1000 MeV, 1100 MeV. The peak moves from bottom to top as the integration limit increases.

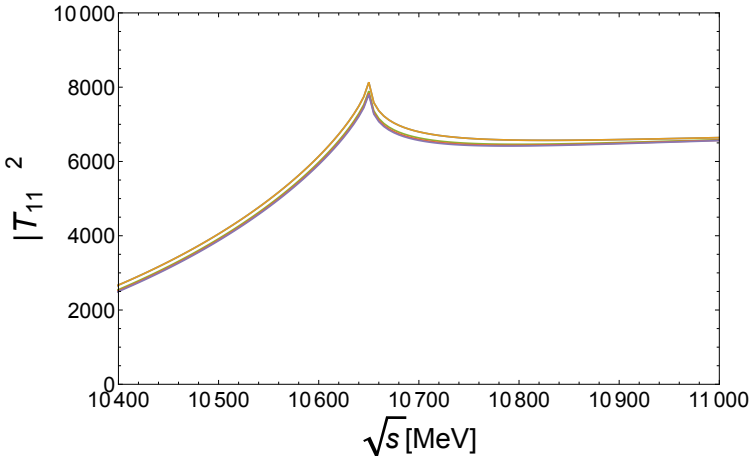

Figure 6.32: $|T_{11}|^2$ as a function of the $\sqrt{s}$ center of mass energy for the case of $B^*\bar{B}^*$ for $J = 2$. Each curve is associated with a value of the integration limit: 700 MeV, 800 MeV, 900 MeV, 1000 MeV, 1100 MeV. The peak moves slightly from bottom to top as the integration limit increases.

channel.

From these figures we can see that the variations of the integration limit cause no effect to the peak position, as we already noted in the $B\bar{B}^*$ case. It is interesting to stress that, even with the large uncertainties in the potential admitted, we always find a structure for the peak of $|T_{11}|^2$ which corresponds clearly to a cusp. Whether to call this a resonant state or not it is a question of criterion. However, we should remember that the $a_0(980)$ appears in the experiments (or in the theories) [32, 298] as a cusp and is universally accepted as a resonance. Our findings, a cusp for the $|T_{11}|^2$ amplitude in this case, would come to support the claims of the former works [255, 256].

For the sake of completeness, we repeat the calculation considering the spin $J = 1$ case. Here we have a single channel problem,

$$T_{11} = \frac{\tilde{t}_{B^*\bar{B}^*\to B^*\bar{B}^*}}{1 - \tilde{t}_{B^*\bar{B}^*\to B^*\bar{B}^*}\, G_{B^*\bar{B}^*}}\,, \tag{6.77}$$

where $G_{B^*\bar{B}^*}$ is the loop function for the $B^*\bar{B}^*$ channel, while $t_{B^*\bar{B}^*\to B^*\bar{B}^*}$ is the $B^*\bar{B}^* \to B^*\bar{B}^*$ vector exchange potential already defined in the first of Eqs. (6.10), plus the contribution from V_{eff} due to the exchange of two interacting pion exchange. We saw in **Section 6.2.8** that, in this case, the noninteracting pion exchange vanishes, and the interacting two pion exchange was also small, smaller than the vector exchange in all range (see **Figures 6.19(b)** and **6.10(b)**). This is why, in this case, in order to play with uncertainties we follow the strategy used in the case of the $D\bar{D}^*$ and $D^*\bar{D}^*$ interaction and we change the range of the vector exchange potential, by changing the cutoff q_{max} to values from 700 to 1100 MeV.

In **Figure 6.33** we show the plot for $|T_{11}|^2$ as a function of the center of mass energy of the system. Note that in this case, we also have a peak corresponding o about 10650 MeV, which is just the threshold mass of the $B^*\bar{B}^*$ channel. Again, we see essentially a cusp in the amplitude which does not correspond to a bound state. The situation is similar if we increase the value of $t_{B^*\bar{B}^*\to B^*\bar{B}^*}$ of a factor 1.5 to account for possible uncertainties. The value of $|T_{11}|^2$ grows accordingly, but the cusp remains and its shape is like in **Figure 6.33**.

6.5 Summary and conclusions

In this Chapter we studied the $D\bar{D}^*$, $D^*\bar{D}^*$, $B\bar{B}^*$ and $B^*\bar{B}^*$ interactions in $I = 1$ using the extension of the local hidden gauge approach to the heavy sector.

We started with a combined study of a Z_c state of $I = 1$ around 3900 MeV, which has been claimed in several experiments. On the one hand, we used the

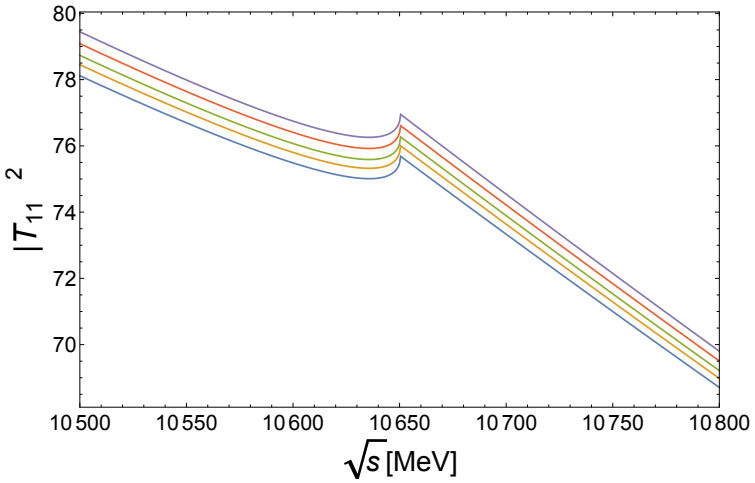

Figure 6.33: $|T_{11}|^2$ as a function of the $\sqrt{s}$ center of mass energy when only the $B^*\bar{B}^*$ channel is considered ($J = 1$ case). Each curve is related to the cutoff values q_{max} equal to 700, 800, 900, 1000 and 1100 MeV. The peak moves from bottom to top as the cutoff increases.

hidden gauge approach to investigate the $D\bar{D}^*$ and $\bar{D}D^*$ interactions, together with coupled channels with a pseudoscalar and a vector meson. The constraints of heavy quark spin symmetry show that the terms which are dominant in other processes, like in $I = 0$, due to the exchange of light mesons, are now forbidden. Hence, one resorts to sub-dominant terms that come from the exchange of heavy vectors or two pions. We found that this last contribution is quite small in comparison with the exchange of heavy vectors and its effect can be included in the uncertainties of the results. We obtained a state with a mass in the range $3867 - 3875$ MeV and a width around 40 MeV with $I = 1$ and positive G-parity. This state, in our formalism, is an isospin partner of the $X(3872)$.

Then, a reanalysis of the experiment of Ref. [291] in the $e^+e^- \to \pi^\pm(D\bar{D}^*)^\mp$ reaction was done. The experimentalists extracted a mass of about 3885 MeV and a width of $25 \pm 3 \pm 11$ MeV from the enhancement of the $D\bar{D}^*$ distribution around threshold. We performed a reanalysis of the data and found a solution close by, with mass of about 3875 MeV and a width of preferably 30 MeV. Hence, the present study shows that the data of Ref. [291] are compatible with a slightly lower mass, as we obtained theoretically. This means that the results reported here offer a natural explanation of the state claimed in Ref. [291] in terms of a $D\bar{D}^*(\bar{D}D^*)$ weakly bound state, that decays into the $\eta_c\rho$ and $\pi J/\psi$ channels.

The question remains whether that state, here reconfirmed, would be the same as the $Z_c(3900)$ claimed by BESIII in [229], or the $Z_c(3894)$ reported by

Belle [243], or the $Z_c(3886)$ reported by CLEO in [244]. Given the uncertainties in the masses and widths in all these experiments, it is quite likely that they are seeing the same state, although other options cannot be ruled out at the present time. In any case, we can say that, given the fact that a single channel $D\bar{D}^*$ with an energy independent potential cannot produce a resonance above the threshold at 3875.87 MeV [96], a state with 3900 MeV could not be easily interpreted as a $D\bar{D}^*(\bar{D}D^*)$ molecular state, while the one at lower energy stands naturally for a molecular interpretation, as we have reported here. Further precise measurements and investigations of other decay channels will help better understanding the issue and they should be encouraged.

When studying the interaction of $D^*\bar{D}^*$ in $I = 1$ from the perspective of the local hidden gauge approach, we have also taken into account the coupled channel $J/\psi\rho$, which is open for decay and is responsible for a width of the state of the order of 100 MeV. As in the previous case, we found that the effect of two pion exchange, with and without interaction, is smaller than the exchange of heavy vectors. The study conducted here complements the one of Ref. [228], where the peak seen in the $D^*\bar{D}^*$ spectrum in the $e^+e^- \to (D^*\bar{D}^*)^{\pm}\pi^{\pm}$ reaction that led the experimental team to claim a $J^P = 1^+$ $Z_c(4025)$ was reinterpreted as a possible 2^+ bound state of $D^*\bar{D}^*$ with $I = 1$. Both the mass and width that we obtained are compatible with the results of Ref. [228], obtained from a fit to the experimental data. This allows us to conclude that the state that we find in our approach can provide a natural explanation of the experimental results of Ref. [213]. One could claim a resonance from this experiment, but with a different energy ($3990 - 4000$ MeV), width (around 100 MeV) and quantum numbers ($I^G = 1^-$, $J^{PC} = 2^{++}$).

In the case of the $B\bar{B}^*$ and $B^*\bar{B}^*$ interactions for isospin $I = 1$, unlike the two previous cases, the vector exchange potential is not the main source of the interactions. In view of this, we consider the vector exchange potential corrected by a factor that takes into account the contributions of the others mesons exchange cases. Then, we use it as the kernel of the Bethe-Salpeter equation in order to solve the transition matrix T. Looking for poles in the T matrix, we tried to relate them with the $Z_b(10610)$ and $Z_b(10650)$ states reported by the Belle collaboration. We found a bound state of $B\bar{B}^*$ with mass in the range $10587 - 10601$ MeV, very close to the experimental mass of the $Z_b(10610)$ at 10608 MeV. In the case of $B^*\bar{B}^*$ interaction, we found a cusp at 10650 MeV for the spin $J = 0$ and $J = 2$ cases. On the other hand, the spin $J = 1$ case is a one channel problem and we do not take into account the $\rho\,\Upsilon$ channel. In this case, again, a cusp at 10650 MeV appears in the $|T_{11}|^2$ as it was also pointed out in Refs. [255, 256].

CHAPTER 7

DECAYS OF THE X(3872) TO $J/\psi\gamma$, $J/\psi\rho$ AND $J/\psi\omega$

7.1 Introduction

In this chapter we will focus on the $X(3872)$ resonance and, in particular, we will study in detail its three decays to $J/\psi\gamma$, $J/\psi\rho$ and $J/\psi\omega$.

The first observation of the $X(3872)$ decay into $J/\psi\gamma$ was reported by the BELLE collaboration in Ref. [299]. Later on this decay mode was confirmed by the BaBar team [300] and, more recently, again by BELLE in Ref. [301]. Theoretically, it had already some early attention and was studied in Refs. [239, 302–304], assuming the $X(3872)$ was either a charmonium or a molecular state.

A thorough discussion of the different models used and results obtained can be found in Ref. [242], and it has been recently updated in Ref. [305]. While in Ref. [306] the $X(3872)$ is assumed to be a charmonium state and in Ref. [307] a tetraquark, in Ref. [241] it is considered as a mixture of a charmonium and a molecular component, and using QCD sum rules a good rate is obtained for the $J/\psi\gamma$ decay mode versus the $J/\psi\pi^+\pi^-$ one, which is evaluated in Ref. [234]. In this latter work, as in Refs. [239, 308], the $X(3872)$ resonance is assumed to be a $D^0\bar{D}^{*0} - cc$ molecule and, in addition, in Ref. [242] the authors include the possibility of a $c\bar{c}$ admixture.

In particular, in Ref. [242] an effective Lagrangian is postulated to provide the coupling of the $X(3872)$ to the $D^0\bar{D}^{*0}$ components with an unknown wave function. The effective coupling needed in the loops for the radiative decay of the $X(3872)$ is obtained using the Weinberg compositeness condition [91, 92], reformulated in Ref. [94] as $g^2 = -(\frac{\partial}{\partial_s}G)^{-1}$ and widely discussed in **Chapter 3**, with G the loop function of the D^0 and $\bar{D}^{*0}$ propagators. In

other works [231, 309, 310], the procedure has been shown to provide a fair description of molecular states. The results of Ref. [242] are tied to unknown constants needed for the regularization of the loop functions, such as the Λ_M parameter, the coupling to the $c\bar{c}$ component and the binding. Once reasonable values for the Λ_M parameter, between 2 and 3 GeV, are taken, the results obtained for the $X(3872)$ decay into the $J/\psi\gamma$ channel are of about 125-250 KeV.

In Ref. [305] the authors also include the charged components of $D^+D^{*-} - cc$, which are proved necessary to explain the ratio of $X(3872)$ to $J/\psi\rho$ and $J/\psi\omega$ in Refs. [56, 94] (further developments in this direction can be in Ref. [217]). The novelty with respect to the work of Ref. [242] is that the authors use a smaller Λ_M cutoff, of the order of 0.5 GeV, to regularize the loop function, such that the wave function of the $D^0\bar{D}^{*0} - cc$ is much more extended in space. The final results of the new evaluations differ quantitatively from the previous ones and are now in the range of 2-17 KeV. It is then clear that a more systematic approach to the problem is needed if one wishes to obtain accurate numbers from a molecular picture of the $X(3872)$. This was the purpose of the work we did in Ref. [127], to which this Chapter is devoted.

A dynamical picture of the $X(3872)$ in the coupled channels $D\bar{D}^* - cc$ was elaborated in Ref. [56] using an extrapolation to $SU(4)$ of the chiral Lagrangians used in the study of the interaction of pseudoscalar mesons with vector mesons [51]. This procedure is equivalent to extending to $SU(4)$ the local hidden gauge approach of Refs. [63–66] with a particular $SU(4)$ breaking. Given the subtlety of the small binding for the neutral $D^0\bar{D}^{*0} - cc$ component versus the about 7 MeV binding for the charged $D^+D^{*-} - cc$ components, a coupled channel approach, considering these explicit channels with their exact masses and not assuming isospin symmetry, was done in Ref. [126], concluding that the couplings of the resonance to the neutral and charged components are very similar. This tells us that in strong processes the $X(3872)$ behaves as a rather good $I = 0$ object. The $D_s^+D_s^{*-} - cc$ components were also included in Refs. [56, 126] and we include them here too [1].

In the present work we follow the path of Refs. [94, 126] where all the couplings are determined from the unitary coupled channel approach and are tied to the binding of the $X(3872)$, which, in this picture, is generated dynamically

[1] We should recall that in any field theory one always selects some channels and ignores others. The ignorance of some channels can be coped by introducing counterterms in the theory, then losing predicting power for some processes, but they can serve to study other processes where the counterterms are negligible. One does not know this a priori but in principle the explicit consideration of close by channels renders the theory more predictive than if they were ignored. One example of this can be found in the study of the scattering of D and D^* mesons off the $X(3872)$ as done in Ref. [311], where the $D\bar{D}^{*0}$ component is by far dominant.

as a composite state of $D\bar{D}^*$. However, we update these couplings considering the latest results for the masses of the particles involved. The mechanisms for the radiative decay are then basically the same as in Ref. [305], except that we also have contributions from the $D_s\bar{D}_s^*$ components and have, although not much, different couplings of the resonance to the neutral and charged $D\bar{D}^*$ components.

Our work is also technically different. The use of wave functions with an arbitrary size parameter is what regularizes the loops in Ref. [305]. Here we use a different regularization scheme. While most of the terms are shown to be convergent, some of them are formally divergent, but we can isolate the divergence into a term proportional to the same loop function G that appears in the scattering problem. The function G is regularized in the scattering problem in order to fit the position of the resonance, such that when it comes to evaluate the radiative decay it is already fixed. Even then, there is still the possibility that a new vertex of the radiative decay loop function introduces a cutoff of longer range (a smaller cutoff in the momentum Λ) which introduces extra uncertainties, but we investigate them and find them small.

Traditionally the $X(3872)$ could be considered as a $J^P = 1^{++}$ or $J^P = 2^{-+}$ state. In a work similar to the one of Ref. [305] it is actually assumed to have $J^P = 2^{-+}$ quantum numbers [312]. However, here we will continue considering the resonance as a $J^P = 1^{++}$ state, idea supported by recent analysis of data in Refs. [313, 314] and, particularly, in the latest LHCB experimental analysis [315].

The Chapter is structured as follows: in the next section we present the formalism and evaluate the amplitudes for the different Feynman diagrams contributing to the decays. In **Section 7.3** we present the results for $X(3872) \to J/\psi\gamma, J/\psi\omega, J/\psi\rho$ and compare them to experiment, discussing the role of the charged components of the $X(3872)$ wave function. In **Section 7.4** we summarize our results. The whole discussion can be found in [127].

7.2 Formalism

7.2.1 Brief summary of the model used for the $D\bar{D}^*$ interaction

In our formalism, the $X(3872)$ resonance is considered as dynamically generated from the interaction of $D\bar{D}^*$ having an eigenstate of positive C-parity with isospin $I = 0$. It also has some component of $D_s\bar{D}_s^*$. In fact, the basis of

positive C-parity and $I = 0$ for these two channels corresponds to:

$$\frac{1}{\sqrt{2}}|(D^*\bar{D} - \bar{D}^*D), I = 0, I_3 = 0\rangle = \frac{1}{2}|(D^{*+}D^- - D^{*-}D^+ + D^{*0}\bar{D}^0 - \bar{D}^{*0}D^0)\rangle$$
$$\frac{1}{\sqrt{2}}|(D_s^*\bar{D}_s - \bar{D}_s^*D_s), I = 0, I_3 = 0\rangle = \frac{1}{\sqrt{2}}|(D_s^{*+}D_s^- - D_s^{*-}D_s^+)\rangle \ . \tag{7.1}$$

In Refs. [56, 126] a contact potential is used, since the works are based on the exchange of vector mesons from the perspective of the local hidden gauge formalism, and, due to the large masses of the vector mesons, their propagators are effectively replaced by constants [2].

Different approaches have been used in the Literature and one of them is pion exchange [257, 316–323]. The way to treat pion exchange differs from one work to another and so do the results and the conclusions. A review of those works can be found in Ref. [324], where a thorough study of the issue is made considering the coupled channels $D\bar{D}^*$, $\bar{D}D^*$ and $D\bar{D}\pi$. It is shown there that a short range $D\bar{D}^* \to D\bar{D}^*$ contact term is needed to arrive at well defined equations, with its strength tied to the regulator needed to make the theory convergent. Because of this ambiguity it was concluded there that no model-independent statement can be made on the importance of the one pion exchange in the formation of the $X(3872)$. However, with respect to what concerns us here, a relevant finding of Ref. [324] is that the $X(3872)$ coupling to the $D^0\bar{D}^{*0}$ component is weakly dependent on the kind of pion dynamics included.

Actually, in a different approach and a similar problem, the interaction of $D^*\bar{D}^*$ mesons leading to X, Y, Z molecules, the π exchange is explicitly taken into account by means of a box diagram that eliminates all possible ambiguities tied to the possibility of having the pion on shell [214]. There it was found that the corrections to the amplitudes induced by the π-exchange driven box diagram were very small using cutoffs or form factors of reasonable size for the effective theories.

The Weinberg compositeness condition is a very accurate tool to determine the coupling and, for a binding of the $D^0\bar{D}^{*0}$ channel below 1 MeV, as it is the case here, the results with a contact potential or with the dynamical pion are practically indistinguishable.

With the $D\bar{D}^{*0}$ coupling under control, a model is needed to obtain the coupling to the charged $D^+D^{*-} - cc$ or charmed-strange $D_S^+D_S^{*-} - cc$ components, and for this we use the model of Refs. [56, 126] as mentioned above.

[2] The formalism also makes approximations setting $|\vec{q}|/M_V$ to zero, with $\vec{q}$ the on shell momentum of the vectors. Improvements on this were done in [51] (see Appendix B), which applied to the present problem lead to negligible corrections.

Channel	$\lvert g_{R\to PV}\rvert$ [MeV]
$(K^- K^{*+} - cc)/\sqrt{2}$	53
$(K^0 \bar{K}^{*0} - cc)/\sqrt{2}$	49
$(D^- D^{*+} - cc)/\sqrt{2}$	3638
$(D^0 \bar{D}^{*0} - cc)/\sqrt{2}$	3663
$(D_s^- D_s^{*+} - cc)/\sqrt{2}$	3395

Table 7.1: Couplings g_R of the pole at $(3871.6 - i0.001)$ MeV to the channels ($\alpha_H = -1.27$ here).

In Ref. [126] it was found that the couplings of the $X(3872)$ to the charged and neutral components of DD^* were very close to each other, implying an approximate $I = 0$ character for the state. Since the masses and bindings used in these previous works have been updated, we have redone the calculation of Refs. [56, 126] with updated masses, assuming the present binding of 0.2 MeV of the $X(3872)$ with respect to the $D^0\bar{D}^{*0} - cc$ component. In Ref. [126] two subtraction constants, α_L and α_H (for the light and heavy sector), are used in the pseudoscalar-vector loop functions and, in view of the minor role played by the light channel, only the α_H parameter was varied to fix the new binding of the $X(3872)$. We evaluate again the couplings to the channels, obtained from the residues at the pole of the $X(3872)$ resonance, and their values are shown in **Table 7.1**.

From these couplings we can notice that there is some isospin violation, which is however very small, less than 1%. Intuitively, one might think that the $D^0\bar{D}^{*0}$ component is the only one that is relevant, since the binding of the $D^0\bar{D}^{*0}$ is very small, of the order of 0.2 MeV, and the wave function extends much further than for the charged component, which is bound by about 7 MeV. However, as we mentioned, the relevant interactions in most processes are short ranged and then the wave functions around the origin, proportional to the couplings in the approach we follow (see **Chapter 3**), are what matters. Thus, the wave function of the $X(3872)$ is very close to the isospin $I = 0$ combination of $D^0\bar{D}^{*0} - cc$ and $D^+D^{*-} - cc$ and has a sizeable fraction of the $D^+D^{*-} - cc$ of Eq. (7.1). However, in a field theoretical approach, like the one we follow, one only needs the couplings to calculate observables, without having to invoke the wave functions explicitly. The dynamics of the process in a reaction like ours, with propagators and couplings in the loops, determine the effective range of the process (see also Ref. [325] in this respect).

From **Table 7.1** we can also notice that the couplings to the $K^-K^{*+} - cc$ and $K^0\bar{K}^{*0} - cc$ channels represent less than the 1% of the contributions from the other channels (the $\pi^-\rho^+ - cc$ has even smaller strength). Therefore, we

will treat the $X(3872)$ as if it were dynamically generated only from the last three channels in the Table.

We have mentioned before that the Weinberg compositeness condition essentially provides the couplings of the $X(3872)$ to the $D^0\bar{D}^{0*}$ component. This can be seen from a different perspective using the generalization of the Weinberg compositeness condition to coupled channels of Eq. (3.80). As shown in **Chapter 3**, each one of the terms in Eq. (3.80) stands for the probability of finding the i channel in the wave function, while gG measures the wave function at the origin. The numerical values obtained for the terms in Eq. (3.80) are: 0.86 for $D^0\bar{D}^{*0}$, 0.124 for D^+D^{*-}, 0.016 for $D_S^+D_S^{*-}$. As one can see, the probability of finding the $D^0\bar{D}^{*0}$ component is the largest, due to the small binding energy [326].

7.2.2 The radiative decay $X(3872) \to J/\psi\gamma$

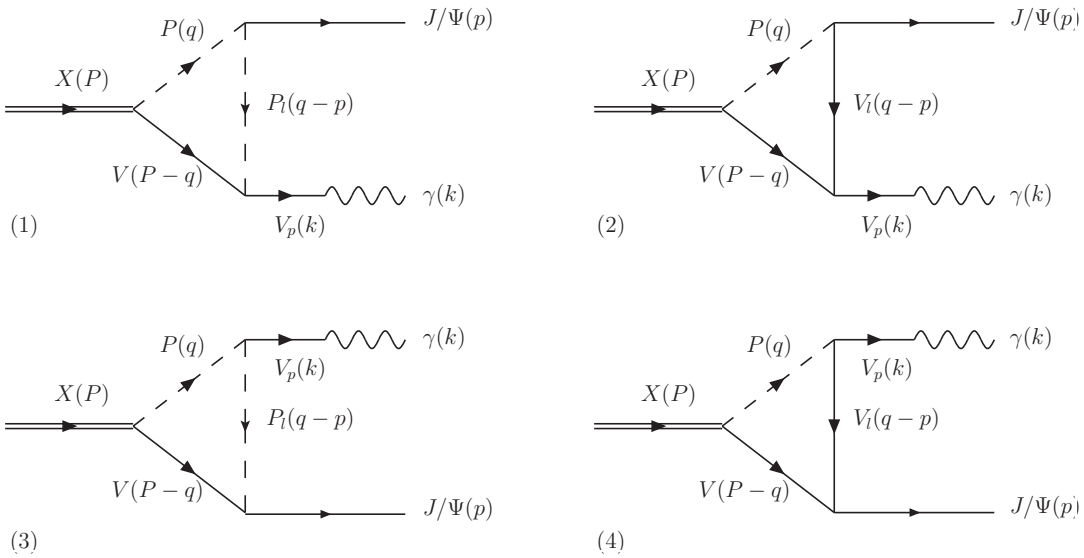

Figure 7.1: Possible types of Feynman diagrams for the decay of the $X(3872)$ into $J/\psi\gamma$.

In the framework described above, the $X(3872)$ decays into $J/\psi\gamma$ through the diagrams shown in **Figure 7.1**. All the diagrams contributing contain an anomalous vertex coupling two vectors and a pseudoscalar (VVP). Then, they can contain a VPP or a VVV vertex and the photon leg can be attached to them or to the anomalous VVP vertex. All this leads to the four types of diagrams shown in **Figure 7.1**. Moreover, there are three different channels: $D^0\bar{D}^{*0}$, D^+D^{*-} and $D_s^+D_s^{*-}$, which lead to 12 Feynman diagrams to evaluate, plus 12 more for the complex conjugate.

The formalism used is very similar to the one of Ref. [327], where the authors study the radiative decay of the dynamically generated resonance $K_2^*(1430)$ [225] into $K\gamma$ via diagrams containing anomalous vector-vector-pseudoscalar vertices. The VPP, VVV and Vγ vertices are evaluated using the local hidden gauge Lagrangians of Eqs. (2.92), (2.96), (2.97), (2.90) which, as already mentioned in **Chapter 2**, automatically incorporate vector meson dominance, such that the photons can couple to other hadrons converting themselves into ρ^0, ω, ϕ and J/ψ. As a consequence of this, we are also able to evaluate the rates of the $X(3872)$ decay into $J/\psi\rho$, $J/\psi\omega$ and the ratios of decay rates, which can be compared to existing data.

We start evaluating the diagram of type (1) of **Figure 7.1**. Using the Lagrangians we can write the vertices involved as

$$\begin{aligned} t_{RVP} &= g_X\ \epsilon^{(V)\mu}\epsilon_\mu^{(X)}\,, \\ t_{V_p\gamma} &= P\ M_{V_p}^2\frac{e}{g}\ \epsilon_\mu^{(\gamma)}\epsilon^{(V_p)\mu}\,, \\ t_{PP_lJ/\psi} &= P_V\ g\ (2q-p)_\mu\epsilon^{(J/\psi)\mu}\,, \\ t_{VV_pP_l} &= A\ G'\ \epsilon^{\alpha\beta\gamma\delta}\ (P-q)_\alpha\epsilon_\beta^{(V)}k_\gamma\epsilon_{\delta(V_l)}\,, \end{aligned} \tag{7.2}$$

where $g_X = 3638/\sqrt{2}, 3663/\sqrt{2}, 3395/\sqrt{2}$ MeV, for D^-D^{*+}, $\bar{D}^0D^{*0}$, $D_s^-D_s^{*+}$ and $-3638/\sqrt{2}$, $-3663/\sqrt{2}, -3395/\sqrt{2}$ MeV, for D^+D^{*-}, $D^0\bar{D}^{*0}$, $D_s^+D_s^{*-}$ respectively and P, P_V and A are numerical factors.

The $V_p \to \gamma$ conversion essentially replaces, up to a constant, $\epsilon_\delta^{(V_p)}$ by $\epsilon_\delta^{(\gamma)}$. Therefore, we can write the amplitude of diagram (1) as

$$\begin{aligned} -it_1 \quad &= -\mathrm{B}\,e\,g_X\,G'\int\frac{d^4q}{(2\pi)^4}\epsilon^{(V)\beta'}\epsilon_{\beta'}^{(X)}\epsilon^{(J/\psi)\mu}(2q-p)_\mu\epsilon^{\alpha\beta\gamma\delta}(P-q)_\alpha \\ &\times\epsilon_\beta^{(V)}k_\gamma\epsilon_\delta^{(\gamma)}\frac{1}{q^2-m_P^2}\frac{1}{(q-p)^2-m_{P_l}^2}\frac{1}{(P-q)^2-m_V^2}\,, \end{aligned} \tag{7.3}$$

where $\mathrm{B} = PAP_V$ (the values of B for each case are shown in **Table D.1** of Appendix **D**). Summing over the polarizations of the internal vector, we have

$$\sum_\lambda \epsilon_\beta^{(V)}\epsilon_{\beta'}^{(V)} = -g_{\beta\beta'} + \frac{(P-q)_\beta(P-q)_{\beta'}}{m_V^2}\ . \tag{7.4}$$

When contracting with the antisymmetric tensor $\epsilon^{\alpha\beta\gamma\delta}$ contained in the anomalous vertex, the symmetric term $(P-q)_\beta(P-q)_{\beta'}$ disappears. Thus, we are left with an integral of the form

$$\begin{aligned} &\int\frac{d^4q}{(2\pi)^4}\frac{(2q-p)_\mu(p+k-q)_\alpha}{(q^2-m_P^2+i\epsilon)((q-p)^2-m_{P_l}^2+i\epsilon)((p+k-q)^2-m_V^2+i\epsilon)} \\ &= i(ag_{\mu\alpha}+bk_\mu k_\alpha+cp_\alpha k_\mu+dk_\alpha p_\mu+ep_\alpha p_\mu) \end{aligned} \tag{7.5}$$

because of Lorentz covariance. After contracting with the antisymmetric tensor $\epsilon^{\alpha\beta\gamma\delta}$ and applying the Lorentz condition $p_\mu \epsilon^{(J/\psi)\mu} = 0$, only the coefficients a and c are left to be evaluated. The a coefficient is related to the logarithmically divergent part of the integral in Eq. (7.5) and, therefore, the evaluation of this coefficient needs a special treatment as we will see later on. We arrive to an amplitude of the form

$$t_1 = \mathrm{B}\, e\, G' g_X\, \epsilon^{\alpha\beta\gamma\delta}(a\epsilon_\alpha^{(J/\psi)} + c p_\alpha k\cdot\epsilon^{(J/\psi)})\epsilon_\beta^{(X)} k_\gamma \epsilon_\delta^{(\gamma)}\,. \tag{7.6}$$

Now we want to evaluate the a and c coefficients. We do it using the Feynman parametrization formula for $n = 3$,

$$\frac{1}{\alpha\beta\gamma} = 2\int_0^1 dx \int_0^x dy \frac{1}{[\alpha + (\beta-\alpha)x + (\gamma-\beta)y]^3}\,. \tag{7.7}$$

In the integral of Eq. (7.5), we can perform the above parametrization taking

$$\begin{aligned} \alpha &= (q-p)^2 - m_{P_l}^2\,, \\ \beta &= q^2 - m_P^2\,, \\ \gamma &= (p+k-q)^2 - m_V^2\,. \end{aligned} \tag{7.8}$$

We define a new variable $q' = q + p(x-y-1) - ky$, such that the integral of Eq. (7.5) can be expressed as

$$4\int_0^1 dx \int_0^x dy \int \frac{d^4q'}{(2\pi)^4} \frac{(q' + p(1-x+y) + ky)_\mu (k - q' - p(y-x) - ky)_\alpha}{(q'^2 + s_1)^3}\,, \tag{7.9}$$

with

$$\begin{aligned} s_1 = &-m_{P_l}^2 + (m_{P_l}^2 - m_P^2)x + (k^2 + m_P^2 - m_V^2)y + p^2(x-y)(1-x+y) \\ &+ 2pky(x-y) - k^2y^2\,. \end{aligned} \tag{7.10}$$

From Eq. (7.9), we must take the $iag_{\mu\alpha}$ and $icp_\alpha k_\mu$ terms. The c coefficient can be evaluated very easily, since

$$\int \frac{d^4q'}{(q'^2 + s_1)^3} = \frac{i\pi^2}{2s_1}\,, \tag{7.11}$$

which means that we have

$$c = \frac{1}{8\pi^2}\int_0^1 dx \int_0^x dy \frac{y(x-y)}{s_1}\,. \tag{7.12}$$

On the other hand, the evaluation of the a coefficient is a little bit more elaborated. We have the identity

$$iag_{\mu\alpha} = -4\int_0^1 dx \int_0^x dy \int \frac{d^4q'}{(2\pi)^4} \frac{q'_\mu q'_\alpha}{(q'^2 + s_1 + i\epsilon)^3} \tag{7.13}$$

and, after taking the trace,

$$ia = -\int_0^1 dx \int_0^x dy \int \frac{d^4q'}{(2\pi)^4} \frac{q'^2}{(q'^2 + s_1 + i\epsilon)^3} \,. \tag{7.14}$$

This part is logarithmically divergent and we will relate it to the two-meson loop function $G(P)$, that has the form

$$G(P = p + k) = i \int \frac{d^4q}{(2\pi)^4} \frac{1}{q^2 - m_P^2 + i\epsilon} \frac{1}{(p + k - q)^2 - m_V^2 + i\epsilon} \,, \tag{7.15}$$

as follows: we multiply the integrand of Eq. (7.15) by the factor $((q-p)^2 - m_{P_l}^2)/((q-p)^2 - m_{P_l}^2)$ and, using the Feynman parametrization with the change of variable $q' = q + p(x - y - 1) - ky$, we obtain

$$G(P) = 2i \int_0^1 dx \int_0^x dy \int \frac{d^4q'}{(2\pi)^4} \frac{q'^2 + (ky)^2 + 2pky(y-x) + p^2(x-y)^2 - m_{P_l}^2}{(q' + s_1)^3} \tag{7.16}$$

and thus

$$a = \frac{G(P)}{2} + \frac{1}{32\pi^2} \int_0^1 dx \int_0^x dy \frac{(ky)^2 + 2pky(y-x) + p^2(x-y)^2 - m_{P_l}^2}{s_1 + i\epsilon} \,. \tag{7.17}$$

However, the assumption that the divergent term of Eq. (7.14) in the three particle loop can be regularized like in the two body loop function appearing in scattering requires a justification. Certainly, this derivation only makes sense if there is a common cutoff in the two integrals. Indeed, as it was also the case in **Chapter 5**, the use of the same cutoff can be justified writing the potential of chiral unitary approach as

$$V(\vec{q}, \vec{q}\,', E) = v(E)\Theta(q_{max} - |\vec{q}|)\Theta(q_{max} - |\vec{q}\,'|) \,, \tag{7.18}$$

which leads to a T matrix with the same factorization

$$T(\vec{q}, \vec{q}\,', E) = T(E)\Theta(q_{max} - |\vec{q}|)\Theta(q_{max} - |\vec{q}\,'|) \,. \tag{7.19}$$

This means that the $PV \to PV$ amplitude in the $X(3872)$ pole goes as

$$T \sim \frac{g_X\ \Theta(q_{max} - |\vec{q}|)\ g_X\ \Theta(q_{max} - |\vec{q}\,'|)}{s - M_X^2} \,, \tag{7.20}$$

and hence the cutoff used for the scattering is the same appearing in the $X \to D\bar{D}^*$ vertex, which is shown in **Figure 7.1**.

The derivation above assumes that no extra cutoffs come from the other vertices in the diagrams, as usually assumed in most calculations, or that they involve bigger cutoffs which become then redundant. In order to test the accuracy of this procedure we introduce an extra cutoff in the $J/\psi DD^*$ vertex, $\Theta(\Lambda' - |\vec{q}|)$. For this we first evaluate the cutoff corresponding to the G function in dimensional regularization used in Refs. [56, 126]. We find a cutoff $q_{max} = 751.7$ MeV for the $D^0\bar{D}^{*0}$ channel and $q_{max} = 733.3$ MeV for the D^+D^{*-} channel. We take $q_{max} = 700$ MeV for the $D_S^+D_S^{*-}$ channel. Any larger value of the $J/\psi DD^*$ cutoff Λ' in $\Theta(\Lambda' - |\vec{q}\,'|)$ will not change anything. So we choose values of Λ' smaller than q_{max} but in a reasonable range.

Another possibility is to take a form factor of the type $e^{\,q^2/\Lambda'^2}$. Such a form factor, with $\Lambda' = 1.2$ MeV, was taken in Ref. [328] in a similar vertex involving D mesons, the $D^*D\pi$ vertex. Normalized such that it is unity when we have the intermediate $D\bar{D}^*$ on shell, the extra factor to be considered in three dimensional integration of the loop function is $e^{(\vec{q}^{\,2}_{on}-\vec{q}^{\,2})/\Lambda'^2}$.

Thus, we consider the two options, $\Lambda' \simeq 600$ MeV with a sharp cutoff and the exponential form factor, and we see how much the results change.

Now, we want to calculate the amplitude for the second diagram in **Figure 7.1**. The only difference with the previous case is the presence of the VVV vertex. The amplitudes corresponding to this vertex and to the anomalous one are, respectively:

$$\begin{aligned} t_{VV_lV_p} &= V_3 g\, [(q-p+k)_\mu \epsilon_\nu^{(V_l)} \epsilon^{(V)\mu} \epsilon^{(V_p)\nu} \\ &\quad - (p+2k-q)_\nu \epsilon_\mu^{(V)} \epsilon^{(V_l)\nu} \epsilon^{(V_p)\mu} \\ &\quad + (2(p-q)+k)_\nu \epsilon_\mu^{(V)} \epsilon^{(V_l)\mu} \epsilon^{(V_p)\nu}] \\ t_{V_lJ/\psi P} &= AG'\, \epsilon^{\alpha\beta\gamma\delta} (q-p)_\alpha \epsilon_\beta^{(V_l)} p_\gamma \epsilon_\delta^{(J/\psi)}\,, \end{aligned} \tag{7.21}$$

where V_3 and A are numerical factors.

Thus, we can write the amplitude of diagram (2) in **Figure 7.1** as

$$\begin{aligned} -it_2 = -eG' g_X \mathrm{C} \int \frac{d^4q}{(2\pi)^4} &\epsilon^{\alpha\beta\gamma\delta} (q-p)_\alpha \epsilon_\beta^{(V_l)} p_\gamma \epsilon_\delta^{(J/\psi)} \epsilon_{\nu'}^{(X)} \epsilon^{(V)\nu'} \\ &\times \{(q-p+k)_\mu \epsilon_\nu^{(V_l)} \epsilon^{(V)\mu} \epsilon^{(\gamma)\nu} - (p+2k-q)_\nu \epsilon_\mu^{(V)} \epsilon^{(V_l)\nu} \epsilon^{(\gamma)\mu} \\ &+ (2(p-q)+k)_\nu \epsilon_\mu^{(V)} \epsilon^{(\gamma)\nu} \epsilon^{(V_l)\mu}\} \frac{1}{q^2 - m_P^2 + i\epsilon} \frac{1}{(q-p)^2 - m_{V_l}^2 + i\epsilon} \\ &\times \frac{1}{(p+k-q)^2 - m_V^2 + i\epsilon}\,, \end{aligned}$$

where $C = V_3 PA$ (the factors C are listed in **Table D.2** of Appendix **D**). In this process the $\bar{D}^{*0}$ is very close to be on-shell with zero three momentum.

To be consistent with the approach of Ref. [126], that is neglecting the three-momentum compared to the mass of the vector meson, $|\vec{q}|/m_V \simeq 0$, $\epsilon^{(V)0} \simeq 0$, we perform the sum over polarizations as

$$\sum_\lambda \epsilon^{(V)\mu}\epsilon^{(V)\nu'} \simeq \delta^{(\mu\nu')_{\rm spatial}} = \delta^{ij}\,. \tag{7.22}$$

We also can keep the covariant formalism and remember at the end that μ, ν' are spatial.

The way to proceed is very similar to that of the previous diagram. The second term of the VVV vertex proportional to $(p+2k-q)_\beta$ does not contribute, since we have $(q-p)_\alpha p_\gamma (p+2k-q)_\beta = q_\alpha (p+2k)_\beta p_\gamma \epsilon^{\alpha\beta\gamma\delta}$, which applying Lorentz covariance in the integral turns into a term like $(a' p_\alpha k_\beta + b' p_\beta k_\alpha) p_\gamma \epsilon^{\alpha\beta\gamma\delta} = 0$. Therefore, we have two kinds of integrals:

$$\begin{aligned}&\int \frac{d^4q}{(2\pi)^4} \frac{q_\alpha (q-p+k)_{\nu'}}{(q^2-m_P^2+i\epsilon)((q-p)^2-m_{V_l}^2+i\epsilon)((p+k-q)^2-m_V^2+i\epsilon)} \\ &= i(a_1 g_{\alpha\nu'} + b_1 k_\alpha k_{\nu'} + c_1 p_\alpha k_{\nu'} + d_1 p_{\nu'} k_\alpha + e_1 p_{\nu'} p_\alpha)\end{aligned} \tag{7.23}$$

and

$$\begin{aligned}&\int \frac{d^4q}{(2\pi)^4} \frac{q_\alpha 2(p-q)_{\nu}}{(q^2-m_P^2+i\epsilon)((q-p)^2-m_{V_l}^2+i\epsilon)((p+k-q)^2-m_V^2+i\epsilon)} \\ &= i(a_2 g_{\alpha\nu} + b_2 k_\alpha k_\nu + c_2 p_\alpha k_\nu + d_2 k_\alpha p_\nu + e_2 p_\alpha p_\nu)\,.\end{aligned} \tag{7.24}$$

One can see that only the coefficients proportional to a_1, b_1, d_1, a_2 and d_2 survive. Thus, we finally get

$$\begin{aligned}t_2 = -{\rm C}\, e\, G' g_X\ \epsilon^{\alpha\beta\gamma\delta}[&(a_1 \epsilon_\alpha^{(X)} + (b_1 k^\mu + d_1 p^\mu)\epsilon_\mu^{(X)} k_\alpha)\epsilon_\beta^{(\gamma)} \\ &+ (a_2 \epsilon_\alpha^{(\gamma)} + d_2 \epsilon_\mu^{(\gamma)} p^\mu k_\alpha)\epsilon_\beta^{(X)}]\, p_\gamma \epsilon_\delta^{(J/\psi)}\,,\end{aligned} \tag{7.25}$$

where now

$$\begin{aligned}a_1 &= -\frac{G(P)}{4} - \frac{1}{64\pi^2}\int_0^1 dx \int_0^x dy \frac{(ky)^2 + 2pky(y-x) + p^2(x-y)^2 - m_{V_l}^2}{s_2 + i\epsilon}\,, \\ b_1 &= \frac{1}{16\pi^2}\int_0^1 dx \int_0^x dy \frac{y(y+1)}{s_2+i\epsilon}\,, \\ d_1 &= \frac{1}{16\pi^2}\int_0^1 dx \int_0^x dy \frac{y(y-x)}{s_2+i\epsilon}\,, \\ a_2 &= -2a_1\,, \\ d_2 &= -2d_1\,,\end{aligned} \tag{7.26}$$

with

$$s_2 = -m_{V_l}^2 + (m_{V_l}^2 - m_P^2)x + (k^2 - m_V^2 + m_P^2)y + p^2(x-y)(1-x+y) + 2kyp(x-y) - k^2y^2 \,. \tag{7.27}$$

In order to evaluate diagrams (3) and (4) in **Figure 7.1**, we only have to do the substitutions $k \to p$ and $\epsilon^{(\gamma)} \to \epsilon^{(J/\psi)}$ in the amplitudes of diagrams (1) and (2). This means that we get

$$t_3 = \mathrm{B}\, e\, G'\, g_X^c\ \epsilon^{\alpha\beta\gamma\delta}(a\epsilon_\alpha^{(\gamma)} + dk_\alpha(p\cdot\epsilon^{(\gamma)}))\epsilon_\beta^{(X)} p_\gamma \epsilon_\delta^{(J/\psi)} \,, \tag{7.28}$$

with

$$a = \frac{G(P)}{2} + \frac{1}{32\pi^2}\int_0^1 dx \int_0^x dy \frac{(py)^2 + 2pky(y-x) - m_{P_l}^2}{s_3 + i\epsilon} \tag{7.29}$$

and

$$d = \frac{1}{8\pi^2}\int_0^1 dx \int_0^x dy \frac{y(x-y)}{s_3} \,, \tag{7.30}$$

where

$$s_3 = -m_{P_l}^2 + (m_{P_l}^2 - m_P^2)x + (p^2 + m_P^2 - m_V^2)y + 2pky(x-y) - p^2y^2 \,, \tag{7.31}$$

for diagram (3), and

$$s_4 = -m_{V_l}^2 + (m_{V_l}^2 - m_P^2)x + (p^2 - m_V^2 + m_P^2)y + 2kyp(x-y) - p^2y^2 \tag{7.32}$$

for diagram (4).

7.2.3 The $X(3872)$ decay to $J/\psi\rho$ and $J/\psi\omega$

This formalism also allows us to evaluate the amplitudes for the decays $X(3872) \to J/\psi\rho)$ and $X(3872) \to J/\psi\omega$ (**Figure 7.2**). We can proceed in complete analogy with the radiative decay to determine these amplitudes, simply removing the final photon and leaving the vector meson in the final state, the ρ^0 or the ω. Moreover, we must take into account that the ρ^0 and the ω do not couple to the strange D mesons, so that we have again four different kinds of diagrams, but only two channels plus their complex conjugate, that is 16 Feynman diagrams to evaluate. Doing this, we can observe that the new amplitudes have the same structure of the previous ones and can be obtained, up

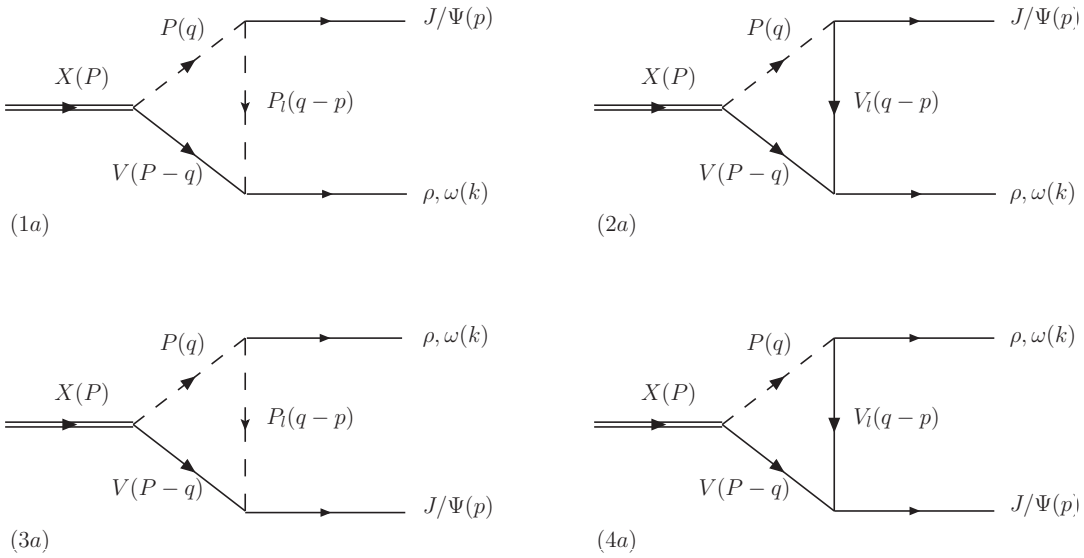

Figure 7.2: Possible types of Feynman diagrams for the decay of the $X(3872)$ into $J/\psi\rho$ and $J/\psi\omega$.

to a coefficient, directly with the substitutions $e \leftrightarrow g$ and $\epsilon^{(\gamma)} \leftrightarrow \epsilon^{(\rho,\omega)}$. For instance, in the case of the diagram $(1a)$ of **Figure 7.2**, we have

$$t_{1a} = \mathrm{B}' g G' g_X \epsilon^{\alpha\beta\gamma\delta} (a\epsilon_\alpha^{(J/\psi)} + c p_\alpha k \cdot \epsilon^{(J/\psi)}) \epsilon_\beta^{(X)} k_\gamma \epsilon_\delta^{(\rho,\omega)} \ , \tag{7.33}$$

with a and c the same as before

$$\begin{aligned} a &= \frac{G(P)}{2} + \frac{1}{32\pi^2} \int_0^1 dx \int_0^x dy \frac{(ky)^2 + 2pky(y-x) + p^2(x-y)^2 - m_{P_l}^2}{s_1 + i\epsilon} \ , \\ c &= \frac{1}{8\pi^2} \int_0^1 dx \int_0^x dy \frac{y(x-y)}{s_1} \end{aligned} \tag{7.34}$$

and $B' = P_V A$ of Eqs. (7.2). However, since we are dealing with different vertices, the new numerical coefficients, that we call B′ and C′, are now different and they are written in **Table D.3**, **Table D.4**, **Table D.5** and **Table D.6** of Appendix **D**.

7.3 Results

Following the procedure in **Section 7.2** we can obtain the total decay amplitude for the radiative decay of the $X(3872)$ and evaluate the correspondent

decay width for this channel by means of the formula

$$\Gamma = \frac{|\vec{k}|}{8\pi M_X^2} \bar{\sum} \sum |t|^2 \,, \tag{7.35}$$

where we sum over the polarizations of the final states and average over the X meson polarizations. Applying Eq. (7.35), we obtain

$$\Gamma(X \to J/\psi\gamma) = 149.5 \text{ keV} \,. \tag{7.36}$$

In order to make an estimation of the theoretical uncertainty on this quantity, we perform a suitable variation of the parameters used to compute the total amplitude: the coupling G' for the VVP vertex, the axial-vector-pseudoscalar couplings g_X for the three channels, and the two subtraction constants in the loop function, α and α_S.

We allow the constant f, contained in G', to vary, but keeping the relationship $G_V = f/\sqrt{2}$ and replacing $M_V = M_\rho$ by M_{D^*}. The couplings g_X for the neutral and strange channels are also varied, independently, by 10%. This might be extreme for the neutral channel, since it is basically determined by the Weinberg compositeness condition, but we also have an uncertainty in the binding which can induce this change. For that reason we perform, later on, another sort of error's analysis based on experimental uncertainties. On the other hand, the variation of the coupling for the charged channel is done in such a way that the ratio between it and the one for the neutral channel is kept constant, in order to preserve the isospin of the $X(3872)$. Then, we let the subtraction constants α and α_S vary between -1.60 and -1.27. This range is motivated by the range chosen for f. Indeed, going to higher values of the constant f causes a decrease of the potential in the Lippman-Schwinger equation used to evaluate the scattering amplitude which determines the position of the resonance. One would need to go to more negative values of the subtraction constants α and α_S in the loop function, which appears in the a coefficients, to keep the pole representing the resonance in the same position. The range is thus chosen such as to produce an effect in the pole position similar to that induced by the change in f.

We obtain the result

$$\Gamma(X \to J/\psi\gamma) = (117 \pm 40) \text{ keV} \,. \tag{7.37}$$

There is another source of error that stems from experimental uncertainties in the binding of the $X(3872)$ and we also evaluate it. We have then performed a different exercise changing just α_H such that the binding goes from 0.1 to 0.4 MeV, which is indeed within the experimental limits but still keeps the

$X(3872)$ bound. We recalculate the couplings and evaluate again the rates and we find

$$\Gamma(X \to J/\psi\gamma) = (117^{+48}_{-35})\ \text{keV}\,. \tag{7.38}$$

This gives a new perspective on the uncertainties, showing that errors from the experimental uncertainties are of the same order of the rough estimate of the theoretical errors.

We can also evaluate the branching ratios for the decays $X(3872) \to J/\psi\rho$ and $X(3872) \to J/\psi\omega$. These two decays, if we consider the ρ and the ω with fixed masses, are not allowed because of the phase space, but they can occur when their mass distributions are taken into account. They are observed in the decays $X(3872) \to J/\psi\pi\pi$ and $X(3872) \to J/\psi\pi\pi\pi$ respectively, where the two and three pions states are produced in the decays of the ρ and the ω.

Thus, the decay widths, convoluted with the spectral functions, are given by the formula

$$\begin{aligned}\Gamma_{\rho/\omega} = \frac{1}{N}\int_{(m_{\rho/\omega}-2\Gamma_{\rho/\omega})^2}^{(m_{\rho/\omega}+2\Gamma_{\rho/\omega})^2} d\tilde{m}^2 \left(-\frac{1}{\pi}\right)\ Im\left[\frac{1}{\tilde{m}^2 - m^2_{\rho/\omega} + i\tilde{\Gamma}_{\rho/\omega}\tilde{m}}\right] \\ \times\, \Gamma_X(\tilde{m})\theta(m_X - m_{J/\psi} - \tilde{m})\,,\end{aligned} \tag{7.39}$$

where

$$N = \int_{(m_{\rho/\omega}-2\Gamma_{\rho/\omega})^2}^{(m_{\rho/\omega}+2\Gamma_{\rho/\omega})^2} d\tilde{m}^2 \left(-\frac{1}{\pi}\right)\ Im\left[\frac{1}{\tilde{m}^2 - m^2_{\rho/\omega} + i\tilde{\Gamma}_{\rho/\omega}\tilde{m}}\right]\,, \tag{7.40}$$

with $\Gamma_X(\tilde{m})$ given by Eq. (7.35), changing m_ρ and m_ω by $\tilde{m}$.

In Eqs. (7.39) and (7.40), $m_\rho = 775.49$ MeV and $m_\omega = 782.65$ MeV are the masses of the mesons, $\Gamma_\rho = 149.1$ MeV and $\Gamma_\omega = 8.49$ MeV are the on shell widths and

$$\tilde{\Gamma}_{\rho/\omega} = \Gamma_{\rho/\omega}\left(\frac{\tilde{q}}{q_{\rho/\omega}}\right)^3\,, \tag{7.41}$$

where $\tilde{q}$ and $q_{\rho/\omega}$ are the on shell relative momenta of the mesons in the center of mass reference frame for the mass $\tilde{m}$ and the physical mass respectively:

$$\begin{aligned}\tilde{q} &= \frac{\sqrt{\tilde{m}^2 - 4m_\pi^2}}{2}\theta(\tilde{m} - 2m_\pi)\,, \\ q_{\rho/\omega} &= \frac{\sqrt{m^2_{\rho/\omega} - 4m_\pi^2}}{2}\,.\end{aligned} \tag{7.42}$$

In Eq. (7.39), Γ_X is the total decay width of the X into $J/\psi\rho$ or $J/\psi\omega$ to simplify the notation and in Eq. (7.42) m_π is the pion mass.

Using Eq. (7.39) we find

$$\begin{aligned} \Gamma_\rho &= 821.9 \text{ keV}\,, \\ \Gamma_\omega &= 1096.6 \text{ keV}\,, \end{aligned} \tag{7.43}$$

and, when the error analysis that leads to Eq. (7.37) is done, the band of values becomes

$$\begin{aligned} \Gamma_\rho &= (645 \pm 221) \text{ keV}\,, \\ \Gamma_\omega &= (861 \pm 294) \text{ keV}\,. \end{aligned} \tag{7.44}$$

Similarly to the case of Eq. (7.38), we have also errors due to the uncertainties in the binding. Taking the same range that led to Eq. (7.37) we find

$$\begin{aligned} \Gamma_\rho &= (645^{+264}_{-192}) \text{ keV}\,, \\ \Gamma_\omega &= (861^{+353}_{-257}) \text{ keV}\,. \end{aligned} \tag{7.45}$$

With the results of Eq. (7.43) we can evaluate the ratio

$$R = \frac{\mathcal{B}(X \to J/\psi\pi\pi\pi)}{\mathcal{B}(X \to J/\psi\pi\pi)} = \frac{\Gamma_\omega}{\Gamma_\rho} = 1.33\,. \tag{7.46}$$

However, the experiment gives the ratio [329]

$$R^{exp} = \frac{\mathcal{B}(X \to J/\psi\pi^+\pi^-\pi^0)}{\mathcal{B}(X \to J/\psi\pi^+\pi^-)} = 0.8 \pm 0.3 \tag{7.47}$$

and, to compare our result with this, we must take into account that the ω decays into $\pi^+\pi^-\pi^0$ with a branching ratio $B_{\omega,3\pi} = 0.892$.

Hence, our ratio to compare with R^{exp} is

$$R^{th} = \frac{\Gamma_\omega}{\Gamma_\rho} \times B_{\omega,3\pi} = 1.19\,, \tag{7.48}$$

well within the experimental error.

The result we obtain for the ratio

$$\frac{\Gamma(X \to J/\psi\gamma)}{\Gamma(X \to J/\psi\pi\pi)} = 0.18\,, \tag{7.49}$$

is also compatible with the two values known from the experiment (0.14 ± 0.05) [299] and (0.22 ± 0.06) [300].

We can also estimate the theoretical errors for the two ratios in Eqs. (7.48) and (7.49), by evaluating the γ, ρ and ω decays with the same set of parameters, and varying these parameters in the range used to evaluate $\Gamma(X \to J/\psi\gamma)$:

$$\begin{aligned} R^{th} &= (0.92 \pm 0.13) \\ \frac{\Gamma(X \to J/\psi\gamma)}{\Gamma(X \to J/\psi\pi\pi)} &= (0.17 \pm 0.02)\,. \end{aligned} \tag{7.50}$$

We should note that changing the binding as done to get the errors in Eq. (7.38) barely changes the ratios of Eq. (7.50), since the ratios of the couplings of the $X(3872)$ to the different channels barely change. This was already found in Ref. [126].

The uncertainties in the ratios are smaller than for the absolute values and they are of the order of 15%.

At this point we also take into account uncertainties from the association of the loop with two propagators to the G function for the scattering, including extra cutoffs or the form factor discussed above. The values that we find are shown in **Table 7.2**, where the errors from the three sources discussed are added in quadrature. We can see that we have good agreement with experiment in the two ratios measured.

Finally, we do another exercise removing the $D^+D^{*-} - c.c$ and $D_S^+D_S^{*-} - c.c$ and keeping only the $D^0\bar{D}^{*0} - c.c$ contribution. The coupling of the $D^0\bar{D}^{*0} - c.c$ is reevaluated taking the same binding for the $X(3872)$, such that Eq. (3.80) is now fulfilled with just this channel. The results that we obtain are

$$\begin{aligned} \Gamma_\gamma &= 0.53 \text{ keV}\,, \\ \Gamma_\rho &= 10589 \text{ keV}\,, \\ \Gamma_\omega &= 429 \text{ keV}\,, \\ R^{th} &= 0.04\,, \\ \frac{\Gamma(X \to J/\psi\gamma)}{\Gamma(X \to J/\psi\pi\pi)} &= 5.05 \cdot 10^{-5}\,. \end{aligned} \tag{7.51}$$

As we can see, the two ratios that we have to compare with experiment largely diverge from the experimental values and Γ_ρ by itself becomes much bigger than the width of the $X(3872)$ ($\Gamma_X < 1.2$ MeV).

In **Table 7.3** we compare our results with a variety of results available in the Literature using different models. It would be interesting to test these models with the new information on the experimental ratios to help discriminate among them.

The ratio of $J/\psi\gamma$ to $J/\psi\pi\pi$ is also evaluated in Ref. [305], where the Weinberg compositeness condition [91] is used to determine the couplings but other assumptions are made, and they find a range of values from 0.18 to

	standard G	$\Theta(\Lambda' - \lvert\vec{q}\rvert)$	$e^{(\vec{q}_{on}^{\,2} - \vec{q}^{\,2})/\Lambda'^2}$	Range [keV]	Experiment [keV]
Γ_γ	150	190	180	117^{+73}_{-53}	
$\Gamma_{\rho(2\pi)}$	821	991	905	645^{+383}_{-293}	
$\Gamma_{\omega(3\pi)}$	1097	1593	1380	861^{+500}_{-390}	
$\frac{\Gamma_\omega}{\Gamma_\rho} \times B_{\omega,3\pi}$	1.19	1.43	1.36	$0.92^{+0.27}_{-0.13}$	0.8 ± 0.3 [329]
$\Gamma_\gamma/\Gamma_{\rho(2\pi)}$	0.18	0.19	0.20	$0.17^{+0.03}_{-0.02}$	(0.14 ± 0.05) [299] (0.22 ± 0.06) [300]

Table 7.2: Values of the partial decay width in units of keV. First column: using the standard G function of scattering. Second column: multiplying the integrand of G by $\theta(\Lambda' - |\vec{q}|)$ with $\Lambda' = 600$ MeV. Third column: multiplying the integrand of G by $e^{(\vec{q}_{on}^{\,2} - \vec{q}^{\,2})/\Lambda'^2}$ with $\Lambda' = 1200$ MeV. Fourth column: range of values for all the rates including the three sources of errors, from uncertainties in the couplings, binding of the X and the G function, summed in quadrature. Fifth column: experimental results.

model	Γ [keV]
$c\bar{c}$	11 [239]
$c\bar{c}$	139 [303]
molecule	8 [303]
molecule	$125-250$ [242]
$c\bar{c}$	$11-71$ [305]
molecule + $c\bar{c}$	$2-17$ [305]
2^{-+}	$1.7-2.1$ [312]
$c\bar{c}$	$45-80$ [306]
tetraquark	$10-20$ [307]
present work	$64-190$

Table 7.3: Results from previous works for the decay width of the $X(3872)$ into $J/\psi\gamma$, using different models.

1.57 depending on the model they consider, as mentioned in the Introduction. We should stress that once the $X(3872)$ is obtained in our case and, hence, the couplings are determined, the uncertainties that we have from theoretical sources and experimental errors in the masses are much smaller than in Ref. [305].

We should note that our results are tied to the masses of the particles in the PDG and there are still large errors. When in the future the binding can be more accurately determined we can also obtain more accurate values of the absolute rates. On the other hand, the values of the ratios will be essentially unaltered.

7.4 Conclusions

In this Chapter we have exploited the picture of the $X(3872)$ as a composite state of $D\bar{D}^* - cc$ dynamically generated by the interaction of the D and D^* states. The couplings of the state to the different $D\bar{D}^* - cc$ channels have been calculated before within this model, but we have recalculated them here to take into account the more precise values of the particle masses tabulated in the PDG [17]. The coupling for the $D^0\bar{D}^{*0} - c.c$ is similar to the one that would be obtained using the compositeness condition of Weinberg, since the state is barely bound in the $D^0\bar{D}^{*0}$ component, but the dynamics of the model produces also couplings for the $D^+D^{*-} - c.c$ and $D_S^+D_S^{*-} - c.c$ states. Using an extension to $SU(4)$ with an explicit breaking of this symmetry of the local hidden gauge approach, already successfully used in the study of related processes, one can determine the widths of the $X(3872)$ to $J/\psi\rho$, $J/\psi\omega$ and

$J/\psi\gamma$ and compare with the ratios determined experimentally in recent works. We find a very good agreement with the experimental results. The absolute numbers obtained for the different widths are also reasonable and their sum within errors, $(1.6^{+0.9}_{-0.7})$ MeV, is compatible with the recent total $X(3872)$ upper limit of the width, $\Gamma = 1.2$ MeV.

We have also conducted a test neglecting the charged and strange components of the wave function and thus keeping only the $D^0\bar{D}^{0*} - cc$ component. We obtain ratios in great disagreement with experiment and an absolute value for the $X(3872)$ partial width into $J/\psi\rho$ which largely exceeds the experimental upper bound for the total width of the $X(3872)$. This exercise confirms the relevance of the charged channels to describe the process that we studied and the approximate $I = 0$ character of this resonance. This does not mean that the use the neutral channel alone is an incorrect way to proceed in general. It is just incomplete, but in any field theoretical approach the missing channels can be accounted for by means of counterterms which, however, make the theory less predictive. For the present case it became clear that the explicit consideration of the charged $D\bar{D}^*$ channels renders the theory more predictive than omitting them.

CHAPTER 8

CONCLUSIONS

In this Thesis we tackled many different issues concerning the understanding of the hadronic spectrum, all of them linked by a common thread: the necessity to describe the structure of resonant states, recently discovered, that have properties impossible to be accommodated in the standard quark model for mesons and baryons.

We dealt with those states from the molecular perspective, exploiting powerful techniques developed starting from Chiral Perturbation Theory. The Chiral Unitary Approach, a non perturbative method able to combine χPT to unitarity constraints, permits to characterize some resonances as *dynamically generated* from the interaction of two fundamental hadrons. The tree level hadron-hadron potentials provided by chiral Lagrangians are used as the kernel for the Bethe-Salpeter equation in coupled channels to calculate the scattering amplitude. Furthermore, with the use of the hidden gauge formalism, vectors and photons can also be included in the theory. Once the amplitude is evaluated, it is possible to look for already experimentally observed resonances and also to predict new ones, searching for them as poles of the scattering amplitude extrapolated to the second Riemann sheet of the complex energy plane. Also the coupling of the state to a given hadron-hadron channel can be easily evaluated, since it corresponds to the residue at the pole of the amplitude. In the following, we make a summary of the objectives accomplished throughout this work by taking advantage of these tools.

1. **Generalization of the Weinberg compositeness condition for bound states to any partial waves.**
   In **Chapter 3** we address the necessity of a general rule to decide if the structure of a state can be considered as composite of other stable hadrons or just genuine. We generalize a specific sum rule, derived in previous works

for s-waves, to higher partial waves. This is done by simply studying the interaction of a hadron pair using an energy independent potential. This leads to a redefinition of the loop function for these intermediate states such that, now, the l-wave character of the interaction is not contained in the potential any more, but absorbed in the loop. Simply evaluating the derivative of the G function for the loop, together with the couplings of the state under study to the relevant channels, the different terms of the sum rule can be calculated. We know that in the case of bound states these terms have a very clear meaning: each one of them is the probability to find that particular channel in the wave function of the state. This happens because the sum rule is derived directly from the normalization condition of the wave function. If we are considering all the possible components that can characterize the structure of our state, then the different terms will sum to one. The difference from unity of their sum gives the probability of having something else in the wave function, for example the genuine quark model component that cannot be accounted for with chiral unitary approach in coupled channels. We also found out that the relations between couplings and wave functions still hold in their generalization to higher partial waves in coupled channels.

2. **Generalization of the compositeness condition to the case of resonances and interpretation.**
Problems arise when extending the formalism to open channels. Dealing with resonances means dealing with complex values for energies and couplings, such that also the different terms of the sum rule are complex and, therefore, cannot be interpreted as probabilities. This is related to the absence of a normalization condition for the wave function. However, the sum rule still holds at the pole. In **Chapter** 4 we showed how now the terms of the sum rule are related to the integral of the square of the wave function instead of the modulus squared. This is a finite quantity under the phase convention that we are using, differently from the integral of the modulus squared, and though it is clearly impossible to consider it as a probability, we can still think about it as the extrapolation, to the case of complex energies, of the concept of probability. We can say that it can be safely interpreted as the weight that a particular hadron-hadron component will have in the wave function of the resonance, but it does not have to be confused with the relevance of a certain channel in a given physical process which is strongly tied to the specific dynamics of the process itself.

3. **Application of the sum rule to concrete cases.**
The compositeness condition is straightforward to apply and we used it to study the structure of some well known resonances. In particular:

- we tried to quantify the importance of the p-wave $\pi\pi$ component in the ρ and πK component in the K^* mesons. None of these resonances qualifies as dynamically generated and we expected the sum rule not to be satisfied. Indeed, with both tests we performed, one relying on chiral unitary theory and a phenomenological one, we obtained a very small amount of compositeness for these states, confirming their genuine nature.
- we applied the two tests to a baryon for the first time, the $\Delta(1232)$, to measure the weight of the πN component in the wave function. The amount of composite character we obtained is considerably high, around 60%, and could seem surprising. However, previous works already stressed the importance of the meson cloud, even in the nucleon. Our result suggests that it should be taken into account when dealing with the $\Delta(1232)$. The investigation continued with the study of the whole $J^P = \frac{3}{2}^+$ decuplet, that manifested a lower composite character as we go to higher energies.
- the last resonance we studied is the $\Lambda(1520)$, dynamically generated in a four-channel problem. We evaluated the relevance of these different components and also their sum, which is very close to one, indicating that we do not have much room left to include other channels in the approach. This is in line with the dynamically generated nature we assume for this state.

4. The triangular $K^*\bar{K}$ loop and the nature of the $a_0(980)$, $f_0(980)$ and $f_1(1285)$.

We used this mechanism to study different decays and better understand the nature of the particles involved in the processes. As already stressed in **Chapter** 5, the novelty of this approach consists in the possibility of regularizing the loop function with a cutoff provided by chiral unitary approach once the $a_0(980)$ and the $f_0(980)$, produced as intermediate states, are assumed as dynamically generated by meson-meson rescattering. Thanks to that, we could evaluate numerical results without arbitrary cutoffs or form factors. We could explain quite successfully the impressive isospin violation measured in the decay of the $\eta(1405)$ to $\pi^0\pi^+\pi^-$ with respect to $\pi^0\pi^0\eta$, and the good agreement between the results we got with our theoretical approach and the experiment encouraged us to apply the same mechanism to the decay of the $f_1(1288)$ to $\pi^0\pi^0\eta$. In this case, also the $f_1(1285)$ is considered as dynamically generated and the fact that it couples to the $K^*\bar{K}$ pair allows us to use the triangular loop. Once again we obtained, at least qualitatively, an agreement between theory and experiment and we could simultaneously study also the decay to $\pi^0\pi^0\eta$, in order to go

further in the investigation of what other works call a_0-f_0 mixing, but that we rather call isospin violation. We found that the amount of this mixing is much smaller than in the case of the $\eta(1405)$ decay, characterizing this quantity as strongly dependent on the process considered. However, the two processes share some peculiar features of the invariant mass spectra. In fact, when looking at the invariant mass distribution for the two decays to $\pi^0\pi^+\pi^-$ in the region of the $f_0(980)$, what we see is a very narrow peak, with the f_0 produced with a width of about 10 MeV, much smaller than its natural one. This width simply indicates the region of energies where the difference between the mass of the charged and neutral kaons, responsible for the production of the f_0 that would be otherwise forbidden, is relevant in the calculation. In both cases, this shape of the mass distribution has been confirmed by experiment providing support to the use of this decay mechanism. The last reaction we studied, the decay of the f_1 to $\pi K\bar{K}$, gave also results compatible with experiment concerning the value of the branching ratio, and we could see how the shapes of the invariant mass distributions are tied to the idea of a molecular $K^*\bar{K} - cc$ nature for the $f_1(1285)$. Though an experimental measure of these distributions would be useful to complete the puzzle, we can safely say that the study of these three decays corroborates the assumption of a dynamically generated nature for the f_0, a_0 and $f_1(1285)$.

5. **Interaction of mesons with charm and beauty and possible molecular Z_c and Z_b states.**
In **Chapter** 6, we studied in detail different possible sources of $D\bar{D}^*$, $D^*\bar{D}^*$, $B\bar{B}^*$ and $B^*\bar{B}^*$ interaction in isospin $I = 1$, in an attempt to put some order among some new Z states observed at different facilities and interpret them from the molecular point of view. Using the extension of the hidden gauge symmetry together with constraints of heavy quark spin symmetry for a more precise evaluation of the couplings, we found interesting results:

   - in the $D\bar{D}^*$ interaction, the dominant process is vector exchange. In our theoretical approach based on chiral unitary theory, we clearly found a peak with mass between $3869 - 3875$ MeV, a weakly bound state decaying to $\eta_c\rho$ and $\pi J/\psi$. Moreover, its energy and width are perfectly compatible with the reanalysis we made of BESIII experimental data for the $D\bar{D}^*$ distribution in the $e^+e^- \to \pi^\pm(D\bar{D}^*)^\mp$ reaction, though slightly lower than predicted by the experimentalists. Still, we cannot infer that this state can be identified with the others observed at other facilities, like the $Z_c(3900)$, $Z_c(3894)$ or $Z_c(3886)$, due to the large uncertainties on the masses. However, while a state with energy below the $D\bar{D}^*$ threshold can be easily accommodated

into the molecular picture, that would not be the case for a state with higher mass. Further investigations are needed to unravel the issue.

- as before, also in the case of $D^*\bar{D}^*$ the major contribution comes from vector exchange. We find a peak with a mass between 3990 and 4000 MeV, considering uncertainties, and with quantum numbers $J^{PC} = 2^{++}$ and $I^G = 1^-$, corresponding to a resonance able to explain BESIII experimental observation from the perspective of the reanalysis of the data made by Torres *et al.*
- in the case of the $B\bar{B}^*$ and $B^*\bar{B}^*$ interaction, the most important contribution comes from different sources and the vector exchange potential needs to be modified to take them into account. We found a BB^* bound state with mass in the range $10587 - 10601$ MeV that we can identify with the $Z_b(10610)$. In the B^*B^* sector we find a cusp corresponding to an energy of 10650 MeV, in perfect agreement with previous theoretical findings.

6. **Decays of the $X(3872)$ and relation with its molecular nature.** In **Chapter 7** we exploit the molecular $D\bar{D}^* - cc$ picture of the $X(3872)$, considering it as a $J^{PC} = 1^{++}$ state. The novelty with respect to previous works is that we consider also the coupling to the $D_s\bar{D}_s^*$ component. We use again the extrapolation of the hidden gauge symmetry to $SU(4)$ to study in detail its decays to $J/\psi\gamma$. Once this is done, the evaluation of the decays to $J/\psi\rho$ and $J/\psi\omega$ is straightforward, since one only has to remove the photon leg from the diagrams describing the process. We find good agreement with experiment for the ratios of the decay widths, and also a value for their sum compatible with the upper limit for the total width of the $X(3872)$ reported in the PDG. However, apart from these results that seem to validate the idea of a molecular state, we went further in the analysis and tested the relevance of the charged component with respect to the neutral one, removing it from the calculation. The results we obtained strongly disagree with experiment, proving that including only the neutral channel in the study of these specific decays, is an incomplete way to proceed. This is in line with the discussion in **Chapter 4**: the fact that the neutral channel, due to its small binding and according to the Weinberg sum rule, is the most relevant component, in terms of probability, in the wave function does not imply that the charged one does not need to be taken into account when dealing with concrete physical reactions.

CHAPTER 9

RESUMEN

9.1 Objetivos

El propósito de esta Tesis es contribuir al extenso esfuerzo que se ha hecho, en las ultimas décadas, a fin de entender la estructura de las partículas hadrónicas, uno de los temas más importantes en física hadrónica.

En los años 50, el desarrollo de los aceleradores de partículas reveló la existencia de una gran cantidad de nuevas resonancias. La proliferación de partículas, poco después, manifestó un patrón, y un esquema de organización para describirlo se hizo necesario. Al principio, se encontró una solución generalizando el concepto de isospín con el modelo de Fermi-Yang de 1959 [6], en el que el protón y el neutrón aparecen como bloques fundamentales y las otras partículas como sus combinaciones. Más tarde, Sakata extendió el modelo de $SU(2)$ a $SU(3)$ incluyendo la Λ como componente.

Sin embargo, el momento crucial fue en 1961, cuando Gell-Mann [9] e, independientemente, Ne'maan [10] propusieron un esquema basado en $SU(3)$, en el que todas las partículas están agrupadas en octetes, la entidad básica del modelo conocido como *eightfold way*.

La idea de la existencia de tres componentes fundamentales, llamados *quarks*, que constituyen todos los hadrones y capaces de explicar la clasificación en multipletes de $SU(3)$, fue propuesta separadamente por Gell-Mann [13] y Zweig [14] en 1964.

El intenso y largo debate sobre el tema llevó a una nueva teoría, llamada Cromodinámica Cuántica (QCD), la teoría de gauge que describe las interacciones fuertes de quarks y gluones. Ahora sabemos que en naturaleza hay seis tipos distintos de quarks ("up", "down", "strange", "charm", "top" y "bottom"), y que cada uno existe en tres diferentes colores (rojo, azul y verde), expresión directa de la simetría de gauge $SU(3)$ de color ($SU(3)_C$). La

QCD representa uno de los bloques fundamentales de Modelo Estándar (SM) de la Física de Partículas, siendo la componente $SU(3)$ del grupo de gauge $SU(3) \times SU(2) \times U(1)$ del SM.

Pruebas experimentales han demostrado su fiabilidad en el régimen de energías altas, donde, gracias a su carácter asintóticamente libre, la teoría de las perturbaciones puede ser aplicada de forma segura. Lamentablemente, esto no es cierto en el dominio de bajas energías, debido al aumento del valor de la constante de acoplamiento y al consecuente confinamiento de quarks y gluones en los hadrones. Es en este momento que entran en juego las teorías efectivas, capaces de tener en cuenta solo los grados de libertad relevantes a bajas energías. La teoría efectiva de QCD, llamada Chiral Perturbation Theory (χPT), se basa en una de sus simetrías fundamentales, la quiral, y proporciona las interacciones entre los estados fundamentales de mesones y bariones. En la próxima sección, abordaremos las propiedades más importantes de la χPT y discutiremos las herramientas que utilizamos en este trabajo.

9.2 Metodología

9.2.1 Teoría Quiral Perturbativa

El Lagrangiano de QCD para los tres quarks más ligeros, en el límite $m_u, m_d, m_s \to 0$ es invariante bajo simetría quiral. No obstante, esta simetría no se manifiesta en el espectro hadrónico, y la simetría quiral está rota espontáneamente al grupo $SU(3)_V$. Según el teorema de Goldstone, deberíamos encontrar un bosón de Goldstone para cada uno de los ocho generadores quirales. Aunque no exactamente sin masa, el octete de los mesones pseudoescalares ligeros (π, K, η) se identifica con los Goldstones, y sus masas físicas se interpretan como la consecuencia de la ruptura explícita de simetría debida a las masas finitas de los quarks.

La diferencia de masa que separa los pseudoescalares del resto del espectro hadrónico, hace que la cosa más natural sea construir una teoría de campo efectiva, llamada Teoría Quiral Perturbativa, que contenga únicamente estos grados de libertad.

A orden más bajo, el Lagrangiano más general invariante bajo transformaciones quirales se puede escribir como

$$\mathcal{L}_2 = \frac{f^2}{4} \langle \partial_\mu U^\dagger \partial^\mu U \rangle \,, \tag{9.1}$$

donde

$$U(\phi) = u(\phi)^2 = \exp\left(i \frac{\sqrt{2}\phi}{f} \right) \,, \tag{9.2}$$

con

$$\phi(x) = \frac{\lambda^a}{\sqrt{2}}\phi^a = \begin{pmatrix} \frac{\eta_8}{\sqrt{6}} + \frac{\pi^0}{\sqrt{2}} & \pi^+ & K^+ \\ \pi^- & \frac{\eta_8}{\sqrt{6}} - \frac{\pi^0}{\sqrt{2}} & K^0 \\ K^- & \bar{K}^0 & -\frac{2\eta_8}{\sqrt{6}} \end{pmatrix} . \tag{9.3}$$

La constante f en la Eq. (9.2) es la constante de desintegración del pion, $f = 93$ MeV. Expandiendo $U(\phi)$ en potencias de ϕ, se obtiene un término cinético más interacciones que involucran un número siempre mayor de mesones pseudoescalares,

$$\mathcal{L}_2 = \frac{1}{2}\langle \partial_\mu \phi \, \partial^\mu \phi \rangle + \frac{1}{12f^2}\langle (\phi \overset{\leftrightarrow}{\partial_\mu} \phi)(\phi \overset{\leftrightarrow}{\partial^\mu} \phi) \rangle + \mathcal{O}(\phi^6/f^4) \, . \tag{9.4}$$

Es importante subrayar que todas las interacciones entre los Goldstones están fijadas por la única constante de acoplamiento, f.

La χPT es una herramienta muy poderosa a energías bajas. Lamentablemente, siendo una expansión perturbativa, no hay manera de reproducir resonancias, ya que están asociadas a polos en la amplitud de scattering. Además, otra desventaja de la teoría es la pérdida de poder de predicción yendo a ordenes más altos, debido al rápido aumento de los parámetros libres. Por lo tanto, fue necesario desarrollar métodos no-perturbativos capaces de extender el rango de validez de la teoría sin reducir su poder de predicción.

Enfoques distintos e independientes se han usado con éxito para describir la interacción mesón-mesón incluyendo resonancias, como el Inverse Amplitude Method (IAM), la ecuación de Bethe-Salpeter (BS) y el método N/D. El de la ecuación de Bethe-Salpeter es el método que utilizamos en esta Tesis y que vamos a resumir en la próxima sección.

9.2.2 Métodos no-perturbativos: la ecuación de Bethe-Salpeter

El punto de partida de la discusión es el Lagrangiano estándar de la χPT a orden más bajo, $\mathcal{L}_2$, ya que contiene las interacciones más generales entre los mesones del octete pseudoescalar. Las amplitudes que se derivan de este Lagragiano constituyen los potenciales que se usarán en la ecuación de scattering en canales acoplados: la ecuación de Lippmann-Schwinger o de Bethe-Salpeter según se use o no un propagador relativista.

Por ejemplo, en el caso sencillo de sólo dos canales acoplados, las ecuaciones de scattering tienen la forma

$$\begin{aligned} T_{11} &= V_{11} + V_{11}G_{11}T_{11} + V_{12}G_{22}T_{21} \, , \\ T_{21} &= V_{21} + V_{21}G_{11}T_{11} + V_{22}G_{22}T_{21} \, , \\ T_{22} &= V_{22} + V_{21}G_{11}T_{12} + V_{22}G_{22}T_{22} \, , \end{aligned} \tag{9.5}$$

con

$$G_{ii} = i\frac{1}{q^2 - m_{1i}^2 + i\epsilon}\frac{1}{(P-q)^2 - m_{2i}^2 + i\epsilon}\,, \tag{9.6}$$

donde P es el cuadrimomento total del sistema mesón-mesón. El término VGT en la Eq. (9.5) representa

$$VGT = \int \frac{dq^4}{(2\pi)^4} V(k,p,q)G(P,q)T(q,k',p')\,. \tag{9.7}$$

El loop en la Eq. (9.7) está regularizado usando un cutoff q_{max}. Este parámetro es el único grado de libertad del modelo y está fijado por los datos experimentales.

En principio, V y T en la Eq. (9.7) se deberían tomar off shell, pero, como se demuestra en [30], sólo las informaciones on shell son necesarias. Esto implica que T y V se pueden factorizar fuera de la integral. La integración en dq^0 se puede hacer analíticamente de manera que las ecuaciones en canales acoplados se puedan ahora escribir como

$$T_{ij} = V_{ij} + V_{il}\,G_{ll}\,T_{lj}\,, \tag{9.8}$$

con

$$G_{ll} = \int_0^{q_{max}} \frac{dq}{(2\pi)^2}\,\frac{q^2\,(\omega_1+\omega_2)}{\omega_1\,\omega_2\,(s-(\omega_1+\omega_2)^2+i\epsilon)}\,. \tag{9.9}$$

En las Eqs. (9.8) y (9.9), $s = P^{02}$ es la energía del centro de masa del sistema mesón-mesón, $\omega_i = \sqrt{q^2+m_i^2}$ y el subíndice $i = 1,2$ representa las dos partículas intermedias en el canal l. En forma matricial, la Eqs. (9.8) viene dada por

$$T = V + VGT\,, \tag{9.10}$$

o, equivalentemente, por

$$T = [1 - VG]^{-1}\,V\,. \tag{9.11}$$

Esta es la ecuación de Bethe-Salpeter en forma matricial, que utilizamos en todo este trabajo para calcular las amplitudes de scattering.

La función de loop G en la Eq. (9.9) se puede también expresar, en regularización dimensional [41], como

$$\begin{aligned} G_{ll} &= \frac{1}{16\pi^2}(\alpha_j(\mu) + \log\frac{m_1^2}{\mu^2} + \frac{m_2^2 - m_1^2 + s}{2s}\log\frac{m_2^2}{m_1^2} \\ &+ \frac{p}{\sqrt{s}}(\log\frac{s - m_2^2 + m_1^2 + 2p\sqrt{s}}{-s + m_2^2 - m_1^2 + 2p\sqrt{s}} \\ &+ \log\frac{s + m_2^2 - m_1^2 + 2p\sqrt{s}}{-s - m_2^2 + m_1^2 + 2p\sqrt{s}})\,. \end{aligned} \tag{9.12}$$

La equivalencia entre las dos prescripciones está demostrada en Ref. [33]. En la Eq. (9.12), p es el trimomento de los mesones en el centro de masa

$$p = \frac{\sqrt{(s-(m_1+m_2)^2)(s-(m_1-m_2)^2)}}{2\sqrt{s}} = \frac{\lambda^{1/2}(s,m_1^2,m_2^2)}{2\sqrt{s}}\,, \tag{9.13}$$

μ es la escala arbitraria de regularización y λ es la función de Källén.

9.2.3 Polos y acoplamientos

La identificación de una resonancia procede por medio de su asociación a un polo de la matriz de scattering. Según la teoría de scattering, los estados ligados corresponden a polos con $\mathrm{Im}(p) > 0$ y $\mathrm{Re}(p) = 0$, es decir el eje s real por debajo del menor umbral. Por otra parte, las resonancias aparecen para $\mathrm{Im}(p) < 0$ y $\mathrm{Re}(s)$ encima del umbral más bajo, una zona del plano s complejo llamada segunda hoja de Riemann de la función $T(s)$. Si estos polos no están demasiado lejos del eje real, sus partes imaginarias se pueden identificar con la mitad de la anchura Γ.

Llamamos la amplitud en la segunda hoja de Riemann

$$T^{II} = [1 - VG^{II}]^{-1}\, V\,, \tag{9.14}$$

donde G^{II}, la función de loop extrapolada a la segunda hoja de Riemann, viene dada por la ecuación

$$G^{II}_{jj}(\sqrt{s}) = G^{I}_{jj}(\sqrt{s}) + i\frac{p}{4\pi\sqrt{s}}\,, \qquad \mathrm{Im}(p) > 0\,, \tag{9.15}$$

con $G^{I}_{jj}(\sqrt{s})$ dada por la Eq. (9.12).

Esta ecuación nos permite evaluar las amplitudes de scattering y buscar resonancias de manera sistemática. En este trabajo, consideramos *dinámicamente generadas* aquellas resonancias que aparecen como polos en la segunda hoja de Riemann de la amplitud de scattering en la Eq. (9.11), usando $G^{II}_{jj}(\sqrt{s})$ cuando un canal está abierto ($\mathrm{Re}\sqrt{s} > m_1 + m_2$) y $G^{I}_{jj}(\sqrt{s})$ cuando $\mathrm{Re}\sqrt{s} < m_1 + m_2$.

Es también posible calcular los acoplamientos g_i del estado a los diferentes canales hadrón-hadrón recordando que, cerca del polo de la resonancia, la amplitud en el plano complejo para una transición diagonal se puede escribir como

$$T_{ii}(s) \simeq \frac{g_i^2}{s - s_R}\,, \tag{9.16}$$

donde s_R es la posición de la resonancia. Por lo tanto, los acoplamientos se pueden evaluar como los residuos en el polo de $T_{ii}(s)$, usando la fórmula

$$\int_0^{2\pi} T_{ii}(z(\theta))\, i\, r\, e^{i\theta} d\theta = 2\pi i\, \mathrm{Res}(T_{ii}) = 2\pi i\, g_i^2\,, \tag{9.17}$$

con $z = z_0 + r\,e^{i\theta}$ y $z_0 = s_R$, con r tal que el circulo $z_0 + r\,e^{i\theta}$ no encierre otros polos o un umbral.

9.2.4 Formalismo de hidden gauge

El formalismo de hidden gauge es el esquema que utilizamos para implementar en la teoría efectiva partículas de spin 1 [63, 64]. Este método es ideal ya que proporciona no solo las interacciones entre vectores y pseudoescalares sino también la de los vectores entre ellos, y permite incluir los fotones en la teoría.

Las interacciones de pseudoescalares, vectores y fotones se pueden describir con las siguientes fórmulas:

$$\mathcal{L}_{V\gamma} = -M_V^2 \frac{e}{g} A_\mu \langle V^\mu Q \rangle \,, \tag{9.18}$$

$$\mathcal{L}_{VPP} = -ig\ \langle V^\mu [\phi, \partial_\mu \phi] \rangle \,, \tag{9.19}$$

$$\mathcal{L}_{PPPP} = -\frac{1}{8f^2} \langle [\phi, \partial_\mu \phi]^2 \rangle \,. \tag{9.20}$$

$$\mathcal{L}_{VVP} = \frac{G}{\sqrt{2}} \epsilon^{\mu\nu\alpha\beta} \langle \partial_\mu V_\nu \partial_\alpha V_\beta P \rangle \ . \tag{9.21}$$

La matriz V es la matriz de $SU(3)$ que contiene los mesones vectoriales

$$V_\mu = \begin{pmatrix} \frac{\omega}{\sqrt{2}} + \frac{\rho^0}{\sqrt{2}} & \rho^+ & K^{*+} \\ \rho^- & \frac{\omega}{\sqrt{2}} - \frac{\rho^0}{\sqrt{2}} & K^{*0} \\ K^{*-} & \bar{K}^{*0} & \phi \end{pmatrix}_\mu \,, \tag{9.22}$$

mientras $Q = \mathrm{diag}(2, -1, -1)/3$, $e = -|e|$ es la carga del electrón y A_μ es el campo del fotón. En la Eq. (9.21), $G = 3M_V^2/16\pi^2 f^3$ y $\epsilon^{\mu\nu\alpha\beta}$ es el tensor totalmente antisimétrico. Además de estas interacciones hay también el vértice de cuatro vectores dado por

$$\mathcal{L}^{(c)} = \frac{g^2}{2} \langle V_\mu V_\nu V^\mu V^\nu - V_\nu V_\mu V^\mu V^\nu \rangle \,, \tag{9.23}$$

y el vértice de tres vectores

$$\mathcal{L}^{(3V)} = ig \langle (\partial_\mu V_\nu - \partial_\nu V_\mu) V^\mu V^\nu \rangle \,. \tag{9.24}$$

El Lagrangiano $\mathcal{L}^{(3V)}$ produce la interacción $VV \to VV$ por medio del intercambio de un mesón vectorial.

9.3 Resultados y conclusiones

En esta parte vamos a resumir los resultados que obtuvimos por medio del formalismo descrito en **Section** 9.2.

9.3.1 "Compositeness" de los estados hadrónicos: resonancias mesónicas

En el **Chapter** 3, hicimos un estudio analítico de la matriz de scattering y de las funciones de onda en el caso de la interacción entre dos hadrones. La novedad en nuestro análisis es la generalización al caso de cualquier onda parcial. Usando el formalismo de la teoría quiral unitarizada junto a la mecánica cuántica, derivamos detalladamente muchas relaciones de interés.

Empezamos con el caso de estados ligados, inicialmente para un solo canal y luego extendiendo el procedimiento a muchos canales acoplados y también a canales abiertos. Encontramos una importante relación entre el acoplamiento del estado al canal hadron-hadron considerado y la función de onda en el origen. De especial relevancia es la regla de suma, o *Weinberg compositeness condition*,

$$\sum_i g_i^2 \left[\frac{dG_i}{dE}\right]_{E=E_P} = -1\,, \tag{9.25}$$

con E_P la posición del polo complejo y donde g_i es el acoplamiento al canal i, definido como

$$g_i g_j = \lim_{E\to E_P} (E - E_P) t_{ij}\,. \tag{9.26}$$

En el caso de estados ligados, la regla de suma tiene una interpretación inequívoca, ya que se deduce directamente de la condición de normalización de la función de onda. Cada término representa la probabilidad de encontrar una determinada componente hadron-hadron en la función de onda y, cuando la suma de estas probabilidades es uno, podemos decir que el estado considerado es un estado compuesto. Su diferencia de uno nos da la probabilidad que haya algo distinto en la función de onda, como, por ejemplo, una componente genuina de naturaleza no molecular. Al contrario, el caso de canales abiertos es más controvertido, dado que no existe una renormalización para la función de onda. Sin embargo, la regla de suma sigue siendo válida en el polo de la resonancia.

La compositeness condition se puede utilizar para extraer importantes informaciones sobre la naturaleza de las resonancias utilizando los datos experimentales. En particular, la aplicamos a dos casos concretos: los mesones ρ y K^*, para hacer una estimación de sus componentes de $\pi\pi$ y πK respectivamente. En primer lugar, calculamos sus acoplamientos a las componentes

moleculares usando el potencial quiral a nivel árbol. Los polos correspondientes a la posición de la resonancia en el plano complejo se obtuvieron con un fit del modelo a los datos de phase-shift y, junto a los acoplamientos, fueron utilizados para evaluar la cantidad de carácter compuesto en el estado, que resulta ser muy pequeña en ambos casos. Aplicamos también un método fenomenológico, basado exclusivamente en la relación entre acoplamientos y masa y anchura de las partículas, para corroborar estos resultados. Los valores que obtuvimos para polos y acoplamientos son perfectamente consistentes con los anteriores y, también en este caso, el carácter molecular de las resonancias es muy pequeño, de acuerdo con la idea comúnmente aceptada que los mesones ρ y K^* no son dinámicamente generados por la interacción de dos mesones.

9.3.2 Aplicación de la regla de suma a los bariones y su interpretación

En el **Chapter** 4 aplicamos la regla de suma generalizada al decuplete de la $\Delta(1232)$ para estimar su carácter mesón-barión. Es interesante notar que, con ambos métodos utilizados, llegamos a un valor para la posición del polo de la $\Delta(1232)$ en muy buen acuerdo con el PDG [17]. La componente hadron-hadron que encontramos es considerable, alrededor del 60%. A continuación, extendimos el procedimiento a todo el decuplete y pudimos constatar que la componente molecular decrece yendo a estados de energía más alta, indicando que la $\Sigma(1385)$ y la $\Xi(1535)$ se describen mejor con una componente genuina. En el caso de la Ω^-, donde solo está presente el canal cerrado $\bar{K}\Xi$, estimamos un carácter molecular bastante pequeño, del orden del 25%. Lo que encontramos nos sugiere que, en el momento de hacer cálculos realistas de las propiedades de la $\Delta(1232)$, se tenga en cuenta la importante nube mesón-barión en su función de onda.

Sucesivamente, clarificamos el significado de la generalización de la compositeness condition en el caso de resonancias, formulando una interpretación en el caso de energías complejas. Pudimos ver que $-g^2 \frac{\partial G_{II}}{\partial E}$ mide $\int d^3p \, \langle \vec{p} \, | \Psi \rangle^2$, en vez de $\int d^3p \, |\langle \vec{p} \, | \Psi \rangle|^2$ como en el caso de estados ligados. Por lo tanto, el concepto de probabilidad se sustituye por el cuadrado de la función de onda. Integrando su parte real, se obtiene una cantidad natural para proporcionar una medida de la relevancia de un canal abierto en la función de onda, ya que la integral del módulo cuadrado es divergente. Por otra parte, $\int d^3p \, \langle \vec{p} \, | \Psi \rangle^2$ no diverge, y la suma de estas cantidades para diferentes canales acoplados es uno, en una determinada convención de fase, como muestra la regla de suma de Weinberg.

Dimos también una interpretación de los términos de la regla de suma para un potencial dependiente de la energía. En el caso de un conjunto completo de

canales acoplados que genere un determinado estado ligado, podemos truncar el espacio y definir un potencial dependiente de la energía en un espacio de dimensión inferior. Por lo tanto, la probabilidad Z que el estado se solape con la parte eliminada del espacio está relacionada con la derivada del potencial con respecto a la energía.

Extendimos el análisis a la $\Lambda(1520)$ para cuantificar sus componentes $\pi\Sigma^*$, $K\Xi^*$ (en onda-d) y $\bar{K}N$, $\pi\Sigma$ (en onda-s). Obtuvimos la amplitud de scattering implementando las técnicas de chiral unitary approach, donde algunos parámetros desconocidos se fijaron con un fit a los datos de scattering $\bar{K}N$ and $\pi\Sigma$. La dependencia del momento proveniente de los canales en onda-d se puede incorporar en la función de loop. Entonces, es posible calcular los términos de la regla de suma, que proporcionan una medida del peso de los diferentes canales en la función de onda, y también la misma suma total.

Mientras el acoplamiento más grande es al canal $\pi\Sigma^*$, el peso más grande en la función de onda pertenece al canal $\bar{K}N$. Esto podría parecer una contradicción, pero las dos cantidades representan conceptos distintos. En efecto, el acoplamiento estima la función de onda en el origen en el caso de onda-s, mientras que el término de la regla de suma, X_i representa la probabilidad de encontrar ese canal.

Explicamos también que el peso muy relevante obtenido para los canales abiertos es consecuencia de la contribución de la integral del cuadrado de la función de onda a distancias más grandes que en el caso de estados ligados, y no constituye una medida de la contribución del canal en diferentes procesos, la mayoría de los cuales son sensibles a distancias pequeñas. El valor de los acoplamientos y la dinámica específica de esos procesos es lo que por último determina la relevancia de cada canal.

9.3.3 Loops triangulares $K\bar{K}$ y rotura de la simetría de isospín

En el **Chapter** 5 calculamos las tasas de desintegración de las reacciones $\eta(1405) \to \pi^0 f_0(980)(\pi^+\pi^-)$ y $\eta(1405) \to \pi^0 a_0(980)(\pi^0\eta)$, con el objetivo de analizar la violación de isospín en el primer proceso. Este fenómeno está relacionado con lo que otros autores llaman $f_0(980)$-$a_0(980)$ mixing. Nosotros preferimos no adoptar esta terminología, ya que en nuestro formalismo no hay transiciones de una resonancia a otra. Por otro lado, lo que se verifica es una producción simultánea de las dos, debida a la violación de isospín que se produce en el momento de utilizar estados mesónicos en la base de la carga.

Siendo ambas resonancias generadas por la interacción de parejas de mesones, el proceso procede por medio de un primer paso en el que se produce un π^0 y una pareja de pseudoescalares y un segundo paso en el que esta pareja de

mesones interacciona. Entonces, hay dos fuentes de violación de isospín: el primer loop después de la producción y la matriz de scattering mesón-mesón. En ambos casos, la violación está relacionada con la diferencia entre las masas de los kaones neutros y cargados. La consecuencia es que la forma del pico que se obtiene para la producción de $\pi^+\pi^-$ en la primera reacción tiene una anchura muy pequeña, del orden de esta diferencia de masas (9 MeV). Esto es directa consecuencia de nuestro formalismo y está perfectamente de acuerdo con las observaciones experimentales.

En la primera parte del capítulo, no usamos ningún modelo explícito para la reacción, sino que asumimos que la producción de $\pi^0 PP$ sea dada por un término de contacto. Con esta asunción, obtuvimos una razón entre la tasa de producción de $\pi^+\pi^-$ frente a $\pi^0\eta$, del orden del 1%. Este resultado está de buen acuerdo con el mixing de $f_0(980)$ y $a_0(980)$ obtenido por el experimento BES en las reacciones $J/\psi \to \phi\pi\eta$ y $\chi_{c1} \to \pi^0\pi\pi$ [164] y también con previsiones teóricas [161, 162]. Sin embargo, es un orden de magnitud más pequeño que el resultado experimental [165] para $\eta(1405) \to \pi^0 f_0(980)(\pi^+\pi^-)$. Tratamos de entender la situación suponiendo una mezcla importante de $I = 1$ en la función de onda de la $\eta(1405)$, pero una componente tan grande de $I = 1$ no es fácilmente aceptable ya que llevaría a una señal para la producción de la $f_0(980)$ con una anchura de aproximadamente 20 MeV, mucho mayor que la experimental.

En la segunda parte, seguimos el método en Ref. [166] usando el mecanismo de producción dado por $\eta' \to K^*\bar{K}$ y seguido por $K^* \to K\pi$. El primer loop, ahora, es bastante distinto de lo que vimos en el caso de la interacción de contacto, ya que la nueva singularidad asociada a $\eta' \to K^*\bar{K}$ juega un papel esencial en la reacción. La consecuencia del uso de este mecanismo es un aumento de un orden de magnitud de la razón $\Gamma(\pi^0, \pi^+\pi^-)/\Gamma(\pi^0, \pi^0\eta)$, que lleva a un resultado muy parecido al experimental. Estos resultados confirman los argumentos de los autores en Ref. [166], donde, en cambio, no era posible determinar la razón con precisión, debido a unos factores de forma desconocidos necesarios para regularizar los loop divergentes. El uso del chiral unitary approach en nuestro trabajo soluciona el problema de manera natural, ya que nos permitió asociar el cutoff para regularizar el nuevo loop al que se utiliza en el scattering de mesón-mesón para generar dinámicamente la $f_0(980)$ y $a_0(980)$. Gracias a eso, pudimos hacer previsiones cuantitativas para $\Gamma(\pi^0, \pi^+\pi^-)/\Gamma(\pi^0, \pi^0\eta)$, con un valor de (0.16 ± 0.03), muy próximo al valor experimental de (0.179 ± 0.04).

Después, evaluamos la tasa de desintegración de $f_1(1285) \to \pi^0\pi^0\eta$, que muestra un pico prominente en la región de la resonancia $a_0(980)$. Utilizamos un esquema en el que la $f_1(1285)$ es también generada dinámicamente en la interacción de un vector con un pseudoescalar en el canal $K\bar{K}^* - cc$. Nos

beneficiamos del mismo mecanismo triangular usado en el caso de la $\eta(1405)$ y encontramos una tasa de desintegración de la $f_1(1285)$ del orden de 20%, de acuerdo cualitativo con el resultado experimental. Al mismo tiempo, evaluamos la tasa de desintegración de $f_1(1285) \to \pi^0\pi^+\pi^-$ explotando el mismo mecanismo. Este último proceso, en principio, estaría prohibido por la conservación de isospín y daría cero en nuestro esquema si consideráramos masas iguales para los kaones neutros y cargados. Cuando usamos las masas físicas, se produce una leve violación de isospín y encontramos un pico, aunque de baja intensidad, en la región de la $f_0(980)$. Una vez más, la anchura del pico es muy estrecha, como en el caso de $\eta(1405) \to \pi\pi\eta$. Estas previsiones fueron confirmadas por un reciente experimento de BESIII [194] y, como en el caso anterior, la distribución de masa invariante para el estado final $\pi^0\pi^+\pi^-$ no refleja la anchura natural de la $f_0(980)$ sino simplemente la región donde la diferencia entre las masas físicas de los kaones es más apreciable comparada con sus masas. También la forma obtenida es parecida a la del caso de las reacciones $\eta(1405) \to \pi^0\pi^+\pi^-$ y $J/\psi \to \phi\pi^0\eta$, pero la ruptura de simetría de isospín es bastante distinta de la de estos dos procesos. Sin embargo, el valor de 1% que obtenemos para la violación de isospín es compatible con el resultado reportado en Ref. [194].

Considerado todo esto, podemos concluir que, en nuestro formalismo , el concepto de $f_0(980)$-$a_0(980)$ mixing no es apropiado: esta cantidad es muy distinta en distintas reacciones y preferimos hablar de violación de isospín, algo estrictamente ligado a la naturaleza de los procesos estudiados. La habilidad del chiral unitary approach para describir estos procesos da apoyo a la idea que las resonancias $f_0(980)$, $a_0(980)$ y $f_1(1285)$ sean básicamente estados moleculares.

La última parte del capítulo se dedicó al cálculo de la tasa de desintegración de $f_1(1285) \to \pi K\bar{K}$. Consideramos antes el nivel árbol y luego incluimos las interacciones de estado final de $K\bar{K} \to K\bar{K}$ y $\pi K \to \pi K$, en las que el loop triangular juega un papel fundamental. Los resultados que obtuvimos son compatibles con el valor experimental dentro de las incertidumbres. Vimos también que las distribuciones de masa invariante de $f_1(1285) \to \pi K\bar{K}$ tienen una forma que está relacionada con la asunción de estado molecular que hicimos sobre la $f_1(1285)$. Su observación experimental proporcionaría valiosa información sobre la naturaleza de esta resonancia.

9.3.4 Hidden charm and hidden bottom states

En el **Chapter** 6 estudiamos las interacciones $D\bar{D}^*$, $D^*\bar{D}^*$, $B\bar{B}^*$ y $B^*\bar{B}^*$ en $I = 1$ usando la extensión al sector pesado del local hidden gauge approach.

Empezamos con un estudio combinado de un estado Z_c de $I = 1$ alrededor

de 3900 MeV, observado en muchos experimentos. Por otro lado, usamos el hidden gauge approach para estudiar las interacciones $D\bar{D}^*$ y $\bar{D}D^*$ en canales acoplados. Las restricciones de heavy quark spin symmetry muestran que los términos dominantes en otros procesos, como en $I = 0$, debidos al intercambio de mesones ligeros, ahora están prohibidos. Entonces, consideramos términos subdominantes que vienen del intercambio de vectores pesados o de dos piones. Encontramos que esta última contribución es bastante pequeña en comparación con el intercambio de vectores pesados y su efecto se puede incluir en las incertidumbres de los resultados. Obtuvimos un estado con masa en el rango $3869 - 3875$ MeV y anchura alrededor de 40 MeV con $I = 1$ y G-paridad positiva. Este estado, en nuestro formalismo, es un partner de isospín de la $X(3872)$.

Luego, hicimos un nuevo análisis del experimento de Ref. [291] en la reacción $e^+e^- \to \pi^\pm(D\bar{D}^*)^\mp$. El equipo experimental extrajo una masa de 3885 MeV y una anchura de $25 \pm 3 \pm 11$ MeV de un aumento en la masa invariante de $D\bar{D}^*$ alrededor del umbral. Nuestro análisis llevó a una solución bastante parecida, con una masa de 3875 MeV y una anchura de 30 MeV.

Por lo tanto, el presente trabajo muestra que los datos de Ref. [291] son compatibles con una masa levemente más baja, como obtuvimos a nivel teórico. Esto implica que los resultados reportados aquí ofrezcan una explicación natural del estado anunciado en Ref. [291] en términos de un estado débilmente ligado de $D\bar{D}^*(\bar{D}D^*)$, que se desintegra en los canales $\eta_c\rho$ y $\pi J/\psi$.

No obstante, todavía no está claro si este estado se puede identificar con el $Z_c(3900)$ de BESIII [229], o $Z_c(3894)$ de Belle [243] o $Z_c(3886)$ de CLEO [244]. De todas formas, podemos decir que, debido a la imposibilidad de producir una resonancia encima del umbral del solo canal $D\bar{D}^*$ con un potencial independiente del energía [96], un estado de 3900 MeV no se podría fácilmente interpretar como un estado molecular $D\bar{D}^*(\bar{D}D^*)$. Por otro lado, la interpretación molecular es natural para el estado de energía inferior. Ulteriores medidas e investigaciones ayudarán a una mejor comprensión del problema.

En el estudio de la interacción $D^*\bar{D}^*$ en $I = 1$ desde el punto de vista del formalismo de hidden gauge, tuvimos en cuenta también el estado acoplado $J/\psi\rho$, que está abierto para la desintegración y es responsable de la importante anchura del estado, alrededor de 100 MeV. Como en el caso anterior, pudimos constatar que el efecto del intercambio de dos piones, con y sin interacción, es menos relevante que el intercambio de vectores pesados. El estudio llevado a cabo en esta Tesis completa el de Ref. [228], en el que el pico observado en el espectro de $D^*\bar{D}^*$ de la reacción $e^+e^- \to (D^*\bar{D}^*)^\pm\pi^\pm$, que llevó el equipo experimental a anunciar el estado $Z_c(4025)$ ($J^P = 1^+$), fue interpretado como un posible estado ligado 2^+ de $D^*\bar{D}^*$ con $I = 1$. La masa y la anchura que obtuvimos son ambas compatibles con los resultados de Ref. [228], que fueron

obtenidos por medio de un fit a los datos experimentales. Todo esto nos permite concluir que el estado que encontramos proporciona una explicación de los resultados experimentales de Ref. [213]. Es posible identificar la observación experimental con una resonancia, pero con energía $(3990 - 4000$ MeV), anchura (100 MeV) y números cuánticos ($I^G = 1^-$, $J^{PC} = 2^{++}$) diferentes.

En el caso de las interacciones $B\bar{B}^*$ y $B^*\bar{B}^*$ en isospín $I = 1$, a diferencia de los dos casos anteriores, el potencial para el intercambio de vectores pesados no es la fuente más relevante de la interacción. Por eso, corregimos este potencial por medio de un factor multiplicativo para que se tuvieran en cuenta las contribuciones de los otros intercambios de mesones. Luego, utilizamos este potencial eficaz como kernel de la ecuación de Bethe-Salpeter para calcular la matriz de scattering T. Intentamos relacionar los polos de la matriz T con los estados $Z_b(10610)$ y $Z_b(10650)$ observados por Belle. Encontramos un estado ligado de $B\bar{B}^*$ con masa en el rango $10587 - 10601$ MeV, muy cerca de la masa experimental del $Z_b(10610)$ de 10608 MeV. En el caso de la interacción $B^*\bar{B}^*$, encontramos un cusp alrededor de 10650 MeV para $J = 0$ y $J = 2$. En el caso de spin $J = 1$, no tuvimos en cuenta el canal $\rho\,\Upsilon$ y el problema se redujo a un único canal. Una vez más encontramos un cusp de energía 10650 MeV en $|T_{11}|^2$, como ya fue señalado en Refs. [255, 256].

9.3.5 Decays of the X(3872) to $J/\psi\gamma$, $J/\psi\rho$ and $J/\psi\omega$

Por último, explotamos la idea de la $X(3872)$ como estado compuesto de $D\bar{D}^* - cc$, generado dinámicamente de la interacción de D y D^*. Volvimos a calcular los acoplamientos del estado a los diferentes canales $D\bar{D}^* - cc$ para tener en cuenta las actualizaciones de los valores de las masas de las partículas tabuladas en el PDG [17]. El acoplamiento para el canal $D^0\bar{D}^{*0} - c.c$ es parecido al que se obtendría utilizando la compositeness condition de Weinberg, ya que el estado está apenas ligado en la componente $D^0\bar{D}^{*0}$, pero la dinámica del modelo produce también acoplamientos para los canales $D^+D^{*-} - c.c$ y $D_S^+D_S^{*-} - c.c$.

Utilizando una extensión a $SU(4)$ del formalismo de hidden gauge, con una ruptura explícita de su simetría, ya usado con éxito en el estudio de otros procesos, fue posible determinar las tasas de desintegración de la $X(3872)$ yendo a $J/\psi\rho$, $J/\psi\omega$ y $J/\psi\gamma$ y compararlas con las razones determinadas experimentalmente en trabajos recientes. Obtuvimos un muy buen acuerdo entre nuestros resultados y los resultados experimentales. También los valores absolutos obtenidos para las distintas tasas de desintegración son razonables, y su suma, dentro de las incertidumbres, $(1.6^{+0.9}_{-0.7})$ MeV, es compatible con el límite superior para la anchura de la $X(3872)$ recientemente medido de $\Gamma = 1.2$ MeV.

Llevamos a cabo un test para averiguar la importancia de la componente cargada y extraña de la función de onda, dejando en el cálculo sólo la componente neutra $D^0\bar{D}^{0*} - cc$. Obtuvimos razones en gran desacuerdo con los valores experimentales y valores absolutos para las tasas de desintegración a $J/\psi\rho$ que superan en gran medida el límite superior experimental de la anchura total de la X. Este ejercicio es una confirmación de la relevancia de los canales cargados en la descripción de los procesos que consideramos y del carácter aproximadamente de $I = 0$ de esta resonancia. En cambio, esto no implica que el uso del canal neutro únicamente no sea una manera correcta de proceder, en general, sino simplemente incompleta. En una teoría de campo, los canales que faltan se pueden tener en cuenta por medio de contra-términos que, en cambio, hacen la teoría menos predictiva. En el presente caso, demostramos claramente que la consideración explícita de los canales cargados hace la teoría más predictiva que su omisión.

APPENDICES

APPENDIX **A**

WAVE FUNCTIONS IN COORDINATE SPACE

Remembering that, as we saw in **Chapter 3**, the wave function in momentum space is given by

$$\Psi(\vec{p}) = g\frac{\theta(\Lambda - p)\,|\vec{p}|}{E - \vec{p}^{\,2}/2\mu}Y_{10}(\hat{p}) \equiv \tilde{\Psi}(\vec{p})Y_{10}(\hat{p})\,, \tag{A.1}$$

where, for simplicity, we only take the spherical harmonic $Y_{10}(\hat{p})$, we move to the coordinate space writing

$$\Psi(\vec{r}) = \int \frac{d^3p}{(2\pi)^{3/2}}e^{i\vec{p}\,\vec{r}}\Psi(\vec{p})\,. \tag{A.2}$$

Integrating over the coordinate space we have

$$\begin{aligned}\int d^3r\,(\Psi(\vec{r}))^2 &= \int d^3r \int \frac{d^3p}{(2\pi)^{3/2}}e^{i\vec{p}\,\vec{r}}\Psi(\vec{p}) \int \frac{d^3p\,'}{(2\pi)^{3/2}}e^{i\vec{p}\,'\vec{r}}\Psi(\vec{p}\,') \\ &= \int d^3p \int d^3p\,'\,\Psi(\vec{p})\Psi(\vec{p}\,')\delta(\vec{p}+\vec{p}\,')\ .\end{aligned} \tag{A.3}$$

Then, due to the behaviour of the spherical harmonics under parity transformations, we have

$$\Psi(\vec{p}\,') = \Psi(-\vec{p}) = (-1)^l\Psi(\vec{p})\,, \tag{A.4}$$

and, for $l = 1$, we get

$$\int d^3r\,(\Psi(\vec{r}))^2 = -\int d^3p\,(\Psi(\vec{p}))^2\,. \tag{A.5}$$

Now we can define again

$$\Psi(\vec{r}) = \tilde{\Psi}(\vec{r}) Y_{10}(\hat{r}\,)\,, \tag{A.6}$$

where

$$\tilde{\Psi}(\vec{r}) = g \int_{p<\Lambda} \frac{d^3p}{(2\pi)^{3/2}}\, i\, j_1(pr) \frac{|\vec{p}\,|}{E - \vec{p}^{\,2}/2\mu}\,. \tag{A.7}$$

If we remove the factor i in $\tilde{\Psi}(\vec{r}\,)$ and call

$$\bar{\Psi}(\vec{r}) = g \int_{p<\Lambda} \frac{d^3p}{(2\pi)^{3/2}}\, j_1(pr) \frac{|\vec{p}\,|}{E - \vec{p}^{\,2}/2\mu}\,, \tag{A.8}$$

then we see that

$$\int d^3p\, (\tilde{\Psi}(\vec{p}\,))^2 = -\int d^3p\, (\bar{\Psi}(\vec{p}\,))^2\,. \tag{A.9}$$

Now we substitute the explicit expression of $j_1(x)$ in Eq. (A.9),

$$j_1(x) = \frac{\sin x}{x^2} - \frac{\cos x}{x}\,, \tag{A.10}$$

and use the symmetry of the integral, getting

$$\begin{aligned} \bar{\Psi}(\vec{r}\,) = &-2\mu g\, \frac{1}{2i}\, \frac{4\pi}{(2\pi)^{3/2}}\, \frac{1}{|\vec{r}\,|^{\,2}} \int_{-\Lambda}^{\Lambda} dp\, \frac{|\vec{p}\,|}{\vec{p}^{\,2} - 2\mu E} e^{ipr} \\ &+ 2\mu g\, \frac{1}{2}\, \frac{4\pi}{(2\pi)^{3/2}}\, \frac{1}{|\vec{r}\,|} \int_{-\Lambda}^{\Lambda} dp\, \frac{|\vec{p}\,|^2}{\vec{p}^{\,2} - 2\mu E} e^{ipr}\,. \end{aligned} \tag{A.11}$$

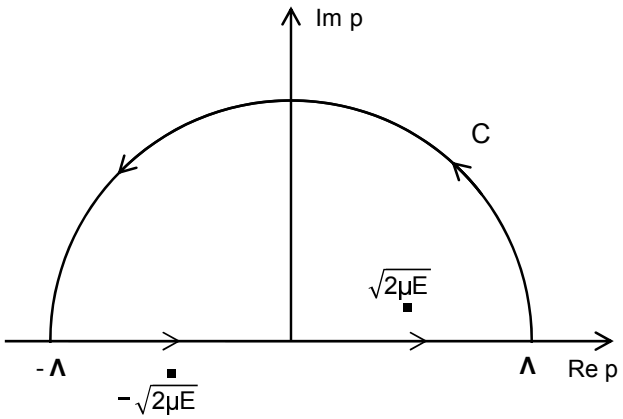

Figure A.1: Integration path in the complex p plane for the wave function.

We can perform the integration in p by integrating over the circuit in the complex plane of **Figure A.1**, and thus

$$\int_{-\Lambda}^{\Lambda} dp \ldots = 2\pi i \, Res(p = \sqrt{2\mu E}) - \int_{\mathcal{C}} dp \ldots \, . \tag{A.12}$$

The circuit picks up the pole at $p = \sqrt{2\mu E}$ and, for the first Riemann sheet, we find the result

$$\begin{aligned} \bar{\Psi}(\vec{r}) = & - \mu g \, \frac{4\pi^2}{(2\pi)^{3/2}} \, \frac{1}{|\vec{r}|^2} \, e^{i\sqrt{2\mu E}\, r} + \mu g \, \frac{4\pi^2}{(2\pi)^{3/2}} \, \frac{i}{|\vec{r}|} \sqrt{2\mu E} \, e^{i\sqrt{2\mu E}\, r} \\ & + \mu g \, \frac{4\pi}{(2\pi)^{3/2}} \, \frac{1}{|\vec{r}|^2} \int_0^{\pi} d\theta \frac{\Lambda^2 \, e^{2i\theta}}{\Lambda^2 \, e^{2i\theta} - 2\mu E} e^{i\Lambda r \cos\theta} e^{-\Lambda r \sin\theta} \\ & - \mu g \frac{4\pi}{(2\pi)^{3/2}} \frac{i}{|\vec{r}|} \int_0^{\pi} d\theta \frac{\Lambda^3 \, e^{3i\theta}}{\Lambda^2 \, e^{2i\theta} - 2\mu E} e^{i\Lambda r \cos\theta} e^{-\Lambda r \sin\theta} \, . \end{aligned} \tag{A.13}$$

To go to the second Riemann sheet we must change $\sqrt{2\mu E}$ to $-\sqrt{2\mu E}$, getting

$$\begin{aligned} \bar{\Psi}^{II}(\vec{r}) = & - \mu g \, \frac{4\pi^2}{(2\pi)^{3/2}} \, \frac{1}{|\vec{r}|^2} \, e^{-i\sqrt{2\mu E}\, r} - \mu g \, \frac{4\pi^2}{(2\pi)^{3/2}} \, \frac{i}{|\vec{r}|} \sqrt{2\mu E} \, e^{-i\sqrt{2\mu E}\, r} \\ & + \mu g \, \frac{4\pi}{(2\pi)^{3/2}} \, \frac{1}{|\vec{r}|^2} \int_0^{\pi} d\theta \frac{\Lambda^2 \, e^{2i\theta}}{\Lambda^2 \, e^{2i\theta} - 2\mu E} e^{i\Lambda r \cos\theta} e^{-\Lambda r \sin\theta} \\ & - \mu g \frac{4\pi}{(2\pi)^{3/2}} \frac{i}{|\vec{r}|} \int_0^{\pi} d\theta \frac{\Lambda^3 \, e^{3i\theta}}{\Lambda^2 \, e^{2i\theta} - 2\mu E} e^{i\Lambda r \cos\theta} e^{-\Lambda r \sin\theta} \, . \end{aligned} \tag{A.14}$$

As we can see, for large values of r the integrals over the half circle in **Figure A.1** are strongly suppressed by the factor $e^{-\Lambda r \sin\theta}$ ($\theta \in [0, \pi]$), which makes these integrals vanish when $r \to \infty$.

Then, the dominant term for $r \to \infty$ is given by

$$\bar{\Psi}^{II}(\vec{r}) \simeq -i \frac{1}{r} \sqrt{2\mu E} \, e^{-i\sqrt{2\mu E}\, r} \, , \tag{A.15}$$

which has been used in the discussion in **Section 4.4**.

APPENDIX B

S-WAVE $PV \to P'V'$ TREE LEVEL AMPLITUDES IN THE BOTTOM SECTOR

The matrix in Eq. (6.9) contains the coefficients C_{ij} for the $PV \to P'V'$ transition amplitudes in the bottom sector. Here we show how they are evaluated by means of the hidden gauge approach.

We choose as an example the $(B\bar{B}^* + cc)/\sqrt{2} \to \eta_c \rho$ transition. The diagrams contributing to the process are shown in **Figure B.1**. We only consider the contributions from the t-channel and neglect the ones coming from the channels s and u due to the presence of anomalous VVP vertices that lead to suppressions. Moreover, we evaluate in detail only the amplitude of the first diagram of **Figure B.1**, being the procedure for the others completely analogous.

We start from the vertices appearing in the diagram. Using the hidden gauge Lagrangian of Eq. (2.92) we obtain, for the $B^0 B^{*0} \eta_c$ vertex,

$$t_{VPP} = -g\epsilon_V^\mu (k + k')_\mu \ , \tag{B.1}$$

where ϵ_V is the polarization four-vector of the exchanged B^{*0} vector meson. For the $\bar{B}^{*0} B^{*0} \rho^0$ vertex we can use Eq. (2.96), leading to

$$t_{VVV} = -\frac{g}{\sqrt{2}} \epsilon^\mu \epsilon'_\mu \epsilon_V^\nu (p + p')_\nu \ , \tag{B.2}$$

with ϵ and ϵ' the polarization four-vectors of the initial and final vector meson, respectively.

From the two vertices we can derive the amplitude of the diagram,

$$t_{B^0 \bar{B}^{*0} \to \eta_c \rho^0} = -\frac{g}{\sqrt{2} M_{B^{*0}}^2} \vec{\epsilon} \cdot \vec{\epsilon}\,' (k + k') \cdot (p + p') \ , \tag{B.3}$$

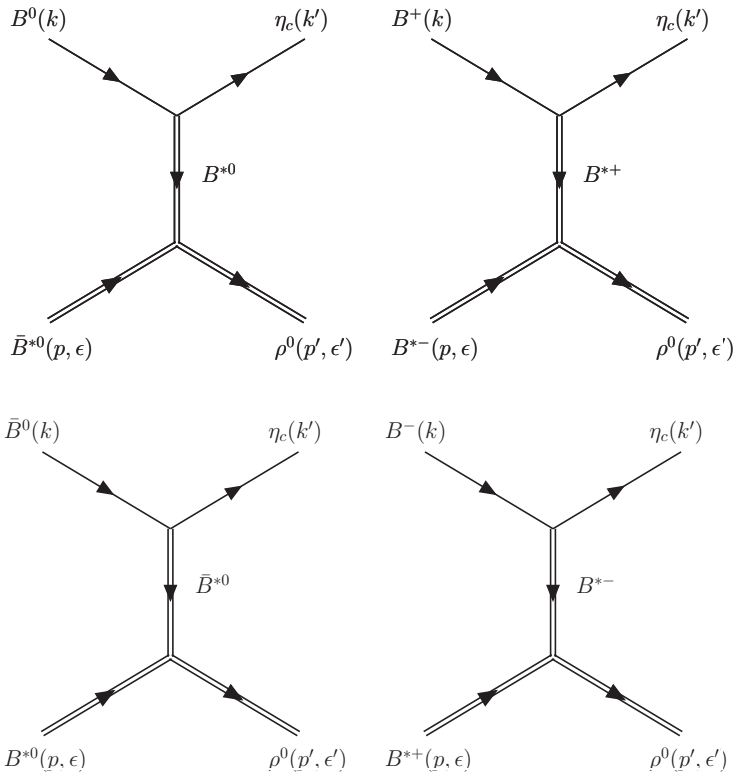

Figure B.1: Feynman diagrams for the $(B\bar{B}^* + cc)/\sqrt{2} \to \eta_c\rho$ interaction via vector exchange.

where we have approximated the propagator of the B^{*0} with $\frac{-i}{M^2_{B^{*0}}}$ and considered that, in the approximation of low three-momenta of the external vectors compared to their masses, the zero'th components of the polarization vectors ϵ and ϵ' are negligible, which implies $\epsilon^\mu \epsilon'_\mu \simeq -\vec{\epsilon}\cdot\vec{\epsilon}\,'$.

We are interested in the $I = 1$ combination of $B\bar{B}^*$ with positive G-parity, which corresponds to

$$|B\bar{B}^*\rangle^{I=1,G=+} = \frac{1}{2}(|B^0\bar{B}^{*0}\rangle - |B^+B^{*-}\rangle + |\bar{B}^0B^{*0}\rangle - |B^-B^{*+}\rangle) \ . \tag{B.4}$$

Taking it into account, the total amplitude of the process will be given by

$$\begin{aligned} t_{B\bar{B}^*\to\eta_c\rho} &= \frac{1}{2}(t_{B^0\bar{B}^{*0}\to\eta_c\rho^0} - t_{B^+B^{*-}\to\eta_c\rho^0} + t_{\bar{B}^0B^{*0}\to\eta_c\rho^0} - t_{B^-B^{*+}\to\eta_c\rho^0}) \\ &= 2t_{B^0\bar{B}^{*0}\to\eta_c\rho^0} = -\sqrt{2}\frac{g}{M^2_{B^{*0}}}\,\vec{\epsilon}\cdot\vec{\epsilon}\,'\,(k+k')\cdot(p+p') \ , \end{aligned} \tag{B.5}$$

where in the last step we used that $t_{B^+B^{*-}\to\eta_c\rho^0} = -t_{B^0\bar{B}^{*0}\to\eta_c\rho^0}$, $t_{\bar{B}^0B^{*0}\to\eta_c\rho^0} = t_{B^0\bar{B}^{*0}\to\eta_c\rho^0}$ and $t_{B^-B^*\to\eta_c\rho^0} = -t_{B^0\bar{B}^{*0}\to\eta_c\rho^0}$. Now, recalling that $g = M_V/2f$, Eq. (B.5) can be rewritten as

$$t_{B\bar{B}^*\to\eta_c\rho} = -\sqrt{2}\frac{M_V}{M^2_{B^{*0}}}\,\frac{\vec{\epsilon}\cdot\vec{\epsilon}\,'}{4f^2}\,(s-u) \ , \tag{B.6}$$

with $s = (k+p)^2 = (p'+k')^2$ and $u = (p'-k)^2 = (k'-p)^2$.

We want to project the amplitude in s-wave,

$$f_{l=0}(s) = \frac{1}{2}\int_{-1}^{1} T(s,t(x'),u(x'))P_{l=0}(x')\,dx' \ , \tag{B.7}$$

where $P_{l=0}(x)$ is the Legendre polynomial for $l = 0$ and $x = cos\theta$, with θ the scattering angle in the center of mass reference frame. In order to do that, we write u as a function of x,

$$u(x) = m'^{\,2} + M^2 - 2E(k')E(p) - 2|\vec{k}'||\vec{p}|x \ , \tag{B.8}$$

where

$$\begin{aligned} E(k') &= \frac{1}{2\sqrt{s}}(s - M'^{\,2} + m'^{\,2}), \\ E(p) &= \frac{1}{2\sqrt{s}}(s + M^2 - m^2) \ . \end{aligned} \tag{B.9}$$

Substituting Eqs. (B.8) and (B.9) in Eq. (B.5) and performing the s-wave projection we obtain

$$t_{B\bar{B}^*\to\eta_c\rho} = -\sqrt{2}\frac{M_V}{M^2_{B^{*0}}}\,\frac{\vec{\epsilon}\cdot\vec{\epsilon}\,'}{8f^2}\,[3s-(M^2+m^2+M'^{\,2}+m'^{\,2})-\frac{1}{2}(M^2-m^2)(M'^{\,2}-m'^{\,2})] \ , \tag{B.10}$$

which is exactly the expression for the potential that we have in Eq. (6.5), and

$$C_{12} = \sqrt{2}\frac{M_V^2}{M_{B^{*0}}^2} \simeq \sqrt{2}\gamma \ , \tag{B.11}$$

like in Eq. (6.9).

APPENDIX C

$VV \to V'V'$ TREE LEVEL AMPLITUDES IN THE BOTTOM SECTOR

We want to evaluate the tree level $VV \to V'V'$ transition amplitudes in the bottom sector. We start with the reaction $B^*\bar{B}^* \to B^*\bar{B}^*$. As in Ref. [214], where the authors treat the $D^*\bar{D}^*$ case, we also consider that the external vectors have negligible three-momentum with respect to their masses. The most important diagrams contributing to the exchange term of the amplitude are shown in **Figure C.1**.

As an example, we calculate in detail the amplitude of the first diagram of **Figure C.1** since the evaluation of the other ones is completely analogous. To this end, we must calculate the three-vector vertices which are given by the Lagrangian of Eq. (2.96). **Figure C.2** (a) and (b) illustrate the two vertices $B^{*+}\bar{B}^{*+}\rho^0$ and $B^{*-}\bar{B}^{*-}\rho^0$ with the momenta assignment. The corresponding vertex functions are

$$t_{B^{*+}B^{*+}\rho^0} = \frac{g}{\sqrt{2}}\epsilon_{1\mu}\epsilon_3^{\mu}(k_1+k_3)_{\nu}\epsilon_V^{\nu}\,, \tag{C.1}$$

$$t_{B^{*-}B^{*-}\rho^0} = \frac{g}{\sqrt{2}}\epsilon_{2\mu}\epsilon_4^{\mu}(k_2+k_4)_{\nu}\epsilon_V^{\nu}\,. \tag{C.2}$$

Once we have determined the vertices, it is possible to calculate the amplitude for the first diagram of **Figure C.1**. Considering all the particles involved in the exchange, we obtain

$$\begin{aligned} t_{B^{*+}B^{*-}\to B^{*+}B^{*-}} = -\frac{1}{2}g^2\left[\frac{2}{M_\Upsilon^2} - \frac{1}{M_\rho^2} + \frac{1}{M_\omega^2}\right]\epsilon_{1\mu}\epsilon_{2\nu}\epsilon_3^{\mu}\epsilon_4^{\nu} \\ \times\,(k_1+k_3)\cdot(k_2+k_4)\,, \end{aligned} \tag{C.3}$$

where M_Υ, M_ρ and M_ω are the masses of the Υ, ρ and ω mesons, respectively.

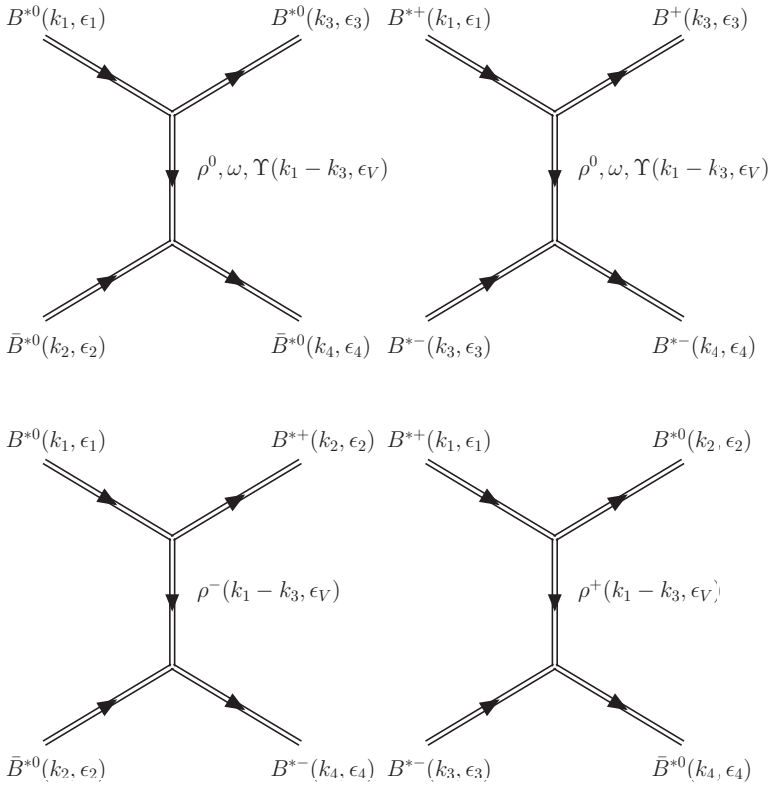

Figure C.1: Vector exchange diagrams contributing to the process $B^*\bar{B}^* \to B^*\bar{B}^*$.

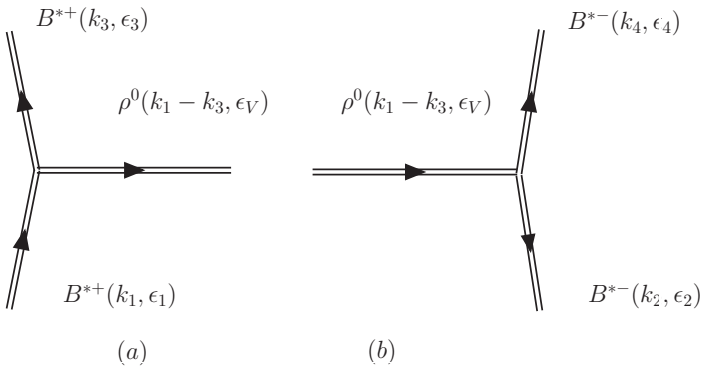

Figure C.2: Three-vector vertices associated with $B^{*+}\,B^{*+}\,\rho^0$ (a) and $B^{*-}\bar{B}^{*-}\rho^0$ (b).

Since we are interested in the $B^*\bar{B}^*$ interaction in the $I = 1$ channel, we must rewrite Eq. (C.3) in the isospin basis. The isospin states are

$$|B^*\bar{B}^*\rangle^{I=1} = -\frac{1}{\sqrt{2}}|B^{*+}\bar{B}^{*-}\rangle + \frac{1}{\sqrt{2}}|B^{*0}\bar{B}^{*0}\rangle\,,$$
$$|B^*\bar{B}^*\rangle^{I=0} = \frac{1}{\sqrt{2}}|B^{*+}\bar{B}^{*-}\rangle - \frac{1}{\sqrt{2}}|B^{*0}\bar{B}^{*0}\rangle\,.$$

Once all the four diagrams of **Figure C.1** are taken into account, we get

$$t^{I=1}_{B^*\bar{B}^*\to B^*\bar{B}^*} = g^2\left[\frac{2M_\rho^2M_\omega^2 + M_\Upsilon^2(-M_\omega^2+M_\rho^2)}{2M_\Upsilon^2M_\omega^2M_\omega^2}\right]\epsilon_{1\mu}\epsilon_{2\nu}\epsilon_3^\mu\epsilon_4^\nu \times (k_1+k_3)\cdot(k_2+k_4)\,, \tag{C.4}$$

which shows explicitly the cancellation of ρ and ω exchange in the limit of equal masses.

In order to rewrite the amplitude of Eq. (C.4) in terms of spin 0, 1 and 2 states, we use the spin projectors $\mathcal{P}^{(0)}$, $\mathcal{P}^{(1)}$ and $\mathcal{P}^{(2)}$ given by Ref. [214],

$$\begin{aligned}\mathcal{P}^{(0)} &= \frac{1}{3}\epsilon_\mu\epsilon_\mu\epsilon^\nu\epsilon^\nu\,,\\ \mathcal{P}^{(1)} &= \frac{1}{2}\left(\epsilon_\mu\epsilon_\nu\epsilon^\mu\epsilon^\nu - \epsilon_\mu\epsilon_\nu\epsilon^\nu\epsilon^\mu\right)\,,\\ \mathcal{P}^{(2)} &= \frac{1}{2}\left(\epsilon_\mu\epsilon_\nu\epsilon^\mu\epsilon^\nu + \epsilon_\mu\epsilon_\nu\epsilon^\nu\epsilon^\mu\right) - \frac{1}{3}\epsilon_\mu\epsilon_\mu\epsilon^\nu\epsilon^\mu\,,\end{aligned} \tag{C.5}$$

where the order of the particles 1, 2, 3 and 4 is implicit. In terms of those projectors the polarization vector combination $\epsilon_{1\mu}\epsilon_{2\nu}\epsilon_3^\mu\epsilon_4^\nu$ appearing in Eq. (C.4) is equal to

$$\epsilon_{1\mu}\epsilon_{2\nu}\epsilon_3^\mu\epsilon_4^\nu = \mathcal{P}^{(0)} + \mathcal{P}^{(1)} + \mathcal{P}^{(2)}. \tag{C.6}$$

Therefore, substituting Eq. (C.6) into Eq. (C.4) and projecting it in s-wave, we obtain

$$t^{I=1,S=0,1,2}_{B^*\bar{B}^*\to B^*\bar{B}^*} = g^2\left[\frac{2M_\rho^2M_\omega^2 + M_\Upsilon^2(-M_\omega^2+M_\rho^2)}{4M_\Upsilon^2M_\omega^2M_\rho^2}\right](4M_{B^*}^2 - 3s)\,, \tag{C.7}$$

where s stands for the square of the center of mass energy of the $B^*\bar{B}^*$ system.

Let us consider now the other channel, $B^*\bar{B}^* \to \rho\Upsilon$. The most relevant diagrams are depicted in **Figure C.3**. The procedure to get the amplitude for this channel is analogous to what we have done earlier. Thus, the amplitude in isospin $I = 1$ basis for the spin $S = 0$, 2 states in s-wave, corresponding to all diagrams of **Figure C.3** is given by

$$t^{I=1,S=0,2}_{B^*\bar{B}^*\to\rho\Upsilon} = g^2\left[\frac{2M_{B^*}^2 + M_\Upsilon^2 + M_\rho^2 - 3s}{M_{B^*}^2}\right]. \tag{C.8}$$

The interaction in $S = 1$ vanishes as a consequence of a cancellation of terms where the ρ^0 and Υ are interchanged in the diagrams. The diagonal $\rho\Upsilon \to \rho\Upsilon$ transition is again OZI forbidden and null in this approach.

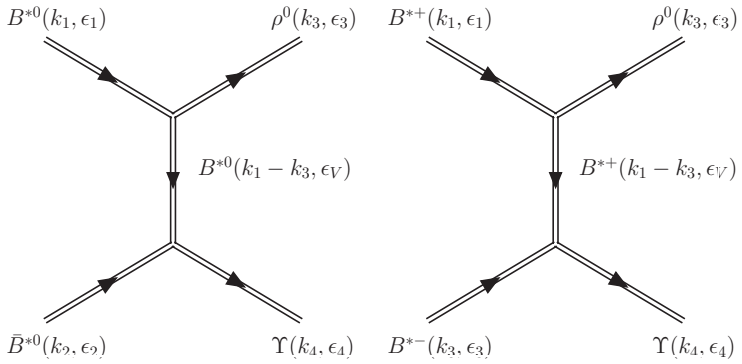

Figure C.3: Vector exchange diagrams contributing for the $B^*\bar{B}^* \to \rho\,\Upsilon$ channel.

APPENDIX D

COEFFICIENTS FOR THE DECAYS OF THE $X(3872)$ TO $J/\psi\gamma$, $J/\psi\rho$ AND $J/\psi\omega$

Diagram	P	V	P_l	B
1	D^0	$\bar{D}^{*0}$	D^0	$4/3\sqrt{2}$
	D^+	D^{*-}	D^+	$1/3\sqrt{2}$
	D_s^+	D_s^{*-}	D_s^+	$1/3\sqrt{2}$
$\bar{1}$	$\bar{D}^0$	D^{*0}	$\bar{D}^0$	$-4/3\sqrt{2}$
	D^-	D^{*+}	D^-	$-1/3\sqrt{2}$
	D_s^-	D_s^{*+}	D_s^-	$-1/3\sqrt{2}$
3	D^0	$\bar{D}^{*0}$	D^0	0
	D^+	D^{*-}	D^+	$1/\sqrt{2}$
	D_s^+	D_s^{*-}	D_s^+	$-1/\sqrt{2}$
$\bar{3}$	$\bar{D}^0$	D^{*0}	$\bar{D}^0$	0
	D^-	D^{*+}	D^-	$-1/\sqrt{2}$
	D_s^-	D_s^{*+}	D_s^-	$-1/\sqrt{2}$

Table D.1: Coefficients B of the different diagrams in **Figure 7.1** for the decay $X(3872) \to J/\psi\gamma$.

Diagram	P	V	V_l	C
2	D^0	$\bar{D}^{*0}$	D^{*0}	0
	D^+	D^{*-}	D^{*+}	$-1/\sqrt{2}$
	D_s^+	D_s^{*-}	D_s^{*+}	$1/\sqrt{2}$
$\bar{2}$	$\bar{D}^0$	D^{*0}	$\bar{D}^{*0}$	0
	D^-	D^{*+}	D^{*-}	$1/\sqrt{2}$
	D_s^-	D_s^{*+}	D_s^{*-}	$1/\sqrt{2}$
4	D^0	$\bar{D}^{*0}$	D^{*0}	$-4/3\sqrt{2}$
	D^+	D^{*-}	D^{*+}	$-1/3\sqrt{2}$
	D_s^+	D_s^{*-}	D_s^{*+}	$-1/3\sqrt{2}$
$\bar{4}$	$\bar{D}^0$	D^{*0}	$\bar{D}^{*0}$	$4/3\sqrt{2}$
	D^-	D^{*+}	D^{*-}	$1/3\sqrt{2}$
	D_s^-	D_s^{*+}	D_s^{*-}	$1/3\sqrt{2}$

Table D.2: Coefficients C of the different diagrams in **Figure 7.1** for the decay $X(3872) \to J/\psi\gamma$.

Diagram	P	V	P_l	B'
1	D^0	$\bar{D}^{*0}$	D^0	1/2
	D^+	D^{*-}	D^+	$-1/2$
$\bar{1}$	$\bar{D}^0$	D^{*0}	$\bar{D}^0$	$-1/2$
	D^-	D^{*+}	D^-	1/2
3	D^0	$\bar{D}^{*0}$	D^0	$-1/2$
	D^+	D^{*-}	D^+	1/2
$\bar{3}$	$\bar{D}^0$	D^{*0}	$\bar{D}^0$	1/2
	D^-	D^{*+}	D^-	$-1/2$

Table D.3: Coefficients B' of the different diagrams in **Figure 7.2** for the decay $X(3872) \to J/\psi\rho$.

Diagram	P	V	V_l	C'
2	D^0	$\bar{D}^{*0}$	D^{*0}	$1/2$
	D^+	D^{*-}	D^{*+}	$-1/2$
$\bar{2}$	$\bar{D}^0$	D^{*0}	$\bar{D}^{*0}$	$-1/2$
	D^-	D^{*+}	D^{*-}	$1/2$
4	D^0	$\bar{D}^{*0}$	D^{*0}	$1/2$
	D^+	D^{*-}	D^{*+}	$-1/2$
$\bar{4}$	$\bar{D}^0$	D^{*0}	$\bar{D}^{*0}$	$-1/2$
	D^-	D^{*+}	D^{*-}	$1/2$

Table D.4: Coefficients B' of the different diagrams in **Figure 7.2** for the decay $X(3872) \to J/\psi\rho$.

Diagram	P	V	P_l	B'
1	D^0	$\bar{D}^{*0}$	D^0	$1/2$
	D^+	D^{*-}	D^+	$1/2$
$\bar{1}$	$\bar{D}^0$	D^{*0}	$\bar{D}^0$	$-1/2$
	D^-	D^{*+}	D^-	$-1/2$
3	D^0	$\bar{D}^{*0}$	D^0	$-1/2$
	D^+	D^{*-}	D^+	$-1/2$
$\bar{3}$	$\bar{D}^0$	D^{*0}	$\bar{D}^0$	$1/2$
	D^-	D^{*+}	D^-	$1/2$

Table D.5: Coefficients B' of the different diagrams in **Figure 7.2** for the decay $X(3872) \to J/\psi\omega$.

Diagram	P	V	P_l	C'
2	D^0	$\bar{D}^{*0}$	D^{*0}	$1/2$
	D^+	D^{*-}	D^{*+}	$1/2$
$\bar{2}$	$\bar{D}^0$	D^{*0}	$\bar{D}^{*0}$	$-1/2$
	D^-	D^{*+}	D^{*-}	$-1/2$
4	D^0	$\bar{D}^{*0}$	D^{*0}	$1/2$
	D^+	D^{*-}	D^{*+}	$1/2$
$\bar{4}$	$\bar{D}^0$	D^{*0}	$\bar{D}^{*0}$	$-1/2$
	D^-	D^{*+}	D^{*-}	$-1/2$

Table D.6: Coefficients C' of the different diagrams in **Figure 7.2** for the decay $X(3872) \to J/\psi\omega$.

BIBLIOGRAPHY

[1] H. L. Anderson, E. Fermi, E. A. Long, and D. E. Nagle, Phys. Rev. **85**, p. 936 (1952).

[2] M. Alston, L. W. Alvarez, P. H. Eberhard, M. L. Good, W. Graziano, H. K. Ticho, and S. G. Wojcicki, Phys. Rev. Lett. **5**, 520–524 (1960).

[3] M. Alston, L. W. Alvarez, P. Eberhard, M. L. Good, W. Graziano, H. K. Ticho, and S. G. Wojcicki, Phys. Rev. Lett. **6**, 300–302 (1961).

[4] A. R. Erwin, R. March, W. D. Walker, and E. West, Phys. Rev. Lett. **6**, 628–630 (1961).

[5] B. Maglich, L. W. Alvarez, A. H. Rosenfeld, and M. L. Stevenson, Phys. Rev. Lett. **7**, 178–182 (1961), [Adv. Exp. Phys.5,106(1976)].

[6] E. Fermi and C.-N. Yang, Phys. Rev. **76**, 1739–1743 (1949).

[7] R. Cahn and G. Goldhaber, *The Experimental Foundations of Particle Physics* (Cambridgle University Press, The Edinburgh Building, Cambridge CB2 8RU, UK).

[8] S. Sakata, Prog. Theor. Phys. **16**, 686–688 (1956).

[9] M. Gell-Mann, Phys. Rev. **125**, 1067–1084 (1962).

[10] Y. Ne'eman, Nucl. Phys. **26**, 222–229 (1961).

[11] A. Pevsner *et al.*, Phys. Rev. Lett. **7**, 421–423 (1961).

[12] J.-M. Richard, "An introduction to the quark model," in *Ferrara International School Niccolò Cabeo 2012: Hadronic spectroscopy Ferrara, Italy, May 21-26, 2012* (2012).

[13] M. Gell-Mann, Phys. Lett. **8**, 214–215 (1964).

[14] G. Zweig, in *Developments in the Quark Theory of hadrons, Vol. 1. 1964 - 1978*, edited by D. Lichtenberg and S. P. Rosen (1964), pp. 22–101.

[15] D. J. Gross and F. Wilczek, Phys.Rev.Lett. **30**, 1343–1346 (1973).

[16] H. D. Politzer, Phys.Rev.Lett. **30**, 1346–1349 (1973).

[17] K. Olive *et al.* (Particle Data Group), Chin.Phys. **C38**, p. 090001 (2014).

[18] S. L. Olsen, Front. Phys. **10**, p. 101401 (2015).

[19] E. Klempt and A. Zaitsev, Phys.Rept. **454**, 1–202 (2007).

[20] E. Klempt and J.-M. Richard, Rev.Mod.Phys. **82**, 1095–1153 (2010).

[21] N. Kaiser, P. Siegel, and W. Weise, Nucl.Phys. **A594**, 325–345 (1995).

[22] E. Oset and A. Ramos, Nucl.Phys. **A635**, 99–120 (1998).

[23] L. Roca, T. Hyodo, and D. Jido, Nucl. Phys. **A809**, 65–87 (2008).

[24] S. Weinberg, Physica **A96**, p. 327 (1979).

[25] J. Gasser and H. Leutwyler, Annals Phys. **158**, p. 142 (1984).

[26] S. Weinberg, Phys.Rev. **166**, 1568–1577 (1968).

[27] G. Ecker, Prog.Part.Nucl.Phys. **35**, 1–80 (1995).

[28] V. Bernard, N. Kaiser, and U.-G. Meissner, Int. J. Mod. Phys. **E4**, 193–346 (1995).

[29] N. Kaiser, T. Waas, and W. Weise, Nucl.Phys. **A612**, 297–320 (1997).

[30] J. Oller and E. Oset, Nucl.Phys. **A620**, 438–456 (1997).

[31] N. Kaiser, Eur.Phys.J. **A3**, 307–309 (1998).

[32] J. Oller, E. Oset, and J. Pelaez, Phys.Rev. **D59**, p. 074001 (1999).

[33] J. Oller and U. G. Meissner, Phys.Lett. **B500**, 263–272 (2001).

[34] D. Jido, A. Hosaka, J. Nacher, E. Oset, and A. Ramos, Phys.Rev. **C66**, p. 025203 (2002).

[35] C. Garcia-Recio, J. Nieves, E. Ruiz Arriola, and M. Vicente Vacas, Phys.Rev. **D67**, p. 076009 (2003).

[36] C. Garcia-Recio, J. Nieves, and L. Salcedo, Phys.Rev. **D74**, p. 034025 (2006).

[37] T. Hyodo, S. Nam, D. Jido, and A. Hosaka, Phys.Rev. **C68**, p. 018201 (2003).

[38] D. Jido, J. Oller, E. Oset, A. Ramos, and U. Meissner, Nucl.Phys. **A725**, 181–200 (2003).

[39] J. Oller, E. Oset, and A. Ramos, Prog.Part.Nucl.Phys. **45**, 157–242 (2000).

[40] J. A. Oller, E. Oset, and J. R. Pelaez, Phys. Rev. Lett. **80**, 3452–3455 (1998).

[41] J. Oller and E. Oset, Phys.Rev. **D60**, p. 074023 (1999).

[42] E. Oset, A. Ramos, and C. Bennhold, Phys. Lett. **B527**, 99–105 (2002), [Erratum: Phys. Lett.B530,260(2002)].

[43] A. Ramos, E. Oset, and C. Bennhold, Phys. Rev. Lett. **89**, p. 252001 (2002).

[44] N. Kaiser, P. B. Siegel, and W. Weise, Phys. Lett. **B362**, 23–28 (1995).

[45] C. Garcia-Recio, M. F. M. Lutz, and J. Nieves, Phys. Lett. **B582**, 49–54 (2004).

[46] T. Hyodo, A. Hosaka, E. Oset, A. Ramos, and M. J. Vicente Vacas, Phys. Rev. **C68**, p. 065203 (2003).

[47] T. Hyodo, S. Sarkar, A. Hosaka, and E. Oset, Phys. Rev. **C73**, p. 035209 (2006), [Erratum: Phys. Rev.C75,029901(2007)].

[48] M. Doring, E. Oset, and S. Sarkar, Phys.Rev. **C74**, p. 065204 (2006).

[49] M. C. Birse, Z. Phys. **A355**, 231–246 (1996).

[50] M. F. M. Lutz and E. E. Kolomeitsev, Nucl. Phys. **A730**, 392–416 (2004).

[51] L. Roca, E. Oset, and J. Singh, Phys. Rev. **D72**, p. 014002 (2005).

[52] A. Faessler, T. Gutsche, S. Kovalenko, and V. E. Lyubovitskij, Phys. Rev. **D76**, p. 014003 (2007).

[53] A. Faessler, T. Gutsche, V. E. Lyubovitskij, and Y.-L. Ma, Phys. Rev. **D76**, p. 114008 (2007).

[54] C. Garcia-Recio, L. S. Geng, J. Nieves, and L. L. Salcedo, Phys. Rev. **D83**, p. 016007 (2011).

[55] F.-K. Guo, P.-N. Shen, and H.-C. Chiang, Phys. Lett. **B647**, 133–139 (2007).

[56] D. Gamermann and E. Oset, Eur. Phys. J. **A33**, 119–131 (2007).

[57] F.-K. Guo, C. Hanhart, and U.-G. Meissner, Eur. Phys. J. **A40**, 171–179 (2009).

[58] M. Altenbuchinger, L. S. Geng, and W. Weise, Phys. Rev. **D89**, p. 014026 (2014).

[59] D. Gamermann, E. Oset, D. Strottman, and M. J. Vicente Vacas, Phys. Rev. **D76**, p. 074016 (2007).

[60] A. Pich, "Effective field theory: Course," in *Probing the standard model of particle interactions. Proceedings, Summer School in Theoretical Physics, NATO Advanced Study Institute, 68th session, Les Houches, France, July 28-September 5, 1997. Pt. 1, 2* (1998), pp. 949–1049.

[61] G. Ecker, *Broken symmetries. Proceedings, 37. Internationale Universitätswochen für Kern- und Teilchenphysik*, Lect. Notes Phys. **521**, 83–129 (1999).

[62] S. Scherer and M. R. Schindler, (2005), arXiv:hep-ph/0505265 [hep-ph] .

[63] M. Bando, T. Kugo, S. Uehara, K. Yamawaki, and T. Yanagida, Phys. Rev. Lett. **54**, p. 1215 (1985).

[64] M. Bando, T. Kugo, and K. Yamawaki, Phys. Rept. **164**, 217–314 (1988).

[65] M. Harada and K. Yamawaki, Phys. Rept. **381**, 1–233 (2003).

[66] U. G. Meissner, Phys. Rept. **161**, p. 213 (1988).

[67] W. E. Burcham and M. Jobes, *Nuclear and Particle Physics* (Pearson - Prentice Hall, Edimburgh).

[68] R. J. Crewther, Phys. Lett. **B70**, p. 349 (1977).

[69] C. G. Callan, Jr., R. F. Dashen, and D. J. Gross, Phys. Lett. **B63**, 334–340 (1976).

[70] G. 't Hooft, Phys. Rev. Lett. **37**, 8–11 (1976).

[71] C. Vafa and E. Witten, Nucl. Phys. **B234**, p. 173 (1984).

[72] S. Coleman, J. Math. Phys. **7**, p. 787 (1966).

[73] J. Goldstone, Nuovo Cim. **19**, 154–164 (1961).

[74] J. Goldstone, A. Salam, and S. Weinberg, Phys. Rev. **127**, 965–970 (1962).

[75] J. Gasser and H. Leutwyler, Phys. Rept. **87**, 77–169 (1982).

[76] J. Gasser and H. Leutwyler, Nucl. Phys. **B250**, p. 465 (1985).

[77] H. W. Fearing and S. Scherer, Phys. Rev. **D53**, 315–348 (1996).

[78] T. N. Truong, Phys. Rev. Lett. **61**, p. 2526 (1988).

[79] T. N. Truong, Phys. Rev. Lett. **67**, 2260–2263 (1991).

[80] G. F. Chew and S. Mandelstam, Phys. Rev. **119**, 467–477 (1960).

[81] A. Dobado and J. R. Pelaez, Phys. Rev. **D47**, 4883–4888 (1993).

[82] H. Nagahiro, L. Roca, A. Hosaka, and E. Oset, Phys. Rev. **D79**, p. 014015 (2009).

[83] G. Ecker, J. Gasser, H. Leutwyler, A. Pich, and E. de Rafael, Phys. Lett. **B223**, p. 425 (1989).

[84] H. Nagahiro, L. Roca, and E. Oset, Eur. Phys. J. **A36**, 73–84 (2008).

[85] N. Kaiser and U. G. Meissner, Nucl. Phys. **A519**, 671–696 (1990).

[86] J. Sakurai (University of Chicago Press, Chicago, IL, 1969).

[87] E. Pallante and R. Petronzio, Nucl. Phys. **B396**, 205–242 (1993).

[88] M. F. M. Lutz and M. Soyeur, Nucl. Phys. **A813**, 14–95 (2008).

[89] H. Nagahiro, L. Roca, E. Oset, and B. S. Zou, Phys. Rev. **D78**, p. 014012 (2008).

[90] S. Ozaki, H. Nagahiro, and A. Hosaka, Phys. Lett. **B665**, 178–181 (2008).

[91] S. Weinberg, Phys.Rev. **137**, B672–B678 (1965).

[92] V. Baru, J. Haidenbauer, C. Hanhart, Y. Kalashnikova, and A. E. Kudryavtsev, Phys.Lett. **B586**, 53–61 (2004).

[93] C. Hanhart, Y. Kalashnikova, and A. Nefediev, Phys.Rev. **D81**, p. 094028 (2010).

[94] D. Gamermann, J. Nieves, E. Oset, and E. Ruiz Arriola, Phys.Rev. **D81**, p. 014029 (2010).

[95] T. Hyodo, D. Jido, and A. Hosaka, Phys.Rev. **C85**, p. 015201 (2012).

[96] J. Yamagata-Sekihara, J. Nieves, and E. Oset, Phys.Rev. **D83**, p. 014003 (2011).

[97] F. Aceti and E. Oset, Phys.Rev. **D86**, p. 014012 (2012).

[98] C. Xiao, F. Aceti, and M. Bayar, Eur.Phys.J. **A49**, p. 22 (2013).

[99] J. Oller, E. Oset, and J. Palomar, Phys.Rev. **D63**, p. 114009 (2001).

[100] M. Doring and U. G. Meissner, JHEP **1201**, p. 009 (2012).

[101] S. Theberge, A. W. Thomas, and G. A. Miller, Phys.Rev. **D22**, p. 2838 (1980).

[102] L. Castillejo, R. Dalitz, and F. Dyson, Phys.Rev. **101**, 453–458 (1956).

[103] J. Pelaez, Phys.Rev.Lett. **92**, p. 102001 (2004).

[104] H.-X. Chen and E. Oset, Phys.Rev. **D87**, p. 016014 (2013).

[105] R. Garcia-Martin, R. Kaminski, J. Pelaez, J. Ruiz de Elvira, and F. Yndurain, Phys.Rev. **D83**, p. 074004 (2011).

[106] P. Estabrooks, R. Carnegie, A. D. Martin, W. Dunwoodie, T. Lasinski, *et al.*, Nucl.Phys. **B133**, p. 490 (1978).

[107] R. Mercer, P. Antich, A. Callahan, C. Chien, B. Cox, *et al.*, Nucl.Phys. **B32**, 381–414 (1971).

[108] D. Boito, R. Escribano, and M. Jamin, JHEP **1009**, p. 031 (2010).

[109] D. R. Boito, R. Escribano, and M. Jamin, Eur.Phys.J. **C59**, 821–829 (2009).

[110] F. Aceti, L. Dai, L. Geng, E. Oset, and Y. Zhang, Eur.Phys.J. **A50**, p. 57 (2014).

[111] Y. Kamiya and T. Hyodo, (2015), arXiv:1509.00146 [hep-ph] .

[112] C. Garcia-Recio, C. Hidalgo-Duque, J. Nieves, L. L. Salcedo, and L. Tolos, Phys. Rev. **D92**, p. 034011 (2015).

[113] E. Kolomeitsev and M. Lutz, Phys.Lett. **B585**, 243–252 (2004).

[114] S. Sarkar, E. Oset, and M. Vicente Vacas, Nucl.Phys. **A750**, 294–323 (2005).

[115] L. Roca, S. Sarkar, V. Magas, and E. Oset, Phys.Rev. **C73**, p. 045208 (2006).

[116] L. Roca, C. Hanhart, E. Oset, and U.-G. Meissner, Eur.Phys.J. **A27**, 373–380 (2006).

[117] F. Aceti, E. Oset, and L. Roca, Phys.Rev. **C90**, p. 025208 (2014).

[118] J.-J. Xie and E. Oset, Eur.Phys.J. **A48**, p. 146 (2012).

[119] C. S. Center for Nuclear Studies Data Analysis Center CNS-DAC, `http://gwdac.phys.gwu.edu/`, .

[120] H. Sazdjian, Phys.Rev. **D33**, p. 3401 (1986).

[121] J. Formánek, R. Lombard, and J. Mareš, Czechoslovak Journal of Physics **54**, 289–315 (2004).

[122] T. Hyodo, Int.J.Mod.Phys. **A28**, p. 1330045 (2013).

[123] H. Feshbach, Annals Phys. **5**, 357–390 (1958).

[124] G. Gopal *et al.* (Rutherford-London Collaboration), Nucl.Phys. **B119**, p. 362 (1977).

[125] M. Alston-Garnjost, R. Kenney, D. Pollard, R. Ross, R. Tripp, *et al.*, Phys.Rev. **D18**, p. 182 (1978).

[126] D. Gamermann and E. Oset, Phys.Rev. **D80**, p. 014003 (2009).

[127] F. Aceti, R. Molina, and E. Oset, Phys.Rev. **D86**, p. 113007 (2012).

[128] W.-C. Chang and J.-C. Peng, Phys.Lett. **B704**, 197–200 (2011).

[129] W.-C. Chang and J.-C. Peng, Phys.Rev.Lett. **106**, p. 252002 (2011).

[130] A. Gomez Nicola, J. Nieves, J. Pelaez, and E. Ruiz Arriola, Phys.Rev. **D69**, p. 076007 (2004).

[131] A. Gomez Nicola, J. Nieves, J. Pelaez, and E. Ruiz Arriola, Phys.Lett. **B486**, 77–85 (2000).

[132] G. Brown, M. Rho, and V. Vento, Phys.Lett. **B84**, p. 383 (1979).

[133] S. D. Protopopescu, M. Alston-Garnjost, A. Barbaro-Galtieri, S. M. Flatte, J. H. Friedman, T. A. Lasinski, G. R. Lynch, M. S. Rabin, and F. T. Solmitz, Phys. Rev. **D7**, p. 1279 (1973).

[134] R. Ammar, R. Davis, W. Kropac, J. Mott, D. Slate, B. Werner, M. Derrick, T. Fields, and F. Schweingruber, Phys. Rev. Lett. **21**, 1832–1835 (1968).

[135] D. Morgan, Phys. Lett. **B51**, p. 71 (1974).

[136] D. Morgan and M. R. Pennington, Z. Phys. **C48**, 623–632 (1990).

[137] D. Morgan and M. R. Pennington, Phys. Rev. **D48**, 1185–1204 (1993).

[138] D. Morgan and M. R. Pennington, Phys. Rev. **D48**, 5422–5424 (1993).

[139] N. A. Tornqvist, Z. Phys. **C68**, 647–660 (1995).

[140] A. Bramon and E. Masso, Phys. Lett. **B93**, p. 65 (1980), [Erratum: Phys. Lett.B107,455(1981)].

[141] C. R. Munz, J. Resag, B. C. Metsch, and H. R. Petry, Nucl. Phys. **A578**, 418–440 (1994).

[142] R. L. Jaffe, Phys. Rev. **D15**, p. 267 (1977).

[143] R. L. Jaffe, Phys. Rev. **D15**, p. 281 (1977).

[144] J. D. Weinstein and N. Isgur, Phys. Rev. Lett. **48**, p. 659 (1982).

[145] J. D. Weinstein and N. Isgur, Phys. Rev. **D27**, p. 588 (1983).

[146] J. D. Weinstein and N. Isgur, Phys. Rev. **D41**, p. 2236 (1990).

[147] G. Janssen, B. C. Pearce, K. Holinde, and J. Speth, Phys. Rev. **D52**, 2690–2700 (1995).

[148] M. Locher, V. Markushin, and H. Zheng, Eur.Phys.J. **C4**, 317–326 (1998).

[149] J. Nieves and E. Ruiz Arriola, Nucl.Phys. **A679**, 57–117 (2000).

[150] J. Pelaez and G. Rios, Phys.Rev.Lett. **97**, p. 242002 (2006).

[151] J. Nebreda, J. Pelaez, and G. Rios, Phys.Rev. **D83**, p. 094011 (2011).

[152] J. Palomar, L. Roca, E. Oset, and M. Vicente Vacas, Nucl.Phys. **A729**, 743–768 (2003).

[153] U.-G. Meissner and J. Oller, Nucl.Phys. **A679**, 671–697 (2001).

[154] L. Roca, J. Palomar, E. Oset, and H. Chiang, Nucl.Phys. **A744**, 127–155 (2004).

[155] T. A. Lahde and U.-G. Meissner, Phys.Rev. **D74**, p. 034021 (2006).

[156] B. Liu, M. Buescher, F.-K. Guo, C. Hanhart, and U.-G. Meissner, Eur.Phys.J. **C63**, 93–99 (2009).

[157] C.-b. Li, E. Oset, and M. Vicente Vacas, Phys.Rev. **C69**, p. 015201 (2004).

[158] E. Marco, E. Oset, and H. Toki, Phys.Rev. **C60**, p. 015202 (1999).

[159] N. Achasov, S. Devyanin, and G. Shestakov, Phys.Lett. **B88**, p. 367 (1979).

[160] J.-J. Wu, Q. Zhao, and B. Zou, Phys.Rev. **D75**, p. 114012 (2007).

[161] C. Hanhart, B. Kubis, and J. R. Pelaez, Phys.Rev. **D76**, p. 074028 (2007).

[162] L. Roca, Phys.Rev. **D88**, p. 014045 (2013).

[163] J.-J. Wu and B. S. Zou, Phys. Rev. **D78**, p. 074017 (2008).

[164] M. Ablikim *et al.* (BESIII), Phys.Rev. **D83**, p. 032003 (2011).

[165] M. Ablikim *et al.* (BESIII), Phys.Rev.Lett. **108**, p. 182001 (2012).

[166] J.-J. Wu, X.-H. Liu, Q. Zhao, and B.-S. Zou, Phys.Rev.Lett. **108**, p. 081803 (2012).

[167] Y. Zhou, X.-L. Ren, H.-X. Chen, and L.-S. Geng, Phys. Rev. **D90**, p. 014020 (2014).

[168] L.-S. Geng, X.-L. Ren, Y. Zhou, H.-X. Chen, and E. Oset, Phys. Rev. **D92**, p. 014029 (2015).

[169] K. Chen, C.-Q. Pang, X. Liu, and T. Matsuki, Phys. Rev. **D91**, p. 074025 (2015).

[170] P. Gavillet, R. Armenteros, M. Aguilar-Benitez, M. Mazzucato, and C. Dionisi, Z. Phys. **C16**, p. 119 (1982).

[171] L. De-Min, Y. Hong, and S. Qi-Xing, Chinese Physics Letters **17**, p. 558 (2000).

[172] J. Vijande, F. Fernandez, and A. Valcarce, J. Phys. **G31**, p. 481 (2005).

[173] S. Godfrey and J. Napolitano, Rev. Mod. Phys. **71**, 1411–1462 (1999).

[174] R. Aaij *et al.* (LHCb), Phys. Rev. Lett. **112**, p. 091802 (2014).

[175] F. Aceti, W. H. Liang, E. Oset, J. J. Wu, and B. S. Zou, Phys. Rev. **D86**, p. 114007 (2012).

[176] F. Aceti, J. M. Dias, and E. Oset, Eur. Phys. J. **A51**, p. 48 (2015).

[177] F. Aceti, J.-J. Xie, and E. Oset, Phys. Lett. **B750**, 609–614 (2015).

[178] A. Bramon, R. Escribano, and M. Scadron, Eur.Phys.J. **C7**, 271–278 (1999).

[179] V. Mathieu and V. Vento, Phys.Lett. **B688**, 314–318 (2010).

[180] F. Ambrosino, A. Antonelli, M. Antonelli, F. Archilli, P. Beltrame, *et al.*, JHEP **0907**, p. 105 (2009).

[181] K. Nakamura *et al.* (Particle Data Group), J.Phys. **G37**, p. 075021 (2010).

[182] C. Amsler, A. Anisovich, C. Baker, B. Barnett, C. Batty, *et al.*, Eur.Phys.J. **C33**, 23–30 (2004).

[183] J. Nacher, E. Oset, H. Toki, and A. Ramos, Phys.Lett. **B455**, 55–61 (1999).

[184] E. Marco, S. Hirenzaki, E. Oset, and H. Toki, Phys.Lett. **B470**, 20–26 (1999).

[185] A. Bramon, R. Escribano, J. Lucio M, M. Napsuciale, and G. Pancheri, Eur.Phys.J. **C26**, 253–260 (2002).

[186] R. Escribano, Phys.Rev. **D74**, p. 114020 (2006).

[187] J. Bai *et al.* (BES), Phys.Lett. **B476**, 25–32 (2000).

[188] J. Bai *et al.* (BES), Phys.Lett. **B446**, 356–362 (1999).

[189] A. Anisovich, V. Anisovich, V. Nikonov, and L. Montanet, Eur.Phys.J. **A6**, 247–249 (1999).

[190] A. Anisovich, (2001), arXiv:hep-ph/0104005 [hep-ph] .

[191] E. Klempt, "The Glueball candidate eta(1440) as eta radial excitation," in *Proceedings, 32nd International Conference on High Energy Physics (ICHEP 2004)* (2004), pp. 1082–1085, arXiv:hep-ph/0409148 [hep-ph] .

[192] T. Gutsche, V. E. Lyubovitskij, and M. C. Tichy, Phys.Rev. **D80**, p. 014014 (2009).

[193] J.-J. Xie, L. R. Dai, and E. Oset, Phys. Lett. **B742**, 363–369 (2015).

[194] M. Ablikim *et al.* (BESIII), Phys. Rev. **D92**, p. 012007 (2015).

[195] D. Barberis *et al.* (WA102), Phys. Lett. **B413**, 225–231 (1997).

[196] D. Barberis *et al.* (WA102), Phys. Lett. **B440**, 225–232 (1998).

[197] T. Sekihara, T. Hyodo, and D. Jido, PTEP **2015**, p. 063D04 (2015).

[198] A. W. Thomas, Ad. Nucl. Phys. **13** (1984).

[199] W. H. Liang and E. Oset, Phys. Lett. **B737**, 70–74 (2014).

[200] M. Bayar, W. H. Liang, and E. Oset, Phys. Rev. **D90**, p. 114004 (2014).

[201] R. Aaij *et al.* (LHCb), Phys. Rev. **D87**, p. 052001 (2013).

[202] S. K. Choi *et al.* (Belle), Phys. Rev. Lett. **91**, p. 262001 (2003).

[203] V. M. Abazov *et al.* (D0), Phys. Rev. Lett. **93**, p. 162002 (2004).

[204] D. Acosta *et al.* (CDF), Phys. Rev. Lett. **93**, p. 072001 (2004).

[205] B. Aubert *et al.* (BaBar), Phys. Rev. **D71**, p. 071103 (2005).

[206] E. S. Swanson, Phys. Rept. **429**, 243–305 (2006).

[207] S.-L. Zhu, Int. J. Mod. Phys. **E17**, 283–322 (2008).

[208] M. Nielsen, F. S. Navarra, and S. H. Lee, Phys. Rept. **497**, 41–83 (2010).

[209] S. L. Olsen, *Particles and nuclei. Proceedings, 18th International Conference, PANIC08, Eilat, Israel, November 9-14, 2008*, Nucl. Phys. **A827**, 53C–60C (2009), [,53(2009)].

[210] N. Brambilla *et al.*, Eur. Phys. J. **C71**, p. 1534 (2011).

[211] A. Ali, *Proceedings, 13th International Conference on B-physics at hadron machines (Beauty 2011)*, PoS **BEAUTY2011**, p. 002 (2011).

[212] M. Ablikim *et al.* (BESIII), Phys. Rev. Lett. **111**, p. 242001 (2013).

[213] M. Ablikim *et al.* (BESIII), Phys. Rev. Lett. **112**, p. 132001 (2014).

[214] R. Molina and E. Oset, Phys. Rev. **D80**, p. 114013 (2009).

[215] P. Pakhlov *et al.* (Belle), Phys. Rev. Lett. **100**, p. 202001 (2008).

[216] D. Gamermann and E. Oset, Eur. Phys. J. **A36**, 189–194 (2008).

[217] C. Hidalgo-Duque, J. Nieves, and M. P. Valderrama, Phys. Rev. **D87**, p. 076006 (2013).

[218] J. Nieves and M. P. Valderrama, Phys. Rev. **D86**, p. 056004 (2012).

[219] F.-K. Guo, C. Hidalgo-Duque, J. Nieves, and M. P. Valderrama, Phys. Rev. **D88**, p. 054007 (2013).

[220] Y.-R. Liu, M. Oka, M. Takizawa, X. Liu, W.-Z. Deng, and S.-L. Zhu, Phys. Rev. **D82**, p. 014011 (2010).

[221] Y.-J. Zhang, H.-C. Chiang, P.-N. Shen, and B.-S. Zou, Phys. Rev. **D74**, p. 014013 (2006).

[222] M. T. Li, W. L. Wang, Y. B. Dong, and Z. Y. Zhang, Int. J. Mod. Phys. **A27**, p. 1250161 (2012).

[223] A. Martinez Torres, K. P. Khemchandani, F. S. Navarra, M. Nielsen, and E. Oset, Phys. Lett. **B719**, 388–393 (2013).

[224] M. Ablikim *et al.* (BES), Phys. Rev. Lett. **96**, p. 162002 (2006).

[225] L. S. Geng and E. Oset, Phys. Rev. **D79**, p. 074009 (2009).

[226] M. Ablikim *et al.* (BES), Phys. Lett. **B685**, 27–32 (2010).

[227] J.-J. Xie, M. Albaladejo, and E. Oset, Phys. Lett. **B728**, 319–322 (2014).

[228] A. Martinez Torres, K. P. Khemchandani, F. S. Navarra, M. Nielsen, and E. Oset, Phys. Rev. **D89**, p. 014025 (2014).

[229] M. Ablikim *et al.* (BESIII), Phys. Rev. Lett. **110**, p. 252001 (2013).

[230] X. Liu, Z.-G. Luo, Y.-R. Liu, and S.-L. Zhu, Eur. Phys. J. **C61**, 411–428 (2009).

[231] Y. Dong, A. Faessler, T. Gutsche, S. Kovalenko, and V. E. Lyubovitskij, Phys. Rev. **D79**, p. 094013 (2009).

[232] I. W. Lee, A. Faessler, T. Gutsche, and V. E. Lyubovitskij, Phys. Rev. **D80**, p. 094005 (2009).

[233] T. Fernandez-Carames, A. Valcarce, and J. Vijande, Phys. Rev. Lett. **103**, p. 222001 (2009).

[234] R. D. Matheus, F. S. Navarra, M. Nielsen, and C. M. Zanetti, Phys. Rev. **D80**, p. 056002 (2009).

[235] P. G. Ortega, J. Segovia, D. R. Entem, and F. Fernandez, Phys. Rev. **D81**, p. 054023 (2010).

[236] S. Coito, G. Rupp, and E. van Beveren, Eur. Phys. J. **C71**, p. 1762 (2011).

[237] S. Prelovsek and L. Leskovec, Phys. Rev. Lett. **111**, p. 192001 (2013).

[238] M. Takizawa and S. Takeuchi, PTEP **2013**, p. 0903D01 (2013).

[239] E. Braaten and M. Kusunoki, Phys. Rev. **D69**, p. 074005 (2004).

[240] F. E. Close and P. R. Page, Phys. Lett. **B578**, 119–123 (2004).

[241] M. Nielsen and C. M. Zanetti, Phys. Rev. **D82**, p. 116002 (2010).

[242] Y.-b. Dong, A. Faessler, T. Gutsche, and V. E. Lyubovitskij, Phys. Rev. **D77**, p. 094013 (2008).

[243] Z. Q. Liu *et al.* (Belle), Phys. Rev. Lett. **110**, p. 252002 (2013).

[244] T. Xiao, S. Dobbs, A. Tomaradze, and K. K. Seth, Phys. Lett. **B727**, 366–370 (2013).

[245] M. B. Voloshin, Phys. Rev. **D87**, p. 091501 (2013).

[246] E. Wilbring, H. W. Hammer, and U. G. Meissner, Phys. Lett. **B726**, 326–329 (2013).

[247] Q. Wang, C. Hanhart, and Q. Zhao, Phys. Lett. **B725**, 106–110 (2013).

[248] Y. Dong, A. Faessler, T. Gutsche, and V. E. Lyubovitskij, Phys. Rev. **D88**, p. 014030 (2013).

[249] H.-W. Ke, Z.-T. Wei, and X.-Q. Li, Eur. Phys. J. **C73**, p. 2561 (2013).

[250] J. M. Dias, F. S. Navarra, M. Nielsen, and C. M. Zanetti, Phys. Rev. **D88**, p. 016004 (2013).

[251] C.-F. Qiao and L. Tang, Eur. Phys. J. **C74**, p. 3122 (2014).

[252] A. Bondar *et al.* (Belle), Phys. Rev. Lett. **108**, p. 122001 (2012).

[253] I. Adachi *et al.* (Belle), (2012), arXiv:1207.4345 [hep-ex] .

[254] A. E. Bondar, A. Garmash, A. I. Milstein, R. Mizuk, and M. B. Voloshin, Phys. Rev. **D84**, p. 054010 (2011).

[255] D. V. Bugg, Europhys. Lett. **96**, p. 11002 (2011).

[256] E. S. Swanson, Phys. Rev. **D91**, p. 034009 (2015).

[257] Y.-R. Liu, X. Liu, W.-Z. Deng, and S.-L. Zhu, Eur. Phys. J. **C56**, 63–73 (2008).

[258] D.-Y. Chen, X. Liu, and S.-L. Zhu, Phys. Rev. **D84**, p. 074016 (2011).

[259] M. Cleven, Q. Wang, F.-K. Guo, C. Hanhart, U.-G. Meissner, and Q. Zhao, Phys. Rev. **D87**, p. 074006 (2013).

[260] Y. Dong, A. Faessler, T. Gutsche, and V. E. Lyubovitskij, J. Phys. **G40**, p. 015002 (2013).

[261] Z.-F. Sun, J. He, X. Liu, Z.-G. Luo, and S.-L. Zhu, Phys. Rev. **D84**, p. 054002 (2011).

[262] J.-R. Zhang, M. Zhong, and M.-Q. Huang, Phys. Lett. **B704**, 312–315 (2011).

[263] I. V. Danilkin, V. D. Orlovsky, and Yu. A. Simonov, Phys. Rev. **D85**, p. 034012 (2012).

[264] C.-Y. Cui, Y.-L. Liu, and M.-Q. Huang, Phys. Rev. **D85**, p. 074014 (2012).

[265] T. Guo, L. Cao, M.-Z. Zhou, and H. Chen, (2011), arXiv:1106.2284 [hep-ph] .

[266] W. Chen and S.-L. Zhu, Phys. Rev. **D83**, p. 034010 (2011).

[267] Z.-G. Wang and T. Huang, Nucl. Phys. **A930**, 63–85 (2014).

[268] A. Ali, C. Hambrock, and W. Wang, Phys. Rev. **D85**, p. 054011 (2012).

[269] E. Braaten, Phys. Rev. Lett. **111**, p. 162003 (2013).

[270] M. P. Valderrama, Phys. Rev. **D85**, p. 114037 (2012).

[271] H.-W. Ke, X.-Q. Li, Y.-L. Shi, G.-L. Wang, and X.-H. Yuan, JHEP **04**, p. 056 (2012).

[272] Y. Yang, J. Ping, C. Deng, and H.-S. Zong, J. Phys. **G39**, p. 105001 (2012).

[273] M. Cleven, F.-K. Guo, C. Hanhart, and U.-G. Meissner, Eur.Phys.J. **A47**, p. 120 (2011).

[274] M. B. Voloshin, Phys. Rev. **D84**, p. 031502 (2011).

[275] J. Nieves and M. P. Valderrama, Phys. Rev. **D84**, p. 056015 (2011).

[276] T. Mehen and J. W. Powell, Phys. Rev. **D84**, p. 114013 (2011).

[277] D.-Y. Chen and X. Liu, Phys. Rev. **D84**, p. 094003 (2011).

[278] S. Ohkoda, Y. Yamaguchi, S. Yasui, and A. Hosaka, Phys. Rev. **D86**, p. 117502 (2012).

[279] F.-K. Guo, C. Hidalgo-Duque, J. Nieves, and M. P. Valderrama, *Proceedings, 9th International Workshop on the Physics of Excited Nucleons (NSTAR 2013)*, Int. J. Mod. Phys. Conf. Ser. **26**, p. 1460073 (2014).

[280] M. T. Li, W. L. Wang, Y. B. Dong, and Z. Y. Zhang, J. Phys. **G40**, p. 015003 (2013).

[281] M. B. Wise, Phys. Rev. **D45**, 2188–2191 (1992).

[282] W. H. Liang, C. W. Xiao, and E. Oset, Phys. Rev. **D89**, p. 054023 (2014).

[283] N. Isgur and M. B. Wise, Phys. Lett. **B232**, 113–117 (1989).

[284] N. Isgur and M. B. Wise, *DPF Conf.1990:0459-464*, Phys. Lett. **B237**, 527–530 (1990).

[285] M. Neubert, Phys. Rept. **245**, 259–396 (1994).

[286] A. Anastassov *et al.* (CLEO), Phys. Rev. **D65**, p. 032003 (2002).

[287] E. Oset, H. Toki, M. Mizobe, and T. T. Takahashi, Prog. Theor. Phys. **103**, 351–365 (2000).

[288] B. Ananthanarayan, G. Colangelo, J. Gasser, and H. Leutwyler, Phys. Rept. **353**, 207–279 (2001).

[289] R. Garcia-Martin, R. Kaminski, J. R. Pelaez, and J. Ruiz de Elvira, Phys. Rev. Lett. **107**, p. 072001 (2011).

[290] J. R. Pelaez, (2015), arXiv:1510.00653 [hep-ph] .

[291] M. Ablikim *et al.* (BESIII), Phys. Rev. Lett. **112**, p. 022001 (2014).

[292] F. Aceti, M. Bayar, E. Oset, A. Martinez Torres, K. P. Khemchandani, J. M. Dias, F. S. Navarra, and M. Nielsen, Phys. Rev. **D90**, p. 016003 (2014).

[293] F. Aceti, M. Bayar, J. M. Dias, and E. Oset, Eur. Phys. J. **A50**, p. 103 (2014).

[294] J. M. Dias, F. Aceti, and E. Oset, Phys. Rev. **D91**, p. 076001 (2015).

[295] J.-J. Wu, R. Molina, E. Oset, and B. S. Zou, Phys. Rev. Lett. **105**, p. 232001 (2010).

[296] J.-J. Wu, R. Molina, E. Oset, and B. S. Zou, Phys. Rev. **C84**, p. 015202 (2011).

[297] J.-J. Wu and B. S. Zou, Phys. Lett. **B709**, 70–76 (2012).

[298] P. Rubin *et al.* (CLEO), Phys. Rev. Lett. **93**, p. 111801 (2004).

[299] K. Abe *et al.* (Belle), "Evidence for $X(3872) \to \gamma J/\psi$ and the sub-threshold decay $X(3872) \to \omega J/\psi$," in *Lepton and photon interactions at high energies. Proceedings, 22nd International Symposium, LP 2005, Uppsala, Sweden, June 30-July 5, 2005* (2005) arXiv:hep-ex/0505037 [hep-ex] .

[300] B. Aubert *et al.* (BaBar), Phys. Rev. **D74**, p. 071101 (2006).

[301] V. Bhardwaj *et al.* (Belle), Phys. Rev. Lett. **107**, p. 091803 (2011).

[302] T. Barnes and S. Godfrey, Phys. Rev. **D69**, p. 054008 (2004).

[303] E. S. Swanson, Phys. Lett. **B598**, 197–202 (2004).

[304] E. Braaten and M. Kusunoki, Phys. Rev. **D72**, p. 054022 (2005).

[305] Y. Dong, A. Faessler, T. Gutsche, and V. E. Lyubovitskij, J. Phys. **G38**, p. 015001 (2011).

[306] A. M. Badalian, V. D. Orlovsky, Yu. A. Simonov, and B. L. G. Bakker, Phys. Rev. **D85**, p. 114002 (2012).

[307] S. Dubnicka, A. Z. Dubnickova, M. A. Ivanov, J. G. Koerner, P. Santorelli, and G. G. Saidullaeva, Phys. Rev. **D84**, p. 014006 (2011).

[308] E. Braaten and M. Lu, Phys. Rev. **D77**, p. 014029 (2008).

[309] A. Faessler, T. Gutsche, V. E. Lyubovitskij, and Y.-L. Ma, Phys. Rev. **D76**, p. 014005 (2007).

[310] T. Branz, T. Gutsche, and V. E. Lyubovitskij, Phys. Rev. **D79**, p. 014035 (2009).

[311] D. L. Canham, H. W. Hammer, and R. P. Springer, Phys. Rev. **D80**, p. 014009 (2009).

[312] M. Harada and Y.-L. Ma, Prog. Theor. Phys. **126**, 91–113 (2011).

[313] C. Hanhart, Yu. S. Kalashnikova, A. E. Kudryavtsev, and A. V. Nefediev, Phys. Rev. **D85**, p. 011501 (2012).

[314] H.-W. Ke and X.-Q. Li, Phys. Rev. **D84**, p. 114026 (2011).

[315] R. Aaij *et al.* (LHCb), Phys. Rev. Lett. **110**, p. 222001 (2013).

[316] M. B. Voloshin and L. B. Okun, JETP Lett. **23**, 333–336 (1976), [Pisma Zh. Eksp. Teor. Fiz.23,369(1976)].

[317] N. A. Tornqvist, Phys. Rev. Lett. **67**, 556–559 (1991).

[318] N. A. Tornqvist, Phys. Lett. **B590**, 209–215 (2004).

[319] E. S. Swanson, Phys. Lett. **B588**, 189–195 (2004).

[320] C. E. Thomas and F. E. Close, Phys. Rev. **D78**, p. 034007 (2008).

[321] E. Braaten, M. Lu, and J. Lee, Phys. Rev. **D76**, p. 054010 (2007).

[322] S. Fleming, M. Kusunoki, T. Mehen, and U. van Kolck, Phys. Rev. **D76**, p. 034006 (2007).

[323] M. Suzuki, Phys. Rev. **D72**, p. 114013 (2005).

[324] V. Baru, A. A. Filin, C. Hanhart, Yu. S. Kalashnikova, A. E. Kudryavtsev, and A. V. Nefediev, Phys. Rev. **D84**, p. 074029 (2011).

[325] C. Hanhart, Yu. S. Kalashnikova, A. E. Kudryavtsev, and A. V. Nefediev, Phys. Rev. **D75**, p. 074015 (2007).

[326] P. Artoisenet, E. Braaten, and D. Kang, Phys. Rev. **D82**, p. 014013 (2010).

[327] R. Molina, H. Nagahiro, A. Hosaka, and E. Oset, Phys. Rev. **D83**, p. 094030 (2011).

[328] F. S. Navarra, M. Nielsen, and M. E. Bracco, Phys. Rev. **D65**, p. 037502 (2002).

[329] S. K. Choi *et al.*, Phys. Rev. **D84**, p. 052004 (2011).